## Title

Zinc finger antiviral protein (ZAP) interaction with ancient viruses and host factors shapes its antiviral activity



## Author

Huang, Serina

## Publication Date

2024

Peer reviewed|Thesis/dissertation

UNIVERSITY OF CALIFORNIA

Los Angeles

# Zinc finger antiviral protein (ZAP) interaction with ancient viruses and host factors shapes its antiviral activity

A dissertation submitted in partial satisfaction of the requirements for the degree

Doctor of Philosophy in Human Genetics

by

Serina Huang

2024

ABSTRACT OF THE DISSERTATION

Zinc finger antiviral protein (ZAP) interaction with ancient viruses and host factors shapes its antiviral activity

by

Serina Huang

Doctor of Philosophy in Human Genetics

University of California, Los Angeles, 2024

Professor Melody Man Hing Li, Co-Chair

Professor Nandita Garud, Co-Chair

Alphaviruses are arthropod-borne viruses that infect mammals and cause arthritogenic and/or encephalitic disease. The risk of an alphavirus outbreak increases as urbanization and global warming alter the habitats of alphaviruses' vectors and host species. Zinc finger antiviral protein (ZAP) is an interferon-stimulated gene that is upregulated to combat alphavirus infections. While the functions of individual ZAP domains in viral infection are known, it is unclear if and how they—along with other cofactors—may work together to create a strong defense against alphaviruses. This dissertation aims to understand the anti-alphaviral mechanism of ZAP using evolutionary approaches and molecular biology.

To determine the sites that have functional importance in ZAP throughout its evolutionary history with viruses, we harnessed the power of positive selection analysis. Using complementary computational approaches that model codon substitution rates, we identified the sites on ZAP that have been the targets of positive selection in the host-virus arms race. We found seven positively selected sites distributed across the ZAP gene. When one of the positively selected sites is mutated to an alanine, we observed that the mutant is almost 10-fold better at inhibiting alphaviruses. This improvement is not due to differences in ZAP's interaction with viral RNA or its cofactor tripartite motif containing 25 (TRIM25), but is associated with a reduced ability to bind to poly(ADP-ribose).

Next, to understand how TRIM25 cofactors contribute to ZAP-mediated antiviral activity, we followed up on poly(A) binding protein cytoplasmic 4 (PABPC4) and investigated its role in regulating viral RNA translation. We found that TRIM25 ubiquitination bolsters PABPC4's enhancement of alphavirus inhibition. We also demonstrated that PABPC4 binds to alphaviral RNA and blocks its translation early on in infection. The work presented here shows that ZAP's interactions with ancient viruses and host factors have shaped its antiviral activity, and implicates translational regulation and modification as key components of the host defense against alphaviruses.

The dissertation of Serina Huang is approved.

Kirk Edward Lohmueller, Committee Chair

Ting-Ting Wu, Committee Chair

Melody Man Hing Li, Committee Co-Chair

Nandita Garud, Committee Co-Chair

University of California, Los Angeles

2024

DEDICATION

For 爺爺奶奶

# TABLE OF CONTENTS

**CHAPTER 1: INTRODUCTION ..... 1**

EVOLUTION ..... 1

ALPHAVIRUS ..... 3

INNATE IMMUNITY ..... 6

SIGNIFICANCE AND DISSERTATION OVERVIEW ..... 9

**CHAPTER 2: POSITIVE SELECTION ANALYSES IDENTIFY A SINGLE WWE DOMAIN RESIDUE THAT SHAPES ZAP INTO A MORE POTENT RESTRICTION FACTOR AGAINST ALPHAVIRUSES 10**

ABSTRACT ..... 10

INTRODUCTION ..... 11

RESULTS ..... 14

DISCUSSION ..... 36

ACKNOWLEDGMENTS ..... 42

MATERIALS AND METHODS ..... 43

SUPPLEMENTARY MATERIAL ..... 52

**CHAPTER 3: PABPC4 ENHANCES ZAP-TRIM25 SYNERGY IN ALPHAVIRAL TRANSLATION BLOCK ..... 57**

INTRODUCTION ..... 57

RESULTS ..... 58

DISCUSSION ..... 62

MATERIALS AND METHODS ..... 64

**CHAPTER 4: CONCLUSION ..... 68**

SUMMARY ..... 68

FUTURE DIRECTIONS ..... 69

**APPENDIX 1: ELUCIDATION OF TRIM25 UBIQUITINATION TARGETS INVOLVED IN DIVERSE CELLULAR AND ANTIVIRAL PROCESSES ..... 71**

**APPENDIX 2: INTERACTION OF CHIKUNGUNYA VIRUS GLYCOPROTEINS WITH MACROPHAGE FACTORS CONTROLS VIRION PRODUCTION** ..... **106**

**BIBLIOGRAPHY** ..... **138**

## LIST OF FIGURES

Figure 1.1 Virus infection activates the type I interferon (IFN) pathway. ..... 7

Figure 1.2 Poly(ADP-ribose) polymerases (PARPs) catalyze the attachment of ADP-ribose onto substrates. ..... 8

Figure 2.1 Identification of seven positively selected sites across ZAP protein. ..... 17

Figure 2.2 Each positively selected site in ZAP was mutated and its antiviral activity against Sindbis virus (SINV) was tested. ..... 19

Figure 2.3 Mutating both positively selected sites in the second WWE domain of ZAP does not further enhance antiviral activity. ..... 22

Figure 2.4 The N658A mutant is better at inhibiting virion production and SINV RNA translation ..... 24

Figure 2.5 The ZAPL N658A mutant inhibits many other alphaviruses better than WT. ..... 26

Figure 2.6 The improved antiviral activity of the N658A mutant is not due to changes in ZAP binding to SINV RNA or interaction with TRIM25. ..... 29

Figure 2.7 The N658A mutant is correlated with decreased binding to poly(ADP-ribose) (PAR). ..... 32

Figure 2.8 Asparagine is the predominant amino acid at site 658 yet confers weaker antiviral activity ..... 36

Figure 3.1 PABPC4 siRNA knockdown (KD) restores SINV replication when TRIM25 wild-type (WT) or R54P are overexpressed. ..... 59

Figure 3.2 Ability of PABPC4 to bind SINV RNA. ..... 60

Figure 3.3 PABPC4 affects SINV translation. ..... 62

## LIST OF SUPPLEMENTARY MATERIALS

Supplementary Figure 2.1 Positive selection and domains of ZAP. ..... 52

Supplementary Figure 2.2 Characterization of WT ZAP inducible single clone cell lines..... 53

Supplementary Figure 2.3 Densitometric analysis of ZAP positive selection mutants. ..... 54

Supplementary Figure 2.4 N658A mutant induces interferon (IFN) and interferon-stimulated gene (ISG) levels similar to WT. ..... 55

Supplementary Figure 2.5 The ZAPL PAR binding deficient Q668R negative control pulls down less PAR. ..... 56

## ACKNOWLEDGEMENTS

This work would not be possible without the scientific mentors who have guided me. First, I am grateful to Dr. Melody Li for nurturing my passion for research. She has supported me when I feel lost and distressed, and celebrated me when I grow and succeed. She is a true inspiration when it comes to being a scientist and a mentor. I would also like to thank my committee members Drs. Nandita Garud, Kirk Lohmueller, and Ting-Ting Wu; all of whom are brilliant and have given me encouragement and valuable insights during the whole process. My lab mates have been a huge source of strength and joy. Just seeing them as I walk into lab brightens up my morning every day. I learned a great deal from Dr. Emily Yang, who modeled efficient experimental work and critical thinking for me. Besides having scientific discussions, I have loved talking and laughing with Dr. Zhenlan Yao, Dr. LeAnn Nguyen, Pablo Alvarez, Sangeetha Ramachandran, Erin Kim, Martin Ruvalcaba, and Maria Gutierrez. I am in awe of our former undergraduate assistants Faith St. Amant and Jules Girdner, who have infused our lab with excitement. In particular, Jules Girdner was integral in helping me with my experiments and has an admirably positive attitude. Dr. Oliver Fregoso and his lab members, especially Dr. Carina Sandoval, Dr. Vivian Yang, and Andrew Saluna, have likewise provided so much support and community. I am also grateful to all the people who have shared their experiences and advice with me.

Thank you to all the staff, directors, and personnel in the Departments of Human Genetics and of Microbiology, Immunology, and Molecular Genetics; including Issa Lutfi, Jerome Keh, Lorraine Hartman, Alonzo Cortez, and Joey Silva. They are always on top of things and uphold the infrastructure that is essential for our research.

I feel so incredibly lucky to have my friends. At UCLA, Gloria Bartolo, Dana Franklin, Ryan Kan, Dr. Minsub Lee, and Aileen Nava (and many more!) have listened empathetically when I vent about my trials and tribulations. Outside of UCLA, I cherish and appreciate my friendships with numerous people, including but not limited to Kailin Li, Vanessa Rodriguez, Catherine Yang, Dr. Jiarong Zhou, and folks in the LA COVID Conscious Community. My friends never cease to amaze me with their kindness and wonderfulness.

I hold so much love and appreciation for my family. The Hakomoris have cheered me on since day one of graduate school. I am forever grateful to my grandparents, who raised me up after I immigrated to the United States and who continue to love me wholeheartedly. I am thankful to my parents, siblings, aunts, uncles, and cousins, who have shown their support for me in so many different ways. My husband Tyler Hakomori has evolved with me in the last eleven years and has accepted my every iteration. His warmth and care have made my life infinitely more colorful.

Lastly, I would like to thank all the people who contributed to the following chapters in the dissertation:

Chapter 2 is adapted from "Huang S, Girdner J, Nguyen LP, Sandoval C, Fregoso OI, et al. (2024) Positive selection analyses identify a single WWE domain residue that shapes ZAP into a more potent restriction factor against alphaviruses. PLOS Pathogens 20(8): e1011836." This work was supported by the National Institute of Allergy and Infectious Diseases R01AI158704, Faculty Seed Grant CRN-20-637544 from University of California Cancer Research Coordinating Committee, 2019 Seed Grant from UCLA AIDS Institute and Charity Treks, and Endowed Chair in Microbiology from Johanna F. and Joseph H. Shaper Family

(all to M.M.H.L.). Author contributions were: Conceptualization – S.H., M.M.H.L.; Data curation – M.M.H.L.; Formal analysis: S.H., J.G.; Funding acquisition – M.M.H.L.; Investigation – S.H., J.G., L.P.N., C.S.; Methodology – S.H., J.G., L.P.N., C.S.; Project administration: S.H., M.M.H.L.; Resources – O.I.F., D.E., M.H.H.L.; Software – S.H., D.E.; Supervision – O.I.F., M.M.H.L.; Validation – S.H., J.G., L.P.N., C.S.; Visualization – S.H., J.G., L.P.N., C.S.; Writing-original draft – S.H., J.G., M.M.H.L.; Writing-review & editing – S.H., J.G., L.P.N., C.S., O.I.F., D.E., M.M.H.L.

Chapter 3 is adapted from a manuscript in preparation and is possible with the contributions of Erin Kim and Melody M.H. Li.

Appendix 1 is a reprint of "Yang E, Huang S, Jami-Alahmadi Y, McInerney GM, Wohlschlegel JA, et al. (2022) Elucidation of TRIM25 ubiquitination targets involved in diverse cellular and antiviral processes. PLOS Pathogens 18(9): e1010743." This work was supported by NIH grant R01AI158704 (M.M.H.L.), Faculty Seed Grant CRN-20-637544 from University of California Cancer Research Coordinating Committee (M.M.H.L.), 2019 Seed Grant from UCLA AIDS Institute and Charity Treks (M.M.H.L.), Endowed Chair in Microbiology from Johanna F. and Joseph H. Shaper Family (M.M.H.L.), Ruth L. Kirschstein MPTG (NRSA AI007323; E.Y.), Warsaw Fellowship (E.Y.), and Whitcome Fellowship (E.Y.). Author contributions were: Conceptualization – E.Y., G.M.M., J.A.W., M.M.H.L; Investigation – E.Y., S.H., Y.J.; Methodology – E.Y., Y.J., J.A.W., M.M.H.L.; Formal analysis, Software – E.Y., Y.J.; Project administration – E.Y., J.W., M.M.H.L.; Validation, Visualization, Writing-Original Draft – E.Y.; Writing-Review and Editing – E.Y., S.H., G.M.M., J.A.W.,

M.M.H.L.; Resources – G.M.M., J.A.W., M.M.H.L.; Supervision – J.A.W., M.M.H.L; Funding acquisition – M.M.H.L.

Appendix 2 is a reprint of "Yao Z, Ramachandran S, Huang S, Kim E, Jami-Alahmadi Y, et al. (2024) Interaction of chikungunya virus glycoproteins with macrophage factors controls virion production. EMBO Journal 43:4625-4655." This work was supported by NIH grants R01AI158704 (M.M.H.L.), GM089778 (J.A.W.), R35GM153408 (J.A.W.), Faculty Seed Grant CRN-20-637544 from University of California Cancer Research Coordinating Committee (M.M.H.L.), 2019 Seed Grant from UCLA AIDS Institute and Charity Treks (M.M.H.L.), the HIV Accessory and Regulatory Complexes (HARC) Collaborative Development Award (M.B.), Ruth L. Kirschstein MPTG (NRSA AI007323; E.K.), and the UCLA Sydney Finegold Post-Doctoral Fellow Award (Z.Y.).

# VITA

## Education

University of California, San Diego, CA, Sep 2014 - Dec 2018
B.S. in Chemical Engineering, Biology Minor

## Research Experience

**Graduate Researcher**, University of California, Los Angeles
Advisor: Dr. Melody Li, Department of Microbiology, Immunology, and Molecular Genetics
Sep 2019 - Present

**Undergraduate Researcher**, University of California, San Diego
Advisor: Dr. Kyle Gaulton
Jan 2016 - Mar 2019

**Research Intern**, Palo Alto Veterans Institute for Research
Advisor: Dr. Brian Zabel
Apr 2016 - Aug 2016

## Publications

**Huang S**, Girdner J, Nguyen LP, Sandoval C, Fregoso OI, Enard D, Li MMH. Positive selection analyses identify a single WWE domain residue that shapes ZAP into a more potent restriction factor against alphaviruses. PLoS Pathog. 2024 Aug; 20(8):e1011836.

Yao Z, Ramachandran S, **Huang S**, Jami-Alahmadi Y, Wohlschlegel JA, Li MMH. Interaction of chikungunya virus glycoproteins with macrophage factors controls virion production. EMBO J. 2024 Sep;1-31.

Yang E, **Huang S**, Jami-Alahmadi Y, McInerney GM, Wohlschlegel JA, Li MMH. Elucidation of TRIM25 ubiquitination targets involved in diverse cellular and antiviral processes. PLoS Pathog. 2022 Sep;18(9):e1010743.

Chiou J, Geusz RJ, Okino ML, Han JY, Miller M, Melton R, Beebe E, Benaglio P, **Huang S**, Korgaonkar K, Heller S, Kleger A, Preissl S, Gorkin DU, Sander M, Gaulton KJ. Interpreting type 1 diabetes risk with genetics and single-cell epigenomics. Nature. 2021 Jun;594(7863):398-402.

Chiou J, Zeng C, Cheng Z, Han JY, Schlichting M, Miller M, Mendez R, **Huang S**, Wang J, Sui Y, Deogaygay A, Okino ML, Qiu Y, Sun Y, Kudtarkar P, Fang R, Preissl S, Sander M, Gorkin DU, Gaulton KJ. Single-cell chromatin accessibility identifies pancreatic islet cell type- and state-specific regulatory programs of diabetes risk. Nat Genet. 2021 Apr;53(4):455-466.

Salazar N, Carlson JC, Huang K, Zheng Y, Oderup C, Gross J, Jang AD, Burke TM, Lewén S, Scholz A, **Huang S**, Nease L, Kosek J, Mittelbronn M, Butcher EC, Tu H, Zabel BA. A Chimeric Antibody against ACKR3/CXCR7 in Combination with TMZ Activates Immune Responses and Extends Survival in Mouse GBM Models. Mol Ther. 2018 May;26(5):1354-1365.

## Conference Presentations

**Huang S**, Girdner J, Nguyen LP, Sandoval C, Fregoso OI, Enard D, Li MMH. Positive selection analyses identify a single WWE domain residue that shapes ZAP into a more potent restriction factor against alphaviruses. Presented at the Annual Society for American Virology Meeting in 2022 (poster), 2023 (talk), and 2024 (poster).

**Huang S**, Aylward A, Chiou J, Okino ML, Gaulton KJ. Type 2 diabetes risk variants affect NOTCH2 activity in the liver. (2018). Poster presented at the Annual American Society of Human Genetics Meeting, San Diego, CA.

## Service

**Judge**, San Bernardino Inyo and Mono Science and Engineering Fair, 2024
**Math Tutor**, Bruin Tutor Network, Pritzker Center, UCLA, 2021 - 2022
**Mentor**, EmpowHer Institute, Los Angeles, 2020 - 2021

## Honors

**American Society for Virology Conference Travel Award**, 2022, 2023, 2024
**Best Poster Award at the Annual Molecular Biology Institute Retreat**, 2021
**Phi Beta Kappa Honor Society**, 2019
**UC Scholars Summer Research Scholarship**, 2018
**Tau Beta Pi Engineering Honor Society**, 2016

## Teaching and Mentorship

**Teaching Assistant** for MIMG 102: Introduction to Virology at UCLA
Winter 2020, Winter 2021
**Graduate Mentor** for Juliana Girdner, undergraduate in Biochemistry at UCLA
2022 - 2024

# Chapter 1: Introduction

## Evolution

Evolution, in the pithy words of Charles Darwin, is "descent with modification" (Darwin & Kebler, 1859). All organisms living today are the products of evolution from a common ancestor. Evolution happens when mutations—which naturally occur when an organism's genetic material is altered by replication, external stimuli, or cellular processes—are inherited by the progenies of a population. When a species experiences a selective force, for example, death from malaria, the individual(s) in the population with a mutation that confers resistance to malaria is able to pass down its variant of the gene to future generations. This beneficial mutation will increase in frequency within the population, a phenomenon known as positive selection.

In addition to environmental conditions and agents outside of the cell, positive selection can also be driven by mutualistic or parasitic intracellular pathogens. The latter antagonistic dynamic is typified by the genetic conflict between hosts and viruses (Daugherty & Malik, 2012). If there is a host antiviral protein that can restrict a viral protein, there will be a selective pressure on the viral protein to evade host restriction. Among all the protein variants generated by the virus naturally, the one that is able to elude the host will be positively selected and become more prevalent. This viral adaptation in turns drives the host protein to restore the recognition. Throughout generations of one-upping each other in this conflict, both the host and viral genes will have gone through rapid adaptation. Thus, sites that are positively selected are likely to be interaction hotspots, functionally important, or both.

Since positively selected sites can facilitate the study of both host and viral genes, several statistical and computational methods have been developed to identify positively selected sites (Z. Yang, 2006). Fundamentally, positive selection analysis compares the non-synonymous substitution rate to the synonymous substitution rate in a phylogeny of gene orthologs. If this ratio (oftentimes represented by dN/dS or ω) exceeds one, it suggests that there is positive selection because non-synonymous mutations that change the amino acid is more likely to negatively impact the function of a protein (Goldman & Yang, 1994; Nielsen, 2005). To identify positive selection at specific sites, more sophisticated analyses have incorporated codon substitution models and Markov chains to estimate the distribution of substitution rates (Kosakovsky Pond & Frost, 2005a; Kosakovsky Pond et al., 2011; Murrell et al., 2013; M. D. Smith et al., 2015; Rodrigue et al., 2021). The analysis is followed by a likelihood ratio test against the neutral theory of evolution, which hypothesizes that the variation observed is due to random genetic drift or negative selection against deleterious mutations—rather than positive selection—and thus has no functional significance (Kimura, 1983). More complex and accurate approximation and implementation of evolutionary analyses are under active research.

Meanwhile, existing methods have identified multiple cases of positive selection in genes involved in host innate immunity (Enard et al., 2016; McDougal et al., 2022). For instance, TRIM5α is a host factor that has a patch of positively selected sites in primate orthologs. When substituted with the patch found in human TRIM5α, rhesus TRIM5α loses its restriction against the retroviral capsid (Sawyer et al., 2004), reflecting that positive selection can determine species specificity. Another host factor, SAMHD1, hydrolyzes and depletes

deoxynucleotide triphosphates so they cannot be used by DNA viruses and retroviruses in replication. SAMHD1 is positively selected in both primate and non-primate lineages (Laguette et al., 2012; Monit et al., 2019), and these positively selected sites can alter SAMHD1's sensitivity to degradation mediated by the retroviral proteins Vpx/Vpr (Lim et al., 2012). These studies have demonstrated the utility of how positive selection analyses can provide windows into host-virus interactions.

## Alphavirus

Alphaviruses (family *Togaviridae*) are RNA viruses that are transmitted by arthropod vectors, usually *Culex* or *Aedes* mosquitoes. Alphaviruses are able to infect most vertebrates and have a wide host repertoire, ranging from fish to birds to mammals (Weaver et al., 2012). However, due to sampling biases and lack of surveillance, the list of reservoir hosts of each alphavirus is incomplete. For instance, marsupials such as kangaroos and wallabies are reservoirs that predominantly contribute to the endemic status of Ross River virus in Australia. Serological and experimental studies have also named horses, possums, cats, dogs, foxes, and humans as potential reservoir or spillover hosts (Claflin & Webb, 2015; Lau et al., 2017; Stephenson et al., 2018; Yuen & Bielefeldt-Ohmann, 2021). In general, mammals are susceptible to alphavirus infections (Griffin & Weaver, 2021; D. W. Smith et al., 2009).

### Health impact and pathogenesis

Because alphaviruses have broad host tropism, deforestation and urbanization have increased human exposure to wildlife and thus to alphaviruses. Moreover, global warming is projected to change and expand the distribution of their mosquito vectors (Ryan et al., 2019).

There is no widely available vaccine or antiviral treatment, underscoring the need for more research about alphaviruses, their hosts, and host immunity.

Alphaviral infections can be categorized into two types based on the disease symptoms: arthritogenic and encephalitic. Arthritogenic symptoms are typically caused by Old World alphaviruses (named for the continents in which they were first discovered) and manifest as rash, muscle pain, and fever early in the infection. Acute symptoms caused by an Old World alphavirus, chikungunya virus (CHIKV) for example, usually resolve within two weeks, but sometimes progress to chronic arthritis lasting from months to years. Encephalitic disease caused by New World alphaviruses includes headache, convulsion, seizure, loss of muscle control, and other neurological symptoms.

The array of disease manifestations is partly attributed to the route of exposure and dissemination. When a mosquito feeds on the blood of a host, the alphaviruses it carries can infect local muscle cells and later spread through the lymph nodes and into the bloodstream, where they can infect other cells in distal tissues including fibroblasts, osteoblasts, macrophages, and even neuronal cells (Kafai et al., 2022).

**Structure, genome, and life cycle**

The alphavirus virion is enveloped by a lipid bilayer embedded with viral E1-E2 glycoproteins which are important for binding to and entering new cells (Strauss & Strauss, 1994). The viral envelope surrounds a nucleocapsid that encloses and protects the viral genome. The virus first enters a cell when the E2 glycoproteins bind to receptors on the host cell surface, and its entry is enhanced by binding to other attachment factors. Several host receptors for alphaviruses have been proposed, including MXRA8 and LDLRAD3 (Kafai et

al., 2022; Zimmerman et al., 2023). After the virus binds to host cell receptors, the virion is internalized into the cell through clathrin-mediated endocytosis. As the early endosome matures into late endosome, the internal pH drops, dissociating the E1-E2 glycoproteins and triggering a conformational change in E1 that allows the viral membrane to fuse with the endosomal membrane.

Upon fusion, the envelope is disassembled and the nucleocapsid is deposited into the cytoplasm for viral RNA genome uncoating. The alphavirus genome is a single-stranded, positive-sense 12kb RNA which contains a non-structural protein (nsP) region and a structural protein (sP) region. Because the alphavirus genome resembles host RNA, it can be immediately translated by the host ribosomal machinery. The nsP region is translated first, predominantly as the P123 polyprotein with a subset of P1234. The nsP polyprotein is cleaved and processed into individuals nsPs by the nsP2 protease. The nsP1 is a guanylyltransferase and a methyltransferase that caps the viral RNA at its 5' end to imitate host RNA. The role of nsP3 in viral infection is not well understood, but it contains a highly conserved macrodomain that binds and hydrolyzes ADP-ribose, both activities that are critical for CHIKV replication (Abraham et al., 2018). nsP4 is an RNA polymerase that, with the nsP polyprotein and nsPs, forms a replication complex to generate negative and positive strands of the viral RNA. Later in the replication cycle, the subgenomic RNA is translated to produce the sP polyprotein, which is processed to aid in the assembly of a mature virus particle. Mature virions are then released out of the cell and ready to infect new cells and hosts. Any of the viral components can interact with host proteins throughout the viral life cycle, providing opportunities for evolutionary adaptation on both sides.

## Innate immunity

The type I interferon (IFN) pathway is a key initial response triggered by the host innate immune system to combat a viral infection (Fig 1.1) (Iwasaki, 2012). The type I IFN pathway is activated when pathogen-associated molecular patterns (PAMPs) are detected by pattern recognition receptors (PRRs) on the cell surface, within the endosomes, or in the cytoplasm (Y. Zhou et al., 2017). PAMPs can be any pathogenic component or feature that appears to be "non-self," such as lipopolysaccharides from bacteria (Wu & Chen, 2014). For viruses, replication intermediates, inadequately capped viral RNA, and viral glycoproteins can all be flagged by PRRs as an intruder to the host (Iwasaki, 2012). Once activated, PRRs set off a signaling cascade that produces IFNs and a subset of interferon-stimulated genes (ISGs). A second wave of the type I IFN response commences as IFNs are secreted and bind to IFN receptors, upregulating the full repertoire of ISGs through the Janus/kinase (JAK) and signal transducers and activators of transcription (STAT) pathway.

One major way IFNs interfere with viral infection is by inducing a vast repertoire of ISGs, which tightly regulates the IFN response or holds antiviral function. Some ISGs encode

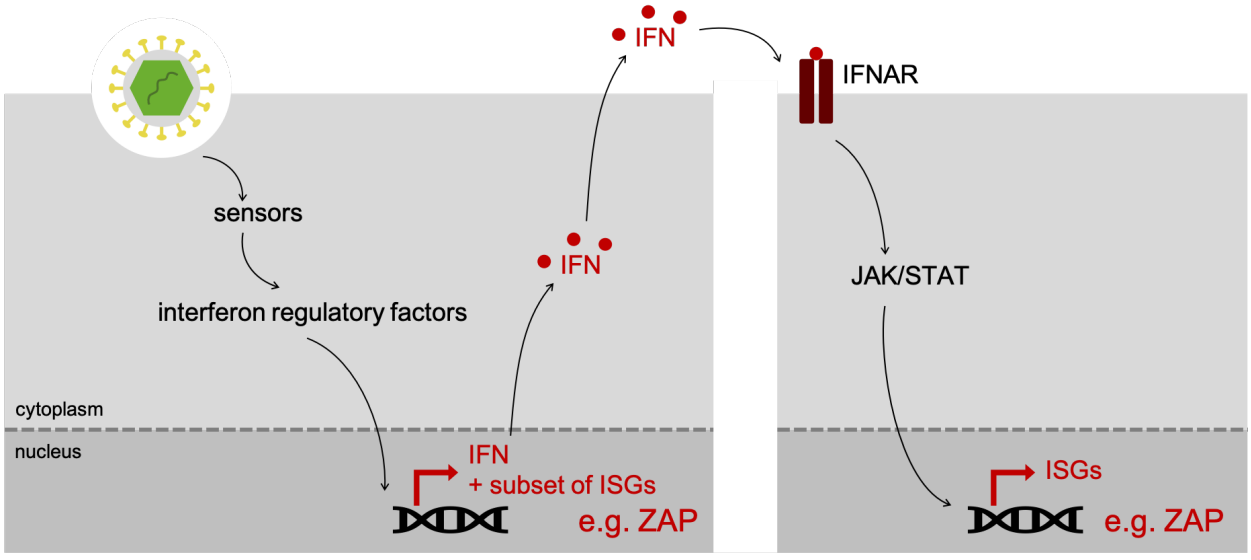

Figure 1.1 Virus infection activates the type I interferon (IFN) pathway.
When a virus enters the cell, its pathogen-associated molecular patterns are recognized by host surface, cytoplasmic, and endosomal sensors. The activate interferon regulatory factors, which translocate to the nucleus and upregulate IFNs and IFN-stimulated genes.

PRRs and transcription factors that amplify the immune response, while other ISGs prevent the activation of JAK/STAT signaling and dampen the immune response (Schneider et al., 2014). Lastly, there are ISGs with antiviral function that target different steps in the viral life cycle (Schoggins, 2019; E. Yang & Li, 2020). The type I IFN is finely orchestrated to achieve an optimal antiviral state while mitigating the risk of chronic or hyperinflammation.

**ZAP**

Zinc finger antiviral protein (ZAP) is one ISG that potently inhibits a diverse group of viruses such as Japanese encephalitis virus (Chiu et al., 2018), severe acute respiratory syndrome-related coronavirus 2 (Zimmer et al., 2021), influenza A virus (Liu et al., 2015), retroviruses (G. Gao et al., 2002), and various species in the *Alphavirus* genus (Bick et al., 2003). On the other hand, it is unable to inhibit viruses such as poliovirus, herpes simplex virus type 1 (Bick et al., 2003), and Zika virus (Chiu et al., 2018). This broad yet specific efficacy suggests that there may be distinct mechanisms underlying ZAP's antiviral activity based on the virus. For its antiviral activity against alphaviruses, ZAP requires the cofactor tripartite motif containing 25 (TRIM25), a host E3 ubiquitin ligase (Li et al., 2017).

ZAP, also known as poly(ADP-ribose) polymerase (PARP) 13, is one of 17 members in the PARP family. Canonical PARP enzymes use nicotinamide adenine dinucleotide to catalyze the addition of ADP-ribose on target substrates in a monomeric, polymeric, and/or branched manner (Fig 1.2) (Malgras et al., 2021; Suskiewicz et al., 2023). The consequences of ADP-ribosylation on a substrate have not been thoroughly explored and likely depend on the

writer, length, and targets of the poly(ADP-ribose) (PAR) (Lüscher et al., 2018). Both proteins and nucleic acids can be ADP-ribosylated (Groslambert et al., 2021; Lüscher et al., 2018). PARP1 PARylates itself and chromatin-associated proteins to enlist repair complexes to DNA breaks. PAR chains on the protein axin are recognized by the E3 ubiquitin ligase RNF146 to facilitate ubiquitination-dependent degradation (Groslambert et al., 2021), illustrating crosstalk between two post-translational modification pathways. PAR chains can also promote liquid-liquid phase separation, which is essential to the formation of antiviral stress granules (Shang et al., 2024). ADP-ribosylation on the 5' end of RNA could serve as a cap to protect the RNA from nuclease or act as a translation signal (Groslambert et al., 2021). Importantly, PARP9 can only mono-ADP-ribosylate when in complex with the E3 ubiquitin ligase DTX3L, and ZAP is the sole PARP that has no ADP-ribosylating activity.

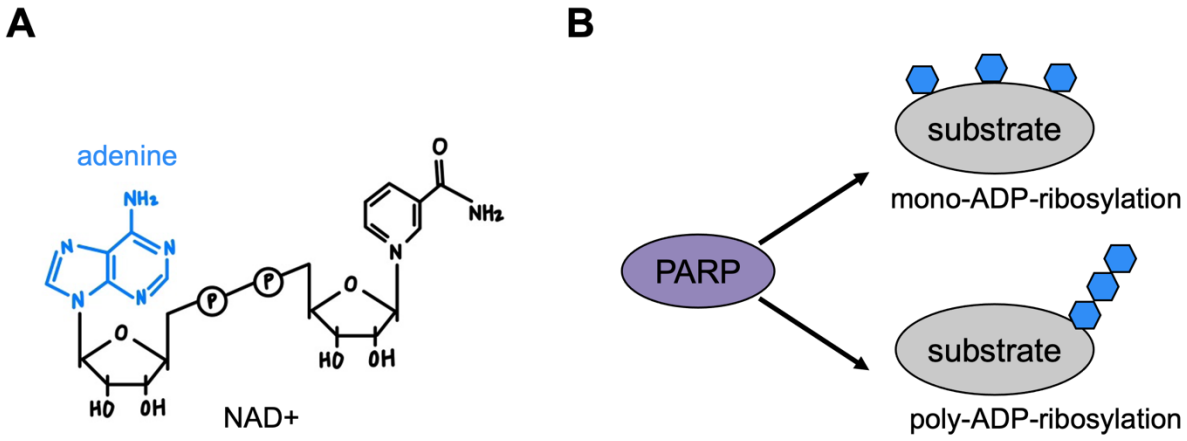


Figure 1.2 Poly(ADP-ribose) polymerases (PARPs) catalyze the attachment of ADP-ribose onto substrates. (A) The chemical structure of nicotinamide adenine dinucleotide (NAD+), which is used to catalyze ADP-ribosylation. Encircled P indicates phosphate groups. (B) Two types of ADP-ribosylation linkages onto substrates.

ZAP has four zinc fingers at the N terminus which mediate its binding to RNA rich in CG- or UA-dinucleotides (X. Guo et al., 2004; Takata et al., 2017; Odon et al., 2022). ZAP's central domain consists of a fifth zinc finger and two WWE domains, the second of which

binds to PAR. The RNA binding and central domains are shared by all four ZAP alternatively spliced isoforms: ZAPS (short), ZAPM (medium), ZAPL (long), and ZAPXL (extralong) (Li et al., 2019). ZAPM has comparable anti-alphavirus activity to ZAPS, and ZAPXL has comparable anti-alphavirus activity to ZAPL. The two longer ZAP isoforms have a unique C-terminal PARP-like domain whose altered triad motif renders its PARP activity inactive. When the triad is mutated to that of an active PARP, ZAP substantially loses its antiviral activity (Gläsker et al., 2014). The PARP-like domain also localizes ZAPL to endolysosomes as opposed to the cytoplasm, where the shorter isoform ZAPS resides (Charron et al., 2013; Kmiec et al., 2021). Even though the activities of the individual domains have been revealed, how they function together in ZAP's antiviral activity is not completely elucidated.

**Significance and dissertation overview**

The picture of how ZAP inhibits alphaviruses is not yet complete. Even though ZAP interacts with viral RNA, PAR, and TRIM25, it is unclear how all of these activities contribute to ZAP's ability to block alphaviral RNA translation. In the following chapters, my work attempts to uncover these answers by looking at the positively selected sites in ZAP throughout evolution (Chapter 2) and following up on a TRIM25 substrate that may be involved in ZAP-mediated anti-alphaviral activity (Chapter 3).

# Chapter 2: Positive selection analyses identify a single WWE domain residue that shapes ZAP into a more potent restriction factor against alphaviruses

**Abstract**

The host interferon pathway upregulates intrinsic restriction factors in response to viral infection. Many of them block a diverse range of viruses, suggesting that their antiviral functions might have been shaped by multiple viral families during evolution. Host-virus conflicts have led to the rapid adaptation of host and viral proteins at their interaction hotspots. Hence, we can use evolutionary genetic analyses to elucidate antiviral mechanisms and domain functions of restriction factors. Zinc finger antiviral protein (ZAP) is a restriction factor against RNA viruses such as alphaviruses, in addition to other RNA, retro-, and DNA viruses, yet its precise antiviral mechanism is not fully characterized. Previously, an analysis of 13 primate ZAP orthologs identified three positively selected residues in the poly(ADP-ribose) polymerase-like domain. However, selective pressure from ancient alphaviruses and others likely drove ZAP adaptation in a wider representation of mammals. We performed positive selection analyses in 261 mammalian ZAP using more robust methods with complementary strengths and identified seven positively selected sites in all domains of the protein. We generated ZAP inducible cell lines in which the positively selected residues of ZAP are mutated and tested their effects on alphavirus replication and known ZAP activities. Interestingly, the mutant in the second WWE domain of ZAP (N658A) is dramatically better than wild-type ZAP at blocking replication of Sindbis virus and other ZAP-sensitive

alphaviruses due to enhanced viral translation inhibition. The N658A mutant is adjacent to the previously reported poly(ADP-ribose) (PAR) binding pocket, but surprisingly has reduced binding to PAR. In summary, the second WWE domain is critical for engineering a more potent ZAP and fluctuations in PAR binding modulate ZAP antiviral activity. Our study has the potential to unravel the role of ADP-ribosylation in the host innate immune defense and viral evolutionary strategies that antagonize this post-translational modification.

## Introduction

Host and viral proteins are constantly engaging in genetic conflicts that create selective pressures on the other side to evolve. In a host immune protein, an advantageous mutation that successfully maintains recognition of a viral protein or evades a viral antagonist will rise in frequency, a phenomenon called positive selection. The amino acid sites on which positive selection has acted can be identified by bioinformatic approaches when the non-synonymous substitution rate is estimated to exceed the synonymous substitution rate (Goldman & Yang, 1994; Nielsen, 2005). The signatures of positive selection on a protein can inform us about historical interaction hotspots between the host and virus (Daugherty & Malik, 2012), as well as highlight sites that have important antiviral roles in winning the host-virus arms race.

Signatures of positive selection are especially prevalent in host interferon (IFN)-stimulated genes (ISGs) that are induced to counteract viral infections (Daugherty & Malik, 2012). One of these ISGs is zinc finger antiviral protein (ZAP), also known as poly(ADP-ribose) polymerase 13 (PARP13) (Fehr et al., 2020). ZAP inhibits a diverse range of virus genera, yet its antiviral activity can be specific to particular members in a genus, suggesting viral evasion or antagonism of ZAP inhibition (Ficarelli et al., 2021; E. Yang & Li, 2020). For

example, ZAP blocks many species of mosquito-borne alphaviruses to varying degrees, where Sindbis virus (SINV) and Ross River virus (RRV) are more sensitive than o'nyong'nyong virus (ONNV) and chikungunya virus (CHIKV) vaccine strain 181/clone 25 (Li et al., 2019; L. P. Nguyen et al., 2023). Alphaviruses have a positive-sense RNA genome, which can be immediately translated into viral proteins by host ribosomes upon entry into the host cell (Ahola et al., 2021; Holmes et al., 2020). The viral proteins then replicate the viral genome, leading to the production of structural proteins and the assembly of mature virus particles. It is in the early stages of infection that ZAP acts to prevent the translation of alphaviral RNA by synergizing with the host E3 ubiquitin ligase, tripartite motif containing 25 (TRIM25) (Li et al., 2017; Zheng et al., 2017).

ZAP has two major splice isoforms, ZAPS (short) and ZAPL (long), with distinct antiviral and immunomodulatory activities (Kerns et al., 2008; Li et al., 2019; Schwerk et al., 2019; Todorova et al., 2014). Recently discovered isoforms ZAPM (medium) and ZAPXL (extralong) resemble the antiviral activities of ZAPS and ZAPL, respectively (Li et al., 2019). The N-terminus of ZAP contains four zinc fingers (ZnFs) that bind RNA. It is followed by a central region that consists of a fifth ZnF and two WWE domains, named for the WWE motif containing tryptophan, tryptophan, and glutamic acid. The ADP-ribose-binding ability of the second WWE domain (WWE2) has only been recently discovered (Kuttiyatveetil et al., 2022; Xue et al., 2022). At the C-terminus, ZAPL has a PARP-like domain that is catalytically inactive and cannot ADP-ribosylate substrates (Karlberg et al., 2015; Kleine et al., 2008), but confers more antiviral activity on the longer isoforms (Gläsker et al., 2014; Kerns et al., 2008; Kmiec et al., 2021; Li et al., 2019). Even though the RNA binding activity of ZAP has been extensively

studied, the manner in which the other domains contribute to ZAP's antiviral activity is not well characterized.

While ZAP has been shown to be positively selected (Daugherty et al., 2014; Kerns et al., 2008), there are outstanding questions about the antiviral mechanism of ZAP and how its cellular functions contribute to viral inhibition. A previous study performed positive selection analysis on ZAP sequences from 13 primate species and found three positively selected sites, all in the PARP-like domain. However, limiting positive selection analyses to primate ZAP sequences only identifies sites that have been selected for rapid adaptation throughout primate evolution. While primates are thought to be the natural hosts of HIV and simian immunodeficiency viruses (F. Gao et al., 1999), ZAP has broad-spectrum antiviral activity against diverse viruses which infect a wider range of mammals (e.g. alphaviruses, flaviviruses, coronaviruses to name a few). Thus, we inferred that other mammalian ZAP orthologs must have also faced selective pressure from this host-virus arms race. By restricting positive selection analyses to only primate ZAP, one might miss positive selection signals contributed by non-primate species. ZAP has a long-standing history of host-virus interactions and likely arose from a gene duplication event after the divergence of tetrapods (Gonçalves-Carneiro et al., 2021). Assuming that at least some of the positively selected sites are driven by the ancestors of extant ZAP-sensitive viruses, we would expect to detect positive selection signals from a broader range of mammals which these viruses tend to infect.

Here, we performed positive selection analyses on 261 mammalian ZAP sequences using four complementary and sophisticated models that make more realistic assumptions about the substitution rates. We identified seven residues that are positively selected in ZAP,

most of which are outside the PARP-like domain. We mutated each positively selected site and found that one mutant in the WWE2 (N658A) has antiviral activity that is almost 10 times stronger than wild-type (WT) ZAP against SINV, creating a restrictor that is more antiviral than any versions of ZAP that were previously reported. The N658A mutant is more efficient than ZAPL WT at inhibiting virion production of SINV and replication of a panel of alphaviruses in a manner that is dependent on viral translation suppression. Interestingly, mutation of both positively selected sites in the WWE2 that form a potential interaction surface does not further increase the antiviral activity of ZAP.

We then investigated the role of viral RNA binding, TRIM25 interaction, IFN response, and poly(ADP-ribose) (PAR) binding in mediating the activity of a more potent restrictor ZAP. We found that the superior antiviral activity of the N658A mutant is correlated with changes in PAR binding by the ZAPL mutant. We mutated site 658 to orthologous residues found in other mammalian species and observed that none of them is as antiviral as the N658A mutant. This surprising finding suggests that evolutionary forces did not steer human ZAP to be the most antiviral, at least not against alphaviruses. By taking into account the history of host-virus conflicts, positive selection analyses allow us to identify specific sites with high impact on the effectiveness of the host antiviral program, providing a blueprint for generating stronger restriction factors.

## Results

### ZAP is positively selected throughout mammalian evolution at novel sites

We used the longest isoform of ZAP, ZAPXL, to curate and align 261 high quality mammalian orthologs. We ran four positive selection tests with complementary strengths on

the alignment of mammalian ZAP sequences: Fixed Effects Likelihood (FEL); Mixed Effects Model of Evolution (MEME); Fast, Unconstrained Bayesian AppRoximation (FUBAR); and the Bayesian mutation-selection model by Rodrigue *et al* (Kosakovsky Pond & Frost, 2005b; Murrell et al., 2012, 2013; Rodrigue et al., 2021). FEL does not make assumptions about the distribution of selection parameters over sites but assigns independent non-synonymous and synonymous rates to each site. MEME accounts for the fact that positive selection occurs episodically, rather than remaining constant over time. FUBAR improves upon random effect likelihood models (Kosakovsky Pond et al., 2011) by implementing more parametrically complex models. Rodrigue *et al.*'s method is the first Bayesian mutation-selection model, offering higher sensitivity.

To validate the robustness of our tests, we ran the 13 primate ZAP sequences from the study by Kerns *et al.* (Kerns et al., 2008) and were able to replicate the three positively selected sites previously identified. Using the 261 mammalian ZAP, we identified seven positively selected sites that are shared by all four tests (Supp Fig 2.1A) and mapped them to human ZAP isoforms (Supp Fig 2.1B). For consistency, the positively selected sites are numbered in the context of ZAPS and ZAPL, which are the better studied isoforms with antiviral activities similar to ZAPM and ZAPXL, respectively. The positively selected sites we identified are concentrated in specific regions spanning across the ZAP gene (Fig 2.1A). Two of these sites are within the first 254 amino acids of the protein, which comprise the RNA binding domain that is necessary for ZAP recognition and inhibition of viral RNA. These residues, Q28 and C38, are relatively close to each other but are positioned opposite the RNA binding groove, with both of their side chains pointing away from the rest of the structure (Meagher et al.,

2019) (Fig 2.1B). RNA binding is essential to ZAP's antiviral activity against murine leukemia virus (Chen et al., 2012), CpG-enriched HIV-1 (Meagher et al., 2019), and SINV (Luo et al., 2020; E. Yang, Nguyen, et al., 2022). However, the identification of these two sites raises the possibility that viral proteins can interact with ZAP at a different location in its N-terminal region without interfering with binding to viral RNA.

More than half of the positively selected sites are in the central domain, three of which are tightly clustered in the WWE2, which has only recently been found in ZAP to bind PAR. When mapped to the available crystal structure of the central region consisting of the fifth zinc finger and the two WWE domains (Kuttiyatveetil et al., 2022; Xue et al., 2022), two of the sites, N658 and A672, are next to the PAR binding pocket and face outward, suggesting

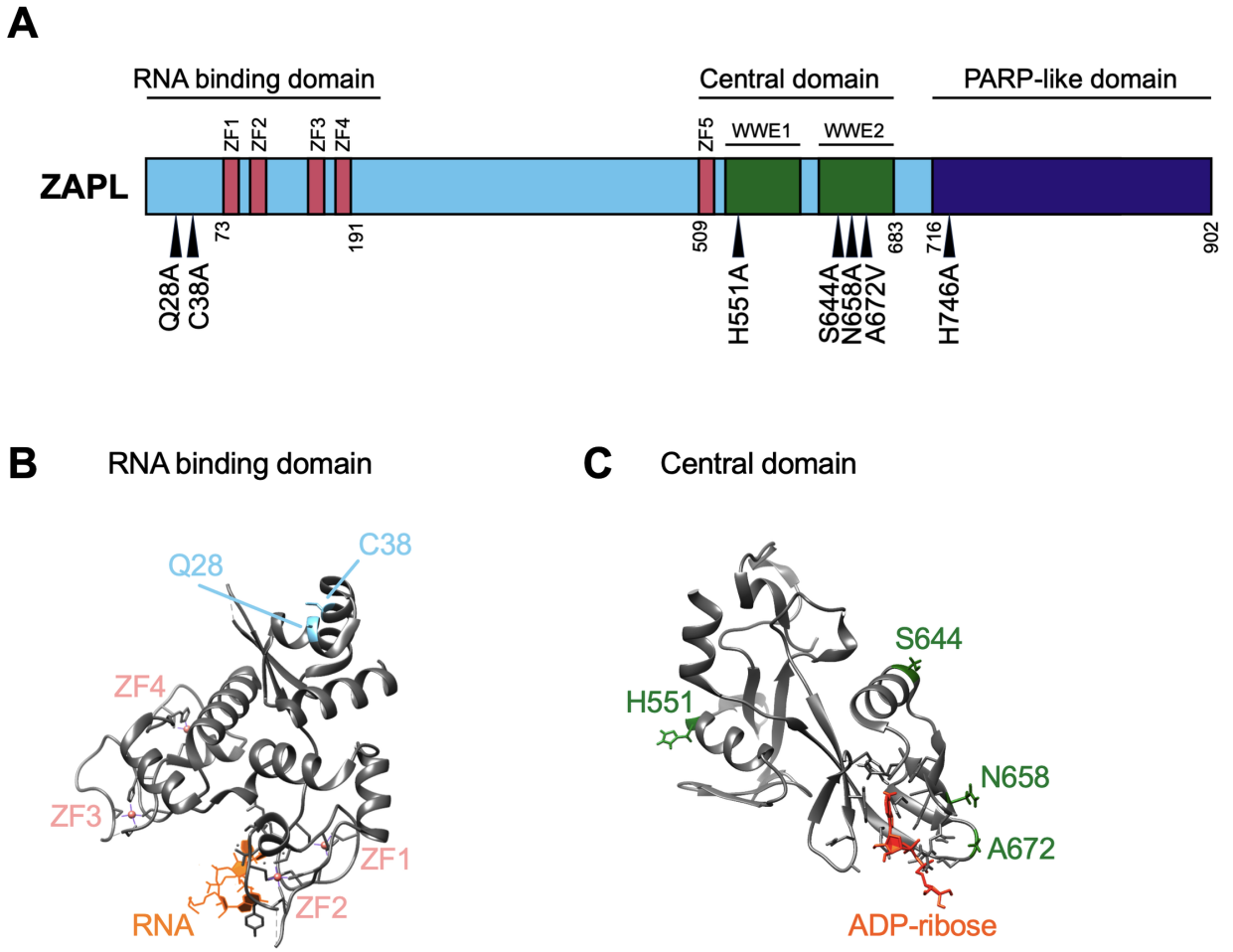

Figure 2.1 Identification of seven positively selected sites across ZAP protein.
(A) A schematic of the ZAPL isoform annotated with its domains. Triangles indicate positively selected sites identified from the overlap of four methods: Fixed Effects Likelihood; Mixed Effects Model of Evolution; Fast, Unconstrained Bayesian AppRoximation; and the Bayesian mutation-selection model by Rodrigue et al. (B) ZAP RNA binding domain bound to RNA. The structure (PDB: 6UEJ) was visualized with UCSF Chimera. Positively selected Q28 and C38 residues shown in blue; RNA in orange; zinc fingers in salmon. (C) ZAP central domain bound to ADP-ribose. The structure (PDB: 7TGQ) was visualized with UCSF Chimera. Positively selected sites H551, S644, N658, and A672 shown in green; ADP-ribose in dark orange.

that there is space to be accessed by viral proteins (Fig 2.1C). Taken together, our positive selection analyses demonstrate that ZAP has been rapidly evolving not just during primate evolution, but also during mammalian evolution. These novel positively selected residues in ZAP are found in all domains of ZAP, suggesting that ancient viruses have likely targeted and antagonized ZAP at distinct sites.

**One of the positively selected site mutants we generated affects ZAP antiviral phenotype against SINV**

To probe the effect of the positively selected sites, we mutated each site from the WT amino acid in humans to alanine because alanine is chemically inert and would not dramatically change the secondary structure of the protein (Cunningham & Wells, 1989). In the case where the WT amino acid is alanine, we mutated it to valine, the next closest amino acid. We cloned either WT or mutant ZAPS and ZAPL with an N-terminal 3XFLAG tag into the ePiggyBac (ePB) transposon system and generated stable cell lines in ZAP knockout (KO) HEK293T cells (Supp Fig 2.2) (Hayakawa et al., 2011; Lacoste et al., 2009). We tested the mutants in the ZAPS and ZAPL background because ZAPS and ZAPL are most commonly studied and have comparable antiviral activities to ZAPM and ZAPXL, respectively.

Almost all the mutant cell lines have robust ZAP expression when induced by doxycycline (dox) (Fig 2.2A and 2.2D), with the exception of ZAPS Q28A which appears to

have a truncation at the C-terminus, as it is still able to be detected by the N-terminal FLAG tag (Fig 2.2A). Since our candidate sites are positively selected throughout mammalian evolution, we chose to test their antiviral activity against alphaviruses, whose primary hosts are mammals such as primates, horses, and rodents (Griffin & Weaver, 2021). We first infected the ZAP cell lines with SINV, a prototype alphavirus that is susceptible to ZAP inhibition.

We infected ZAPS and ZAPL WT and mutant cell lines with a luciferase-expressing SINV reporter virus. To quantify the antiviral activity, we divided the averaged -dox values by the individual triplicate +dox values in each cell line to get three fold inhibition values. Despite differences in absolute fold inhibitions between independent experiments featuring ZAPS and ZAPL mutants, we found that ZAPL WT is invariably more antiviral than ZAPS WT, consistent with previous reports (Kerns et al., 2008; Li et al., 2019). While a couple of mutants have lower fold inhibition than WT ZAP, others have higher fold inhibition (Fig 2.2B and 2.2E), though they are not statistically significant. Notably, the N658A mutant located in the WWE2 shows a statistically significant improvement in ZAP antiviral activity than the WT (Fig 2.2C and 2.2F, three times better than ZAPS WT and eight times better than ZAPL WT). In addition, some mutants displayed isoform-specific effects. For instance, ZAPL C38A has higher fold inhibition than ZAPL WT, but its ZAPS counterpart is similarly antiviral to ZAPS WT. Densitometric quantification of the amount of ZAP in each cell line seems to have no correlation with anti-SINV activity (Supp Fig 2.3). These results suggest that altering the naturally occurring amino acid at a positively selected site *a posteriori* changes the antiviral activity of ZAP against SINV and that adaptations at a site can have important functional consequences.

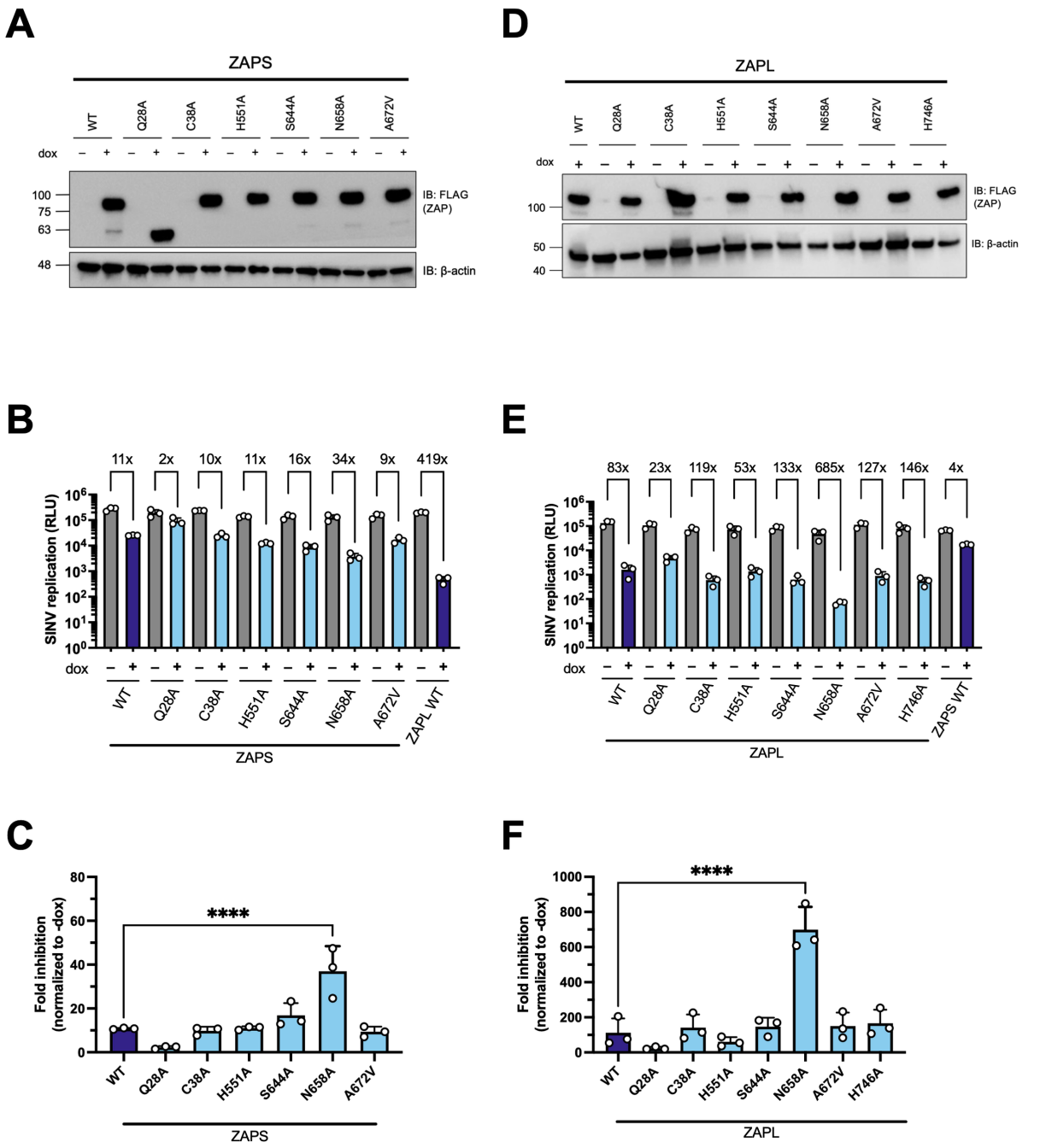


Figure 2.2 Each positively selected site in ZAP was mutated and its antiviral activity against Sindbis virus (SINV) was tested.

(A, D) Western blot of (A) ZAPS or (D) ZAPL wild-type (WT) or positive selection mutants inducible ZAP knockout (KO) HEK293T whole cell lysates (WCL). (B, E) (B) ZAPS or (E) ZAPL WT or mutant ZAP KO HEK293T cells were induced for ZAP expression for 24 hours before infection with SINV Toto1101/Luc at a multiplicity of infection (MOI) of 0.01 plaque forming units (PFU)/cell and harvested at 24 hours post-infection (h.p.i.) for luciferase assay by measuring relative luciferase units (RLU). Data are representative of two independent experiments. 1μg/mL doxycycline (dox) is used to induce ZAP expression. (C, F) Fold inhibition values of each ZAPS (C) and ZAPL (F) cell line are calculated by dividing the averaged -dox RLU by the individual +dox RLU. The averaged fold inhibition for each cell line is shown on top of the bars in (B) and (E). Error bars indicate standard deviation. Asterisks indicate statistically significant differences as compared to the corresponding WT cell line (one-way ANOVA and Bartlett's test: ****, $p<0.0001$).

Since both sites 658 and 672 are located in the WWE2 and flank the PAR binding pocket in the crystal structure (Fig 2.1A and 2.1C), we wondered if site 672 can bolster the superior antiviral effect of site 658, as in the case with TRIM5α (Sawyer et al., 2005). We generated the double mutant N658A/A672V (NA) in the same ZAP KO ePB system and assessed its ability to restrict SINV replication. Both ZAPS and ZAPL NA double mutants are as stably expressed as the single mutants (Fig 2.3A and 2.3D). To our surprise, the antiviral activity of the ZAPS NA double mutant is not an intermediate between ZAPS N658A and A672V; rather, it diminishes the antiviral activity of N658A to that of ZAPS WT and A672V (Fig 2.3B and 2.3C), suggesting that A672V may have a dominant negative effect on N658A in ZAPS. The ZAPL NA double mutant likewise does not approach the strength of ZAPL N658A (Fig 2.3E and 2.3F). The differential antiviral activity of the A672V single mutant and the NA double mutant in ZAPS and ZAPL again highlights isoform specificity at particular sites. Together, the WWE2 mutations in combination lessen the increase in antiviral activity we observed with the single N658A mutation in both ZAPS and ZAPL backgrounds, suggesting that these mutations may not act as a single protein interaction surface.

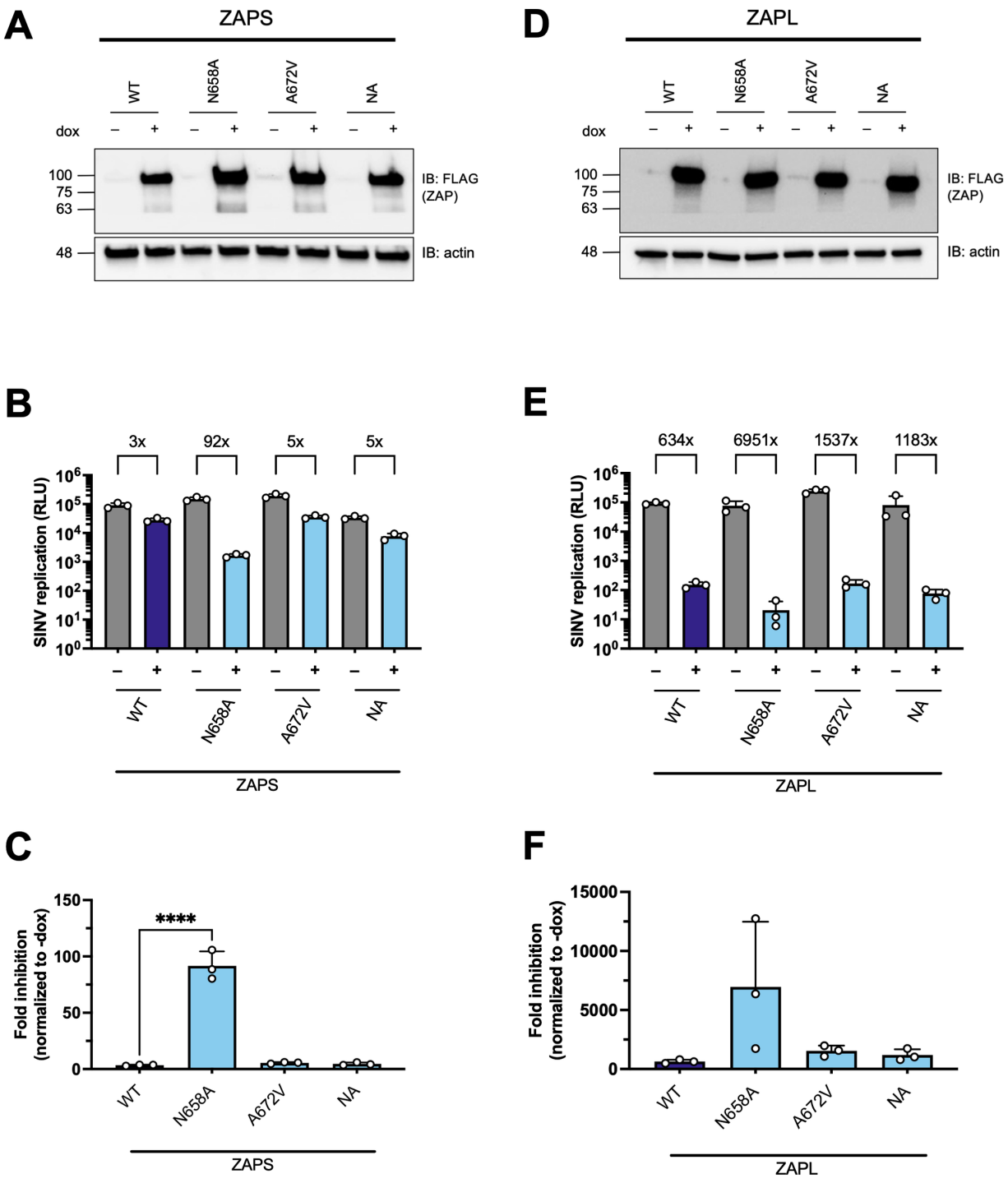
A
ZAPS
WT
N658A
A672V
NA
dox
100
75
63
48
IB: FLAG (ZAP)
IB: actin
D
ZAPL
B
3x
92x
5x
5x
SINV replication (RLU)
E
634x
6951x
1537x
1183x
C
Fold inhibition (normalized to -dox)
****
F

Figure 2.3 Mutating both positively selected sites in the second WWE domain of ZAP does not further enhance antiviral activity.
(A, D) Western blot of (A) ZAPS or (D) ZAPL WT, N658A, A672V, or N658A/A672V (NA) double mutant inducible ZAP KO HEK293T cell lysates. (B, E) (B) ZAPS or (E) ZAPL WT or mutant ZAP KO HEK293T cells were induced for ZAP expression for 24 hours before infection with SINV Toto1101/Luc at an MOI of 0.01 PFU/cell and harvested at 24 h.p.i for luciferase assay. Data are representative of three (B) and three out of four (E) independent experiments. 1μg/mL dox is used to induce ZAP expression. (C, F) Fold inhibition values of each ZAPS (C) and ZAPL (F) cell line are calculated by dividing the averaged -dox RLU by the individual +dox RLU. The averaged fold inhibition for each cell line is shown on top of the bars in (B) and (E). Error bars indicate standard deviation. Asterisks indicate statistically significant differences as compared to the corresponding WT cell line (one-way ANOVA and Dunnett's test: ****, $p<0.0001$).

**The ZAPL N658A mutant blocks the early steps of alphaviral infection more effectively**

We were interested by the superior antiviral activity of the N658A mutant alone and focused on the ZAPL isoform to study the mutant in the presence of all domains of ZAP, including the PARP-like domain. We wanted to determine whether the effects on viral replication impact the overall virion production. We infected ZAPL WT or N658A cells with SINV and collected the cell supernatant containing mature and released virions at 0, 6, 12, 24, and 36 hours post-infection (h.p.i.). We determined the viral titer on BHK-21 cells via plaque assay. We found that both ZAPL WT and N658A inhibited SINV virion production, but at 24 h.p.i., ZAPL N658A is about 4-fold more inhibitory (Fig 2.4A, 11x vs. 40x), consistent with the phenotype we observed with viral replication.

Next, we sought to determine the stage in the viral life cycle at which the ZAPL N658A mutant acts. Because ZAP is known to act by blocking alphaviral RNA translation, we tested the positively selected ZAP mutant N658A against a temperature-sensitive replication-deficient SINV luciferase reporter virus (Bick et al., 2003). The temperature-sensitive SINV luciferase reporter virus (ts6 mutant) has a single glycine to glutamine mutation in the viral RNA-dependent RNA polymerase (Hahn et al., 1989) and is therefore unable to replicate the viral genome at the non-permissive temperature (40ºC) at which infection was carried out. As

a result, only the incoming viral genomic RNA is translated. We infected ZAP WT and N658A cell lines with the replication-deficient virus at the non-permissive temperature and found that the N658A mutant is about two times better at blocking SINV RNA translation at 3 h.p.i. and 6 h.p.i. (Fig 2.4B and 2.4C), which is a difference that is statistically significant. Our finding supports that the superior antiviral activity of the N658A mutant is likely due to an enhanced block at the step of incoming viral RNA translation.

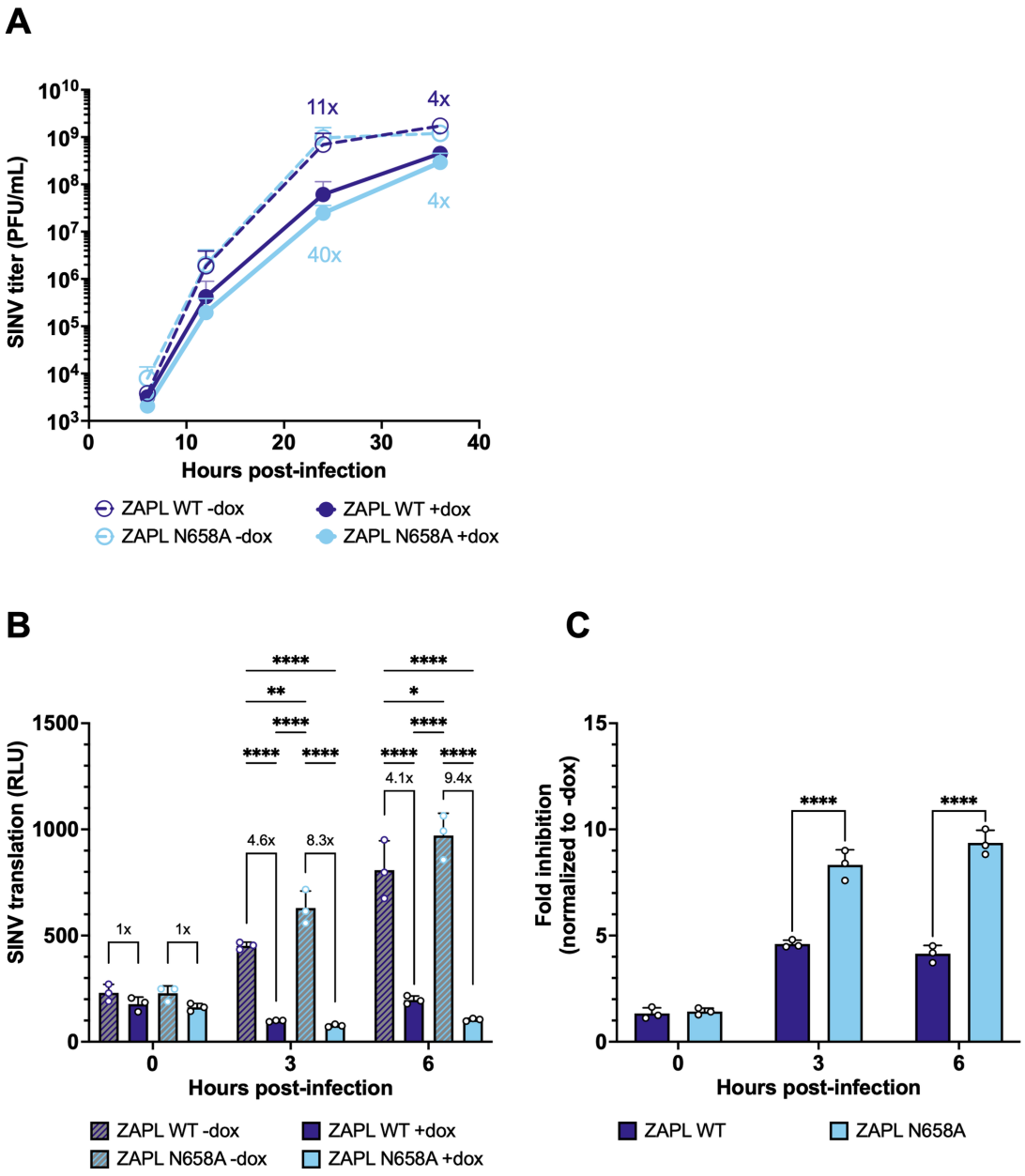

Figure 2.4 The N658A mutant is better at inhibiting virion production and SINV RNA translation.
ZAPL WT or N658A ZAP KO HEK293T cells were induced for ZAP expression with 1μg/mL dox 24 hours prior to infection. Cells were infected with (A) SINV Toto1101 at an MOI of 0.01 PFU/cell, harvesting supernatant at 6, 12, 24, and 36 h.p.i. for plaque assays. Viral titers of plaque assays are determined in BHK-21 cells. Data are combined from two independent experiments. Fold inhibition values of each cell line are calculated by dividing the averaged -dox titer by the individual +dox titer. The averaged fold inhibition for each cell line is shown on top of the bars. Error bars indicate standard deviation; or (B, C) SINV Toto1101/Luc:ts6 at an MOI of 10 PFU/cell, and harvested at 0, 3, and 6 h.p.i. for luciferase assay. Data are representative of two independent experiments. Fold inhibition values of each cell line are calculated by dividing the averaged -dox RLU by the individual +dox RLU. The averaged fold inhibition for each cell line is shown on top of the bars in (B). Error bars indicate standard deviation. Asterisks indicate statistically significant differences as compared to every other condition at each timepoint (B, two-way ANOVA and Tukey's multiple comparisons test: *, $p<0.05$; **, $p<0.01$; ***, $p<0.001$; ****, $p<0.0001$) or compared to the WT cell line (C, two-way ANOVA and Šídák's multiple comparisons test: ****, $p<0.0001$).

Since we hypothesized that the positive selection of ZAP may be driven by ancient alphavirus-like viruses, we tested whether the N658A mutant also inhibits other alphaviruses better. We infected the ZAPL WT or N658A cell line with GFP-expressing SINV, RRV, ONNV, CHIKV vaccine strain 181/clone 25, and Venezuelan equine encephalitis virus (VEEV). Alphaviruses known to be more sensitive to ZAP inhibition are more inhibited by the N658A mutant (Fig 2.5A, 7x vs. 58x against SINV; Fig 2.5B, 16x vs. 69x against RRV), while the ones that are less sensitive (Bick et al., 2003; Li et al., 2019) are similarly resistant to both ZAPL WT and N658A (Fig 2.5C, 4x vs. 9x against ONNV; Fig 2.5E, 1.1x vs. 1.0x against VEEV). Interestingly, even though we previously observed that the non-reporter CHIKV vaccine strain is less susceptible to ZAP inhibition (Li et al., 2019), we saw that both ZAPL WT and N658A dramatically inhibited GFP-expressing CHIKV vaccine strain, with the N658A mutant being more antiviral than WT (Fig 2.5D). Since the CHIKV strain we tested expresses the GFP reporter under the control of the viral subgenomic promoter, our results suggest that ZAP might inhibit step(s) at or prior to viral subgenomic mRNA expression. The smaller difference in virion production between WT and N658A ZAP might be partly due to the fact that by the time we assay for virion production, there are many steps in the virus life

cycle post-ZAP restriction for the virus to "catch up." On the other hand, luciferase- and GFP-expressing alphaviruses have allowed us to see the effect of ZAP at isolated, specific steps leading up to viral RNA replication, where ZAP exerts its strongest effect during viral RNA translation.

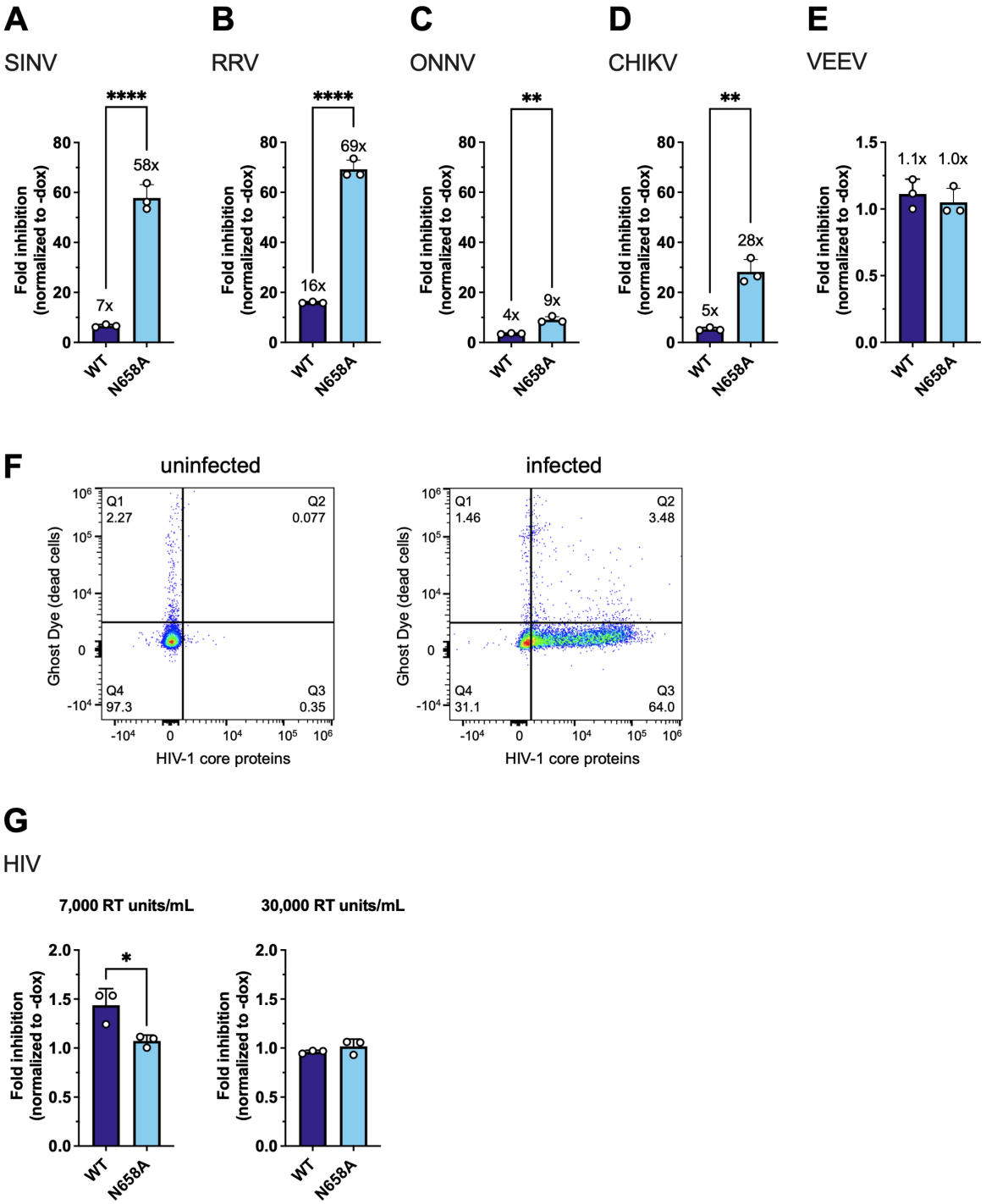

Figure 2.5 The ZAPL N658A mutant inhibits many other alphaviruses better than WT.
After 24 hours of 1μg/mL dox treatment, ZAPL WT or N658A ZAP KO HEK293T cells were infected with (A) GFP-expressing Sindbis virus (SINV, MOI = 0.01), (B) Ross River virus (RRV, MOI = 1), (C) o'nyong'nyong virus (ONNV, MOI = 1), (D) chikungunya virus (CHIKV, MOI = 0.1), or (E) Venezuelan equine encephalitis virus (VEEV, MOI = 0.1) PFU/cell for 24 hours before their percentage of infection was determined by flow cytometry. Data are representative of at least two independent experiments of biological replicates in triplicate wells. Fold inhibition values of each cell line are calculated by dividing the averaged -dox % GFP infection by the individual +dox % GFP. The averaged fold inhibition for each cell line is shown on top of the bars. Error bars indicate standard deviation. Asterisks indicate statistically significant differences as compared to the WT cell line (unpaired t-test: **, $p<0.01$; ****, $p<0.0001$). (F, G) Following 24 hours of 1μg/mL dox treatment, ZAPL WT or N658A ZAP KO HEK293T cells were spinfected by an HIV-1 isolate BRU ΔEnv pseudotyped with the vesicular stomatitis virus glycoprotein at 7,000 or 30,000 reverse transcriptase (RT) units/mL. 24 hours later, the cells were analyzed for the percentage of infection (HIV-1 core antigen) and viability (Ghost Dye) via flow cytometry. Flow cytometry plots of an uninfected (left) and infected (right) sample (F). The fold inhibition is calculated by normalizing the percentage of infection in the +dox samples to the averaged percentage of infection in the corresponding -dox samples (G). Data are representative of two independent experiments of biological replicates in triplicate wells. Error bars indicate standard deviation. Asterisks indicate statistically significant differences (Unpaired t-test: *, $p<0.05$).

As a broad-spectrum antiviral protein, it is very likely that ZAP has to balance its inhibitory activity against one virus at the expense of its inhibitory activity against other viruses. To test this evolutionary hypothesis, we infected our ZAPL WT and N658A mutant cell lines with HIV-1 Bru ΔEnv, a single-round infection virus that is deficient in the viral envelope gene and pseudotyped with the glycoprotein from vesicular stomatitis virus which infects broad cell types. We measured infection via flow cytometry and confirmed that more than 95% of the infected cells were viable (negative for the Ghost Dye stain), and gated for infected cells using an antibody against HIV-1 core proteins (Fig 2.5F). With a lower virus input of 7,000 reverse transcriptase (RT) units/mL, WT ZAP exhibits weak anti-HIV-1 activity (~1.5-fold inhibition) while the N658A mutant does not (~1-fold inhibition) (Fig 2.5G). Even though there is statistical significance between WT and N658A ZAP against HIV-1 at lower infection, the difference is minimal. With a higher virus input (30,000 RT units/mL), neither WT nor N658 ZAP inhibits HIV-1 replication. Taken together, these results show that the N658A mutant is not better than WT ZAP at inhibiting HIV-1.

**The improved antiviral activity of the N658A mutant is not due to changes in binding to SINV RNA, interaction with TRIM25, or increased activation of ISGs**

To determine the mechanism of the enhanced antiviral activity of the N658A mutant, we characterized the mutant in terms of known abilities of ZAP. Since ZAP is recognized as a sensor of CpG-rich viral RNA, we wondered if N658A binds better to SINV genomic RNA than ZAPL WT does. We performed an *in vitro* RNA pulldown assay by incubating protein lysates from either the ZAPL WT or N658A cell line with equal amounts of biotinylated SINV genomic RNA. We pulled down the biotinylated viral RNA using streptavidin beads and probed for ZAP. We generated and tested a ZAP KO HEK293T cell line with inducible expression of a ZAPS C86A/Y96A mutant (ZAPS CY), which is deficient in RNA binding (Luo et al., 2020; E. Yang, Nguyen, et al., 2022), as negative control. As expected, markedly less ZAPS CY is bound to equal amounts of SINV RNA compared to ZAPL WT (Fig 2.6A). Similar amounts of ZAPL WT and ZAPL N658A are bound to SINV RNA (Fig 2.6A). Averaged across three independent trials, a slightly higher amount of ZAPL N658A was bound to SINV RNA compared to ZAPL WT, but the difference was minimal (1.3x vs. 1x) and was not statistically significant (Fig 2.6B). Our results suggest that factors other than viral RNA binding may contribute to the enhanced antiviral activity of the mutant.

We then asked whether the N658A mutant changes ZAP's ability to interact with TRIM25, a host E3 ubiquitin ligase that is a requisite cofactor for ZAP's inhibition of SINV RNA translation (Li et al., 2017; Zheng et al., 2017). We transfected 3XFLAG-ZAPL and myc-TRIM25 into ZAP KO HEK293T cells and performed a co-immunoprecipitation assay with FLAG beads. We found that ZAPL WT and N658A interact with TRIM25 similarly (Fig

2.6C). When we quantified the amount of overall myc-TRIM25 in the cell from the representative experiment shown in Fig 2.6C, we confirmed that the ZAP that was co-transfected had a negligible effect on the overall myc-TRIM25 protein levels (1x when co-transfected with ZAPL WT vs. 1.08x when co-transfected with ZAPL N658A). The amount of myc-TRIM25 immunoprecipitated by FLAG-ZAP is also apparently equal (1x pulled down by ZAPL WT vs. 1.09x pulled down by ZAPL N658A) (Fig 2.6C). From all four independent experiments we have performed, we found no statistically significant differences in interaction with TRIM25 between ZAPL WT and ZAPL N658A (Fig 2.6D), suggesting that the increased antiviral activity of the N658A mutant is not related to changes to its synergy with TRIM25.

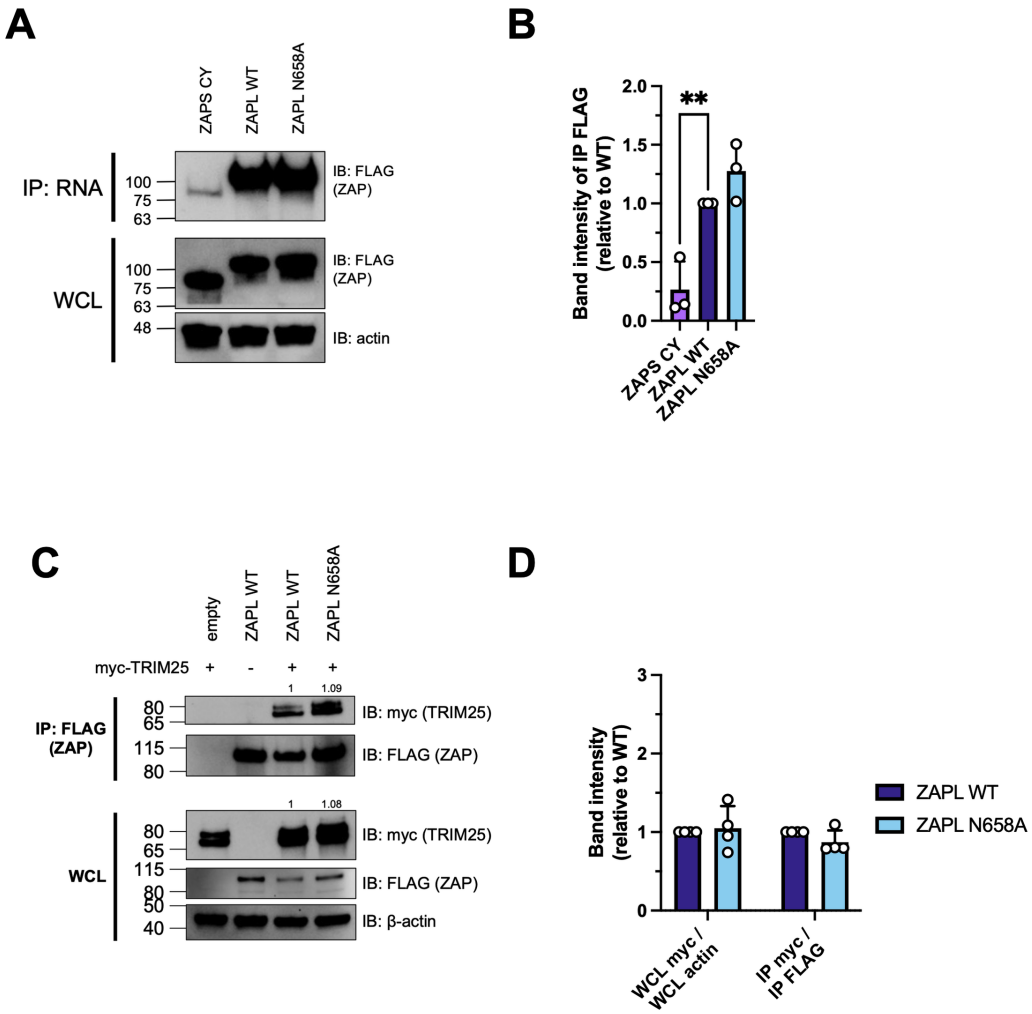

Figure 2.6 The improved antiviral activity of the N658A mutant is not due to changes in ZAP binding to SINV RNA or interaction with TRIM25.
(A) Western blot of ZAPL CY, WT, or N658A in ZAP inducible ZAP KO HEK293T cell lysates bound to biotinylated SINV genomic RNA immunoprecipitated by streptavidin beads. Data are representative of three independent experiments. (B) Densitometric analysis of the amount of FLAG-ZAP immunoprecipitated by equal amounts of SINV RNA as quantified by Image Lab, normalized to WT, and combined from three independent experiments. Error bars indicate standard deviation. Asterisks indicate statistically significant differences as compared to the WT cell line (one-way ANOVA: **, $p<0.01$). (C) Western blot of TRIM25 bound to ZAP in cell lysates of ZAP KO HEK293T transfected with pcDNA3.1-3XFLAG-ZAPL and pcDNA3.1-myc-TRIM25. Lysates were immunoprecipitated by FLAG beads. Data are representative of four independent experiments. (D) Densitometric analysis of the amount of WCL myc-TRIM25 normalized to β-actin, and of the amount of myc-TRIM25 pulldown normalized to FLAG-ZAP pulldown as quantified by Image Lab, normalized to WT, and combined from four independent experiments. Error bars indicate standard deviation. Asterisks indicate statistically significant differences as compared to the WT cell line (two-way ANOVA and Dunnett's multiple comparisons test).

We further evaluated whether increased IFN induction is responsible for the enhanced antiviral activity of the ZAPL N658A mutant. After treating ZAPL WT and N658A cell lines with poly(I:C), a double-stranded RNA mimic, to stimulate the IFN response, we performed quantitative polymerase chain reaction (qPCR) analysis of the mRNA levels of IFN-β, IFIT1, and IFIT2, the latter two of which are classical antiviral ISGs. We found that poly(I:C) treatment upregulates IFN-β, IFIT1, and IFIT2 RNA levels, and expression of ZAPL WT and N658A further augments the response (Supp Fig 2.4). Importantly, both IFN-β and IFIT1 induction between ZAPL WT and N658A cell lines is similar upon stimulation (Supp Fig 2.4A and Supp Fig 2.4B). WT ZAP induces IFIT2 slightly more than N658A ZAP (728x vs. 401x, Supp Fig 2.4C), but this is in the opposite direction from the superior antiviral activity, as IFIT2 is an antiviral ISG and a higher amount should evoke a more antiviral state. We next asked whether the non-ISG, ZAP-regulated cellular transcript TRAILR4 has distinct RNA levels in ZAPL WT and N658A mutant cell lines. A previous study has shown that siRNA knockdown of ZAP increases TRAILR4 mRNA by about 2.5-fold, and rescue of ZAPL expression by transfection marginally decreases TRAILR4 RNA (Todorova et al., 2014). We found that inducing ZAP with doxycycline in the absence of poly(I:C) treatment reduced

TRAILR4 transcript levels, although the difference is minimal between WT ZAP and N658A (0.9x vs. 0.4x). However, with poly(I:C) treatment to simulate an infected state, TRAILR4 RNA levels are further decreased when ZAPL N658A is expressed (Supp Fig 2.4D, 1.2x for WT vs. 0.4x for N658A). Taken together, our results rule out a heightened IFN response as responsible for the improved antiviral phenotype of N658A.

**The ZAPL N658A mutant has reduced binding to PAR**

Since RNA binding, TRIM25 interaction, and the IFN response do not appear to mediate the superior antiviral activity of ZAPL N658A, we decided to characterize the effect the mutation has on WWE domain function. The WWE2 in ZAP has recently been found to bind to PAR, an ability that enhances ZAP's antiviral function against a CpG-enriched HIV-1 (Xue et al., 2022). We wondered if mutating site 658, which is within the WWE2, changes ZAP's ability to bind to PAR. We performed a co-immunoprecipitation assay in which we pulled down ZAP and probed for PAR. PAR levels in the whole cell lysate are markedly lower in cells without ZAP induced (Fig 2.7A). Compared to ZAPL WT, ZAPL N658A binds to less PAR (Fig 2.7A). Even though we have seen fluctuating overall PAR levels among independent experiments, the N658A mutant has consistently pulled down less PAR, as demonstrated by our densitometric quantification across three independent experiments (Fig 2.7B). Altogether, these data suggest that the antiviral activity of this mutant negatively corresponds to ZAPL's ability to bind PAR, despite the site being outside of the PAR binding groove. The mutation might prevent an active PARP from accessing and PARylating ZAPL in an uninfected cell. Contrary to the Q668R mutation in the PAR binding pocket which

diminishes ZAP PAR binding and anti-HIV activity (Xue et al., 2022), our N658A mutant is less proficient in binding PAR, but surprisingly more adept at restricting SINV.

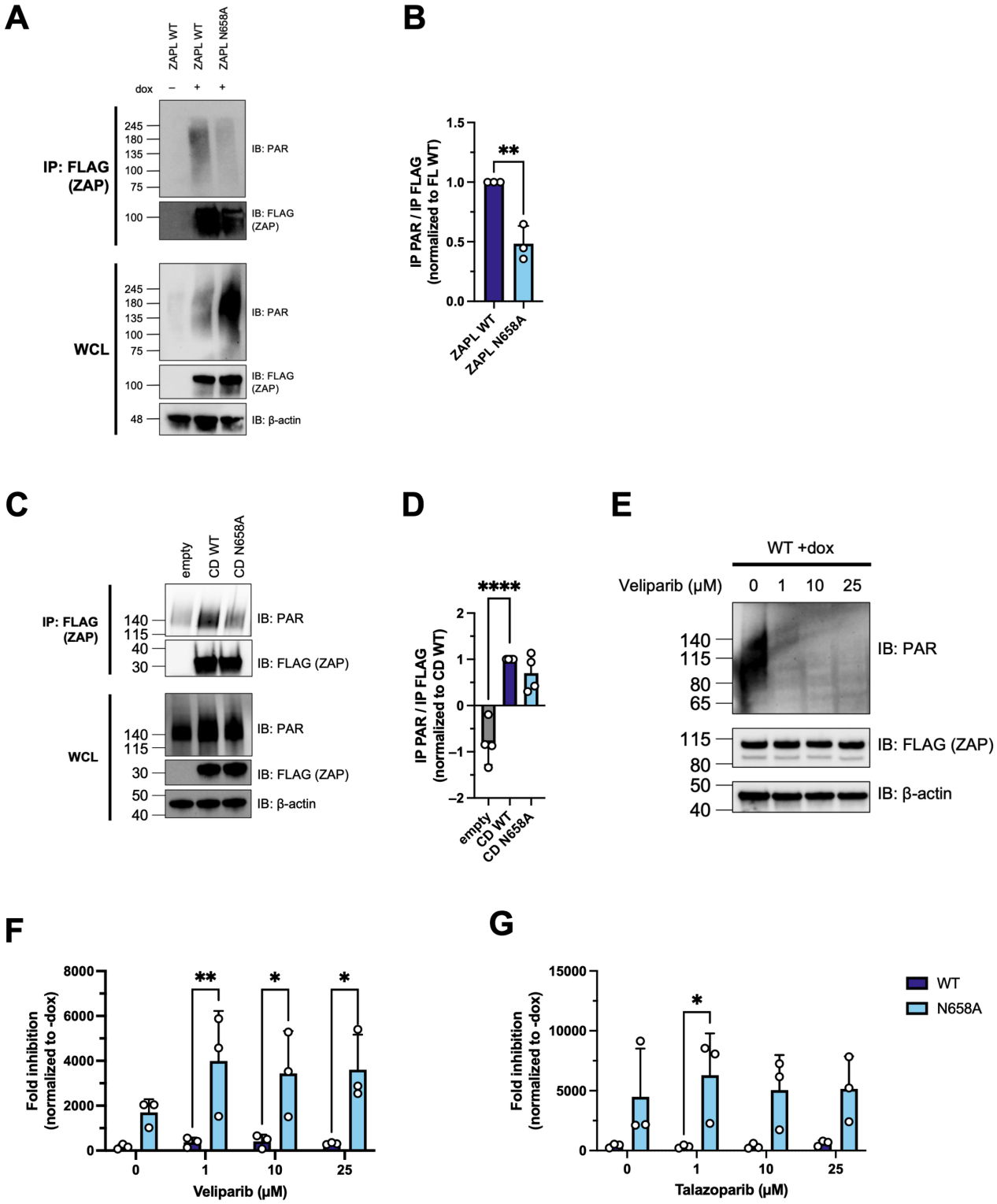

Figure 2.7 The N658A mutant is correlated with decreased binding to poly(ADP-ribose) (PAR).
(A) Western blot of ZAPL WT or N658A in ZAP inducible ZAP KO HEK293T cell lysates immunoprecipitated by FLAG beads after treatment with 1μM PARG inhibitor. Data are representative of three independent experiments. (B) Densitometric analysis of the ratio of PAR pulldown normalized to FLAG-ZAP pulldown as quantified by Image Lab, normalized to WT, and combined from three independent experiments. Error bars indicate standard deviation. Asterisks indicate statistically significant differences as compared to the WT cell line (unpaired t-test: **, $p<0.01$). (C) Western blot of PAR bound to ZAP in cell lysates of ZAP KO HEK293T transfected with empty pcDNA3.1 vector, pcDNA3.1-3XFLAG-ZAPL-WT, or -N658A central domain. ZAP was immunoprecipitated by FLAG beads after treatment with 1μM PARG inhibitor. Data are representative of three out of four independent experiments. (D) Densitometric analysis of the amount of PAR pulldown normalized to FLAG-ZAP pulldown as quantified by Image Lab, normalized to WT, and combined from four independent experiments. Error bars indicate standard deviation. Asterisks indicate statistically significant differences as compared to the WT cell line (one-way ANOVA and Dunnett's multiple comparisons test: ****, $p<0.0001$). (E) ZAPL WT inducible ZAP KO HEK293T cell line treated with 0, 1, 10, and 25μM of the PARP inhibitor Veliparib for 24 hours before harvesting the WCL for western blot. Data is from one experiment. (F, G) ZAPL WT or N658A inducible ZAP KO HEK293T cell line was induced with dox for ZAP expression for 24 hours before infection with SINV Toto1101/Luc at an MOI of 0.01 PFU/cell and treated with 0, 1, 10, and 25μM of the PARP inhibitor Veliparib (F) or Talazoparib (G). The cells were harvested 24 h.p.i for luciferase assay. Fold inhibition is calculated by dividing the averaged -dox RLU by the individual +dox RLU. Data are representative of two independent experiments. Error bars indicate standard deviation. Asterisks indicate statistically significant differences as compared to the corresponding WT cell line (two-way ANOVA and Šídák's multiple comparisons test: *, $p<0.05$; **, $p<0.01$). 1μg/mL dox is used to induce ZAP expression in ePB ZAP inducible cell lines.

To further validate the PAR binding phenotype, we included a negative control mutant that had been reported to have attenuated PAR binding (Q668R) (Xue et al., 2022). Consistent with previous findings, the Q668R ZAP mutant exhibits a loss in PAR binding activity (Supp Fig 2.5). Because the localization of ZAP can change based on the presence of a PARP-like domain, we also tested PAR binding in the context of just the central domain (Charron et al., 2013; Gläsker et al., 2014). We generated plasmid constructs of FLAG-tagged ZAP central domain with WT and N658A sequences, transfected them into ZAP KO HEK293T cells, and performed a PAR binding assay. Similar to our results in the full-length ZAP context, we found that the central domain N658A mutant is still correlated with less PAR binding than the central domain ZAP WT (Fig 2.7C) in three out of four independent trials (average ratio of IP PAR/IP FLAG is 0.7x for N658A vs. 1x for WT), although the difference is not statistically significant likely due to the one outlier trial (Fig 2.7D).

Because PAR binding can be affected by overall PAR levels in the cell, we treated WT and N658A ZAP cell lines with the PARP inhibitors Veliparib and Talazoparib from 1 to 25μM (Delgado-Rodriguez et al., 2023; T. Guo et al., 2019; Kim et al., 2020; Lee et al., 2021; Maya-Mendoza et al., 2018). Veliparib is superior in selectively inhibiting PARP1 and PARP2, while Talazoparib inhibits PARP1, PARP2, and tankyrases (Thorsell et al., 2017). We pre-treated the cells with the inhibitors for 1 hour before SINV addition to allow enough time to block PARP activities prior to virus infection, during which we maintained the same concentration of each PARP inhibitor. We harvested the cells for western blot and luciferase assay 24 h.p.i. Consistent with a previous study that used Veliparib (Albert et al., 2007), PAR is markedly decreased past 1μM of Veliparib treatment (Fig 2.7E). We found that the antiviral activity of WT ZAP is not enhanced and that the N658A mutant is still more potent than WT ZAP regardless of the concentration of the PARP inhibitor tested (Fig 2.7F and 2.7G).

**Asparagine is the predominant amino acid at site 658 in ZAP yet the least antiviral**

To further understand the requirements at site 658 for ZAP to become a more potent restrictor, we analyzed the amino acid distribution in our mammalian ZAP sequences. We observed that site 28, one of the positively selected sites, displays an even distribution of amino acids (Fig 2.8A). In contrast, at site 658, asparagine is the most prevalent amino acid in our 261 mammalian ZAP sequences (68%, Fig 2.8A). Interestingly, when we looked at what species do not have an asparagine, we found that marine mammals in the Pinnipedia clade all have a serine (Fig 2.8C). However, there are also other non-pinniped mammals that have a serine, such as the long-tongued fruit bat, Asian palm civet, and the meerkat, suggesting that there is convergent evolution from distinct clades. In terms of the amino acid property, there

is less variation at site 658 than at site 28 (Fig 2.8A and 2.8D). Even though site 658 has rapidly evolved, polar amino acids seem to be favored by evolution. 80% of the mammals in our alignment have a polar amino acid at site 658: 177 out of the 261 mammals (68%) have asparagine and 32 (12%) have serine (Fig 8A). This is in stark contrast to Q28, where every amino acid property is present: 7% have a nonpolar amino acid (alanine, glycine); 38% have a polar amino acid (glutamine, asparagine, serine); 38% have a negatively charged amino acid (aspartic acid, glutamic acid); and 23% have a positively charged amino acid (histidine, lysine, arginine) (Fig 2.8A and 2.8D), demonstrating that site 28 is able to tolerate more flexibility in the chemical property of its amino acid. Adjacent sites that are not under positive selection, 657 and 659, show even less amino acid diversity (Fig 2.8B). Site 657 is dominated by a polar (glutamine) or positive (arginine) amino acid, and site 659 permits only nonpolar amino acids with an aromatic ring (tyrosine and phenylalanine).

To ascertain if a specific amino acid or a nonpolar property is required at site 658 to achieve better antiviral activity, we generated additional ZAPL N658 mutants by mutating the WT residue in humans, asparagine, to residues found in other mammalian species such as glycine (nonpolar; in African woodland thicket rat), serine (polar uncharged; in California deer mouse), lysine (positive; in greater bamboo lemur), or aspartic acid (negative; in little brown bat). We infected cell lines with inducible expression of each of these ZAPL site 658 mutants with the same luciferase-expressing SINV and found that only the N658A mutant consistently has significantly higher anti-SINV activity than WT ZAP (N658) (Fig 2.8E and 2.8F). None of the other naturally occurring residues at site 658 confers significantly more potent activity on ZAP, supporting that ZAP has the potential to be further optimized and improved as a

restriction factor. As our findings suggest that the residue at site 658 with the best antiviral activity (N658A) is nonexistent in nature, further studies are required to understand why positive selection has selected for a version of ZAP that does not maximize its anti-alphaviral activity.

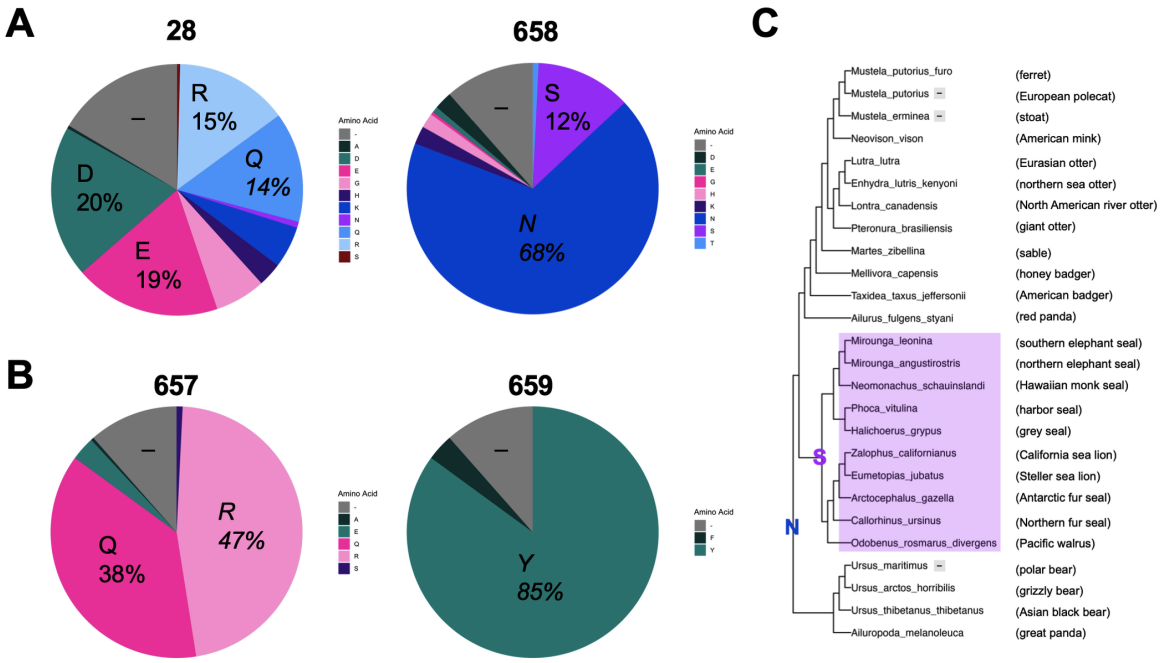


D

| | Site | | | |
|---|---|---|---|---|
| | 28 | 657 | 658 | 659 |
| Human | Q | R | N | Y |
| Common marmoset | Q | R | N | Y |
| Greater bamboo lemur | E | R | K | Y |
| Horse | D | R | N | Y |
| Donkey | K | R | N | Y |
| Mouse | G | Q | N | Y |
| Hispid cotton rat | H | - | - | - |
| California deer mouse | G | Q | S | Y |
| Yellow-bellied marmot | D | R | N | Y |

nonpolar (aliphatic)
nonpolar (aromatic)
polar (uncharged)
polar (positive)
polar (negative)

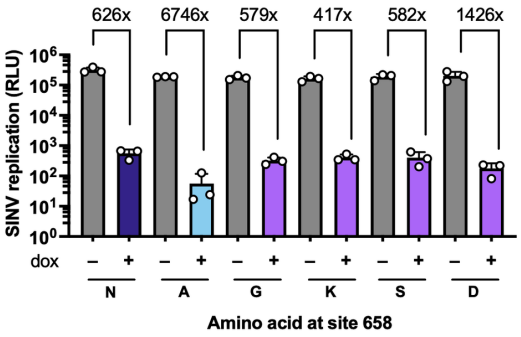


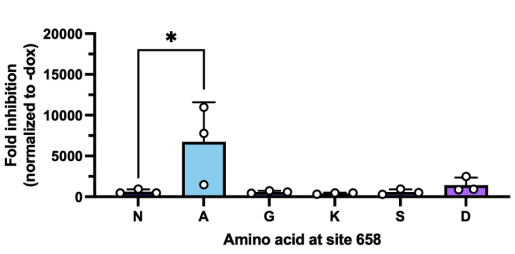

Figure 2.8 Asparagine is the predominant amino acid at site 658 yet confers weaker antiviral activity.
(A, B) The distribution of amino acids at sites 28, 657, 658, and 659. (C) A zoomed in view of the 261-mammals phylogenetic tree showing the nearest relatives of the Pinnipedia clade (seals) and their amino acids at site 658. Gray dashes indicate gaps or deletions. (D) An abridged alignment of amino acids at sites 28, 657, 658, and 659. (E) ZAPL N658 (WT) or N658A/G/K/S/D inducible ZAP KO HEK293T cells were induced for ZAP expression with 1μg/mL dox. Cells were infected with SINV Toto1101/Luc at an MOI of 0.01 PFU/cell and harvested at 24 h.p.i for luciferase assay. Data are representative of two independent experiments. Error bars indicate standard deviation. (F) Fold inhibition of (E) is calculated by dividing the averaged -dox RLU by the individual +dox RLU. Error bars indicate standard deviation. Asterisks indicate statistically significant differences as compared to the corresponding WT cell line (one-way ANOVA and Dunnett's multiple comparisons test: *, $p<0.05$).

## Discussion

In this study, we sought other positively selected sites beyond the three previously identified in the PARP-like domain of ZAP and asked whether they have played a role in response to virus infections. We identified seven positively selected sites in total throughout mammalian evolution of ZAP, with only one residing in the PARP-like domain, supporting the notion that ZAP has been the target in more than one host-virus arms race. Notably, four of these positively selected sites are concentrated in the central region. We found that mutating the positively selected sites did not significantly impair WT ZAP's original antiviral activity, in line with a deep mutational scanning study of TRIM5α (Tenthorey et al., 2020). Interestingly, a mutation at the WWE2 (N658A) was almost 10 times better at inhibiting SINV and other Old World alphaviruses than WT ZAP. Even though an alanine mutation at site 658 is nonexistent in extant mammalian ZAP, our study adds to and is consistent with previous studies on MxA (Cólon-Thillet et al., 2019; Mitchell et al., 2012). Importantly, just one amino acid change in MxA is sufficient to change its species specificity against an orthomyxovirus (Mitchell et al., 2012) and that enhancing mutations do not necessarily have to be naturally occurring (Cólon-Thillet et al., 2019). Furthermore, we have been testing other naturally occurring residues at site 658 in the context of human ZAP, although strong effects might

require testing these residues in the context of ZAP from their cognate species. Together with our findings, these studies highlight the advantage of positive selection analysis, which facilitates the discovery of improved versions of host antiviral proteins, especially when we are not confined to what is sampled in nature.

Our positive selection analysis incorporates high quality ZAP sequences from all orders of mammals, while most analyses of positive selection in innate immune factors have focused on a subset of species. For example, using 17 primate TRIM5α sequences, Sawyer *et al.* identified five residues under positive selection all within a 13-amino acid patch that is responsible for species specificity against lentiviruses (Sawyer et al., 2005). Enabled by the more comprehensive sequences and robust codon substitution models presently, we hypothesized that including more species would allow us to detect positive selection signatures in regions across the whole protein and provide a more well-rounded picture of antiviral effectors. Consistent with a study that identified distinct positively selected sites in SAMHD1 using different subsets of mammals (Monit et al., 2019), we found that positively selected sites in ZAP, while concentrated, are not just restricted to the PARP-like domain (Kerns et al., 2008), but span the N-terminus, central region, and C-terminus. This reflects the highly diverse and long evolutionary history of ZAP, which arose during the emergence of tetrapods (Gonçalves-Carneiro et al., 2021). Further positive selection analyses in subsets of mammals are required to confirm if each positively selected site or domain is driven by distinct viruses.

We found that mutating the N658 site to alanine in the WWE2 of ZAP creates a ZAP that has stronger anti-alphavirus function, unaltered anti-HIV-1 function, and diminished PAR binding ability. We speculated on why our results are different from a previous study in

which it identified a Q668R mutation to have a positive relationship between ZAP's binding to PAR and anti-HIV-1 activity. First, the Q668 residue is buried in the PAR binding pocket, as opposed to the N658 positively selected residue which is outside of the binding pocket. Second, the previous study found differences in antiviral activity only when a CpG-enriched engineered HIV-1 was used (Xue et al., 2022), whereas the Q668R mutant has similar antiviral activity as WT ZAP when the HIV-1 tested was not CpG-enriched. Lastly, the effect of PAR binding deficiency might be different between HIV-1 and SINV because they are different viruses with different replication strategies. For instance, ADP-ribosylation may be a post-translational modification exploited by alphaviruses, as a productive alphaviral infection relies on the binding to and removal of ADP-ribose by the highly conserved alphaviral macrodomains encoded by nonstructural protein 3 (Abraham et al., 2018; Alhammad & Fehr, 2020; McPherson et al., 2017; Park & Griffin, 2009). Thus, ancient HIV-1- and SINV-like viruses have most likely exerted distinct selective pressures on ZAP. Building on the previous study, we recognize that changes in PAR binding may both positively and negatively affect ZAP antiviral activity. In the case of the N658A mutant, we saw that having an alanine is correlated with reduced PAR binding, suggesting that the naturally occurring asparagine residue at this site in human ZAP has maintained relatively higher levels of PAR binding. This can be driven by an evolutionary arms race with PARylated viral proteins. Furthermore, because we can only get a snapshot with extant ZAP sequences, it is not possible to know the directionality of the conflict at this moment in time, i.e. if the asparagine restores recognition of a viral protein, or if a viral protein antagonizes WT ZAP by interacting with the asparagine. On one hand, asparagine could be the "best" version because it is able to balance antiviral

activity with other functions of ZAP like PAR binding. On the other hand, the mammals with asparagine might gradually evolve toward a better amino acid in the future. To our surprise, depleting the amount of PAR in the cell with a PARP inhibitor does not change the antiviral activity of WT ZAP, suggesting that PAR binding may be an unintended side effect in the evolutionary arms race, rather than a cause or consequence. Alternatively, decreased PAR binding to the ZAPL N658A mutant may also be a way to reduce PAR-dependent ubiquitination of other proteins that interact with ZAP (Vivelo et al., 2019). In the future, it would be important to carry out more rigorous biochemical assays for PAR binding, such as isothermal titration calorimetry (Alhammad et al., 2021) or single-molecule fluorescence resonance energy transfer (Badiee et al., 2023). This would allow us to formally elucidate the relationship between PAR binding and antiviral activity, as well as the role of macrodomains, PARylation, and/or ubiquitination in virus infection.

Why has evolution selected for an amino acid at site 658 that makes a less antiviral version of mammalian ZAP against alphaviruses? One hypothesis is that catering to a specific virus would limit ZAP's antiviral activity against another virus. We wondered if our N658A mutant is worse than WT ZAP at inhibiting HIV-1. Consistent with previous studies (Ficarelli et al., 2020; Kerns et al., 2008; Takata et al., 2017; Xue et al., 2022), we found that WT ZAP was only mildly effective against HIV-1 (at best a 2-fold inhibition) and that the N658A mutant had similarly modest anti-HIV activity. Thus, it does not seem that ZAP is in its current form to maintain potency against HIV-1. Since the HIV sensitive to ZAP is an artificially engineered mutant enriched with CpGs in a specific region of the HIV genome, it would be interesting to test our mutant ZAP against this engineered HIV in the context of ZAP sensitivity to CpGs

in future studies to determine the impact of the N658A mutation on the breadth of ZAP antiviral activity. Another possibility is that having a stronger antiviral activity incurs a fitness cost on the host cell by interfering with non-immune-related cellular functions of ZAP. In cells not infected by a virus, PAR was bound to ZAP; when cells were treated with arsenite to induce stress granule formation, the amount of PAR on ZAP increased and miRNA-mediated silencing decreased (Leung et al., 2011). While the direct mRNA targets bound by ZAP and the miRNA complex remain mostly unknown, ZAP is implicated in the regulation of host transcripts in a non-viral context. For example, the transcript of TRAILR4 transcript, which we found to be modestly downregulated in this study by the ZAPL N658A mutant, is a decoy receptor that is involved in TRAIL-induced apoptosis in cancer (Todorova et al., 2014). Furthermore, a recent RNA-seq analysis also discovered that ZAPS and ZAPL bind to host mRNAs involved in the unfolded protein response and the epithelial-mesenchymal transition (Ly et al., 2022). It would be interesting to explore if any of the cellular pathways that are post-transcriptionally regulated by ZAP are affected by the more antiviral N658A mutation.

ZAP is a broad-spectrum antiviral protein that is effective against members from a wide range of virus families. It is possible that some of our positively selected sites did not have a dramatically better antiviral effect compared to WT ZAP because the selection at these other sites were driven by ancient viruses that were not alphavirus-like. We wonder how our other positive selection mutants would behave against other viruses that infect mammals as their primary reservoir hosts. For instance, alphaviruses and flaviviruses share similar transmission cycles where they circulate between wild mammals and domestic mammalian dead-end hosts. Coronaviruses also commonly exploit mammals as hosts, such as camels for MERS and bats

for SARS-CoV-1 (Z. Zhou et al., 2021). If ancient flavivirus- or coronavirus-like viruses drove the positive selection of ZAP, we expect to see a greater impact on its antiviral activity when ZAP mutants are tested against those viruses. Alternatively, viruses that are not susceptible to the increased antiviral activity of the N658A mutant might encode viral antagonists of ZAP. Notably, we saw that there was no difference in the ability of ZAPL WT and N658A to inhibit VEEV. It is possible that VEEV encodes a viral antagonist that can still recognize ZAP despite the mutation and thus is impervious to any improvement in ZAP's antiviral activity. Nevertheless, rapid adaptation can happen outside of the context of a pursuer-target relationship with one virus, as long as the mutation confers a fitness advantage. It is just as possible that a host protein engaged in multiple arms races with different viruses would have positively selected sites and residues that affect the outcome in each of these races. This could explain why other naturally occurring residues at site 658 we have already tested were not as effective as N658A because they might only be able to show an effect against other matched virus(es). Our HIV result suggests that ancient retroviruses might not have been the major selective force that led to the positive selection of ZAP throughout mammalian evolution. ZAP was likely engaged in more than one genetic conflict and thus its positively selected sites would have different effects in each of these conflicts. In this case, site 658 appears to be important in the genetic conflict with alphaviruses but not HIV-1. Future studies should identify the viral proteins that are locked in an evolutionary conflict with ZAP and test more viruses from different families.

Lastly, it has been shown that ZAP's N-terminal domain and TRIM25 from different mammalian species are mostly compatible against CpG-enriched HIV-1 (Gonçalves-Carneiro

et al., 2021). It is possible for our ZAP mutant to behave differently in the cellular backgrounds of species other than that of humans since the N658A mutation is located outside the N-terminal domain of ZAP, in the central domain. Additional bioinformatic analyses can be done to infer the branches or species that contributed to the signals of positive selection. Future studies that look at the compatibility of the human N658A mutant with the ZAP cofactors expressed by those species will be informative.

Our study is one of the first to look at positive selection of a broad-spectrum antiviral protein in a comprehensive and diverse group of mammals. By understanding what makes a strong restrictor and the host cell constraints, we can design better antiviral therapeutics that have the potential to outrun the virus in the host-virus arms race.

**Acknowledgments**

Flow cytometry was performed in the UCLA Jonsson Comprehensive Cancer Center (JCCC) Flow Cytometry Core Facility that is supported by the National Institutes of Health award P30 CA016042 and by the JCCC. RT-qPCR was performed in the UCLA AIDS Institute that is supported by the James B. Pendleton Charitable Trust and the McCarthy Family Foundation.

Molecular structures were performed with UCSF Chimera by the Resource for Biocomputing, Visualization, and Informatics at the University of California, San Francisco (NIH P41-GM103311).

We thank Dr. Nandita Garud, Dr. Kirk Lohmueller, Dr. Ting-Ting Wu, Erin Kim, Martin Ruvalcaba, and Dr. Zhenlan Yao for their invaluable feedback on the project and critical reading of the manuscript.

## Materials and methods

### Cell culture

HEK293T (parental and ZAP KO) cells were gifts from Dr. Akinori Takaoka at Hokkaido University (Hayakawa et al., 2011) and maintained in Dulbecco's Modified Eagle Medium (DMEM; Thermo Fisher Scientific, Waltham, MA) with 10% fetal bovine serum (FBS; Avantor Seradigm, Radnor, PA). BHK-21 cells (American Type Culture Collection, Manassas, VA) were maintained in Minimal Essential Media (Thermo Fisher Scientific) with 7.5% FBS. 0.1mg/mL poly-L-lysine hydrobromide (Millipore Sigma, Darmstadt, Germany) and water were used to coat cell culture dishes when thawing or seeding each cell line to promote cell adhesion and recovery.

### Plasmids

WT or mutant ZAP was cloned into the plasmid pcDNA3.1-3XFLAG (gift from Dr. Oliver Fregoso, University of California, Los Angeles) as previously described (E. Yang, Nguyen, et al., 2022). 3XFLAG-ZAPS and -ZAPL were amplified from the pcDNA3.1-3XFLAG plasmids using primers to add ClaI and NotI restriction sites for ligation into the ePB vector (gift from Dr. Ali Brivanlou, Rockefeller University) (Lacoste et al., 2009). Full-length TRIM25 (gift from Dr. Jae U. Jung at Cleveland Clinic Lerner Research Institute) (Gack et al., 2007) was cloned into pcDNA3.1-myc as previously described (E. Yang, Huang, et al., 2022). The ZAP positive selection mutants, PAR binding deficient Q668R mutant, and N658G/K/S/D mutants were generated by the Q5 Site-Directed Mutagenesis Kit (New England Biolabs, Ipswich, MA) or synthesized as a gene block (Twist Bioscience, South San Francisco, CA) with ClaI and NotI restriction sites and ligated into the ePB vector. The ZAP

CD WT or N658A mutant in pcDNA was cloned using primers that flanked the CD with restriction sites NotI and XbaI. The identity of all plasmids was confirmed by Sanger (Genewiz/Azenta, South Plainfield, NJ) and whole-plasmid sequencing (Primordium, Monrovia, CA).

**Generation of ZAP inducible cell lines**

All ZAP inducible cell lines were made via the ePB transposon system in ZAP KO HEK293T cells. Specifically, ZAP KO HEK293T cells were transfected with equal amounts of the transposase plasmid and an ePB transposon vector containing WT or mutant ZAP using X-tremeGENE9 DNA Transfection Reagent (Roche Life Science, Basel, Switzerland) in Opti-MEM (Thermo Fisher Scientific) following manufacturer's instructions. 1μg/mL puromycin was added 48 hours post-transfection to select for ZAP KO HEK293T cells that have incorporated the ePB transposon. Our ZAPS WT and ZAPL WT cell lines were made by selecting single cell clones that follow two criteria: 1) robustly express ZAP following 24 hours of 1μg/mL doxycycline treatment, and 2) recapitulate differential alphaviral sensitivities (Fig 2.3) similar to previously generated bulk cell lines with inducible ZAP expression (Li et al., 2019; E. Yang, Huang, et al., 2022). The mutant ZAP cell lines in this study were bulk cells that survived after puromycin selection. Comparable inducible ZAP expression in each cell line was validated by immunoblotting following treatment with 1μg/mL doxycycline. After the study was completed, we found out that the original ePB-3XFLAG-ZAPL constructs and subsequent positive selection mutant constructs we generated express haplotype 2, while the ZAPS constructs express haplotype 1. Both haplotypes are naturally occurring in human populations and have very similar antiviral activities against the viruses tested in (Li et al.,

2019). We decided to investigate the effects of the haplotypes on the positive selection mutants in future studies.

**Viruses and infections**

SINV (Toto1101) (Rice et al., 1987), SINV expressing luciferase (Toto1101/Luc and Toto1101/Luc:ts6) (Bick et al., 2003), SINV expressing enhanced green fluorescent protein (EGFP) (TE/5'2J/GFP) (Frolova et al., 2002), RRV expressing EGFP (gift from Dr. Mark Heise, University of North Carolina) (Morrison et al., 2006), ONNV expressing EGFP (gift from Dr. Steve Higgs, Kansas State University) (Brault et al., 2004), CHIKV vaccine strain 181/clone 25 expressing EGFP (gift from Scott Weaver, The University of Texas Medical Branch at Galveston) (Gorchakov et al., 2012), VEEV vaccine strain TC-83 expressing EGFP (gift from Dr. Ilya Frolov, University of Alabama at Birmingham), and HIV-1 Bru ΔEnv pseudotyped with the glycoprotein from vesicular stomatitis virus have been previously described (L. P. Nguyen et al., 2023; Sandoval et al., 2024; E. Yang, Huang, et al., 2022). All alphaviral stocks were generated and titered in BHK-21 cells (Bick et al., 2003). The amount of virus used for each experiment was determined by the multiplicity of infection (MOI), cell number, and virus titer. HIV-1 stocks were generated as previously described (Sandoval et al., 2024) and infection was normalized by units of reverse transcriptase activity (Vermeire et al., 2012).

ZAPS/L WT and mutant cell lines were induced for ZAP expression with 1μg/mL of doxycycline 1 day prior to virus infection. To quantify SINV replication, cells were infected with SINV with a luciferase reporter gene (Toto1101/Luc) and harvested 24 h.p.i. To quantify SINV translation, cells were infected with a replication-deficient temperature-sensitive SINV

(Toto1101/Luc:ts6) at 37ºC for 1 hour to allow virus adsorption, followed by incubation at 40ºC and harvested at the specified timepoints. Harvested lysates were measured for luciferase units following manufacturer's instructions of the Luciferase Assay System (Promega, Madison, WI).

To quantify infection by GFP-alphaviruses, infection was performed as described above and fixed in PBS with 1% FBS and 2% formaldehyde 24 h.p.i. The fixed cells were analyzed on the Attune NxT Flow Cytometer (Thermo Fisher Scientific), courtesy of the UCLA Flow Cytometry Core.

For HIV-1 infection, cells were spinfected at 1200xg for 90 min at 37ºC at 7,000 units/mL and 30,000 units/mL of reverse transcriptase activity. Infection was assessed at 24 hours via flow cytometry by an antibody against the HIV-1 core antigen-RD1 (Beckman Coulter) and viability was assessed by Ghost Dye Red 780 (CytekBio).

**Quantification of SINV virion production via plaque assays**

To quantify SINV virion production in ZAPL WT or mutant cells, ZAP expression was induced by 1μg/mL doxycycline 1 day prior to infection and infected with SINV Toto1101. The viral supernatant was collected at specific timepoints. To determine viral titers, BHK-21 cells were infected with the viral supernatant at six 10-fold dilutions and incubated at 37ºC for 1 hour with gentle rocking every 15 min. Avicel (RC-581 NF, pharm grade, DuPont Nutrition & Health) overlay consisting of 2X MEM and 4.5% Avicel was added to each well and the plate was incubated at 37ºC overnight. On the following day, cells were fixed with 7% formaldehyde for 15 min and stained with 1X crystal violet. The plates were washed and the plaques counted after drying.

**Poly(I:C) stimulation, RNA extraction, and reverse transcription quantitative polymerase chain reaction (RT-qPCR)**

To stimulate cells with a double-stranded RNA mimic, poly(I:C) diluted in Opti-MEM was incubated with Lipofectamine RNAiMax Transfection Reagent (Thermo Fisher Scientific) before being added to ZAPL WT or mutant cells. 1 day after poly(I:C) stimulation, total RNA was extracted from cells using the Quick-RNA kit (Zymo Research). The amount of RNA template was equalized for reverse transcription using the Protoscript II First Strand cDNA Synthesis Kit and random hexamers (New England Biolabs). RT-qPCR was performed using 10-fold-diluted cDNA and the Luna Universal qPCR Master Mix (New England Biolabs) in the CFX Real-Time PCR system (Bio-Rad), courtesy of the UCLA Virology Core. qPCR conditions were as previously described (E. Yang, Huang, et al., 2022, p. 20). Target transcript levels were determined by normalizing the target transcript CT value to the RPS11 transcript CT value. Fold change was calculated using this normalized value relative to that of the corresponding cell line untreated with dox and unstimulated with poly(I:C) (CT method).

**Immunoblot analysis**

Proteins were visualized using SDS-PAGE with 4-20% Mini-PROTEAN TGX Precast Protein Gels (Bio-Rad) in NuPAGE MOPS SDS Running Buffer (Invitrogen) and transferred to a PVDF membrane (Bio-Rad). The proteins of interest were probed with the corresponding primary and secondary antibodies, followed by visualization on a ChemiDoc imager (Bio-Rad, Hercules, CA) using the ProSignal Pico ECL Reagent detection reagent (Genesee Scientific, El Cajon, CA).

Primary antibody 1:20,000 anti-FLAG (Sigma-Aldrich), 1:20,000 anti-actin-HRP (Sigma-Aldrich), or 1:1000 anti-poly(ADP-ribose) (Abcam); and secondary antibody 1:20,000 goat anti-mouse HRP (Jackson ImmunoResearch, West Grove, PA) or 1:20,000 goat anti-rabbit HRP (Thermo Fisher Scientific) were used to probe the protein of interest.

Band intensity was quantified by Image Lab (Bio-Rad) using Volume Tools and the default local background subtraction method. Detailed description of how the quantification was performed for each experiment can be found in the respective Figure captions.

***In vitro* biotinylation of SINV RNA and RNA pulldown assays**

The genomic SINV DNA template was digested by XhoI and *in vitro* transcribed using SP6 RNA polymerase (New England Biolabs) and 0.5mM biotin-16-UTP (Roche Life Science, Penzberg, Germany) as previously described (E. Yang, Nguyen, et al., 2022). RNA biotinylation was confirmed by streptavidin-HRP dot blot as previously described (L. P. Nguyen et al., 2023).

*In vitro* RNA pulldown was performed as previously described (E. Yang, Nguyen, et al., 2022). ZAP expression was induced in ePB ZAP cell lines and the protein lysates were harvested in CHAPS buffer (10mM Tris-HCl pH7.5, 1mM $MgCl_2$, 1mM EDTA, 0.5% CHAPS, 10% glycerol, 5mM beta-mercaptoethanol, and protease inhibitor) 24 hours later. 0.4pmol of biotinylated SINV RNA was incubated with normalized amounts of protein lysates and RNA binding buffer containing RNaseOUT (Thermo Fisher), heparin (Sigma-Aldrich), and yeast tRNA (Thermo Fisher) to minimize non-specific binding. The lysate-RNA samples were incubated with Dynabeads M-280 Streptavidin (Invitrogen) on a shaker for 30 min at room temperature. Protein visualization on a ChemiDoc imager was as described above.

**Immunoprecipitation assays**

To test interaction with TRIM25, ZAP KO HEK293T cells were transfected with pcDNA3.1-3XFLAG-ZAPL and pcDNA3.1-myc-TRIM25. Cells were lysed in FLAG buffer (100mM Tris HCl pH8.0, 150mM NaCl, 5mM EDTA, 5% glycerol, 0.1% NP-40, 1mM DTT, and protease inhibitor) and incubated on a rotator at 4ºC for 30 min. After equilibration, FLAG beads were incubated with lysates on a rotator at 4ºC for 45 min. Immunoprecipitated samples were washed three times with FLAG buffer and eluted in Laemmli buffer for immunoblotting.

PAR binding assay was based on (Xue et al., 2022) with modification. Briefly, ZAP inducible cells, ZAP KO HEK293T cells transfected with ZAP CD plasmids, or cells treated with PARP inhibitors were lysed in lysis buffer containing 50mM Tris-HCl pH7.5, 150mM NaCl, 0.2% Triton X-100, protease inhibitor, and 1μM PARG inhibitor PDD 00017273 (Tocris Bioscience, Bristol, UK). After equilibration, FLAG beads were incubated with lysates on a rotator at 4ºC for 1 hour and 30 min. Bound lysates were washed three times with IP buffer (50mM Tris-HCl pH7.5, 150mM NaCl, and 0.2% Triton X-100) and eluted in Laemmli buffer for immunoblotting.

**PARP inhibitor treatment**

To block PARP activity, the PARP inhibitors Veliparib (Selleck Chemicals, Houston, TX) and Talazoparib (Selleck Chemicals) were added to cells 1 hour before virus infection and maintained at the same concentration during the 24 hours of infection such that the volume of the diluent (DMSO) did not exceed a 1:1000 dilution in the culture media.

**Sequence alignment, phylogenetic tree, and positive selection analysis**

The coding sequence (CDS) of human ZAPXL was used to search for orthologs in 260 other mammalian genome assemblies with a contig size of at least 30kb in the NCBI assembly database as of July 2020 to minimize truncated orthologous coding sequences. To extract the orthologous coding sequences of ZAP, we used best Blat reciprocal hits from the human CDS to every other mammalian genome, and back to the human genome (matching all possible reading frames, minimum identity of 30%, and the "fine" option activated).

The 261 orthologous ZAP were aligned to human ZAPXL with MACSE v2 (Ranwez et al., 2018) with maximum accuracy settings. The alignments generated by MACSE v2 were then cleaned by HMMcleaner (Di Franco et al., 2019) using default parameters to remove errors from genome sequencing and "false exons" that might have been introduced during the Blat search. Visual inspection confirmed that the resulting alignment had a very low number of visibly ambiguous or erroneous segments.

The phylogenetic tree of the 261 mammals was built using IQ-Tree (L.-T. Nguyen et al., 2015) to generate the consensus, maximum likelihood tree with a GTR substitution model with six parameters (GTR-6) which provided the best fit. The tree was visualized using the ggtree R package (Yu et al., 2017).

More complete details on the alignment and phylogenetic tree reconstruction are given in (Bowman et al., 2024) as the same exact pipeline was used for this study.

The positive selection analyses FEL, MEME, and FUBAR were performed using HyPhy from the command line (Kosakovsky Pond & Frost, 2005b; Murrell et al., 2012, 2013), with the aforementioned alignment and mammalian tree as inputs. Rodrigue *et al.*'s positive selection test based on a Mutation-Selection balance (Mutselomega) was used as described in

(Rodrigue et al., 2021). Briefly, Mutation-Selection balance tests attempt to provide higher statistical power to detect positive selection by better accounting for selective constraint in coding sequences, beyond the usual arbitrary use of the dN/dS>1 threshold by other selection tests.

**Statistical analysis**

Experiments were performed at least two independent times and statistical analyses were performed on biological replicates from triplicate wells using GraphPad Prism. All graphical presentations have error bars above the plotted bars.

## Supplementary material

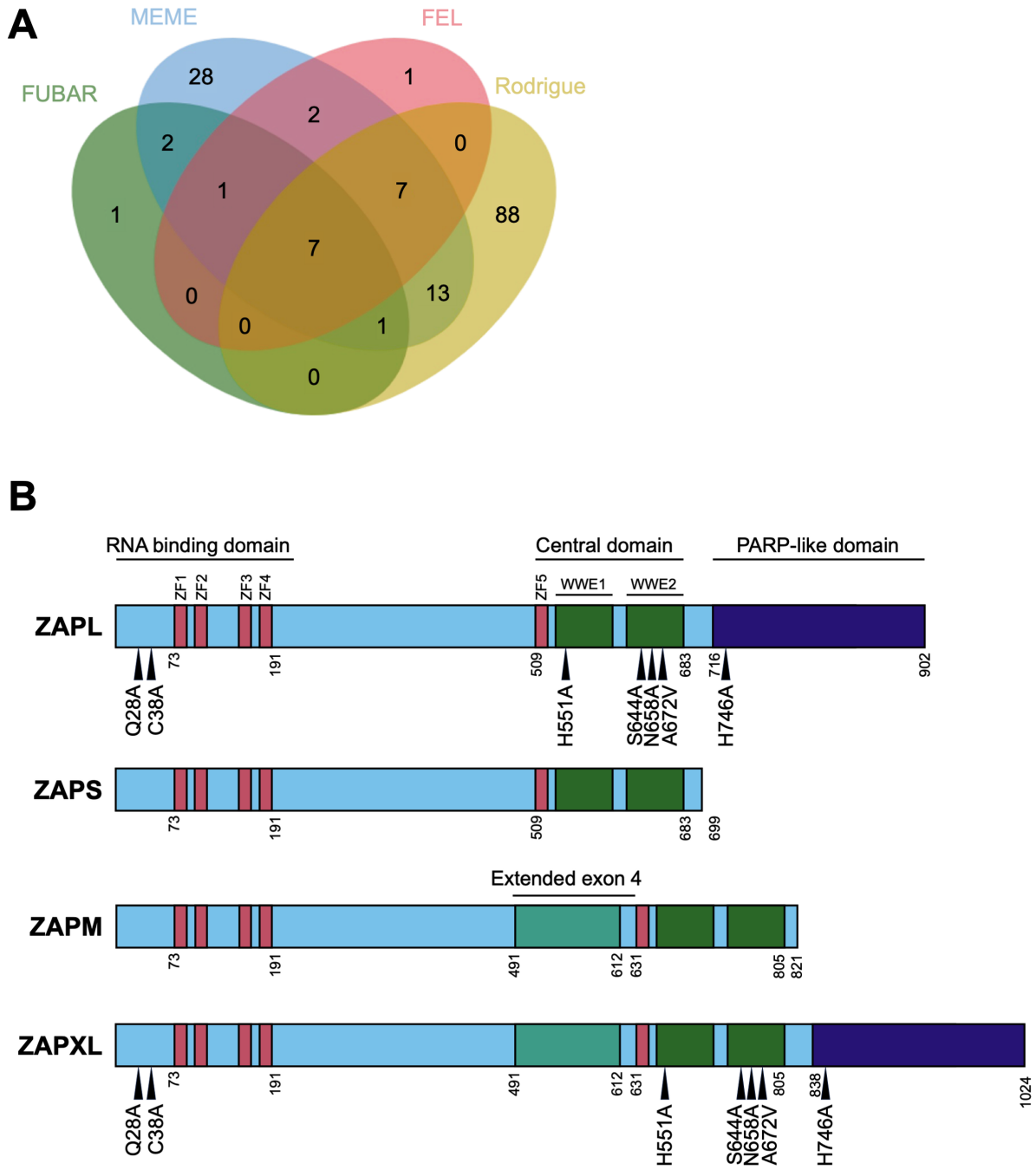


Supplementary Figure 2.1 Positive selection and domains of ZAP.
(A) Positive selection analyses on ZAPXL of 261 mammalian species detected by the FEL, MEME, FUBAR, and Rodrigue methods. (B) ZAP isoforms annotated with their domains. The four ZAP splice variants are depicted here: ZAPS (short), ZAPM (medium), ZAPL (long), and ZAPXL (extra-long). All isoforms contain the zinc finger (Z1-Z5, pink) and WWE domains (green), but only ZAPXL and ZAPL have a catalytically inactive PARP-like domain (indigo). ZAPXL and ZAPM also share an extended exon 4 (teal). The amino acid numbering of domains is based on Ficarelli et al., 2021 and Li et al., 2019.

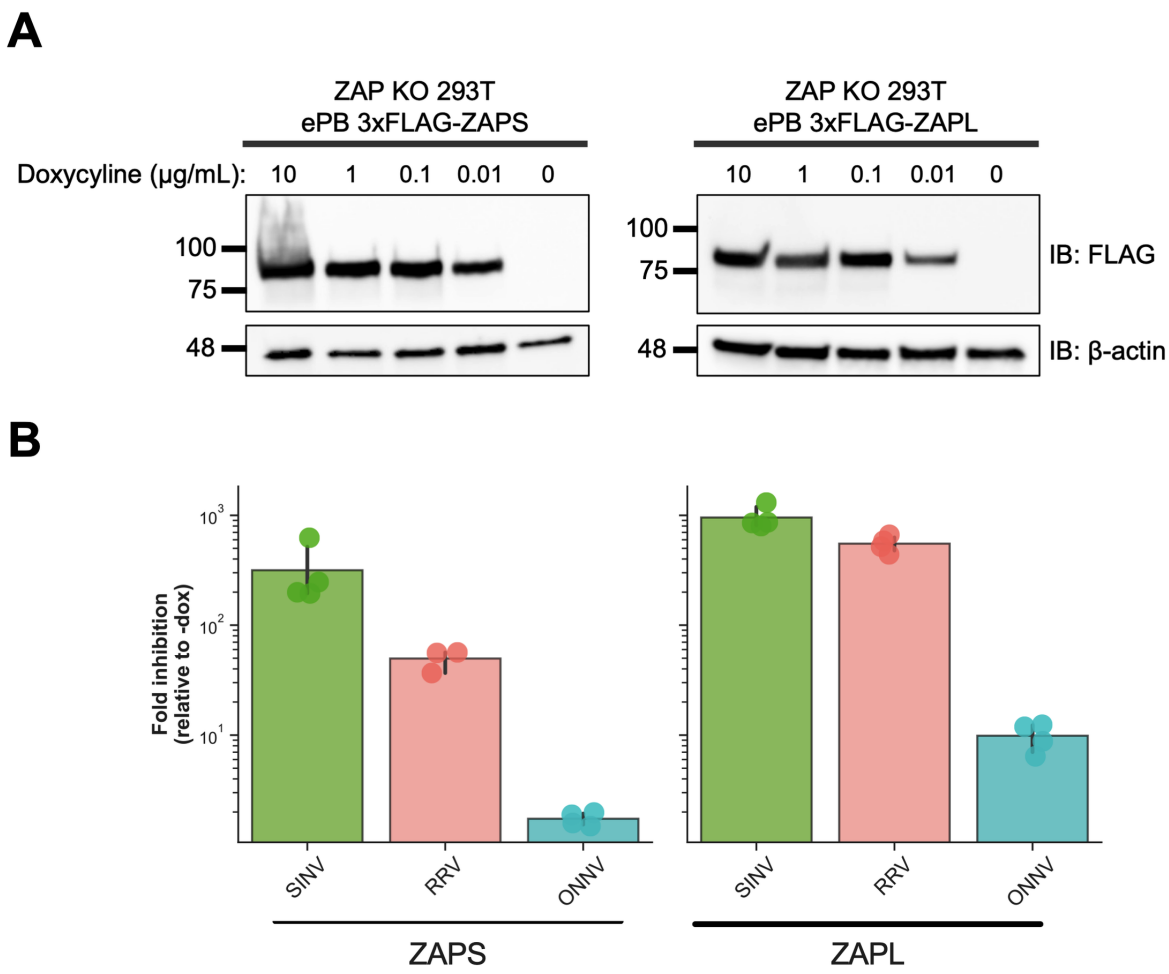


Supplementary Figure 2.2 Characterization of WT ZAP inducible single clone cell lines.
(A) Western blot of ZAPS and ZAPL WT inducible ZAP KO HEK293T cell lysates. Each single clone cell line was treated with dilutions of dox 24 hours after seeding. Cell lysates were harvested 24 hours after dox treatment. (B) ZAPS and ZAPL WT inducible ZAP KO HEK293T cells were induced for ZAP expression 24 hours before infection by GFP-expressing alphaviruses and harvested at the time listed for flow cytometry (SINV, MOI = 10, harvest 8 h.p.i.; RRV, MOI = 10, harvest 24 h.p.i.; ONNV, MOI = 0.1, harvest 18 h.p.i.). Data are representative of two independent experiments. Error bars indicate standard deviation.

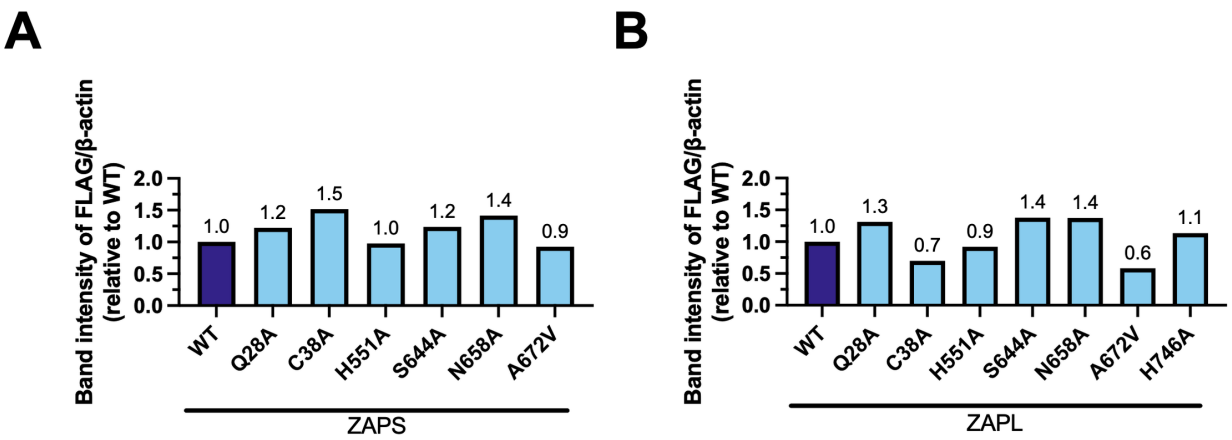


Supplementary Figure 2.3 Densitometric analysis of ZAP positive selection mutants.
Densitometric analysis on the western blot of ZAPS (A) and ZAPL (B) positive selection mutants as shown in Fig 2A and 2D. The band intensity of FLAG was divided by the band intensity of β-actin for all +dox samples, and the ratios were normalized to that of the corresponding WT ZAP.

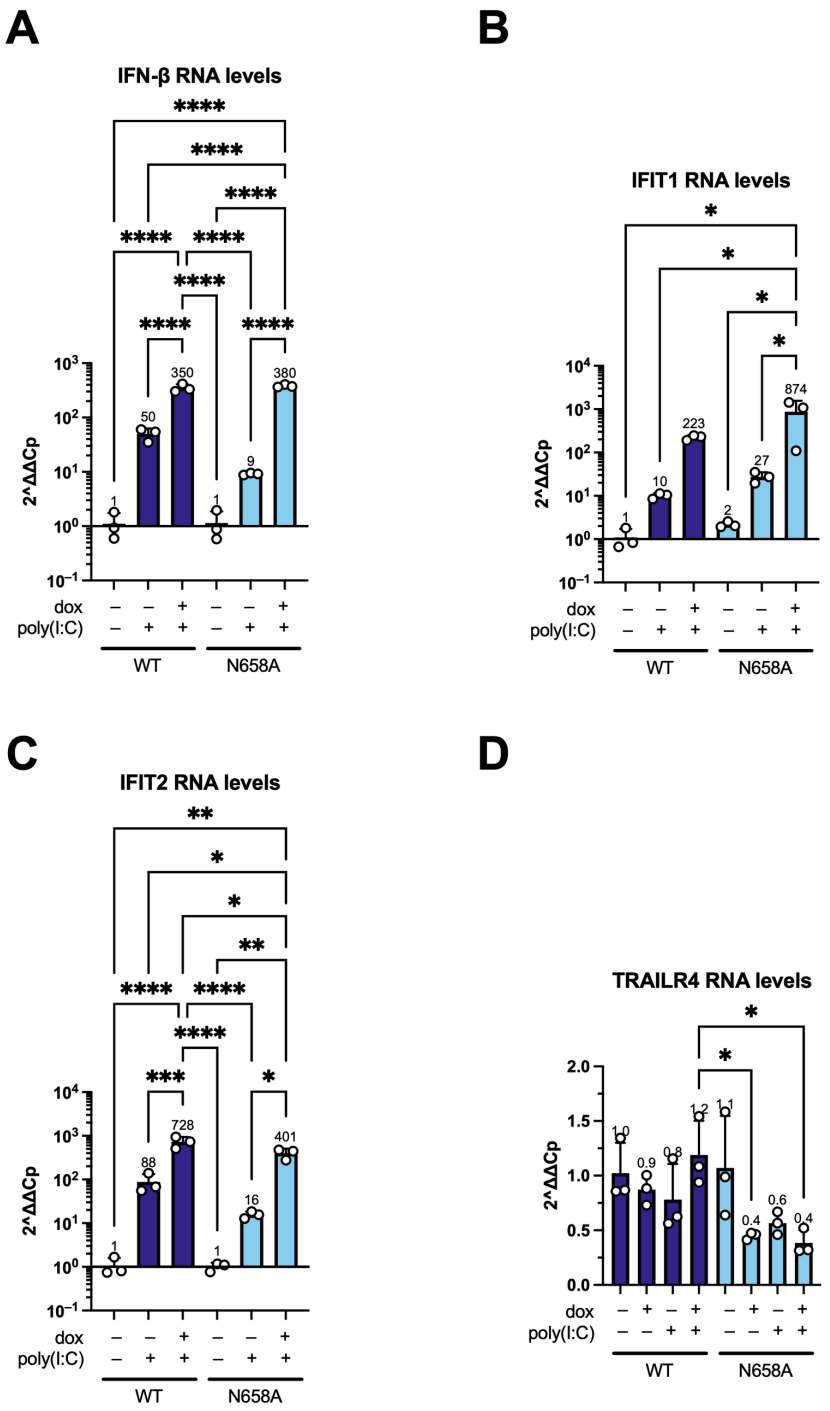


Supplementary Figure 2.4 N658A mutant induces interferon (IFN) and interferon-stimulated gene (ISG) levels similar to WT.
ZAPL WT or N658A inducible ZAP KO HEK293T cells were untreated, treated with poly(I:C), or treated with both poly(I:C) and dox. RNA was harvested for RT-qPCR. mRNA levels of IFN-β (A), the ISGs IFIT1 (B) and IFIT2 (C), and TRAILR4 (D) in each condition were normalized to that of the respective cell line without poly(I:C) and without dox. Data are representative of two independent experiments. Asterisks indicate statistically significant differences as compared to every other condition and to each cell line (two-way ANOVA and Tukey's multiple comparisons test: *, p<0.05; **; p<0.01; ***, p<0.001; ****, p<0.0001).

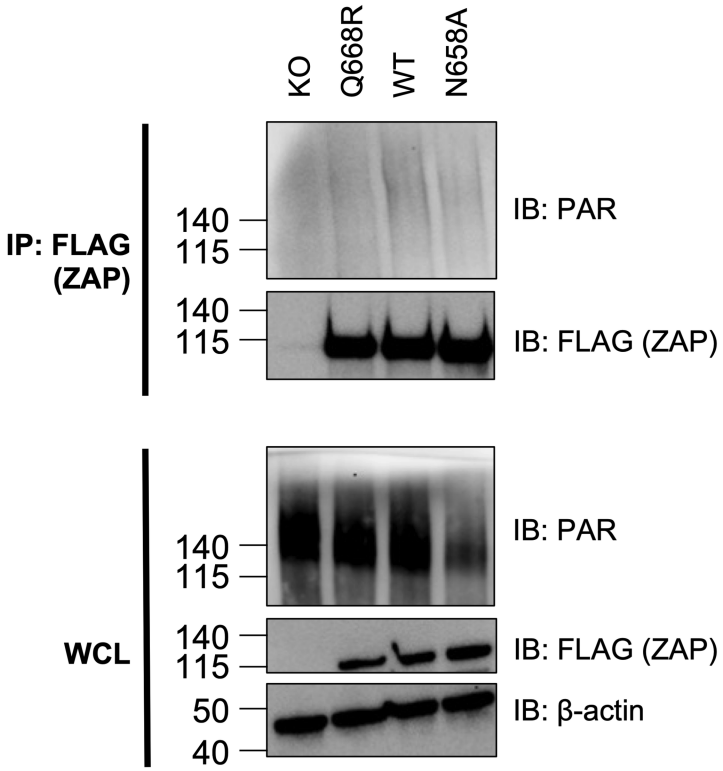


Supplementary Figure 2.5 The ZAPL PAR binding deficient Q668R negative control pulls down less PAR. Western blot of ZAP KO HEK293T cells, ZAPL Q668R, WT, and N658A inducible ZAP KO HEK293T cell lysates are immunoprecipitated by FLAG beads after treatment with 1μM PARG inhibitor. Data are representative of two independent experiments.

# Chapter 3: PABPC4 enhances ZAP-TRIM25 synergy in alphaviral translation block

## Introduction

When a virus infects a cell, the host activates the type I interferon pathway and upregulates interferon-stimulated genes (ISGs) to combat each step of infection (Schneider et al., 2014). One of the most effective antiviral strategies is to block viral translation at an early stage to prevent viral protein expression and preemptively curb the viral life cycle.

Alphaviruses are a genus of mosquito-borne viruses whose viral RNA translation is blocked by the ISG zinc finger antiviral protein (ZAP) (Bick et al., 2003; Zhu et al., 2012). One proposed mechanism of ZAP's antiviral activity is that ZAP interferes with the formation of the eIF4A-4G translation initiation complex (Zhu et al., 2012). However, this mechanism has not been studied in alphaviruses and it is also unclear if ZAP interferes with other cellular factors present in the translation initiation complex.

ZAP's inhibition of alphaviral translation requires tripartite motif containing protein 25 (TRIM25), a host E3 ubiquitin ligase. E3 ubiquitin ligases are part of the pathway that post-translationally modifies substrates with the ubiquitin protein. Ubiquitin is covalently attached on the substrate either as a single ubiquitin (monoubiquitination) or a ubiquitin chain (polyubiquitination). While monoubiquitination is involved in histone regulation, endocytic internalization, and degradation of small and disordered proteins (Hicke, 2001; Kwon & Ciechanover, 2017), polyubiquitination has a variety of consequences depending on the linkage type. Polyubiquitin chains can be formed on the initial methionine or on the lysine residue(s) of the ubiquitin protein (K6, K11, K27, K29, K33, K48, and K63). So far, TRIM25 is known

to mediate both K48- and K63-polyubiquitination (E. Yang, Huang, et al., 2022). K48 ubiquitin chains target substrates for proteasomal degradation, whereas K63 chains mark substrates for intracellular transport, signal transduction, and DNA repair.

Because TRIM25 ubiquitin ligase activity is required for ZAP antiviral mechanism, we hypothesized that TRIM25 substrates ubiquitinated during alphavirus infection play a role in ZAP-mediated translation repression of viral RNA. Previously, our lab identified TRIM25 substrates via immunoprecipitation/mass spectrometry in an infection by Sindbis virus (SINV), a prototypical alphavirus (E. Yang, Huang, et al., 2022). Among the substrates whose interaction with TRIM25 is validated, we found that nucleoside diphosphate kinase 1 (NME1) and poly-adenylate binding protein cytoplasmic 4 (PABPC4) restore SINV replication when it is knocked down by siRNA. Here, we follow up on PABPC4 and explore its potential role in enhancing ZAP-TRIM25 synergy against alphaviral translation.

## Results

### PABPC4-mediated anti-SINV activity requires TRIM25 ubiquitination

Given that ZAP inhibits viral RNA translation, we decided to focus on PABPC4 which binds to poly(A) tails on RNA and have known roles in RNA translation and decay. From our previous siRNA data, we deduced that PABPC4 may have additional antiviral activity that PABPC1 does not have (E. Yang, Huang, et al., 2022).

We hypothesized that TRIM25 ubiquitination may required for PABPC4-mediated antiviral effect against alphaviruses. We silenced PABPC4 in TRIM25 knockout (KO) HEK293T cells with inducible expression (TRIM25 KO ePB hereafter) of wild-type (WT) or ubiquitin ligase activity-deficient (R54P) TRIM25. We infected each cell line with SINV at an MOI of 0.01 and measured viral replication. To calculate fold rescue, we divided the luciferase value of each siRNA to that of the averaged non-targeting (NT) negative control for the corresponding cell line (Fig 3.1).

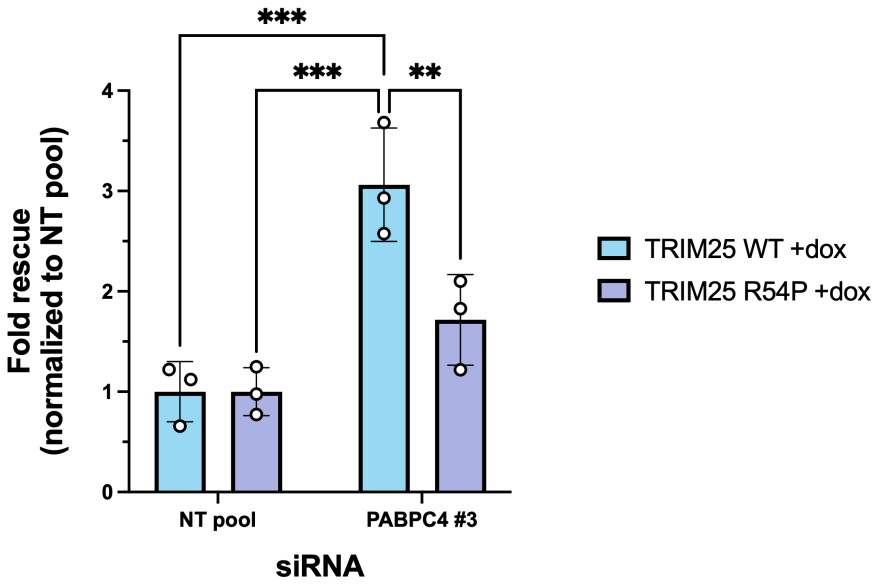


Figure 3.1 PABPC4 siRNA knockdown (KD) restores SINV replication when TRIM25 wild-type (WT) or R54P are overexpressed.
TRIM25 knockout (KO) HEK293T with inducible TRIM25 WT or R54P were seeded with non-targeting (NT) negative control or PABPC4 siRNAs. One day after TRIM25 expression is induced with 1µg/mL doxcycyline (dox), cells were infected with a luciferase reporter Sindbis virus (SINV). Data are representative of two independent experiments. Error bars indicate standard deviation. Asterisks indicate statistically significant differences (two-way ANOVA and uncorrected Fisher's LSD: **, p<0.01; ***, p<0.001).

Consistent with our previous report (E. Yang, Huang, et al., 2022), PABPC4 siRNA #3 significantly rescues SINV replication when TRIM25 WT is overexpressed (3.1x). The same siRNA is less able to restore viral replication when TRIM25 R54P is overexpressed

(1.7x), a statistically significant difference. This suggests that PABPC4 may depend on TRIM25 ubiquitination for its antiviral phenotype in SINV infection.

**Both PABPC1 and PABPC4 interact with SINV RNA**

Since the PABPs have been shown to bind to cellular RNA through their four RNA recognition motifs, we next asked if PABPC4 can bind to viral RNA (Fig 3.2).

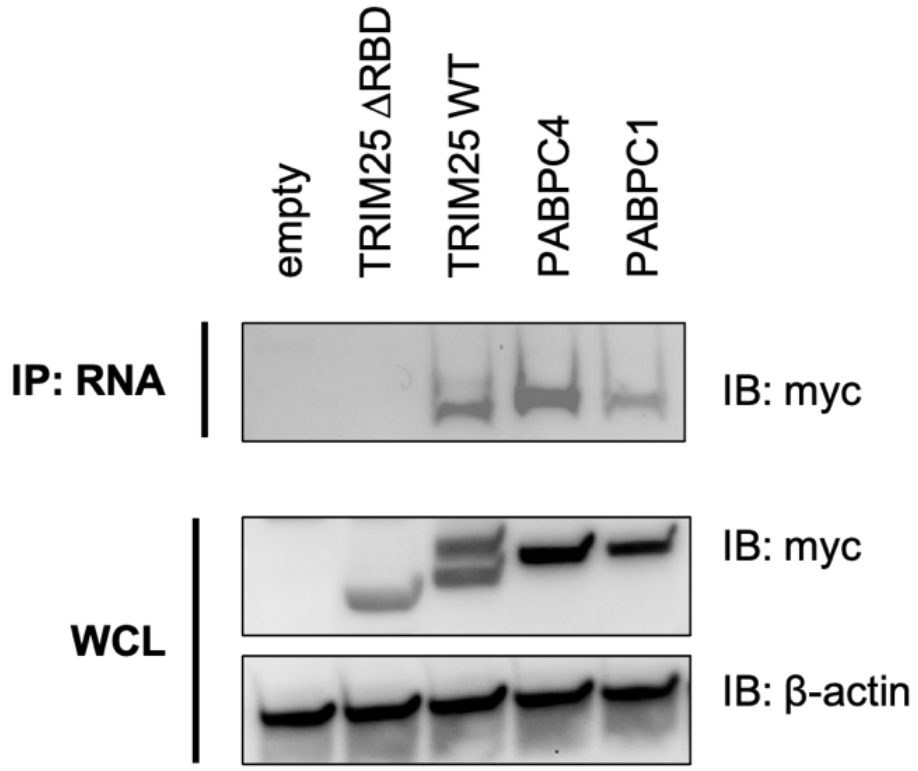


Figure 3.2 Ability of PABPC4 to bind SINV RNA.
HEK293T cells were transfected with myc-tagged constructs and harvested for an in vitro RNA binding assay. Cell lysates were incubated with biotinylated SINV RNA, followed by immunoprecipitation by streptavidin beads.

We transfected the following myc-tagged constructs into HEK293T and tested their ability to bind to SINV RNA. For negative control, we included the empty vector and a TRIM25 truncation mutant with its RNA binding domain deleted (ΔRBD). We used TRIM25 WT as a positive control (E. Yang, Nguyen, et al., 2022). As PABPs, PABPC1 and PABPC4 contain RNA recognition motifs (J. Gao et al., 2022), so we tested both identified TRIM25

substrates. We harvested the lysates and incubated each sample with biotinylated SINV RNA *in vitro*. We pulled down the viral RNA with streptavidin beads and probed for each protein with a myc antibody. As expected, neither the empty vector nor TRIM25 ΔRBD interacts with SINV RNA (Fig 3.2). TRIM25 WT has a strong additional band in the input, affirming its autoubiquitination. Consistent with our former study, TRIM25 WT interacts with SINV RNA. PABPC4 and PABPC1 both have robust expression in the input and bind with SINV RNA, though PABPC4's binding is slightly stronger.

**PABPC4 enhances TRIM25's block of SINV translation**

Next, we wanted to investigate how PABPC4 binding to SINV RNA enhances ZAP-TRIM25 mediated anti-SINV activity. Since ZAP both degrade and inhibit the translation of viral RNA, we tested whether PABPC4 can do either. We silenced PABPC4 and induced TRIM25 KO HEK293T cells for TRIM25 WT expression, then infected the cells with a temperature-sensitive replication-deficient SINV (ts6 mutant) that also contains a luciferase reporter. The ts6 mutant is unable to replicate its genome at 40ºC, thus any luciferase activity is due to the translation of just the incoming viral RNA. Over 6 hours, we quantified the amount of viral RNA to assess RNA stability and measured the amount of luciferase to assess RNA translation (Fig 3.3).

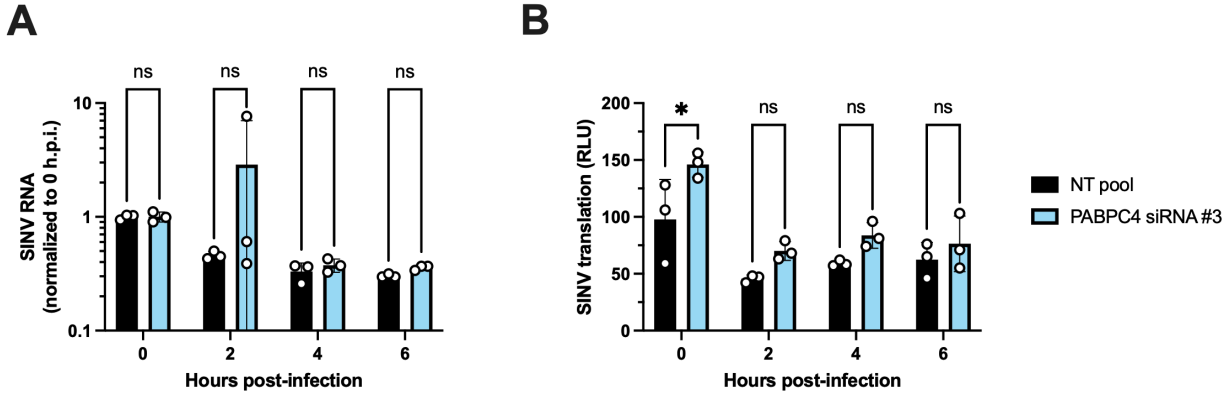

Figure 3.3 PABPC4 affects SINV translation.
TRIM25 KO HEK293T with inducible TRIM25 WT expression were seeded with NT or PABPC4 siRNA. After TRIM25 induction by 1μg/mL dox, cells were infected by SINV Toto1101/ts6 and harvested one day later. (A) Lysates were extracted for RNA and qPCR was performed to quantify the amount of SINV RNA. The RNA level of each siRNA is normalized to its averaged RNA level at 0 hour post-infection. (B) Lysates were prepared for luciferase assay and viral translation was quantified. Data are representative of two independent experiments. Error bars indicate standard deviation. Asterisks indicate statistically significant differences using two-way ANOVA and Šídák's multiple comparisons test: ns, not significant; *, $p<0.05$. 1μg/mL dox is used to induce ZAP expression in ePB ZAP inducible cell lines.

We saw that there is no significant difference in viral RNA regardless of the presence of PABPC4 at all timepoints (Fig 3.3A). In contrast, PABPC4 KD already leads to higher SINV translation at 0 hour post-infection (h.p.i.) and onwards (Fig 3.3B), though this difference does not reach statistical significance at 2, 4, and 6 h.p.i. These results suggest that PABPC4 may contribute to ZAP-TRIM25 inhibition of alphaviruses through a block against viral RNA translation early on in the infection.

## Discussion

In this study, we followed up on PABPC4, a TRIM25 substrate we previously identified in the context of SINV infection, and aimed to understand the role of PABPC4 in ZAP-TRIM25-mediated inhibition of alphaviruses. We observed that TRIM25 ubiquitination activity is required for PABPC4 to enhance anti-SINV replication (Fig 3.1). We found that apart from their known ability to bind host RNA, both PABPC1 and PABPC4 also bind viral RNA (Fig 3.2). Using a temperature-sensitive replication-deficient SINV, we saw that silencing PABPC4 does not have any effect on SINV RNA at all timepoints compared to the non-targeting control (Fig 3.3). However, SINV translation is higher at 0 h.p.i. and 2 h.p.i. when PABPC4 is knocked down.

In the cell, PABPs regulate both mRNA translation and stability (Kajjo et al., 2022). On one hand, they promote host translation and protect host mRNA by binding to the 3'

poly(A) tail and forming a loop with the eIF4 translation initiation complex (J. Gao et al., 2022). On the other hand, PABPC1 binding to the protein PAIP2 displaces PABPC1 from the poly(A) tail, thereby repressing translation (Khaleghpour et al., 2001). PABPC1 is also capable of destabilizing RNA by interacting with deadenylase or silencing complexes (Tritschler et al., 2010; Burgess et al., 2011). We observed that PABPC4 knockdown rescues SINV translation, suggesting that during alphavirus infection, PABPC4 may have an inhibitory effect on viral RNA translation. The preponderance of evidence of PABPs regulating RNA is for PABPC1, but PABPC4 seems to work with PABPC1 in supporting cell viability and protein synthesis (Kajjo et al., 2022). Thus, more studies are required to see if PABPC4 is involved in translation inhibition processes.

Another possibility for PABPC4's antiviral phenotype is that PABPC4 bolsters host mRNA translation. Since alphaviruses are known to arrest host translation (Ventoso et al., 2024), it is possible PABPC4 binding to poly(A) tails and interaction with eIF4G protect host (and viral) RNA from translation termination. Perhaps PABPC4 interaction with cofactors such as ZAP and TRIM25 allows it to distinguish between host and viral RNAs, though a comprehensive characterization of the RNA targets of PABPC4 is required to understand the nuances of PABPC4's impact on host RNA translation.

An unresolved question is how ZAP, TRIM25, and PABPC4 work together to create an anti-alphavirus state. When individually silenced, each of these three proteins restores SINV replication. We have previously discovered that ZAP binding to SINV RNA is positively correlated with SINV inhibition and negatively correlated with ZAP interaction with TRIM25 (E. Yang, Nguyen, et al., 2022). Moreover, while TRIM25 ubiquitination ligase activity is

required for ZAP-mediated antiviral activity, ubiquitination of ZAP is not required (Li et al., 2017). PABPC4 is ubiquitinated (E. Yang, Huang, et al., 2022), and it is probable that ubiquitination of PABPC4 targets the protein to stress granules, where both ZAP (Law et al., 2019) and TRIM25 (Shang et al., 2024) localize upon alphavirus infection. That interactome studies have identified PABPC1 and PABPC4 as a ZAP-interacting proteins in stress granules (Youn et al., 2018) makes this explanation plausible. Future investigation into the lysine(s) and ubiquitin linkages on PABPC4 will clarify the consequences of TRIM25 ubiquitination of PABPC4, and how it may play a role in the anti-alphavirus activity mediated by ZAP and TRIM25.

## Materials and methods

### Cell culture

HEK293T (parental) cells were gifted by Dr. Akinori Takaoka at Hokkaido University (Hayakawa et al., 2011) and cultured in Dulbecco's Modified Eagle Medium (DMEM; Thermo Fisher Scientific, Waltham, MA) with 10% fetal bovine serum (FBS; Avantor Seradigm, Radnor, PA). TRIM25 KO HEK293T cell lines with inducible TRIM25 expression were generated as previously described (E. Yang, Huang, et al., 2022).

### Plasmids

The myc-tagged TRIM25 WT and ΔRBD mutant constructs were cloned as previously described (E. Yang, Nguyen, et al., 2022) into the pcDNA3.1 backbone (gift from Dr. Oliver Fregoso, University of California, Los Angeles). The coding sequences of PABPC1 (#155805) and PABPC4 (#19877) were amplified from Addgene plasmids using flanking NotI and XbaI primers and ligated into the myc-tagged pcDNA3.1 backbone.

**siRNA knockdown**

Non-targeting siRNA controls and Ambion silencer siRNAs (Thermo Fisher Scientific) were mixed with DharmaFECT 1 Transfection Reagent (Horizon Discovery, Cambridge, United Kingdom) and diluted in HBSS at a final concentration of 25nM as previously described (E. Yang, Huang, et al., 2022). 50µL of siRNA mix were added to each well in a 24-well plate followed by the seeding of 1.2e5 TRIM25 KO HEK293T cells with inducible expression of TRIM25 WT or R54P.

**Viruses and infections**

SINV (Toto1101) (Rice et al., 1987) and SINV expressing luciferase (Toto1101/Luc and Toto1101/Luc:ts6) (Bick et al., 2003) have been previously described (Huang et al., 2024; L. P. Nguyen et al., 2023; E. Yang, Huang, et al., 2022). The multiplicity of infection (MOI) accounted for cell number and virus titer. Tissue culture plates were coated with 0.1mg/mL poly-L-lysine hydrobromide (Millipore Sigma, Darmstadt, Germany) and washed with water to maintain cell adhesion after virus infection. 1 day before virus infection, TRIM25 KO HEK293T were induced with 1µg/mL of doxycycline for TRIM25 expression. To quantify SINV replication, cells were infected with SINV with a luciferase reporter gene (Toto1101/Luc) and harvested 24 h.p.i. To quantify SINV RNA and translation, cells were infected with a replication-deficient temperature-sensitive SINV (Toto1101/Luc:ts6) at 37°C for 1 hour to allow virus adsorption, followed by incubation at 40°C and harvested at the specified timepoints. Harvested lysates were processed for RNA extraction or for analysis with the Luciferase Assay System (Promega, Madison, WI).

**Reverse transcription quantitative polymerase chain reaction (RT-qPCR)**

Cells harvested for RT-qPCR were extracted using the Quick-RNA kit (Zymo Research). cDNA was synthesized using the Protoscript II First Strand cDNA Synthesis Kit and random hexamers (New England Biolabs) as previously described (Huang et al., 2024). RT-qPCR was performed as previously described (Huang et al., 2024) using the Luna Universal qPCR Master Mix (New England Biolabs) and the CFX Real-Time PCR system (Bio-Rad), courtesy of the UCLA Virology Core. Target transcript levels were determined by normalizing the target transcript CT value to the RPS11 transcript CT value. Fold rescue was calculated using this normalized value relative to that of the non-targeting control (CT method).

**Immunoblot analysis**

Proteins were visualized by SDS-PAGE using 4–20% Mini-PROTEAN TGX Precast Protein Gels (Bio-Rad) and NuPAGE MOPS SDS Running Buffer (Invitrogen) followed by transfer to PVDF membrane (Bio-Rad). The proteins of interest were probed with the corresponding primary and secondary antibodies and visualized on a ChemiDoc imager (Bio-Rad, Hercules, CA) using the ProSignal Pico ECL Reagent detection reagent (Genesee Scientific, El Cajon, CA).

Primary antibodies 1:2,400 anti-myc (Cell Signaling Technologies #2276) and 1:20,000 anti-actin-HRP (Sigma-Aldrich); and secondary antibody 1:20,000 goat anti-mouse HRP (Jackson ImmunoResearch, West Grove, PA) were used to probe the protein of interest.

***In vitro* biotinylation of SINV RNA and RNA pulldown assays**

The genomic SINV DNA template was linearized and *in vitro* transcribed using SP6 RNA polymerase (New England Biolabs) and biotin-16-UTP (Roche Life Science, Penzberg,

Germany) as previously described (E. Yang, Nguyen, et al., 2022; L. P. Nguyen et al., 2023; Huang et al., 2024). RNA biotinylation confirmation and *in vitro* RNA pulldown assay was also performed as previously described (E. Yang, Nguyen, et al., 2022; L. P. Nguyen et al., 2023; Huang et al., 2024). HEK293T cells were transfected with the corresponding plasmids and harvested in CHAPS buffer (10mM Tris-HCl pH7.5, 1mM MgCl2, 1mM EDTA, 0.5% CHAPS, 10% glycerol, 5mM beta-mercaptoethanol, and protease inhibitor) 24 hours later. Biotinylated SINV RNA was incubated with equal amounts of protein lysates and RNA binding buffer containing RNaseOUT (Thermo Fisher), heparin (Sigma-Aldrich), and yeast tRNA (Thermo Fisher) to minimize non-specific binding. The lysate-RNA samples were incubated with Dynabeads M-280 Streptavidin (Invitrogen) for 30 min at room temperature. Protein bands were visualized as outlined above.

**Statistical analysis**

Experiments were performed at least two independent times and statistical analyses were performed using GraphPad Prism. Specific statistical tests used for each experiment are listed in the figure captions.

# Chapter 4: Conclusion

## Summary

ZAP is an important antiviral protein on the first line of defense against alphavirus infection. ZAP's antiviral activity is shaped by its engagement with viruses throughout evolution, as well as its collaboration with other host factors which regulate cellular operations critical to viral replication. Due to the nature of host-virus interactions, host antiviral strategies and viral antagonism are intricately linked. Understanding how the innate immune system has evolved allows us to discover processes that are at the center of the host-virus arms race. Leveraging this knowledge can provide us with clues for the assessment of host vulnerabilities and the development of antiviral therapeutics.

In Chapter 2, we looked at how ZAP has evolved in mammals throughout its perpetual genetic conflict with ancient viruses. We identified novel positively selected sites that span the entirety of ZAP and tested its antiviral activity against SINV after mutating each positively selected site. We found that a positive selection mutant in the second WWE domain (N658A) of ZAP substantially improves ZAP's inhibition of SINV replication and viral RNA translation. We also observed a similar improvement when testing the N658A mutant against other members of the *Alphavirus* genus, but there is no difference between WT ZAP and the mutant ZAP against HIV-1. We deduced that the superior anti-alphavirus phenotype of the N658A mutant is not due to differences in interaction with SINV RNA or with TRIM25. However, the mutant is associated with a reduced ability to bind to PAR. Interestingly, we mutated the positively selected site at 658 to other amino acids that are extant in mammals, but none of the amino acids sampled is as good as an alanine. Altogether, our results show

that positive selection has acted on mammalian ZAP orthologs, and that the human WT version of ZAP has the potential to be better, but perhaps is not due to other selective pressures.

In Chapter 3, we explored how PABPC4, a poly(A) tail binding protein and a TRIM25 substrate, aids in ZAP-TRIM25 inhibition of SINV translation. We found that TRIM25's ubiquitin ligase activity enhances PABPC4's antiviral effect. We showed for the first time that PABPC1 and PABPC4 bind to viral RNA. Next, we narrowed down the step PABPC4 exerts its effect to the early translation of the incoming SINV RNA, rather than RNA degradation.

**Future directions**

A mystery that remains unresolved is how does the crosstalk between ubiquitination and ADP-ribosylation contribute to the antiviral activity of ZAP against alphaviruses. First, developing an assay that can more precisely quantify the amount of PAR on a substrate will be very useful, especially if it can tell the difference between the substrate being PARylated versus binding to PAR or another PARylated protein. Moreover, there is a myriad of downstream consequences for ubiquitination and ADP-ribosylation. It will be illuminating to determine the type of post-translational modification(s) on ZAP and decipher its impact on ZAP antiviral activity. Given that ubiquitination and ADP-ribosylation have an effect on alphavirus replication, it is likely that ZAP has a role in enhancing or disrupting either or both of these processes during infection.

More characterization of PABPC4's domains and regulatory mechanism of RNA stability and translation is needed. Much of what is known about PABPC4 is based on studies on PABPC1, and it is unclear whether the PABPCs serve independent purposes in viral

infection. Our data suggest that PABPC4 does have an individual role to play in ZAP-TRIM25 synergy against alphaviruses. If so, does PABPC4 preferentially bind to viral transcripts? Where is PABPC4 ubiquitinated by TRIM25 and what is the effect of TRIM25 ubiquitination? Answers to these questions will help build the model of how TRIM25 and its cofactors support ZAP antiviral activity against alphaviruses.

# Appendix 1: Elucidation of TRIM25 ubiquitination targets involved in diverse cellular and antiviral processes

PLOS PATHOGENS

RESEARCH ARTICLE

# Elucidation of TRIM25 ubiquitination targets involved in diverse cellular and antiviral processes

**Emily Yang[1,2¤], Serina Huang[3], Yasaman Jami-Alahmadi[4], Gerald M. McInerney[5], James A. Wohlschlegel[4], Melody M. H. Li[1,2,6]***

**1** Molecular Biology Institute, University of California, Los Angeles, California, United States of America, **2** Department of Microbiology, Immunology and Molecular Genetics, University of California, Los Angeles, California, United States of America, **3** Department of Human Genetics, David Geffen School of Medicine, University of California, Los Angeles, California, United States of America, **4** Department of Biological Chemistry, David Geffen School of Medicine, University of California, Los Angeles, California, United States of America, **5** Department of Microbiology, Tumor, and Cell Biology, Karolinska Institutet, Stockholm, Sweden, **6** AIDS Institute, David Geffen School of Medicine, University of California, Los Angeles, California, United States of America

¤ Current address: Department of Biological Sciences, Biola University, La Mirada, California, United States of America
* manhingli@mednet.ucla.edu





**Citation:** Yang E, Huang S, Jami-Alahmadi Y, McInerney GM, Wohlschlegel JA, Li MMH (2022) Elucidation of TRIM25 ubiquitination targets involved in diverse cellular and antiviral processes. PLoS Pathog 18(9): e1010743. https://doi.org/10.1371/journal.ppat.1010743

**Editor:** Mark T. Heise, University of North Carolina at Chapel Hill, UNITED STATES

**Received:** June 1, 2022

**Accepted:** July 15, 2022

**Published:** September 6, 2022



**Data Availability Statement:** All mass spectrometry raw data files are available from the PRIDE database (accession number PXD034024). All other relevant data are within the manuscript and its Supporting Information files.

**Funding:** This study was funded by the National Institute of Allergy and Infectious Diseases (NIAID, www.niaid.nih.gov), grant R01AI158704, the US Cancer Research Coordinating Committee (www.ucop.edu/research-initiatives/programs/crcc/index.html), grant CRN-20-637544, the UCLA AIDS

## Abstract

The tripartite motif (TRIM) family of E3 ubiquitin ligases is well known for its roles in antiviral restriction and innate immunity regulation, in addition to many other cellular pathways. In particular, TRIM25-mediated ubiquitination affects both carcinogenesis and antiviral response. While individual substrates have been identified for TRIM25, it remains unclear how it regulates diverse processes. Here we characterized a mutation, R54P, critical for TRIM25 catalytic activity, which we successfully utilized to "trap" substrates. We demonstrated that TRIM25 targets proteins implicated in stress granule formation (G3BP1/2), nonsense-mediated mRNA decay (UPF1), nucleoside synthesis (NME1), and mRNA translation and stability (PABPC4). The R54P mutation abolishes TRIM25 inhibition of alphaviruses independently of the host interferon response, suggesting that this antiviral effect is a direct consequence of ubiquitination. Consistent with that, we observed diminished antiviral activity upon knockdown of several TRIM25-R54P specific interactors including NME1 and PABPC4. Our findings highlight that multiple substrates mediate the cellular and antiviral activities of TRIM25, illustrating the multi-faceted role of this ubiquitination network in modulating diverse biological processes.

## Author summary

Ubiquitin E3 ligases each interact with and ubiquitinate a subset of cellular proteins, thereby regulating specific cellular processes. Tripartite motif containing protein 25 (TRIM25) is one such E3 ligase involved in carcinogenesis and antiviral innate immunity. TRIM25 catalytic activity is indispensable for the host antiviral response against

Institute and Charity Treks (www.uclahealth.org/aidsinstitute) 2019 Seed Grant, the Johanna and Joseph H. Shaper Family, grant Johanna and Joseph H. Shaper Family Chair to MMHL. This study was also funded by the NIH Ruth L. Kirschstein Multidisciplinary Training Grant in Microbial Pathogenesis (www.mimg.ucla.edu/microbial-pathogenesis-training-grant/) grant NRSA AI007323, the UCLA Warsaw Fellowship (www.mimg.ucla.edu) and the UCLA Whitcome Fellowship (www.mbi.ucla.edu/resources-for-students/whitcome-fellowships) to EY. The funders had no role in study design, data collection and analysis, decision to publish, or preparation of the manuscript.

**Competing interests:** The authors have declared that no competing interests exist.

alphaviruses, an arthropod-borne group of RNA viruses possessing expanding distributions and pandemic potential. However, it remains poorly understood which TRIM25 substrates mediate viral inhibition. To complicate the matter, identification of E3 ligase substrates is technically challenging, given the transient nature of ligase-substrate interactions. Here, we present the first comprehensive ubiquitinome study utilizing a novel "substrate-trapping" approach to identify TRIM25 target proteins. We found that TRIM25 ubiquitinates key players in translational and nucleic acid metabolic processes, specifically involving stress granule formation, nonsense-mediated mRNA decay, nucleotide synthesis, and translation initiation. In addition, TRIM25 ligase activity is critical for its inhibition of diverse alphaviruses through viral translation suppression, highlighting the importance of ubiquitination in driving antiviral activity in this context. Our study both provides new insights into understanding the innate immune and cell biology roles of TRIM25 and paves the way forward for identification of novel TRIM substrates at large.

## Introduction

Addition of ubiquitin, or ubiquitination, is a post-translational modification that is highly conserved in eukaryotic organisms, and operates in myriad cellular pathways. Ubiquitin is a small, 76 amino acid protein that must be activated by E1 enzymes, passed to E2 carrier enzymes, and finally covalently attached to lysines on substrates by E3 ligases. Though only one enzyme is needed at each step, their numbers vary widely. Humans encode 2 E1 enzymes, about 40 E2 enzymes, and upwards of 600 E3 ligases [1,2]. This vast number of E3 ligases is needed because they determine substrate specificity; however, the means by which E3 ligases identify their substrates and the array of substrates ubiquitinated by any given E3 ligase remain largely unknown.

The tripartite motif containing protein (TRIM) family is one of the largest families of E3 ligases, with over 70 *TRIM* genes in humans [3]. TRIMs share three common domains at their N-terminus–the catalytic RING domain, 1 to 2 B-Box domains, and a coiled-coil domain–but differ in their C-termini [3]. These varied C-termini determine TRIM substrate specificity, allowing this large family of proteins to regulate diverse cellular processes, including but not limited to viral restriction, immune signaling, stress responses, proliferation, and differentiation [4–7]. Mutations in TRIM genes have been associated with rare genetic diseases, including developmental, muscular, and neurological disorders [8,9]. However, development of targeted therapeutic approaches has been hindered by not only the lack of knowledge on their specific substrates, but also the frequent involvement of TRIMs in multiple cellular processes. One prime example is TRIM25, which functions in both cancer and antiviral innate immunity [10,11]. When examined in the context of cancer, TRIM25-mediated ubiquitination primarily targets varied proteins for proteolytic degradation, which can either enhance or hinder carcinogenesis [12–16].

Many of the TRIM proteins are upregulated by interferon (IFN) and play significant roles in the host innate immune response [7]. Upon detection of viral infection by the host cell, type I IFN is produced, inducing expression of hundreds of IFN-stimulated genes (ISGs) to establish an antiviral environment [17,18]. TRIM25 is one such ISG which not only stimulates innate immune signaling by ubiquitinating and activating the dsRNA sensor RIG-I, but also functions as a critical co-factor of another ISG, zinc finger antiviral protein (ZAP) [19–21]. While TRIM25 has been shown to complex with ZAP in the context of several different viral infections [22], its ligase activity has only been tied to its participation in blocking translation

of incoming RNA genomes of alphavirus (family Togaviridae) [20]. Given that ubiquitination of ZAP or lack thereof fails to affect its viral translation inhibition [20], it is likely that TRIM25 antiviral involvement depends on its ubiquitination of other cellular proteins. Interestingly, both TRIM25 and ZAP not only bind viral RNA but also interact with other RNA binding proteins, implying that proteins involved in RNA processes may feature prominently among TRIM25 substrates [23–26].

In light of this question, we set out to identify novel TRIM25 substrates that may play a role in translation and RNA processes. Because identification of E3 ligase substrates is technically challenging due to the transient nature of ligase-substrate interactions, we utilized a "substrate trapping" approach similar to previously reported [27] to capture TRIM25 interactors in a co-immunoprecipitation (IP)/mass spectrometry (MS) experiment. We sought to generate a TRIM25 mutant that would be unable to interact with the upstream E2 carrier enzyme, thus simultaneously rendering it incapable of ubiquitination and prolonging its interactions with substrates. We identified a point mutation, R54P, in the TRIM25 RING catalytic domain, which almost completely abolishes its autoubiquitination in cells.

While almost all of the more highly enriched interactors are shared by both TRIM25-WT and -R54P, we found that TRIM25-R54P enriches for additional interactors as compared to TRIM25-WT. Further characterization of some of the most highly enriched interactors, Ras-GTPase-activating protein SH3-domain binding proteins (G3BP) 1 and 2, RNA helicase up-frameshift protein 1 (UPF1), nucleoside diphosphate kinase 1 (NME1), and poly-adenylate binding protein cytoplasmic 4 (PABPC4), has validated their identification as novel TRIM25 substrates. We identified NME1 and PABPC4 as TRIM25-R54P-specific interactors during viral infection. Moreover, upon characterization of its antiviral activity, the TRIM25-R54P mutant demonstrates a complete loss of inhibition against a panel of Old World and New World alphaviruses albeit higher IFN and ISG expression compared to WT, suggesting that ubiquitination of TRIM25 substrates directly leads to activation of an antiviral state. Altogether, we have identified both known and novel interactors as TRIM25 substrates, and demonstrated the validity of this "substrate trapping" approach in identifying bona fide E3 ligase substrates. We have shed light on the ways that TRIM25-mediated ubiquitination might target substrates to modulate translation, nucleic acid metabolism, and antiviral response, paving the way for further work characterizing the critical role of TRIMs in diverse cellular and viral processes.

## Results

### Point mutations in TRIM25 RING domain almost completely abolish TRIM25 auto-polyubiquitination

It is technically challenging to identify E3 ligase-substrate interactions as they are often transient, resulting in proteasomal degradation or a change in localization or activity of the substrates. In order to enrich for transient E3 ligase-substrate interactions, we turned to a less conventional co-IP approach that makes use of E3 mutants unable to interact with E2 conjugating enzymes. This prevents ubiquitin transfer to E3 substrates and their subsequent targeting to other cellular pathways and as a result, "trapping" these substrates. This approach successfully identified the cellular 'structural maintenance of chromosomes' (Smc) complex Smc5/6 as being targeted by hepatitis B virus X protein for ligase-mediated degradation [27]. We hypothesized that a similar approach would serve to identify TRIM25 substrates, which will be immunoprecipitated more robustly with a TRIM25 E2 binding mutant than with TRIM25-WT, as the former is unable to mediate transfer of ubiquitin from E2 to substrates.

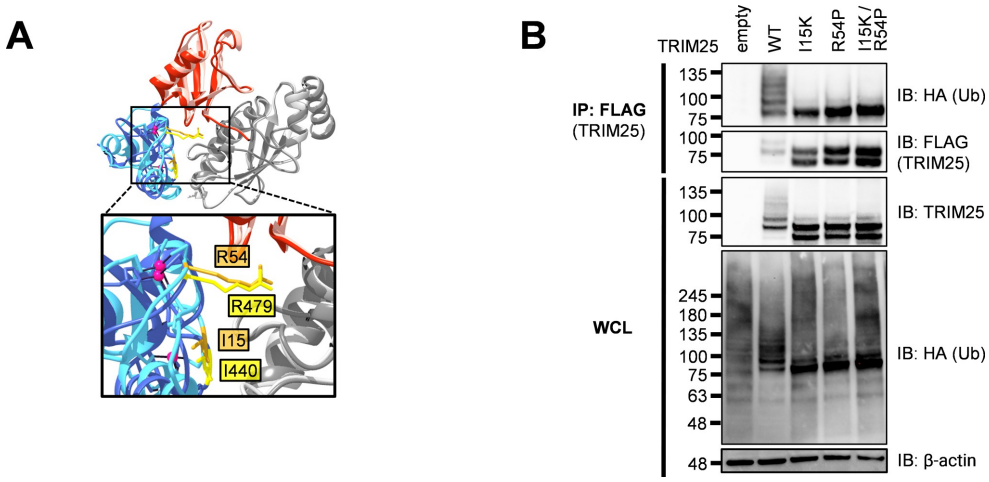


**Fig 1. Individual TRIM25 RING residues required for TRIM25 autoubiquitination.** (A) Alignment of the RING E3 ligases MDM2 (dark blue) and TRIM25 (light blue) in complex with ubiquitin (red) and the E2 UbcH5 (gray), performed using UCSF Chimera [30]. Highlighted in gold (TRIM25) and yellow (MDM2) are homologous residues. PDB: 5MNJ (MDM2), 5EYA (TRIM25). (B) Western blot of 293T cells transfected with FLAG-TRIM25 mutants and HA-ubiquitin (Ub). Lysates were subjected to FLAG IP. Data representative of three independent experiments.

https://doi.org/10.1371/journal.ppat.1010743.g001

Residues important for the RING-E2 interaction and thus necessary for ligase activity have already been identified in the RING E3 ligase MDM2 [28]. We aligned the structure of the TRIM25 RING domain complexed to E2-ubiquitin (Ub) to the analogous MDM2-E2-Ub structure and identified two conserved critical E2 interaction residues in TRIM25 RING, I15 and R54 (Fig 1A). To assess loss of ligase activity, we transfected HA-tagged Ub and FLAG-tagged TRIM25 into 293T cells and immunoprecipitated TRIM25 in denaturing conditions. We then blotted for HA-Ub, wherein polyubiquitination manifests as a ladder of bands. These TRIM25 E2 binding mutants (I15K and R54P), are deficient in auto-polyubiquitination, suggesting successful crippling of ligase activity (Fig 1B). Individual E2 binding mutants retain a mono-Ub band (Fig 1B), so we generated the double mutant I15K/R54P, which did not display further reduction in ligase activity (Fig 1B). Therefore, we selected the R54P mutant for future co-IP/MS studies since this mutation has previously been shown to reduce TRIM25 catalytic activity and polyubiquitin chain formation [29].

## Substrate trapping approach enriches for novel TRIM25 interactors

Next, we asked what proteins are modified by TRIM25, as identification of these substrates will elucidate how ubiquitination facilitates TRIM25-mediated cellular and antiviral activities. We first used CRISPR-Cas9 to generate a TRIM25 KO 293T cell line (S1 Fig). We then stably integrated doxycycline (dox) inducible FLAG-tagged TRIM25 wild-type (WT) and mutant R54P using the ePiggyBac (ePB) transposon system [31], where both TRIM25-WT and TRIM25-R54P are similarly induced in a dose-dependent manner (Fig 2A). TRIM25 protein levels are comparable upon detection using a FLAG or TRIM25-specific antibody (Fig 2A).

To capture TRIM25 substrates, we performed two independent co-IP/MS experiments using our reconstituted TRIM25 KO 293T cell lines (Fig 2B). We induced TRIM25-WT or -R54P expression in the presence or absence of the prototype alphavirus Sindbis virus (SINV),

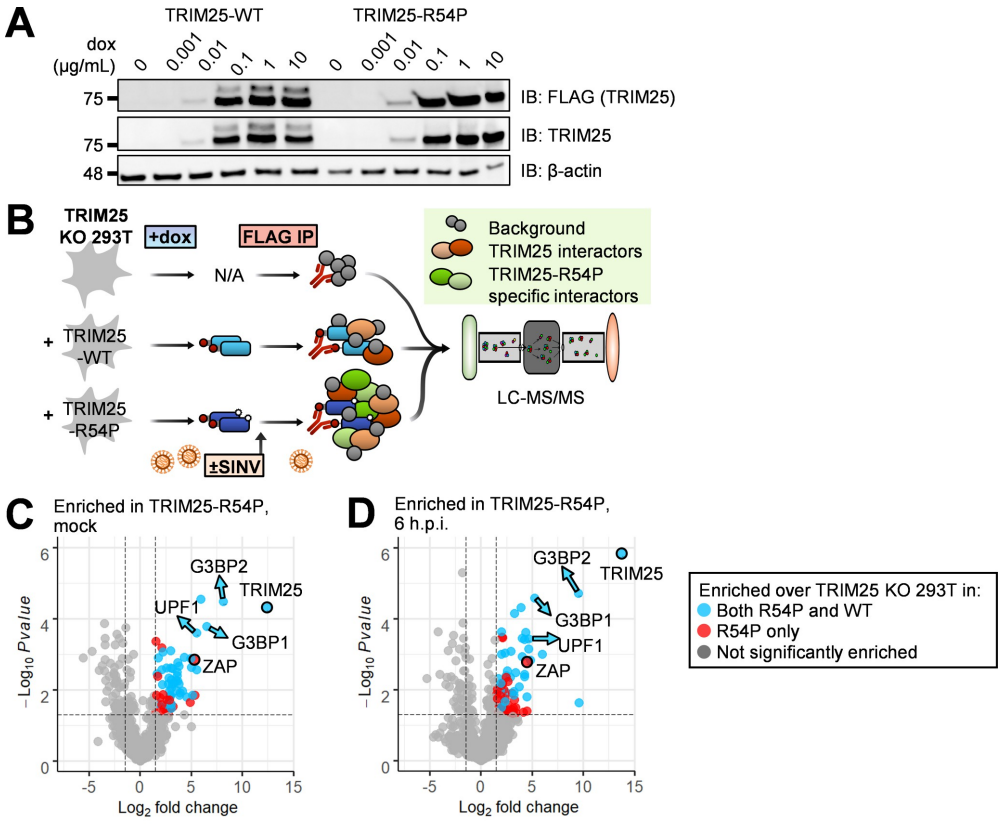


**E**

| | P value | |
|---|---|---|
| **Gene Ontology Term** | **mock** | **6 h.p.i.** |
| Nuclear-transcribed mRNA catabolic process, NMD | 9.17E-26 | 5.55E-09 |
| SRP-dependent cotranslational protein targeting to membrane | 3.68E-23 | 5.12E-06 |
| Translational initiation | 1.03E-22 | 1.30E-08 |
| Viral transcription | 4.96E-22 | 1.03E-05 |
| Translation | 2.41E-20 | 4.95E-07 |
| rRNA processing | 1.00E-19 | 1.29E-04 |

**Fig 2. TRIM25 co-IP/MS identifies TRIM25 interactors.** (A) Western blot of TRIM25-WT and -R54P doxycycline (dox)-inducible 293T cell lines in the presence of increasing amount of dox (0, 0.001, 0.01, 0.1, 1, and 10 μg/mL). Data are representative of two independent experiments. (B) Schematic of co-IP/MS experiment to identify TRIM25 interactors. (C-D) Volcano plots of proteins significantly enriched over TRIM25 KO background in TRIM25-R54P co-IP/MS in the (C) absence or (D) presence of viral infection. Data representative of two independent experiments. Blue dots represent proteins that were also significantly enriched in TRIM25-WT co-IP and red dots represent proteins that were only enriched in TRIM25-R54P co-IP. Proteins were counted as enriched when log2FC>1.5 and -log10Pvalue>1.3 (Pvalue<0.05). The R package EnhancedVolcano [32] was used to generate volcano plots. (E) Gene ontology terms significantly enriched in all unique TRIM25-WT and TRIM25-R54P interactors. Analysis performed for GO terms in biological processes using DAVID [33,34].

https://doi.org/10.1371/journal.ppat.1010743.g002

performed a FLAG IP to enrich for TRIM25, and analyzed the resultant protein mixture using MS. TRIM25 KO 293T cells with dox added were used as a control, since previous work by our lab found that dox treatment nonspecifically affects viral replication in other systems [35]. We found that this "substrate trapping" approach enriches for interactors specific to TRIM25-R54P under both mock and infected conditions (Fig 2C and 2D, red circles). These TRIM25-R54P-specific interactors tend to have lower fold change in abundance over background than interactors common to both TRIM25-WT and TRIM25-R54P (Fig 2C and 2D, blue circles), suggesting that the TRIM25-R54P co-IP/MS captures weaker interactions not identified with TRIM25-WT. After filtering for interactors enriched in both independent experiments, we found that TRIM25-R54P enriches for 14 unique interactors under mock conditions (Table 1) and that almost all TRIM25-WT interactors (25 of 30) are also present as TRIM25-R54P interactors (Table 2), indicating that TRIM25-R54P is otherwise functionally similar to TRIM25-WT. During viral infection, TRIM25-R54P enriches for all TRIM25-WT interactors in addition to 16 unique interactors (Tables 3 and 4), suggesting an effective "substrate trap." Interestingly, we found that the number of TRIM25 interactors drastically decreases during viral infection for both TRIM25-WT (29 to 7 interactors; Tables 2 and 4) and TRIM25-R54P (38 to 23 interactors; Tables 1 and 3). We used DAVID bioinformatics resources [33,34] to find that TRIM25 interactors are highly enriched in GO terms involved in translation, RNA metabolism, and viral transcription (Fig 2E). This is in line with our hypothesis that TRIM25 substrates mediate diverse cellular and viral processes as a consequence of ubiquitination.

## TRIM25 interacts with G3BP1 and 2 through a conserved binding motif and modifies them with predominantly K63 polyubiquitin chains

Among the most enriched TRIM25-R54P interactors in the presence and/or absence of SINV infection (Tables 1 and 3), we identified the core stress granule proteins G3BP1 and 2, RNA helicase UPF1 (Fig 2C and 2D, blue arrows), metastatic suppressor and nucleoside kinase NME1, and poly(A) binding protein PABPC4 as high priority candidates given our interest in RNA metabolic and translation processes (G3BP1 and 2, UPF1, PABPC4) and TRIM25's role in regulating carcinogenesis (NME1). Next, we asked whether any of these are TRIM25 ubiquitination substrates.

Both G3BP1 and G3BP2, hereafter collectively referred to as G3BP, associate very strongly with TRIM25 in the co-IP/MS (Tables 1–4; G3BP1, log2FoldChange 2.5–6.5; G3BP2, log2FoldChange 5.5–9.5). G3BP normally function in stress granule (SG) assembly, interacting with RNA and other cellular proteins to induce SG formation [36,37]. Interestingly, the Old World alphaviruses exploit G3BP to promote their own replication [38–41]. These viruses utilize their non-structural protein 3 (nsP3) to recruit G3BP into viral replication complexes, which disrupts antiviral SG formation [42], clusters viral replication complexes [41], and recruits translation initiation machinery [43]. By doing so, alphaviruses enhance viral replication at the cost of endogenous G3BP function.

Previous work identified an FGDF peptide motif in alphavirus nsP3 which binds with high affinity to G3BP [42,44]. More recent work characterizing viral-host interaction motifs has uncovered a conserved G3BP-binding motif, ΦxFG (where Φ is a hydrophobic residue) [45]. This G3BP interaction motif is present in both viral and host proteins, such as the cellular SG protein and known G3BP interactor USP10, and is remarkably similar to the alphavirus nsP3-G3BP interaction motif, FGDF, but likely binds with lower affinity [45]. Moreover, TRIM25 was identified as a G3BP1 interaction partner [45]. Mutating the latter two amino acids in the TRIM25-specific motif (404-PTFG-407), to alanine (404-PTAA-407) was

**Table 1. TRIM25-R54P interactors in the absence of virus.** Interactors pulled down in both independent experiments shown here; proteins also enriched in TRIM25-WT co-IP are italicized and bolded. Fold change = FC. In EXP #2, the "i" prefacing log2FC and Pvalue refers to how missing data values were imputed.

| Protein | EXP #1 log2FC | EXP #2 ilog2FC | EXP #1 -log10Pvalue | EXP #2 -log10iPvalue |
|---|---|---|---|---|
| ***TRIM25*** | ***12.39*** | ***7.51*** | ***4.29*** | ***2.12*** |
| G3BP2 | 8.11 | 5.55 | 4.48 | 1.50 |
| ***G3BP1*** | ***6.50*** | ***4.03*** | ***3.78*** | ***1.73*** |
| ***PABPC1*** | ***5.93*** | ***5.10*** | ***4.55*** | ***3.28*** |
| ***UPF1*** | ***5.50*** | ***4.79*** | ***3.60*** | ***1.44*** |
| RPL27 | 5.34 | 3.69 | 1.84 | 1.55 |
| ZC3HAV1 | 5.32 | 5.31 | 2.83 | 1.42 |
| ***ZCCHC3*** | ***5.12*** | ***3.75*** | ***1.85*** | ***1.78*** |
| RPL36 | 4.98 | 3.48 | 2.88 | 1.79 |
| MOV10 | 4.91 | 4.49 | 1.64 | 1.80 |
| ***RPLP2*** | ***4.13*** | ***5.86*** | ***1.96*** | ***1.55*** |
| ***SSB*** | ***3.89*** | ***4.48*** | ***1.91*** | ***1.71*** |
| ***RPS3A*** | ***3.79*** | ***2.69*** | ***2.16*** | ***1.89*** |
| ***MRPL11*** | ***3.77*** | ***5.47*** | ***2.66*** | ***1.40*** |
| RPL3 | 3.66 | 2.15 | 2.24 | 1.79 |
| ***RPS12*** | ***3.66*** | ***3.49*** | ***2.76*** | ***1.89*** |
| ***NME1*** | ***3.61*** | ***4.79*** | ***2.39*** | ***1.79*** |
| ***IGF2BP3*** | ***3.56*** | ***3.28*** | ***1.98*** | ***1.50*** |
| ***RPS8*** | ***3.26*** | ***3.27*** | ***2.19*** | ***1.75*** |
| DNAJA1 | 3.17 | 3.92 | 2.61 | 1.91 |
| RPL21 | 3.06 | 2.39 | 1.48 | 1.47 |
| ***DDX21*** | ***3.05*** | ***1.89*** | ***1.59*** | ***1.73*** |
| ***RPL7A*** | ***3.04*** | ***2.52*** | ***2.05*** | ***1.73*** |
| ***DDX50*** | ***3.03*** | ***3.66*** | ***1.48*** | ***1.53*** |
| ***RPL14*** | ***3.01*** | ***2.79*** | ***1.83*** | ***1.79*** |
| ***HSPA9*** | ***2.98*** | ***2.54*** | ***3.10*** | ***1.73*** |
| ***RPL8*** | ***2.95*** | ***2.64*** | ***2.62*** | ***1.50*** |
| ***RPL4*** | ***2.95*** | ***1.93*** | ***1.80*** | ***1.50*** |
| ***RPL30*** | ***2.92*** | ***4.99*** | ***1.86*** | ***1.81*** |
| RPL6 | 2.88 | 1.95 | 1.97 | 1.50 |
| RPL19 | 2.77 | 5.27 | 1.34 | 1.36 |
| CXorf56 | 2.62 | 2.59 | 1.71 | 1.34 |
| ***MRPS25*** | ***2.56*** | ***3.34*** | ***2.61*** | ***1.54*** |
| POLDIP2 | 2.24 | 2.45 | 3.07 | 1.64 |
| ***IGF2BP2*** | ***2.20*** | ***3.23*** | ***2.15*** | ***1.46*** |
| ***HSPA5*** | ***2.10*** | ***2.61*** | ***2.56*** | ***1.79*** |
| NCL | 1.95 | 2.58 | 1.78 | 2.63 |
| ***HSPA8*** | ***1.64*** | ***2.01*** | ***2.45*** | ***1.79*** |
| RTRAF | 1.60 | 1.76 | 1.84 | 1.31 |

https://doi.org/10.1371/journal.ppat.1010743.t001

sufficient to abolish TRIM25-G3BP1 interaction [45]. Meanwhile, TRIM25 and G3BP2 have previously been shown to interact in the context of prostate cancer [46]. To examine whether this motif is also necessary for TRIM25-G3BP2 interaction, we co-transfected myc-tagged G3BP into TRIM25 KO 293T cells along with FLAG-tagged TRIM25-WT, -R54P, or -PTAA, and performed a FLAG IP to pull down TRIM25. While both TRIM25-WT and -R54P robustly associate with both G3BP1 and 2, TRIM25-PTAA does not associate with either G3BP1 or 2 (Fig 3A), validating our co-IP/MS identification of G3BP as TRIM25 interactors.

**Table 2. TRIM25-WT interactors in the absence of virus.** Interactors pulled down in both independent experiments shown here; proteins also enriched in TRIM25-R54P co-IP in both independent experiments are italicized and bolded. Fold change = FC. In EXP #2, the "i" prefacing log2FC and Pvalue refers to how missing data values were imputed.

| Protein | EXP #1 log2FC | EXP #2 ilog2FC | EXP #1 -log10Pvalue | EXP #2 -log10iPvalue |
|---|---|---|---|---|
| ***TRIM25*** | ***12.35*** | ***7.21*** | ***4.29*** | ***2.36*** |
| ***NME1*** | ***5.89*** | ***5.69*** | ***3.19*** | ***2.11*** |
| ***PABPC1*** | ***5.18*** | ***4.36*** | ***4.32*** | ***2.65*** |
| ***UPF1*** | ***4.15*** | ***4.99*** | ***3.13*** | ***1.56*** |
| ***G3BP1*** | ***3.84*** | ***4.38*** | ***2.89*** | ***2.08*** |
| ***SSB*** | ***3.67*** | ***5.28*** | ***1.82*** | ***1.67*** |
| ***RPS12*** | ***3.52*** | ***3.02*** | ***2.70*** | ***2.24*** |
| ***DDX21*** | ***3.52*** | ***1.60*** | ***1.79*** | ***2.07*** |
| ***ZCCHC3*** | ***3.41*** | ***2.47*** | ***1.50*** | ***1.50*** |
| ***MRPL11*** | ***3.11*** | ***4.50*** | ***2.36*** | ***1.83*** |
| ***MRPS25*** | ***3.11*** | ***5.37*** | ***2.93*** | ***1.81*** |
| ***RPS3A*** | ***3.02*** | ***1.92*** | ***1.82*** | ***2.11*** |
| ***RPL14*** | ***2.91*** | ***2.56*** | ***1.78*** | ***1.71*** |
| ***RPS8*** | ***2.86*** | ***3.07*** | ***1.99*** | ***2.11*** |
| RPL23A | 2.83 | 2.50 | 1.42 | 2.29 |
| LARP1 | 2.82 | 2.72 | 1.75 | 1.65 |
| ***HSPA9*** | ***2.78*** | ***2.55*** | ***2.98*** | ***1.98*** |
| ***DDX50*** | ***2.78*** | ***5.52*** | ***1.38*** | ***1.87*** |
| ***RPLP2*** | ***2.71*** | ***5.81*** | ***1.37*** | ***1.36*** |
| ***RPL7A*** | ***2.68*** | ***2.05*** | ***1.87*** | ***2.11*** |
| ***RPL8*** | ***2.67*** | ***1.91*** | ***2.46*** | ***1.46*** |
| ***IGF2BP3*** | ***2.67*** | ***3.65*** | ***1.56*** | ***1.66*** |
| ***HSPA5*** | ***2.36*** | ***2.77*** | ***2.75*** | ***2.05*** |
| FMR1 | 2.16 | 2.14 | 1.38 | 1.56 |
| ***RPL4*** | ***2.09*** | ***1.96*** | ***1.33*** | ***2.08*** |
| ***RPL30*** | ***1.98*** | ***4.99*** | ***1.33*** | ***2.66*** |
| RPL32 | 1.91 | 2.10 | 1.44 | 2.05 |
| ***IGF2BP2*** | ***1.73*** | ***2.16*** | ***1.80*** | ***1.45*** |
| ***HSPA8*** | ***1.66*** | ***2.26*** | ***2.46*** | ***1.65*** |
| FXR1 | 1.52 | 4.86 | 2.66 | 1.59 |

https://doi.org/10.1371/journal.ppat.1010743.t002

We then used the ePB transposon system to reconstitute TRIM25 KO 293T cells with dox inducible TRIM25-PTAA. To establish that TRIM25 ubiquitinates G3BP and that the TRIM25-G3BP interaction is necessary for ubiquitination, we co-transfected myc-tagged G3BP with HA-Ub into TRIM25-WT, -R54P, and -PTAA inducible cell lines. After inducing TRIM25 expression, we performed a myc IP and probed for the presence of ubiquitinated G3BP. We found that both G3BP1 and 2 are robustly polyubiquitinated only in the presence of TRIM25-WT (Fig 3B), again validating our co-IP/MS identification of G3BP as TRIM25 substrates. No ubiquitination is detected in the presence of ligase-deficient TRIM25-R54P, whereas ubiquitination is dramatically diminished in the presence of G3BP-interaction deficient TRIM25-PTAA (Fig 3B). Interestingly, TRIM25 appears to more robustly ubiquitinate G3BP2 as compared to G3BP1 (Fig 3B). Given the TRIM25-mediated polyubiquitination of G3BP1 and 2, we then characterized G3BP ubiquitination linkage type. To do so, we transfected our TRIM25-WT inducible cell line with myc-G3BP1 or -2 and different forms of HA-Ub: -WT, -K48, and -K63. Ub-K48 and -K63 have all lysines mutated to arginine except

**Table 3. TRIM25-R54P interactors during viral infection.** Interactors pulled down in both independent experiments shown here; proteins also enriched in TRIM25-WT co-IP in both independent experiments are italicized and bolded. Fold change = FC. In EXP #2, the "i" prefacing log2FC and Pvalue refers to how missing data values were imputed.

| Protein | EXP #1 log2FC | EXP #2 ilog2FC | EXP #1 -log10Pvalue | EXP #2 -log10iPvalue |
|---|---|---|---|---|
| ***TRIM25*** | ***13.82*** | ***6.87*** | ***5.83*** | ***1.28*** |
| G3BP2 | 9.50 | 7.66 | 4.71 | 1.40 |
| G3BP1 | 5.25 | 2.51 | 4.58 | 1.92 |
| NME1 | 4.81 | 3.43 | 2.84 | 1.40 |
| ***H1FX*** | ***4.65*** | ***4.49*** | ***3.14*** | ***1.46*** |
| ***UPF1*** | ***4.64*** | ***5.24*** | ***3.44*** | ***1.94*** |
| ZC3HAV1 | 4.47 | 2.77 | 2.77 | 1.42 |
| RPL8 | 4.26 | 2.98 | 2.36 | 1.80 |
| PABPC4 | 4.25 | 2.67 | 3.42 | 1.42 |
| PABPC1 | 4.24 | 3.54 | 2.44 | 1.44 |
| ***HP1BP3*** | ***4.00*** | ***4.09*** | ***3.44*** | ***1.50*** |
| ***LARP1*** | ***3.93*** | ***4.59*** | ***4.32*** | ***1.61*** |
| ***DDX50*** | ***3.74*** | ***4.14*** | ***2.08*** | ***1.47*** |
| RPL21 | 3.40 | 3.45 | 1.50 | 1.44 |
| RPL29 | 3.38 | 2.53 | 2.48 | 2.06 |
| ***HSPA9*** | ***3.28*** | ***2.04*** | ***4.15*** | ***2.05*** |
| ***ZCCHC3*** | ***3.23*** | ***4.49*** | ***1.95*** | ***1.54*** |
| RPS3A | 3.18 | 1.53 | 1.36 | 1.38 |
| GLYR1 | 3.01 | 2.59 | 1.43 | 1.59 |
| YBX1 | 2.61 | 1.73 | 1.44 | 1.44 |
| GNL3L | 2.47 | 5.28 | 2.35 | 1.58 |
| RPL19 | 2.44 | 2.90 | 2.39 | 1.75 |
| MRPS26 | 1.98 | 1.90 | 1.49 | 1.31 |
| MRPS9 | 1.58 | 2.56 | 2.02 | 1.38 |

https://doi.org/10.1371/journal.ppat.1010743.t003

K48 and K63, respectively, such that only K48 or K63 polyubiquitin chains are able to be formed [47]. We found that both G3BP1 and 2 are most robustly ubiquitinated in the presence of Ub-K63, suggesting that TRIM25 primarily mediates K63-linked ubiquitination of both proteins (Fig 3C). Interestingly, while both G3BP1 and 2 exhibit a lower level of ubiquitination in the presence of Ub-K48, G3BP1 possesses more K48-linked polyubiquitin chains as compared to G3BP2 (Fig 3C), indicating that TRIM25 is able to distinguish between and differentially ubiquitinate these related proteins.

**Table 4. TRIM25-WT interactors during viral infection.** Interactors pulled down in both independent experiments shown here; proteins also enriched in TRIM25-R54P co-IP in both independent experiments are italicized and bolded. Fold change = FC. In EXP #2, the "i" prefacing log2FC and Pvalue refers to how missing data values were imputed.

| Protein | EXP #1 log2FC | EXP #2 ilog2FC | EXP #1 -log10Pvalue | EXP #2 -log10iPvalue |
|---|---|---|---|---|
| ***TRIM25*** | ***13.19*** | ***6.43*** | ***5.75*** | ***1.15*** |
| ***H1FX*** | ***3.95*** | ***3.23*** | ***2.87*** | ***1.74*** |
| ***UPF1*** | ***3.86*** | ***5.51*** | ***3.13*** | ***1.62*** |
| ***HP1BP3*** | ***2.75*** | ***3.84*** | ***2.82*** | ***1.75*** |
| ***ZCCHC3*** | ***2.65*** | ***4.90*** | ***1.78*** | ***1.41*** |
| ***HSPA9*** | ***2.63*** | ***2.35*** | ***3.77*** | ***1.41*** |
| ***LARP1*** | ***2.62*** | ***4.61*** | ***3.63*** | ***1.42*** |
| ***DDX50*** | ***2.44*** | ***5.21*** | ***1.47*** | ***1.46*** |

https://doi.org/10.1371/journal.ppat.1010743.t004

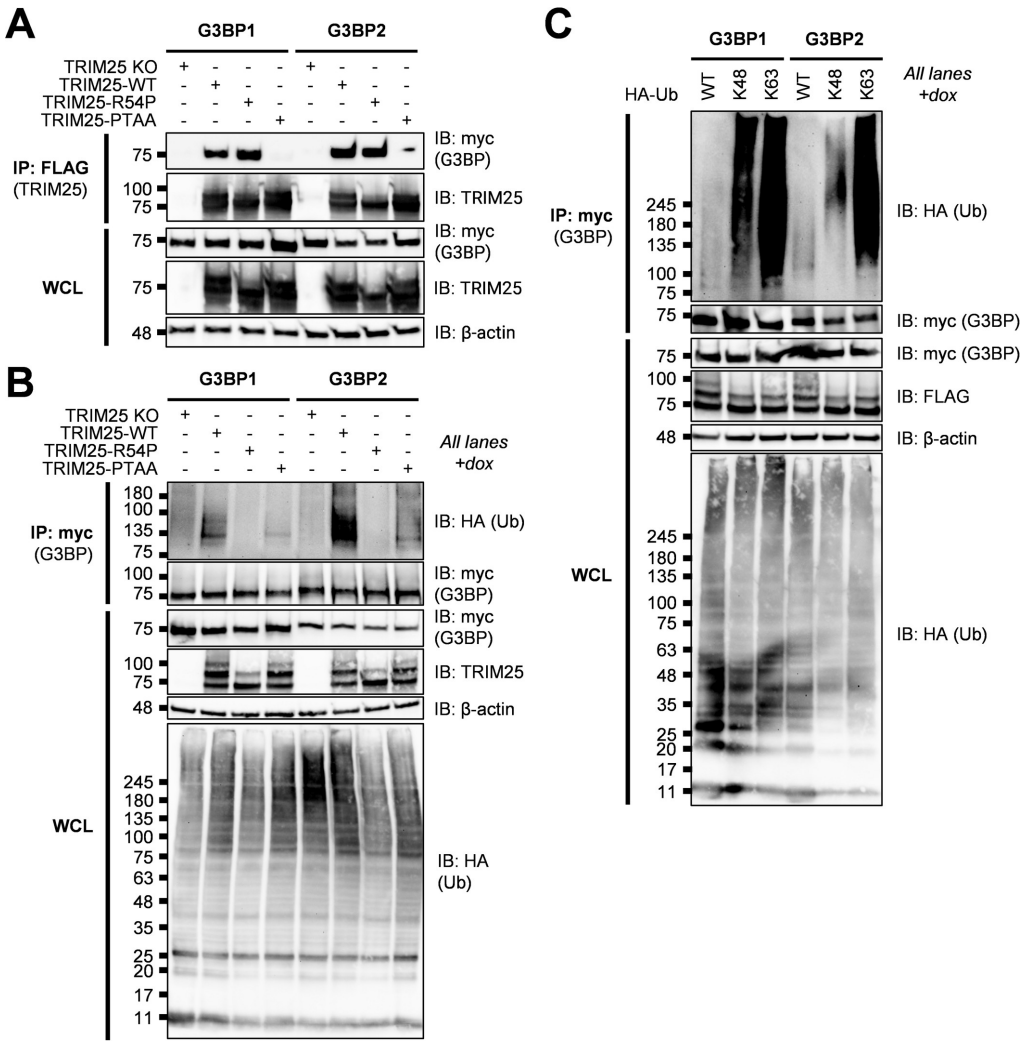


**Fig 3. TRIM25 interacts with and polyubiquitinates G3BP.** (A) Western blot of TRIM25 KO 293T cells transfected with myc-G3BP1/2 and FLAG-TRIM25-WT, -R54P, or -PTAA. Lysates were subjected to FLAG IP. Data are representative of three independent experiments. (B) Western blot of TRIM25 KO and TRIM25-WT, -R54P, or -PTAA inducible cells transfected with myc-G3BP1/2 and HA-Ub-WT in the presence of 1 μg/mL dox. (C) Western blot of TRIM25-WT inducible cells transfected with myc-G3BP1/2 and HA-Ub-WT, -K48, or -K63 in the presence of 1 μg/mL dox. (B-C) Lysates were subjected to myc IP. Data are representative of three independent experiments.

https://doi.org/10.1371/journal.ppat.1010743.g003

We then asked whether TRIM25-G3BP interaction and G3BP ubiquitination are required for TRIM25 antiviral activity. We found that overexpression of TRIM25-PTAA suppresses SINV replication (S2A Fig) and translation (S2B Fig) similarly to TRIM25-WT, suggesting that loss of TRIM25-G3BP interaction or G3BP ubiquitination is not sufficient to restore

SINV infection. It has been demonstrated that different alphaviruses display differing degrees of dependency on G3BP for their replication, wherein SINV is partially reliant and chikungunya virus (CHIKV) is completely reliant on G3BP [41,48]. We hypothesized that a more G3BP-reliant virus such as CHIKV might be more sensitive to any antiviral mechanisms that are dependent on G3BP. In such a system, TRIM25-PTAA, which is unable to interact with and efficiently ubiquitinate G3BP to potentially disrupt their pro-viral functions, may not be as antiviral as TRIM25-WT. Interestingly, inhibition of CHIKV infection is also dependent on TRIM25 with functional ligase activity as TRIM25-R54P restores virion production to similar levels as TRIM25 KO (S2C Fig). However, we found no significant difference between TRIM25-WT and TRIM25-PTAA in their ability to suppress virion production (S2C Fig). Overall, though we validated G3BP interaction with and ubiquitination by TRIM25, we did not find that the TRIM25-G3BP axis is sufficient for TRIM25 antiviral activity.

## TRIM25 interacts with and mono-ubiquitinates UPF1 at K592

Moreover, UPF1 associates very strongly with TRIM25 in the co-IP/MS (Tables 1–4, log2FoldChange 3.9–5.5), supporting a role for UPF1 as a novel TRIM25 interactor. UPF1 is best known for its central role in nonsense-mediated mRNA decay (NMD), where it is recruited to premature termination codons to catalyze the NMD pathway, inhibiting further translation and recruiting other RNA-degrading enzymes [49]. UPF1 has also been implicated in serving an antiviral role in the context of alphavirus infection [50]. The authors of this study found that depletion of NMD components, including UPF1, promotes viral replication; further investigation revealed that UPF1 likely destabilizes incoming viral RNA genomes [50].

We first validated that TRIM25 interacts with UPF1. To do so, we transfected V5-tagged UPF1 into TRIM25 inducible cell lines, then induced for TRIM25-WT or -R54P expression with dox, and performed a FLAG IP to pull down TRIM25. We found that UPF1 is robustly detected only when TRIM25 is induced (Fig 4A), validating the TRIM25-UPF1 interaction identified in our co-IP/MS. To test the hypothesis that TRIM25 ubiquitinates UPF1, we co-transfected V5-tagged UPF1 with HA-Ub into our TRIM25 inducible cell lines and induced TRIM25 expression. We then performed a V5 IP and probed for the presence of ubiquitinated UPF1. We found that UPF1 is more robustly mono-ubiquitinated only in the presence of TRIM25-WT and not ligase-deficient TRIM25-R54P (~50% more by ImageJ quantification, Fig 4B), suggesting that TRIM25 mono-ubiquitinates UPF1. We then identified putative ubiquitination sites by selecting residues that are both identified in a previously published ubiquitinome [51] and predicted via UbPred to be ubiquitinated (Score $>$ 0.70) [52], and mutated these sites to arginine (K281R, K592R). Whereas ubiquitination is unchanged in UPF1 K281R, the introduction of K592R abolishes UPF1 ubiquitination in the presence of TRIM25-WT (Fig 4C). Together, these results validate our co-IP/MS identification of UPF1 as a novel TRIM25 substrate.

Next, we asked whether UPF1 plays a role in TRIM25 antiviral activity. We tested several UPF1 siRNAs and selected the one with the most efficient knockdown (S2D Fig). We observed that UPF1 knockdown only has a significant effect on SINV replication when TRIM25 is absent, though trends toward an effect when TRIM25-WT is induced (S2E and S2F Fig). Together, these data suggest that UPF1 could be antiviral independent of TRIM25 and that it is not critical for the TRIM25 antiviral response.

## TRIM25 polyubiquitinates NME1 but only interacts with endogenous, not ectopically expressed NME1

Finally, we asked whether TRIM25-R54P specific interactors identified in our co-IP/MS were bona fide TRIM25 substrates. We identified NME1 as one of the most enriched TRIM25-R54P

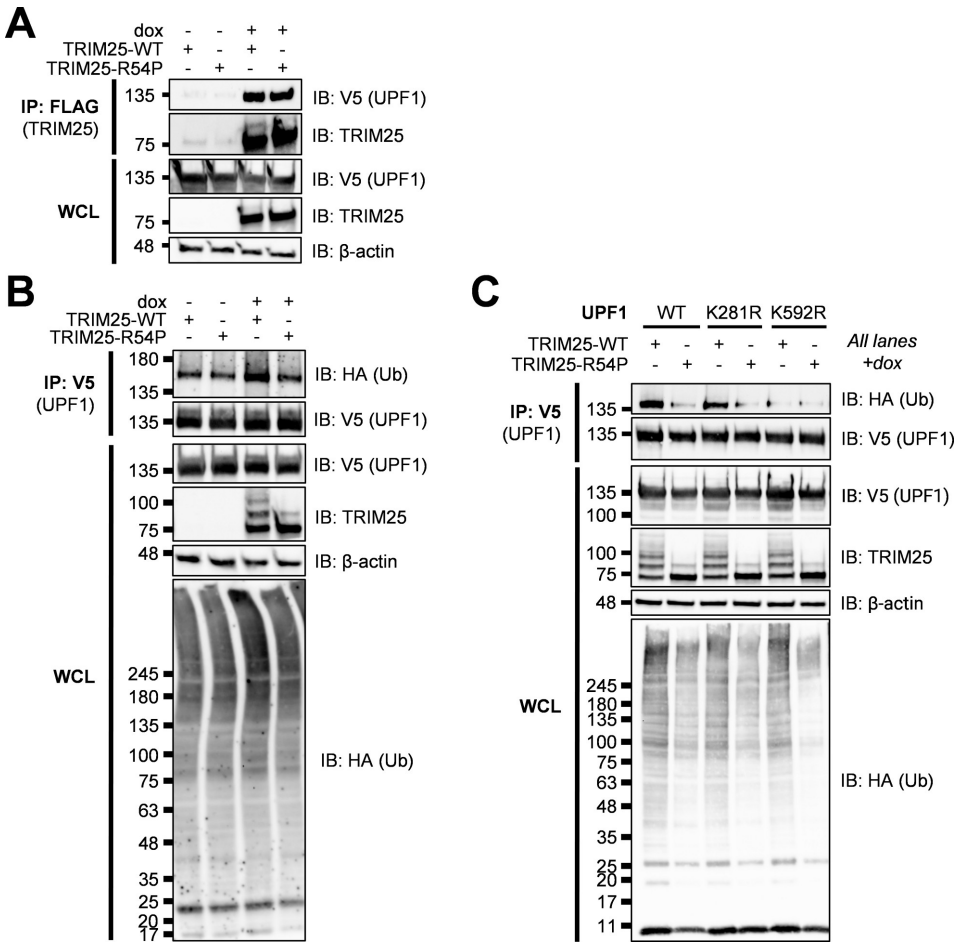


**Fig 4. TRIM25 interacts with and mono-ubiquitinates UPF1.** (A) Western blot of TRIM25 inducible cells transfected with V5-tagged UPF1 in the presence or absence of 1 μg/mL dox. Lysates were subjected to FLAG IP. Data are representative of three independent experiments. (B-C) Western blot of TRIM25 inducible cells transfected with (B) V5-UPF1 or (C) V5-UPF1 WT and mutants (K281R, K592R) and HA-Ub in the presence of 1 μg/mL dox. Lysates were subjected to V5 IP. Data are representative of two independent experiments for (B) and of three independent experiments for (C).

https://doi.org/10.1371/journal.ppat.1010743.g004

interactors in the presence of SINV infection (Table 3, log2FoldChange 3.4–4.8). NME1 is a nucleoside diphosphate kinase and a major synthesizer of non-ATP nucleoside triphosphates, perhaps best characterized in its role in inhibiting cell migration and proliferation of tumor cells via inhibition of MAPK signaling [53]. However, the role of NME1 in viral replication is not well studied [54].

Given its well-characterized role as a metastatic suppressor, we decided to validate NME1 as a TRIM25 ubiquitination substrate. We first set out to validate TRIM25 interaction with

NME1 as identified in our co-IP/MS (Tables 1–3). To do so, we transfected myc-tagged NME1 or UPF1 to serve as a positive control in our TRIM25 inducible lines, induced for TRIM25-WT or -R54P expression, and performed a FLAG IP to pull down TRIM25. We then probed for any associated UPF1 or NME1. While we saw robust association of UPF1 with both TRIM25-WT and -R54P in line with our previous results (Figs 4A and 5A; MW ~135 kDa), we did not identify NME1 (Fig 5A, MW 20–25 kDa). We also performed the reverse IP where we pulled down myc-tagged NME1, but were unable to find any TRIM25 interacting with NME1 (Fig 5B). We hypothesized that this lack of TRIM25-NME1 interaction could be due to functional differences between ectopically expressed myc-NME1 and endogenous NME1, given our successful validation of the other robust TRIM25 interactors from our co-IP/MS, G3BP and UPF1 (Figs 3 and 4). To test this hypothesis, we performed a FLAG IP using our TRIM25 inducible lines and probed for co-IP of endogenous NME1 along with endogenous G3BP and UPF1 as positive controls. In line with our co-IP/MS results, endogenous G3BP, UPF1, and NME1 enrich robustly with TRIM25 pulldown, despite a low level of non-specific binding of NME1 to the FLAG IP in TRIM25 KO 293T cells (Fig 5C).

To test whether TRIM25 ubiquitinates NME1, we transfected myc-tagged NME1 into TRIM25-WT and -R54P inducible cells, induced for TRIM25 expression, and performed a myc IP. We found that NME1 is more robustly polyubiquitinated in the presence of TRIM25-WT as compared to TRIM25-R54P, although we cannot yet rule out the possibility that TRIM25 might mono-ubiquitinate NME1 at multiple sites (Fig 5D).

## TRIM25 interacts with PABPC4 and predominantly modifies it with K63 polyubiquitin chains

We chose PABPC4 as a second example of TRIM25-R54P specific substrate, which was identified as a TRIM25-R54P interactor in the presence of SINV infection (Table 3). PABPC4 is a member of the poly(A) binding protein (PABP) family, which functions in translation initiation by binding the mRNA poly(A) tail, thus regulating mRNA translation and stability [55]. PABPs have been shown to localize to SGs and to inhibit recruitment of UPF1 to 3'UTRs [55,56]. Given their key roles in translation and mRNA metabolism, PABPs are frequently targeted and manipulated by viruses during infection [57]. Interestingly, PABPC4 was recently found to broadly inhibit coronavirus replication by recruiting an E3 ligase to ubiquitinate the viral nucleocapsid protein and target it for degradation [58].

We first validated the TRIM25-PABPC4 interaction by transfecting myc-tagged PABPC4, induced for TRIM25-WT or -R54P expression, and performed a FLAG IP to pull down TRIM25. We then probed for any associated PABPC4. We found that PABPC4 is robustly detected when either TRIM25-WT or TRIM25-R54P is induced (Fig 6A), validating the TRIM25-PABPC4 interaction identified in our co-IP/MS. We also found that both TRIM25-WT and -R54P interact with endogenous PABPC4 (Fig 6B).

We then asked whether TRIM25 ubiquitinates PABPC4. We transfected myc-PABPC4 into TRIM25-WT and -R54P inducible cells, induced for TRIM25 expression, and performed a myc IP. We found that PABPC4 is more robustly polyubiquitinated in the presence of TRIM25-WT as compared to TRIM25-R54P (Fig 6C). Upon characterizing ubiquitination via transfection of Ub-K48 or -K63, we found that like G3BP, PABPC4 is most robustly ubiquitinated in the presence of Ub-K63, suggesting that TRIM25 primarily mediates K63-linked ubiquitination of PABPC4 (Fig 6D).

Taken together, these results suggest that TRIM25-R54P specific interactors identified in our co-IP/MS, such as NME1 and PABPC4, function as bona fide TRIM25 substrates, and that TRIM25 is able to utilize a range of ubiquitin linkages dependent on the substrate context.

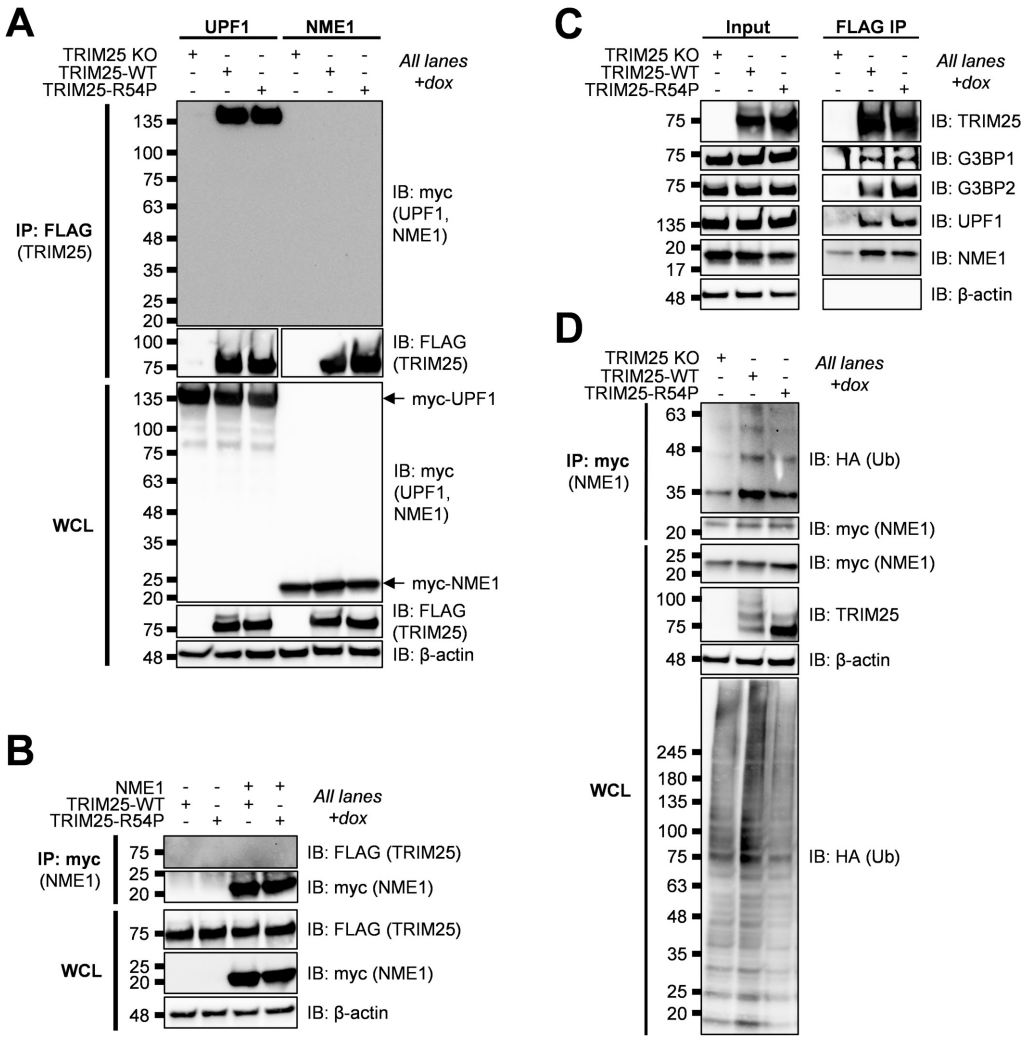


**Fig 5. TRIM25 interacts with and polyubiquitinates NME1.** (A) Western blot of TRIM25 KO and TRIM25 inducible cells transfected with myc-tagged UPF1 or NME1 in the presence of 1 μg/mL dox. Lysates were subjected to a FLAG IP. Data are representative of two independent experiments. (B) Western blot of TRIM25 inducible cells transfected with myc-NME1 in the presence or absence of 1 μg/mL dox. Lysates were subjected to a myc IP. Data are representative of two independent experiments. (C) Western blot of TRIM25 KO and TRIM25 inducible cells in the presence of 1 μg/mL dox. Lysates were subjected to a FLAG IP. Data are representative of two independent experiments. (D) Western blot of TRIM25 KO and TRIM25 inducible cells treated with 1 μg/mL dox and transfected with myc-NME1 and HA-Ub-WT. Lysates were subjected to myc IP. Data are representative of three independent experiments.

https://doi.org/10.1371/journal.ppat.1010743.g005

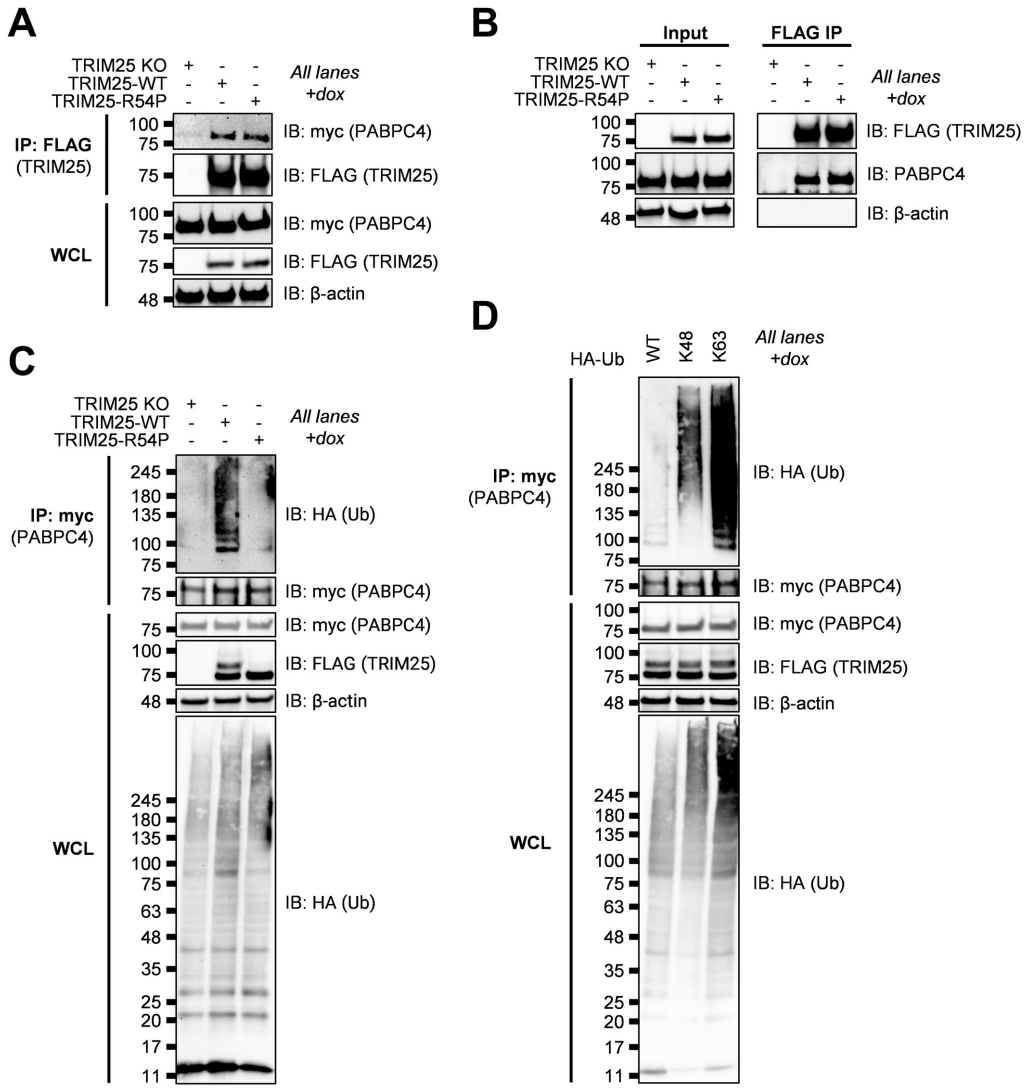


**Fig 6. TRIM25 interacts with and polyubiquitinates PABPC4.** (A) Western blot of TRIM25 KO and TRIM25 inducible cells transfected with myc-tagged PABPC4 in the presence of 1 μg/mL dox. Lysates were subjected to a FLAG IP. Data are representative of two independent experiments. (B) Western blot of TRIM25 KO and TRIM25 inducible cells in the presence of 1 μg/mL dox. Lysates were subjected to a FLAG IP. Data are representative of two independent experiments. (C) Western blot of TRIM25 KO and TRIM25 inducible cells treated with 1 μg/mL dox and transfected with myc-PABPC4 and HA-Ub-WT. Lysates were subjected to myc IP. Data are representative of two independent experiments. (D) Western blot of TRIM25-WT inducible cells treated with 1 μg/mL dox and transfected with myc-PABPC4 and HA-Ub-WT, -K48, or -K63. Lysates were subjected to myc IP. Data are representative of two independent experiments.

https://doi.org/10.1371/journal.ppat.1010743.g006

## TRIM25 antiviral activity is dependent on its ligase activity

Given our identification of diverse host factors as TRIM25 substrates (Figs 3–6), many of which function in translational and RNA processes (Fig 2E) and several of which have known roles in alphavirus replication, we hypothesized that TRIM25 ligase activity is critical for orchestrating an antiviral response.

We used TRIM25 inducible cell lines in the KO background (Fig 2A) to characterize the requirement of ligase activity in TRIM25-mediated viral inhibition. We found that TRIM25-WT, which retains ligase activity, represses SINV replication, whereas ligase mutant TRIM25-R54P does not (Fig 7A). Overexpression of TRIM25-WT (Fig 7A, solid light blue line) dramatically represses SINV replication by 7–15 fold at earlier timepoints (6–12 hours post infection (h.p.i.)) to 43–52 fold at later timepoints (24–40 h.p.i.) compared to TRIM25 KO 293T cell lines (Fig 7A, dotted lines). Interestingly, some replicates fail to initiate infection in the presence of TRIM25-WT, causing seemingly large variability in viral replication. In contrast, overexpression of ligase-deficient TRIM25-R54P (Fig 7A, solid dark blue line) restores SINV replication to levels even higher than the TRIM25 KO background (Fig 7A, dotted lines). Overexpressed TRIM25-R54P may act in a dominant negative manner by binding to and sequestering ZAP, preventing ZAP from interacting with its other co-factors. Similarly, we found that overexpression of TRIM25-WT robustly represses virion production by approximately 36–250 fold at 24–40 h.p.i., whereas overexpression of TRIM25-R54P restores virion production to comparable levels as the TRIM25 KO background (Fig 7B, compare solid light blue line to solid dark blue line).

We then investigated at which step TRIM25 may be acting to inhibit SINV infection. Previous work done by our lab showed that TRIM25 synergized with ZAP in blocking SINV translation [20]. We utilized a temperature-sensitive replication-deficient SINV luciferase reporter virus to characterize the requirement of ligase activity in TRIM25-mediated inhibition of viral translation, since luciferase activity in infected cell lysates represents translation of the incoming viral genome. Overexpressed TRIM25-WT inhibits viral translation by 6 fold at 6 h.p.i. (Fig 7C), supporting our hypothesis that TRIM25 blocks alphavirus replication by inhibiting translation of incoming viral genomes.

While we already examined TRIM25 antiviral activity against the Old World alphavirus CHIKV, wherein TRIM25-WT inhibits robustly and TRIM25-R54P fails to inhibit (S2C Fig), we then asked whether ligase-deficient TRIM25-R54P remains active against other alphaviruses. We tested other Old World (Ross River virus, RRV; o'nyong-nyong virus, ONNV) and New World (Venezuelan equine encephalitis virus, VEEV) alphaviruses. TRIM25-WT remains potently antiviral against all alphaviruses tested (Fig 7D, light blue shaded bar), while overexpression of TRIM25-R54P either has no effect on or restores viral replication to levels higher than the TRIM25 KO background (Fig 7D, dark blue shaded bar). Taken together, these data clearly demonstrate that TRIM25-dependent ubiquitination is required for inhibition of alphavirus replication, specifically through a block in viral translation.

## TRIM25-mediated viral inhibition is independent of changes in the type I IFN response

To exclude the complementary possibility that TRIM25 is exerting antiviral effects through affecting type I IFN or ISG production, we quantified the mRNA of IFN-β and the prominent ISGs IFIT1, ISG15, and OAS2 in the presence of poly(I:C), a dsRNA mimetic and stimulator of innate immune signaling. If TRIM25 antiviral activity is mediated through a strengthened IFN response, we would expect that both IFN and ISG production to increase when TRIM25-WT is induced and to be lower in the presence of TRIM25-R54P due to its defective

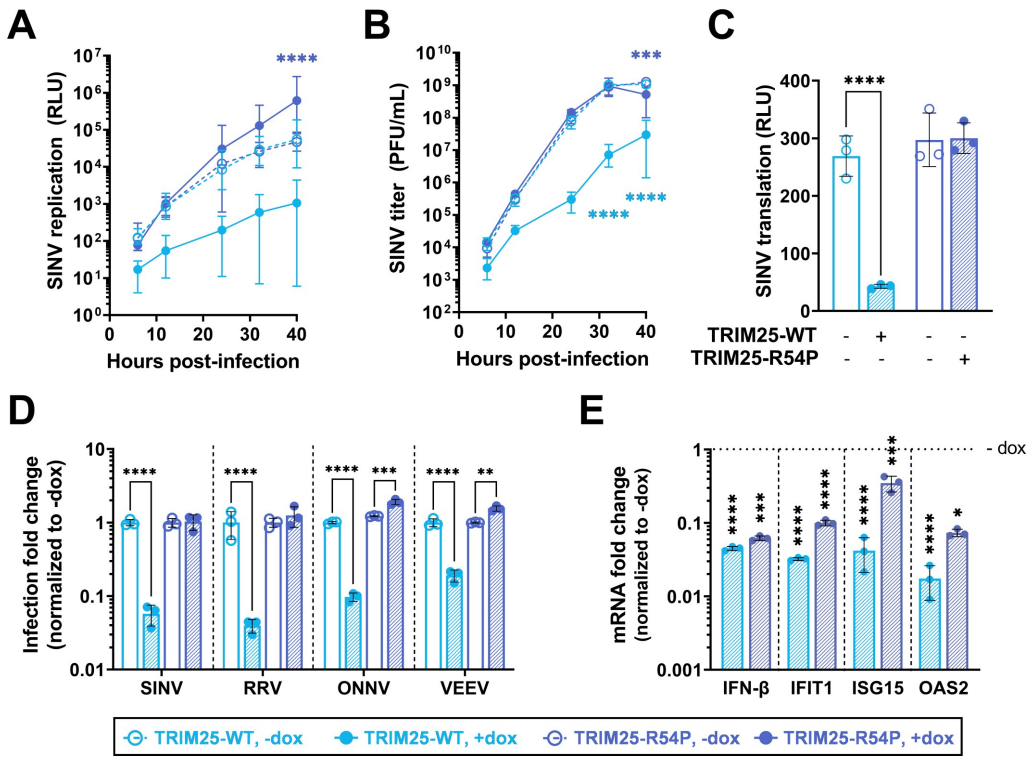


**Fig 7. Point mutation in TRIM25 RING domain cripples TRIM25 antiviral activity.** (A-C) Dox inducible TRIM25-WT or -R54P cells were induced for TRIM25-WT or -R54P expression at 1 μg/mL dox. Cells were infected with (A) SINV Toto1101/Luc at an MOI of 0.01 plaque forming unit (PFU)/cell, and lysed at 6, 12, 24, 32, and 40 hours post infection (h.p.i.); data combined from three independent experiments, error bars indicate range; or (B) Sindbis virus (SINV) Toto1101 at an MOI of 0.01 PFU/cell, harvesting supernatant at 6, 12, 24, 32, and 40 h.p.i. for plaque assays; data representative of two independent experiments, error bars indicate range; or (C) SINV Toto1101/Luc:ts6 at an MOI of 1 PFU/cell and lysed at 6 h.p.i. for measurement of luciferase activity; data representative of two independent experiments, error bars indicate standard deviation. (D) Percent infected cells (GFP+) at MOI of 0.01 PFU/cell (SINV 24 h.p.i.; Ross River virus (RRV) 24 h.p.i.; o'nyong-nyong virus (ONNV) 22 h.p.i.; Venezuelan equine encephalitis virus (VEEV) 10 h.p.i.) were normalized to that of the respective cell line without dox (set to one-fold). Asterisks indicate statistically significant differences, calculated using (A-B, D) Two-way ANOVA and Tukey's multiple comparisons test: **, $p<0.01$; ***, $p<0.001$; ****, $p<0.0001$; (light blue compares WT +/- dox, dark blue compares R54P +/- dox) or (C) Two-way ANOVA and Šidák's multiple comparisons test: ****, $p<0.0001$. Data for each virus (demarcated by dashed lines) was statistically analyzed independently. (E) TRIM25 inducible cells were treated with poly(I:C) in the presence or absence of dox, and RNA was harvested for RT-qPCR analysis. mRNA levels of IFN/ISGs in TRIM25-WT or R54P were normalized to that of the respective cell line without dox (set to one-fold, horizontal dotted line). Data representative of two independent experiments. mRNA fold change for each gene (demarcated by vertical dashed lines) was statistically analyzed independently. Asterisks indicate statistically significant differences as compared to the -dox condition (Two-way ANOVA and Šidák's multiple comparisons test: *, $p<0.05$; ***, $p<0.001$; ****, $p<0.0001$).

https://doi.org/10.1371/journal.ppat.1010743.g007

antiviral activity. Poly(I:C) stimulation works well, inducing IFN-β robustly in the presence and absence of TRIM25 induction (S3 Fig). Surprisingly, we found that overexpression of either TRIM25-WT or TRIM25-R54P significantly suppresses production of IFN-β, IFIT1, ISG15, and OAS2 mRNA in the presence of poly(I:C) (Fig 7E). We also observed that induction of TRIM25-WT results in a more drastic suppression of the ISGs as compared to TRIM25-R54P (Fig 7E, compare light blue to dark blue shaded bar), leading to a higher type I

IFN response in the TRIM25-R54P inducible cell line. Together, these data support our hypothesis that TRIM25 antiviral activity is not mediated through the IFN response.

### Identifying TRIM25-R54P specific interactors as critical for viral inhibition

As we showed that the loss of antiviral activity of TRIM25-R54P does not correlate with the levels of IFN and ISG expression, suggesting a direct consequence of TRIM25-mediated ubiquitination of target proteins, we then decided to examine TRIM25-R54P interactors identified in our co-IP/MS that are not consistently present in the TRIM25-WT enrichment (non-bolded and non-italicized proteins; Tables 1 and 3). These candidate proteins likely exhibit weaker or more transient interactions with TRIM25 and are ubiquitinated by TRIM25. We hypothesized that if any of these interactors are critical for TRIM25 antiviral activity, loss of their expression would result in increased viral replication even in the presence of overexpressed TRIM25-WT. While we initially also assessed a subset of ribosomal proteins identified as TRIM25-R54P interactors, their knockdown results in high cytotoxicity and therefore are excluded from subsequent analyses. We validated most of the TRIM25-R54P interactors that are not present on the TRIM25-WT lists (Tables 1–4) in the absence (Table 1 and Figs 8A and S4A) or presence of viral infection (Table 3 and Figs 8B and S4B). While knockdown of multiple interactors trends towards restoring SINV replication, only loss of RTRAF (Table 1, log2-FoldChange 1.6–1.8) and NME1 (Table 3, log2FoldChange 3.4–4.8) significantly restores SINV replication (Fig 8A and 8B). Moreover, knockdown of MOV10 (Table 1, log2FoldChange 4.5–4.9) approaches significant restoration of SINV replication (Fig 8A, $p = 0.0631$).

We decided to de-convolute the siRNA pools for both NME1 and PABPC4, given our verification of them as bona fide TRIM25 interactors and substrates (Figs 5 and 6). Moreover, loss of NME1 results in the most significant restoration of SINV replication (Fig 8B). We hypothesized that siRNAs that induced greater knockdown of *NME1* or *PABPC4* expression would also result in greater SINV replication. Therefore, we de-convoluted both *NME1* and *PABPC4* siRNA pools in both our inducible TRIM25-WT cell line and in the parental 293T cell line with endogenous TRIM25 and ZAP expression. There, we observed that both the degree of *NME1* and *PABPC4* mRNA expression (Fig 8C and 8D) significantly and negatively correlate with increase of viral replication (Fig 8E and 8F), supporting a role for both NME1 and PABPC4 in TRIM25-dependent alphavirus inhibition. This correlation is more robust in the presence of inducible TRIM25-WT (NME1: $r = -0.83$, $p<0.001$; PABPC4: $r = -0.87$, $p<0.001$) than in the presence of endogenous TRIM25 (NME1: $r = -0.82$, $p<0.01$; PABPC4: $r = -0.74$, $p<0.01$). Altogether, these results suggest that the antiviral activity of TRIM25 is mediated by multiple substrates. Though knockdown of most individual interactors on their own does not significantly restore SINV replication, the fact that several have demonstrated a phenotype implies that together they may have a larger impact on viral replication. Further studies need to be performed to determine their synergistic effects on viral infection and functional consequences of their ubiquitination by TRIM25.

## Discussion

Many TRIMs are involved in and ubiquitinate components of multiple cellular and antiviral processes [3–6]. In this study, we set out to identify TRIM25 substrates by generating a point mutation in the TRIM25 RING domain, R54P, which is predicted to abolish its interaction with E2 carrier enzymes and is sufficient to cripple TRIM25 ligase activity (Fig 1). We reported identification of TRIM25 substrates involved in nucleic acid metabolism and translation (Fig 2E), in line with its role in blocking viral translation [20]. We characterized the ubiquitination of the most enriched TRIM25 interactors, G3BP (Fig 3) and UPF1 (Fig 4), as well as two

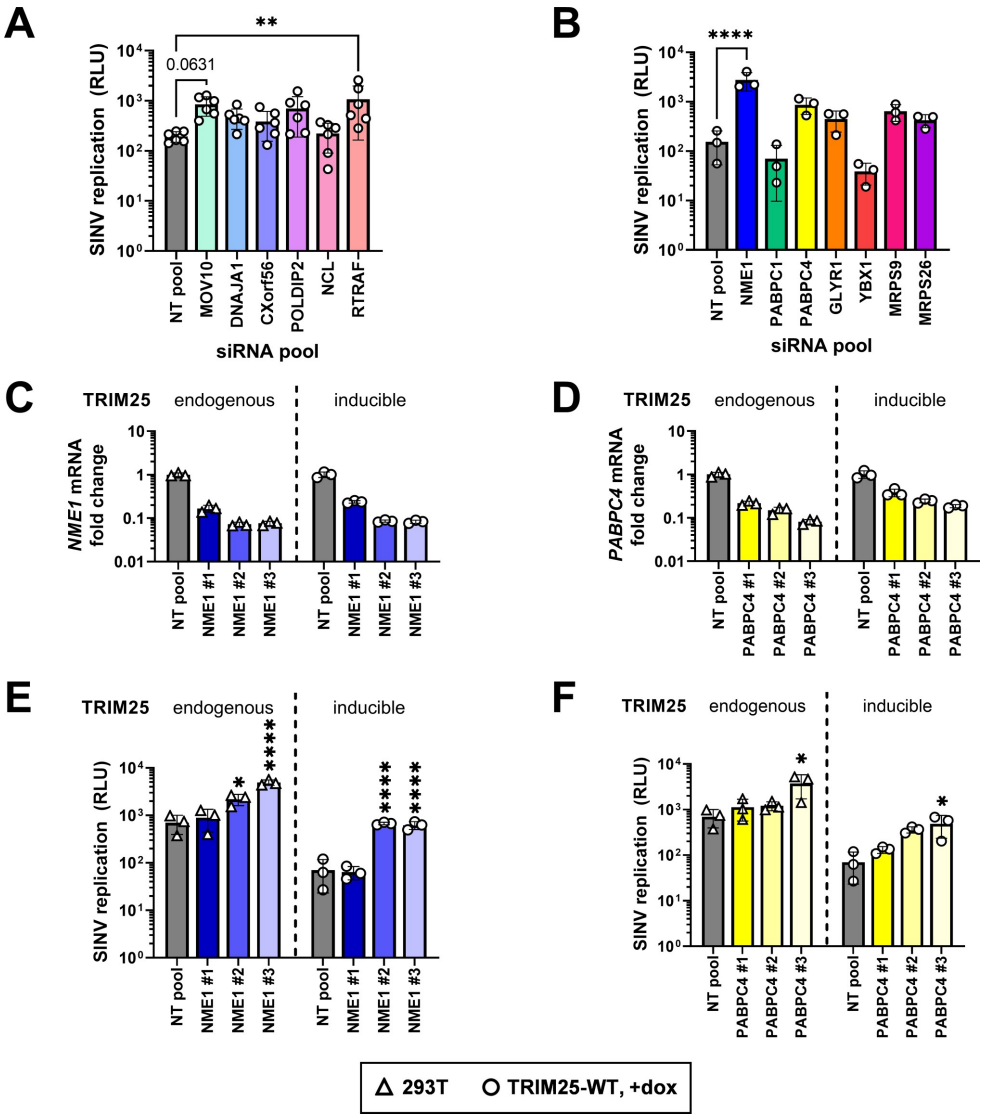


**Fig 8. Knocking down TRIM25-R54P-specific interactors identifies essential substrates for TRIM25 antiviral activity.** (A-B) TRIM25 inducible cells were transfected with pooled siRNAs for either (A) hits specific to TRIM25-R54P in the absence of viral infection or (B) hits specific to TRIM25-R54P in the presence of viral infection. Cells were induced for TRIM25-WT expression at 1 μg/mL dox, infected with Toto1101/Luc at an MOI of 0.01 PFU/cell, and lysed at 24 h.p.i. for measurement of luciferase activity. Asterisks indicate statistically significant differences as compared to the NT pool siRNA (One-way ANOVA, Dunnett's multiple comparison test; **, $p<0.01$; ****, $p<0.0001$). Unlabeled comparisons are not significant. Data are either (A) pooled from or (B) representative of two independent experiments. (C-F) Parental 293T cells (TRIM25: endogenous) or TRIM25 inducible (TRIM25: inducible) cells were transfected with individual siRNAs for (C,E) *NME1* or (D,F) *PABPC4*, induced for TRIM25-WT expression at 1 μg/mL dox, and (C-D) had RNA extracted for RT-qPCR analysis or (E-F) infected with Toto1101/Luc at an MOI of 0.01 PFU/cell. Cells were lysed at 24 h.p.i. for measurement of luciferase activity. Asterisks indicate statistically significant differences as compared to the NT pool for each cell line.

293T and TRIM25-WT inducible cell lines were statistically analyzed independently from one another (One-way ANOVA, Dunnett's multiple comparison test; *, $p<0.05$; ****, $p<0.0001$). Data are representative of two independent experiments for each cell line.

https://doi.org/10.1371/journal.ppat.1010743.g008

TRIM25-R54P specific interactors during infection, NME1 (Fig 5), and PABPC4 (Fig 6). These represent proteins with essential cellular functions, some of which with prior involvement in alphavirus infection [50,59]. We also used the TRIM25-R54P mutant to definitively show the critical role of ubiquitination in TRIM25 antiviral activity that is independent of IFN production and signaling (Fig 7). We then examined proteins that display a preference for association with TRIM25-R54P under mock and viral infection conditions, and found that several of these are necessary for TRIM25 antiviral activity (Fig 8), identifying them as potential TRIM25 substrates mediating viral inhibition. Our results suggest that targeting of any single substrate by TRIM25 is insufficient to mediate the entirety of its cellular and antiviral activities, illustrating the powerful, multi-faceted role of this ubiquitination network in diverse biological processes.

We propose that the success of this "substrate trapping" approach in identifying TRIM25 ubiquitination substrates hinges on preservation of protein structure. Previous reports that unearthed the importance of TRIM25 ligase activity in the ZAP antiviral response depend on either deleting the entire TRIM25 RING catalytic domain or disrupting formation of the zinc finger motif, potentially having an adverse effect on protein folding overall and potentially affecting other TRIM25 cellular functions or interactions [20,21]. The R54P point mutation we generated has been demonstrated to preserve protein structure and cognate interactions in other contexts [29], instilling greater credibility in our identification of novel TRIM25 substrates. Moreover, this mutation is predicted to abolish the E3 ligase-E2 conjugating enzyme interaction [29], preventing any downstream ubiquitination events and thus prolonging transient ligase-substrate interactions. The TRIM25-R54P specific hits may have weaker, more transient, or infection-specific interactions not easily detected by the conventional co-IP/MS approach. Other "substrate trapping" approaches depend on fusing a polyubiquitin binding domain to the ligase of interest [60], which may either disrupt native protein-protein interactions or result in false-positive identification of ubiquitinated proteins. Moreover, this type of approach would fail to identify substrates that are not polyubiquitinated, given that ligases can mono or multi-monoubiquitinate their substrates [61].

For the first time, we identified G3BP1/2, UPF1, NME1, and PABPC4 as bona fide TRIM25 substrates (Figs 3–6). Furthermore, we were able to characterize TRIM25 polyubiquitination of G3BP and PABPC4 as primarily utilizing K63 linkages (Figs 3C and 6D). This type of linkage is commonly used to build signaling scaffolds, as TRIM25 does to activate RIG-I [19], and could potentially play a role in either SG assembly or disassembly by recruiting SG components in the former or generating steric hindrance in the latter. Additionally, our validation of K592 as a mono-ubiquitination site on UPF1 (Fig 4C) overlaps with a predicted acetylation site on the same residue, and neighbors a predicted phosphorylation site at T595, potentially modulating these other post-translational modifications of UPF1 [62]. These residues lie within the AAA ATPase domain of UPF1, suggesting that ubiquitination of UPF1 by TRIM25 might affect its ATP hydrolysis, thus hindering UPF1 in its NMD target discrimination and efficient translation termination [63,64]. Interestingly enough, G3BP1 and UPF1 cooperate to mediate structure-mediated RNA decay [65]. It is entirely possible that TRIM25-mediated ubiquitination could affect this process by modulating their interaction with one another, though further experiments are required to explore this hypothesis.

Though UPF1 and G3BP have previously been implicated as antiviral and pro-viral factors in alphavirus replication, respectively [50,59], we did not find a role for either in the

TRIM25-ZAP antiviral response. UPF1 may have an antiviral role independent of TRIM25, given that its knockdown only significantly rescued viral replication when TRIM25 was absent (S2D Fig). This hypothesis is supported by a previous report which found that UPF1 was involved in regulating half-life stability of viral RNA [50], which TRIM25 does not affect [20], On the other hand, G3BP is known to cluster replication complexes and recruit translation initiation machinery [59], which might be disrupted through G3BP ubiquitination by TRIM25, resulting in translational suppression. Alternatively, given that the G3BP interaction motifs in TRIM25 and nsP3 are similar [45,66], it is tempting to speculate that TRIM25 may compete with the viral nsP3 for G3BP interaction and recruitment, resulting in diminishment of G3BP pro-viral effects. However, the pro-viral roles of G3BP did not seem to be affected by TRIM25 ubiquitination or lack thereof, given that abolishing TRIM25-G3BP interaction through overexpression of the TRIM25-PTAA mutant did not rescue SINV replication and translation nor CHIKV virion production (S2A–S2C Fig). Nevertheless, we noted that the TRIM25-PTAA mutant still preserves some ubiquitination of G3BP despite completely abolishing the TRIM25-G3BP interaction (Fig 3A and 3B). Further studies are warranted to fully elucidate the role of G3BP ubiquitination in TRIM25 antiviral activity.

TRIM25-mediated ubiquitination of NME1 and PABPC4 may interfere with RNA metabolic processes by altering their stability or ability to bind RNA. Both of these proteins have previously been demonstrated to be ubiquitinated by other E3 ligases. Ubiquitination of NME1 by the E3 ligase SCF-FBXO24 targets it for degradation [67]. Seeing as TRIM25 is able to modify G3BP with both proteolytic K48- and non-proteolytic K63-polyubiquitin linkages, TRIM25 may also be targeting NME1 for degradation, thereby hindering nucleotide synthesis and general RNA metabolic processes. On the other hand, ubiquitination of PABPC4 by the E3 ligase MKRN decreases its affinity for binding mRNA poly(A) tails [68]. It is interesting to speculate that TRIM25-mediated polyubiquitination of PABPC4 could regulate PABPC4 binding to the poly(A) tail on viral RNAs, thus modulating the stability of the RNA and reducing its ability to form translation initiation complexes.

We also utilized the TRIM25-R54P mutant to define the requirement for ligase activity in TRIM25 inhibition of alphavirus replication. We found that TRIM25 ligase activity is absolutely required for its inhibition of diverse alphaviruses through a block in viral translation (Fig 7A–7D). Interestingly, overexpression of both TRIM25-WT and -R54P results in a dampened IFN response in our hands (Fig 7E), contrasting with the previously established role of TRIM25 in activating RIG-I signaling and implicating TRIM25 as a negative regulator of the type I IFN response [69]. Moreover, TRIM25-R54P with a complete loss of antiviral activity actually exhibits relatively more production of IFN and a subset of ISG mRNAs (Fig 7E). Still, these data together suggest that the robust TRIM25 antiviral activity against alphaviruses is not mediated through an augmented IFN response, but through its ligase activity and subsequent ubiquitination network.

Our examination of the contribution of a subset of TRIM25-R54P specific interactors to TRIM25 antiviral activity has yielded several hits, namely RTRAF (Fig 8A), NME1 (Fig 8B), and PABPC4 (Fig 8B). Though only pooled siRNA knockdown for *RTRAF* and *NME1* gave statistically significant restored viral replication, pooled siRNA knockdown of PABPC4 still restored viral replication by approximately 5 fold (Fig 8B). Additionally, both NME1 and PABPC4 expression significantly and negatively correlated with viral replication (Fig 8C–8F). RTRAF, also known as hCLE or C14orf166, is an RNA binding protein involved in cellular transcription, translation, and RNA transport, and is required for influenza virus replication [70–72]. Notably, RTRAF is a member of a cap-binding complex that activates mRNA translation [71]. Given RTRAF's role in facilitating translation of mRNAs, it is therefore tempting to speculate that RTRAF may be required for translation of alphavirus RNA, and

TRIM25-mediated ubiquitination of RTRAF may affect its ability to do so. The novel bona fide TRIM25 substrate NME1, which functions as a major synthesizer of non-ATP nucleoside triphosphates, upon ubiquitination may inhibit alphavirus replication via a similar mechanism as the potent restriction factor SAMHD1, which depletes deoxynucleotide pools, effectively preventing replication of varied DNA viruses and reverse transcription of HIV-1 [73]. On the other hand, TRIM25-mediated ubiquitination of NME1 may inhibit its metastatic suppressor activities, potentially serving as a novel mechanism for TRIM25's previously described roles in carcinogenesis. Finally, TRIM25-mediated ubiquitination of PABPC4 could inhibit translation initiation by interfering with necessary protein-protein interactions to form the mRNA closed loop structure for ribosomal recruitment. Alternatively, it is possible that PABPC4 could inhibit alphavirus replication in a manner similar to its general block of coronavirus replication by recruiting TRIM25 to target alphavirus proteins for degradation [58]. Further studies need to be carried out to elucidate the functional consequences of these TRIM25 substrates in blocking viral translation and other cellular processes.

The novelty of this work lies within our innovative approach to uncover the multifaceted TRIM25 ubiquitination network, which is likely involved in mediating TRIM25 cellular and antiviral functions. Many questions remain unanswered as to how TRIM25-mediated ubiquitination modulates the activity of these substrates. In contrast to the more binary consequences of K48-linked dependent degradation, other types of ubiquitin linkage may effect more nuanced cellular changes by modulating substrate activity and localization [61]. Given TRIM25 proclivity for K63 linkages in the context of alphavirus infection and innate immunity [19–21], we are tempted to speculate that TRIM25 eschews a simple degradation approach in favor of a more refined modulation of substrate activity and localization. Current therapeutics that harness E3 ligases focus on their degradative power, generating compounds that bring ligases in close proximity to a target protein for degradation [74]. Further research is warranted to explore the utility of alternate modes of ubiquitination in biological therapeutics.

## Materials and methods

All resources utilized in this study are compiled below (Table 5) and referenced in the relevant methods in the following sections.

### Cell culture, viruses, and infections

ZAP KO 293T cells (clone 89) and its respective parental 293T cells were generously provided by Dr. Akinori Takaoka at Hokkaido University [82]. 293T (parental, ZAP KO, and TRIM25 KO (see below) with or without inducible expression of TRIM25) were cultured in Dulbecco's Modified Eagle Medium (DMEM; Thermo Fisher Scientific, Waltham, MA) supplemented with 10% fetal bovine serum (FBS; Avantor Seradigm, Radnor, PA). Baby hamster kidney 21 (BHK-21; American Type Culture Collection, Manasass, VA) cells were cultured in Minimal Essential Media (Thermo Fisher Scientific) supplemented with 7.5% FBS.

Wild-type SINV (Toto1101), temperature-sensitive SINV (Toto1101/Luc:ts6), SINV expressing firefly luciferase (Toto1101/Luc), SINV expressing EGFP (TE/5'2J/GFP), CHIKV vaccine strain 181/clone 25 (generously provided by Scott Weaver, The University of Texas Medical Branch at Galveston), ONNV expressing EGFP (generously provided by Dr. Steve Higgs, Kansas State University), RRV expressing EGFP (generously provided by Dr. Mark Heise, University of North Carolina), and VEEV vaccine strain TC-83 (generously provided by Dr. Ilya Frolov, University of Alabama at Birmingham) have been previously described [75–80]. Viral stocks and titers for multiplicity of infection (MOI) calculations were generated in BHK-21 cells as previously described [79]. Viral infections and plaque assays were

**Table 5. Key resources.**

| Reagent type (species) or resource | Description | Source or reference | Identifiers | Additional information |
|---|---|---|---|---|
| strain (*Chikungunya virus*) | CHIKV strain 7142.181/25 | [75] | | |
| strain (*O'nyong-nyong virus*) | ONNV-GFP | [76] | GenBank AF079456 | SG650 genome |
| strain (*Ross River virus*) | RR64-GFP | [77] | | |
| strain (*Sindbis virus)* | Toto1101 | [78] | | |
| strain (*Sindbis virus*) | Toto1101/Luc | [79] | | |
| strain (*Sindbis virus*) | Toto1101/Luc:ts6 | [79] | | |
| strain (*Sindbis virus*) | TE-5'2J/GFP | [80] | | |
| strain (*Venezuelan equine encephalitis virus*) | VEEV-GFP | [81] | vaccine strain TC-83 | |
| Antibody | anti-actin-HRP, mouse monoclonal | Sigma-Aldrich | A3854 | WB (1:20,000) |
| Antibody | anti-EFP/TRIM25, mouse monoclonal | BD Biosciences | 610570 | WB (1:5,000) |
| Antibody | anti-FLAG, mouse monoclonal | Sigma-Aldrich | F1804 | WB (1:20,000) |
| Antibody | anti-G3BP1, mouse monoclonal | Santa Cruz | sc-365338 | WB (1:500) |
| Antibody | anti-G3BP2, rabbit polyclonal | Assay Biotech | C18193 | WB (1:1,000) |
| Antibody | anti-HA, rat monoclonal | Roche Life Science | 3F10 | WB (1:1,000) |
| Antibody | anti-myc, rabbit polyclonal | Cell Signaling Technology | 2272S | WB (1:2,500) |
| Antibody | anti-NM23A (NME1), rabbit monoclonal | Abcam | ab171935 | WB (1:10,000) |
| Antibody | anti-PABPC4, rabbit polyclonal | Proteintech | 14960-1-AP | WB (1:2,000) |
| Antibody | anti-UPF1, rabbit monoclonal | Cell Signaling Technology | 12040 | WB (1:1,000) |
| Antibody | anti-V5, mouse monoclonal | Invitrogen | MA5-1523 | WB (1:5,000) |
| Antibody | donkey anti-rat HRP | Jackson ImmunoResearch | 712-035-153 | WB (1:20,000) |
| Antibody | goat anti-mouse HRP | Jackson ImmunoResearch | 115-035-146 | WB (1:20,000) |
| Antibody | goat anti-rabbit HRP | Thermo Fisher Scientific | 31462 | WB (1:20,000) |
| Chemical compound, drug | poly(I:C) HMW | InvivoGen | tlrl-pic | |
| Chemical compound, drug | Poly-L-lysine hydrobromide | Sigma-Aldrich | P2636 | |
| Chemical compound, drug | Roche cOmplete Mini, EDTA-free Protease Inhibitor Cocktail | Sigma-Aldrich | 11836170001 | |
| Commercial assay or kit | DharmaFECT 1 Transfection Reagent | Horizon Discovery | T-2001-01 | |
| Commercial assay or kit | Dynabeads Protein A for Immunoprecipitation | Invitrogen | 10-002-D | |
| Commercial assay or kit | EZview Red ANTI-FLAG M2 Affinity Gel | Sigma-Aldrich | F2426 | |
| Commercial assay or kit | EZview Red ANTI-MYC M2 Affinity Gel | Sigma-Aldrich | E6654 | |
| Commercial assay or kit | KOD Hot Start Master Mix | Sigma-Aldrich | 71842 | |
| Commercial assay or kit | Luna Universal qPCR Master Mix | New England Biolabs | M3003X | |
| Commercial assay or kit | Mini-PROTEAN TGX Gels, 4–15%, 15 well | Bio-Rad | 4568086 | |
| Commercial assay or kit | NuPAGE MOPS SDS running buffer | Invitrogen | NP0001 | |
| Commercial assay or kit | ProSignal Full-Range Prestained Protein Ladder | Genesee Scientific | 83–650 | |
| Commercial assay or kit | ProSignal Pico ECL Reagent | Genesee Scientific | 20-300B | |
| Commercial assay or kit | Protoscript II First Strand cDNA Synthesis Kit | New England Biolabs | E6560L | |
| Commercial assay or kit | Q5 Site-Directed Mutagenesis Kit | New England Biolabs | E0552S | |
| Commercial assay or kit | Quick-DNA Miniprep-Plus kit | Zymo Research | D4068 | |
| Commercial assay or kit | Quick-RNA kit | Zymo Research | R1055 | |
| Commercial assay or kit | QuikChange II XL Site-Directed Mutagenesis Kit | Agilent | 210518 | |

(*Continued*)

**Table 5.** (Continued)

| Reagent type (species) or resource | Description | Source or reference | Identifiers | Additional information |
|---|---|---|---|---|
| Commercial assay or kit | RNeasy mini kit | Qiagen | 74104 | |
| Commercial assay or kit | X-tremeGENE9 Transfection Reagent | Sigma-Aldrich | 6365787001 | |
| Sequence-based reagent | DNA primers for molecular cloning | This work | S1 Table | |
| Sequence-based reagent | RT-qPCR oligonucleotides | PrimerBank | S3 Table | https://pga.mgh.harvard.edu/primerbank/ |
| Sequence-based reagent | siRNA | Ambion | S2 Table | |
| Software, algorithm | Database for Annotation, Visualization and Integrated Discovery v6.8 | Frederick National Laboratory for Cancer Research, Frederick, MD | | https://david.ncifcrf.gov/home.jsp |
| Software, algorithm | EnhancedVolcano | Clinical Bioinformatics Research LTD, United Kingdom | | https://github.com/kevinblighe/EnhancedVolcano |
| Software, algorithm | FlowJo | BD Biosciences, Franklin, NJ | | https://flowjo.com |
| Software, algorithm | Geneious Prime (2021.2) | Biomatters, San Diego, CA | | https://geneious.com |
| Software, algorithm | GraphPad Prism 9 (v.9.2.0) | GraphPad Software, San Diego, CA | | https://graphpad.com |
| Software, algorithm | ImageJ | National Institutes of Health, Bethesda, MD | | https://imagej.net/ |
| Software, algorithm | RStudio software (v.1.4.1106) | RStudio, Boston, MA | | https://rstudio.com |
| Software, algorithm | UCSF Chimera | University of California, San Francisco, San Francisco, CA | | https://www.rbvi.ucsf.edu/chimera/ |

https://doi.org/10.1371/journal.ppat.1010743.t005

performed as previously described [79]. TRIM25 inducible cells (see below) were induced for TRIM25 expression and infected with EGFP expressing viruses at an MOI of 0.01 plaque forming units (PFU)/cell, harvested at 10–24 hours post-infection (h.p.i.), and fixed in 1% paraformaldehyde for flow cytometry analysis. Data was acquired using a MACSQuant Analyzer 10 (Miltenyi Biotec, Auburn, CA) and analyzed using FlowJo (BD Biosciences, Franklin Lakes, NJ). Percent infected (GFP+) cells was calculated and normalized to the -dox condition of each respective cell line.

## Plasmids and transfections

Addgene plasmids for HA-tagged ubiquitin (pRK5-HA-Ubiquitin-WT, #17608; pRK5-HA-Ubiquitin-K48, #17605; pRK5-HA-Ubiquitin-K63, #17606), UPF1 (pCW57.1-Tet-UPF1WT, #99146), and PABPC4 (pDESTmycPABPC4, #19877) were used [47,83,84]. Full-length TRIM25 was generously provided by Dr. Jae U. Jung at the University of Southern California [19]. Dr. Gerald McInerney at the Karolinska Institutet, Sweden, generously provided pGFP-G3BP1 and pGFP-G3BP2a [59]. The coding sequence of NME1 isoform a (NM_198175.1) was synthesized as a gene fragment (Integrated DNA Technologies, Coralville, IA), where the ends were flanked by restriction enzyme sites NotI and XbaI, and random nucleotides were incorporated to maintain the open reading frame. Dr. Oliver Fregoso kindly gifted us a pcDNA3.1-3XFLAG plasmid. The 3XFLAG tag was swapped out for a V5 tag or a myc tag using BamHI and HindIII restriction sites to generate V5-pcDNA3.1 or myc-pcDNA3.1, respectively. The plasmid pcDNA3.1-3XFLAG was used as an expression vector for TRIM25, pcDNA3.1-V5 for UPF1, and pcDNA3.1-myc for G3BP1, G3BP2, NME1, and PABPC4. TRIM25 was cloned into pcDNA3.1-3XFLAG using XhoI and XbaI restriction sites, while UPF1, G3BP, NME1, and PABPC4 were cloned into either pcDNA3.1-V5 (UPF1) or pcDNA3.1-myc (G3BP, NME1, and PABPC4) using the NotI and XbaI restriction sites. TRIM25 RING domain mutants (I15K, R54P, I15K/R54P) were generated by mutagenesis of pcDNA-3XFLAG-TRIM25 using the QuikChange II XL Site-Directed Mutagenesis Kit

(Agilent Technologies, Santa Clara, CA), while the TRIM25-PTAA mutant was generated using the Q5 Site-Directed Mutagenesis Kit (New England Biolabs, Ipswich, MA), by performing sequential mutagenesis reactions to individually mutate each residue to alanine. TRIM25 was cloned into a 3XFLAG expressing ePiggyBac transposon plasmid at the ClaI and NotI restriction sites. For cloning and mutagenesis primers, see S1 Table. All plasmids were verified by sequencing (Genewiz, South Plainfield, NJ).

Cells were transfected using X-tremeGENE9 DNA Transfection Reagent (Roche Life Science, Basel, Switzerland) at a ratio of 3 μL to1 μg DNA according to the manufacturer's instructions. Empty vectors (pcDNA3.1-3XFLAG, V5, or myc) were transfected as necessary to keep total plasmid amount in co-transfections constant.

## *TRIM25* targeting by CRISPR

The MIT Optimized CRISPR Design portal (crispr.mit.edu) and CHOPCHOP [85] (chopchop.cbu.uib.no) were used to design guide RNAs (gRNAs) targeting exon 1 of the human *TRIM25* gene (S1A Fig). The guide with the highest ranking in both scoring programs (5'-CGGCGCAA CAGGTCGCGAACGGG-3') was selected for cloning into the PX459 vector (Addgene, #62988), a non-lentiviral construct that also delivers Cas9 [86]. Oligos containing the gRNA sequences (5'- CACCGCGGCGCAACAGGTCGCGAAC-3' and 5'- AAACGTTCGCGAC CTGTTGCGCCGC-3') were ligated and cloned into PX459 linearized with BbsI. 293T cells were transiently transfected with PX459 expressing TRIM25 gRNA and selected with 1 μg/mL puromycin the next day to eliminate untransfected cells. Following two days of puromycin selection, surviving cells were counted, diluted to 0.3 cell/well in a 96-well plate, and seeded in 10% FBS DMEM. Single cell clones were expanded and treated with or without puromycin. Clones sensitive to puromycin, indicating failure to integrate gRNA expressing vector, were harvested for immunoblot analysis to assess TRIM25 expression. Five clones (3, 6, 8, 9, and 10) were selected based on western blotting results indicating complete loss of TRIM25 protein expression (S1B Fig). Viral replication within these clones was characterized by infection with a luciferase-expressing SINV (Toto1101/Luc). Clone #8 was selected for generation of TRIM25 inducible cell lines based on its intermediate viral replication phenotype (S1C Fig), similar to previous TRIM25 siRNA data [20]. A 600-bp amplicon flanking the gRNA targeting site was amplified from genomic DNA isolated from each clonal population using a Quick-DNA Miniprep Plus kit (Zymo Research, Irvine, CA) and KOD Hot Start Master Mix (Millipore Sigma). Amplicons from clone #8 were sent to Massachusetts General Hospital Center for Computational and Integrative Biology DNA Core for Complete Amplicon Sequencing, confirming that CRISPR targeting results in deletions in exon 1 of TRIM25, leading to frameshift mutations and premature stop codons in both alleles (S1D Fig).

## Generation of TRIM25 inducible cell lines

To reconstitute TRIM25 expression (WT and R54P) in our TRIM25 KO 293T cell line (clone #8; see above for details), we used the enhanced PiggyBac (ePB) transposable element system provided by the Brivanlou laboratory at the Rockefeller University, as previously described [87,88]. TRIM25 KO 293T cells were transfected with 1:1 ePB transposon vector encoding TRIM25-WT or TRIM25-R54P and the transposase plasmid. Two days post-transfection, 1.5 μg/mL of puromycin was used to select a population of TRIM25 KO 293T cells inducible for TRIM25-WT, -R54P, or -PTAA, which were then expanded and treated with different amounts of dox (0.001, 0.01, 0.1, 1, and 10 μg/mL) to confirm TRIM25 inducible expression by immunoblotting.

## Mass spectrometry (MS)

To identify TRIM25 substrates, three 15-cm dishes per condition were seeded with $7.5x10^6$ TRIM25 inducible or TRIM25 KO 293T cells each in the presence of 1 μg/mL dox. Two days later, cells were mock infected or infected with Toto1101 at an MOI of 1 PFU/cell. Six hours post infection, cells were trypsinized, spun down, and lysed in 3 mL of FLAG IP buffer. Supernatant was transferred to a new 15 mL tube and supplemented with 5 mL of FLAG IP buffer before incubating with 80 μL of anti-FLAG beads for 45 min at 4˚C, rotating. Immunoprecipitates were washed three times in FLAG IP buffer before elution with 130 μL of 8M urea in 100 mM Tris-HCl, pH 8, shaken for 10 min at 1200 rpm. Supernatant was carefully transferred to a new tube and proteins were precipitated by addition of 4 volumes of -20˚C acetone and incubation at 4˚C overnight. After centrifugation at 16,100 g for 30 min at 4˚C, pellets were washed with -20˚C acetone and centrifuged again.

Dried pellets were processed at the UCLA Proteomics Core. Protein samples were reduced and alkylated using 5mM Tris (2-carboxyethyl) phosphine and 10mM iodoacetamide, respectively, and then proteolyzed by the sequential addition of trypsin and lys-C proteases at 37˚C as described [89]. Digested peptides were resuspended in 5% formic acid and fractionated online using a 25cm long, 75 μM inner diameter fused silica capillary packed in-house with bulk C18 reversed phase resin (length, 25 cm; inner diameter, 75 μM; particle size, 1.9 μm; pore size, 100 Å; Dr. Maisch GmbH) [90]. The 140 min water-acetonitrile gradient was delivered using a Dionex Ultimate 3000 UHPLC system (Thermo Fisher Scientific) at a flow rate of 300 nL/min (Buffer A: water with 3% DMSO and 0.1% formic acid and Buffer B: acetonitrile with 3% DMSO and 0.1% formic acid). Fractionated peptides were ionized and analyzed by tandem mass spectrometry (MS/MS) Orbitrap Fusion Lumos mass spectrometer (Thermo Fisher Scientific). Label-free quantitation was performed using the MaxQuant software package [91]. The mass spectrometry proteomics data have been deposited to the ProteomeXchange Consortium via the PRIDE [92] partner repository with the dataset identifier PXD034024. The EMBL Human reference proteome (UP000005640 9606) was utilized for all database searches. Statistical analysis of MaxQuant output data was performed with the artMS Bioconductor [93] package which performs the relative quantification of protein abundance using the MSstats Bioconductor package (default parameters). Intensities were normalized across samples by median-centering the log2-transformed MS1 intensity distributions. The abundance of proteins missing from one condition but found in more than 2 biological replicates of the other condition for any given comparison were estimated by imputing intensity values from the lowest observed MS1-intensity across samples and p-values were randomly assigned to those between 0.05 and 0.01 for illustration purposes. Significant hits were defined as interactors that possessed a log2FoldChange of $>1.5$ and a -log10Pvalue $> 1.3$.

## TRIM25 autoubiquitination and co-immunoprecipitation (co-IP) assay

To assess TRIM25 autoubiquitination or co-IP with proteins of interest, transfected or untransfected cells in 6-well plates were collected and lysed by rotating for 30 min at 4˚C in FLAG IP buffer (100 mM Tris-HCl 8.0, 150 mM NaCl, 5 mM EDTA, 1 mM DTT, 5% glycerol, 0.1% NP-40) supplemented with a complete protease inhibitor cocktail (Roche Life Science), before spinning down at 14000 rpm for 15 min at 4˚C. Anti-FLAG beads (EZview Red ANTI--FLAG M2 Affinity Gel, Sigma-Aldrich, St. Louis, MO) or anti-myc beads (EZview Red ANTI--MYC M2 Affinity Gel, Sigma-Aldrich) were equilibrated by washing 3 times in FLAG IP buffer. Three hundred μL of whole cell lysate (WCL) were incubated with 30 μL of anti-FLAG beads for 45 min at 4˚C, rotating. Immunoprecipitates were washed 3 times with the FLAG IP

buffer. Bound proteins were eluted with SDS loading buffer and boiled for 5 minutes for immunoblot analysis.

## Ubiquitination IP assay

To assess TRIM25 ubiquitination of putative substrates, immunoprecipitation was performed essentially as previously described [20]. Briefly, cells were collected and lysed in 0.5% SDS buffer supplemented with complete protease inhibitor cocktail. Three hundred μL of WCL were diluted into 1X TNA buffer (0.25% Triton, 50 mM Tris-HCl, pH 7.5; 200 mM NaCl, 1 mM EDTA) + 2 mg/mL BSA. WCL containing V5-tagged substrates were then incubated with 1 μg of anti-V5 antibody overnight at 4˚C. The next morning, 40 μL Protein A Dynabeads (Invitrogen, Waltham, MA) were added and incubated for 2 h at 4˚C. WCL containing myc-tagged substrates were incubated directly with anti-myc beads for 45 minutes at 4˚C, rotating. Following incubation with beads, both myc-tagged and V5-tagged immunoprecipitates were washed 3 times with 1X TNA buffer + 2 mg/mL BSA. Myc-tagged NME1 underwent an additional two washes with 1X TNA buffer only. Bound proteins were eluted with SDS loading buffer and boiled for 5 minutes for immunoblot analysis.

## Immunoblot analysis

Proteins were resolved through SDS-PAGE using 4–15% precast Mini-PROTEAN TGX Gels (Bio-Rad) and NuPAGE MOPS SDS running buffer (Thermo Fisher Scientific) before transferring to a PVDF membrane (Bio-Rad). Immunodetection was achieved with 1:5,000 anti-ZAP (Abcam, Cambridge, United Kingdom); 1:5,000 anti-TRIM25 (BD Biosciences), 1:1,000 anti-HA (Roche Life Science), 1:5000 anti-V5 (Invitrogen), 1:2,500 anti-myc (Cell Signaling Technology, Danvers, MA), 1:20,000 anti-FLAG (Sigma-Aldrich), 1:500 anti-G3BP1 (Santa Cruz, Dallas, TX), 1:1,000 anti-G3BP2 (Assay Biotech, Fremont, CA), 1:1,000 anti-UPF1 (Cell Signaling Technology), 1:10,000 anti-NME1 (Abcam), 1:2,000 anti-PABPC4 (Proteintech, Rosemont, IL), and 1:20,000 anti-actin-HRP (Sigma-Aldrich). Primary antibodies were detected with 1:20,000 goat anti-mouse HRP (Jackson ImmunoResearch, West Grove, PA), 1:20,000 goat anti-rabbit HRP (Thermo Fisher Scientific), or 1:20,000 donkey anti-rat HRP (Jackson ImmunoResearch). Proteins were resolved on a 4–15% Mini-PROTEAN TGX gel (Bio-Rad, Hercules, CA) and visualized using ProSignal Pico ECL Reagent (Genesee Scientific, San Diego, CA) on a ChemiDoc (Bio-Rad). Quantification of western blots was performed using ImageJ.

## siRNA knockdown and poly(I:C) stimulation

Ambion Silencer siRNAs (S2 Table) and nontargeting controls (Thermo Fisher Scientific) were reverse transfected with DharmaFECT 1 Transfection Reagent (Horizon Discovery, Cambridge, United Kingdom) according to manufacturer protocols. Briefly, siRNAs were mixed with DharmaFECT 1 Transfection Reagent (1:100 dilution in HBSS) and 50 μL of siRNA mix were added to each well in a 24 well plate, or 100 μL in a 12 well plate. $1.2 \times 10^5$ cells were added per well in 250 μL in a 24 well plate or $2.4 \times 10^6$ in 500 μL in a 12 well plate, for a final concentration of 25 nM siRNA. Plates that would be subjected to SINV infection were first poly-L-lysine treated. Cells were induced for TRIM25 expression using a final concentration of 1 μg/mL dox one day post-transfection, as applicable. Cells were harvested for RNA extraction for RT-qPCR to quantify gene knockdown or subjected to SINV infection 48 h post-transfection. To assess ISG induction in TRIM25 inducible cells upon poly(I:C) treatment, cells were treated with 1 μg poly(I:C) HMW (InvivoGen, San Diego, CA) in the presence or absence of 1 μg/mL dox per well, and harvested for RNA extraction for RT-qPCR.

### Quantitative reverse transcription PCR (RT-qPCR)

Total RNA was isolated from siRNA- and poly(I:C)-treated cells using the RNeasy mini kit (Qiagen, Hilden, Germany) or the Quick-RNA kit (Zymo Research). 400 ng to 1 μg of input RNA was used as a template for reverse transcription using Protoscript II First Strand cDNA Synthesis Kit (New England Biolabs) and random hexamers, following manufacturer instructions. RT-qPCR was performed using 5 μL of 4 to 10-fold-diluted cDNA, and Luna Universal qPCR Master Mix (New England Biolabs) in the CFX Real-Time PCR system (Bio-Rad), courtesy of the UCLA Virology Core. qPCR conditions were as follows: initial denaturation step at 95˚C for 1 min, then 40 cycles of 95˚C for 15 sec followed by 60˚C for 30 sec, concluding with a final 10 sec at 60˚C. A melt curve was then calculated by heating to 95˚C incrementally by 0.5˚C/s for 10 sec at each temperature. Transcript levels of R54P specific interactors and ISGs were determined by normalizing the target transcript CT value to the CT value of the RPS11 transcript, an endogenous housekeeping gene. Fold change was calculated using this normalized value relative to the average of cells treated with the NT siRNA control or the -dox condition for respective cell lines (CT method). For RT-qPCR primers, see S3 Table.

### Statistical analysis

Statistical analyses in Figs 7 and 8, and S2 were performed on biological replicates from triplicate wells, unless indicated otherwise, using GraphPad Prism. Spearman's rho was calculated using Microsoft Excel. For statistical analyses and numerical data underlying graphical depictions, see S1 Data.

## Supporting information

**S1 Data. Excel spreadsheet containing, in separate sheets, the underlying numerical data and statistical analysis for Fig panels 7A, 7B, 7C, 7D, 7E, 8A, 8B, 8C, 8D, 8E, 8F, S1C, S2A, S2B, S2C, S2D, S2E, S2F, S3A, S3B, S4A, S4B, and for Spearman's rho calculations for NME1 and PABPC4.**
(XLSX)

**S1 Fig. Validation of TRIM25 KO in CRISPR clones.** (A) Schematic of where TRIM25 sgRNA targets exon 1. (B) Western blot of TRIM25 KO CRISPR single cell clones. (C) Cells were infected with SINV Toto1101/Luc at an MOI of 0.01 PFU/cell and lysed at 6, 12, 24, and 40 h.p.i. for measurement of luciferase activity. (D) CRISPR-targeting region in the genomic sequence of TRIM25 is shown in clone 8. The alignment shown is in the same reading frame of the wild-type TRIM25 protein. A red dash represents a deletion when compared to the wild-type TRIM25 sequence.
(TIF)

**S2 Fig. G3BP and UPF1 are not sufficient to mediate TRIM25 antiviral activity.** (A-C) TRIM25- inducible cells were induced for TRIM25-WT, -R54P, or -PTAA expression at 1 μg/mL dox, infected with (A) SINV Toto1101/Luc at an MOI of 0.01 PFU/cell, and lysed at 6, 12, 24, 32, and 40 h.p.i.; or with (B) SINV Toto1101/Luc:ts6 at an MOI of 1 PFU/cell and lysed at 0, 2, 4, and 6 h.p.i. for measurement of luciferase activity; or (C) CHIKV at an MOI of 0.01 PFU/cell, harvesting supernatant at 6 and 24 h.p.i. for plaque assays. Open circles and dashed lines indicate absence of TRIM25 induction. Data are representative of two independent experiments. Error bars represent (A-B) range or (C) standard deviation. Asterisks indicate statistically significant differences (Two-way ANOVA and Tukey's multiple comparisons test: $^{**}$, $p<0.01$; $^{***}$, $p<0.001$; $^{****}$, $p<0.0001$). Light blue compares WT +/- dox, dark blue for R54P +/- dox, and green for PTAA +/- dox. Unlabeled comparisons are not significant. (D)

TRIM25-WT inducible cells were transfected with NT pool siRNA or UPF1 siRNAs in the absence of dox. RNA was extracted 48 hours post-transfection for RT-qPCR analysis. Data are combined from two independent experiments. (E-F) TRIM25-WT inducible cells were transfected with NT pool siRNA or UPF1 siRNA #1, induced for TRIM25-WT expression at 1 μg/mL dox, and infected with Toto1101/Luc at an MOI of 0.01 PFU/cell. Cells were lysed at 24 h.p.i. for (E) measurement of luciferase activity or (F) quantification of UPF1 knockdown via RT-qPCR. Data are combined from three independent experiments. Asterisks indicate statistically significant differences (Two-way ANOVA and Šídák's multiple comparisons test: ****, $p<0.0001$). Unlabeled comparisons are not significant.
(TIF)

**S3 Fig. Poly(I:C) treatment robustly induces *IFN-β* mRNA expression.** (A-B) TRIM25 inducible cells were treated with poly(I:C) in the presence or absence of (A) TRIM25-WT or (B) TRIM25-R54P induction. RNA was harvested for RT-qPCR analysis. Data are representative of two independent experiments.
(TIF)

**S4 Fig. Validation of pooled siRNA knockdown.** (A-B) TRIM25 inducible cells were transfected with pooled siRNAs for either (A) hits specific to TRIM25-R54P in the absence of viral infection or (B) hits specific to TRIM25-R54P in the presence of viral infection. Cells were induced for TRIM25-WT expression at 1 μg/mL dox. RNA was extracted for RT-qPCR analysis.
(TIF)

**S1 Table. Cloning and mutagenesis primers.**
(DOCX)

**S2 Table. siRNAs.**
(DOCX)

**S3 Table. RT-qPCR primers.**
(DOCX)

## Acknowledgments

We thank Dr. Bill Schneider (Rockefeller University) for help with alignment of TRIM25 KO sequences and Drs. Douglas Black, Irvin Chen, and Oliver Fregoso (UCLA) for critical reading of the manuscript. We want to especially thank Drs. Oliver Fregoso and Michael Emerman (Fred Hutchinson Cancer Center) for their valuable input during the manuscript submission and review process. We also thank the UCLA Proteome Research Center for their services. RT-qPCR and flow cytometry was performed in the UCLA AIDS Institute that is supported by the James B. Pendleton Charitable Trust and the McCarthy Family Foundation. Molecular graphics and analyses performed with UCSF Chimera, developed by the Resource for Biocomputing, Visualization, and Informatics at the University of California, San Francisco.

## Author Contributions

**Conceptualization:** Emily Yang, Gerald M. McInerney, James A. Wohlschlegel, Melody M. H. Li.

**Data curation:** James A. Wohlschlegel, Melody M. H. Li.

**Formal analysis:** Emily Yang, Serina Huang, Yasaman Jami-Alahmadi.

**Funding acquisition:** Melody M. H. Li.

**Investigation:** Emily Yang, Serina Huang, Yasaman Jami-Alahmadi.

**Methodology:** Emily Yang, Yasaman Jami-Alahmadi.

**Project administration:** Emily Yang, James A. Wohlschlegel, Melody M. H. Li.

**Resources:** Yasaman Jami-Alahmadi, Gerald M. McInerney, James A. Wohlschlegel, Melody M. H. Li.

**Software:** Yasaman Jami-Alahmadi, James A. Wohlschlegel.

**Supervision:** James A. Wohlschlegel, Melody M. H. Li.

**Validation:** Emily Yang, Serina Huang.

**Visualization:** Emily Yang, Yasaman Jami-Alahmadi.

**Writing – original draft:** Emily Yang, Melody M. H. Li.

**Writing – review & editing:** Emily Yang, Serina Huang, Yasaman Jami-Alahmadi, Gerald M. McInerney, James A. Wohlschlegel, Melody M. H. Li.

## References

1. Li W, Bengtson MH, Ulbrich A, Matsuda A, Reddy VA, Orth A, et al. Genome-Wide and Functional Annotation of Human E3 Ubiquitin Ligases Identifies MULAN, a Mitochondrial E3 that Regulates the Organelle's Dynamics and Signaling. PLOS ONE. 2008; 3: e1487. https://doi.org/10.1371/journal.pone.0001487 PMID: 18213395
2. Metzger MB, Hristova VA, Weissman AM. HECT and RING finger families of E3 ubiquitin ligases at a glance. Journal of Cell Science. 2012; 125: 531–537. https://doi.org/10.1242/jcs.091777 PMID: 22389392
3. Vunjak M, Versteeg GA. TRIM proteins. Current Biology. 2019; 29: R42–R44. https://doi.org/10.1016/j.cub.2018.11.026 PMID: 30668943
4. Ozato K, Shin D-M, Chang T-H, Morse HC. TRIM family proteins and their emerging roles in innate immunity. Nat Rev Immunol. 2008; 8: 849–860. https://doi.org/10.1038/nri2413 PMID: 18836477
5. Rajsbaum R, García-Sastre A, Versteeg GA. TRIMmunity: The Roles of the TRIM E3-Ubiquitin Ligase Family in Innate Antiviral Immunity. Journal of Molecular Biology. 2014; 426: 1265–1284. https://doi.org/10.1016/j.jmb.2013.12.005 PMID: 24333484
6. Hatakeyama S. TRIM Family Proteins: Roles in Autophagy, Immunity, and Carcinogenesis. Trends in Biochemical Sciences. 2017; 42: 297–311. https://doi.org/10.1016/j.tibs.2017.01.002 PMID: 28118948
7. Hage A, Rajsbaum R. To TRIM or not to TRIM: the balance of host–virus interactions mediated by the ubiquitin system. Journal of General Virology. 2019; 100: 1641–1662. https://doi.org/10.1099/jgv.0.001341 PMID: 31661051
8. Meroni G. TRIM E3 Ubiquitin Ligases in Rare Genetic Disorders. In: Barrio R, Sutherland JD, Rodriguez MS, editors. Proteostasis and Disease: From Basic Mechanisms to Clinics. Cham: Springer International Publishing; 2020. pp. 311–325. https://doi.org/10.1007/978-3-030-38266-7_14 PMID: 32274764
9. Meroni G, Desagher S. Cellular Function of TRIM E3 Ubiquitin Ligases in Health and Disease. Cells. 2022; 11: 250. https://doi.org/10.3390/cells11020250 PMID: 35053366
10. Heikel G, Choudhury NR, Michlewski G. The role of Trim25 in development, disease and RNA metabolism. Biochemical Society Transactions. 2016; 44: 1045–1050. https://doi.org/10.1042/BST20160077 PMID: 27528750
11. Martín-Vicente M, Medrano LM, Resino S, García-Sastre A, Martínez I. TRIM25 in the Regulation of the Antiviral Innate Immunity. Front Immunol. 2017; 8: 1187. https://doi.org/10.3389/fimmu.2017.01187 PMID: 29018447
12. Urano T, Saito T, Tsukui T, Fujita M, Hosoi T, Muramatsu M, et al. Efp targets 14-3-3j for proteolysis and promotes breast tumour growth. 2002; 417: 5.
13. Sato W, Ikeda K, Urano T, Abe Y, Nakasato N, Horie-Inoue K, et al. Efp promotes in vitro and in vivo growth of endometrial cancer cells along with the activation of nuclear factor-κB signaling. PLOS ONE. 2018; 13: e0208351. https://doi.org/10.1371/journal.pone.0208351 PMID: 30586414

14. Dong X-Y, Fu X, Fan S, Guo P, Su D, Dong J-T. Oestrogen causes ATBF1 protein degradation through the oestrogen-responsive E3 ubiquitin ligase EFP. Biochemical Journal. 2012; 444: 581–590. https://doi.org/10.1042/BJ20111890 PMID: 22452784

15. Zang H, Ren S, Cao H, Tian X. The ubiquitin ligase TRIM25 inhibits hepatocellular carcinoma progression by targeting metastasis associated 1 protein. IUBMB Life. 2017; 69: 795–801. https://doi.org/10.1002/iub.1661 PMID: 28861931

16. Liu Y, Tao S, Liao L, Li Y, Li H, Li Z, et al. TRIM25 promotes the cell survival and growth of hepatocellular carcinoma through targeting Keap1-Nrf2 pathway. Nat Commun. 2020; 11: 348. https://doi.org/10.1038/s41467-019-14190-2 PMID: 31953436

17. Schneider WM, Chevillotte MD, Rice CM. Interferon-Stimulated Genes: A Complex Web of Host Defenses. Annu Rev Immunol. 2014; 32: 513–545. https://doi.org/10.1146/annurev-immunol-032713-120231 PMID: 24555472

18. Schoggins JW. Interferon-Stimulated Genes: What Do They All Do? Annual Review of Virology. 2019; 6: 567–584. https://doi.org/10.1146/annurev-virology-092818-015756 PMID: 31283436

19. Gack MU, Shin YC, Joo C-H, Urano T, Liang C, Sun L, et al. TRIM25 RING-finger E3 ubiquitin ligase is essential for RIG-I-mediated antiviral activity. Nature. 2007; 446: 916–920. https://doi.org/10.1038/nature05732 PMID: 17392790

20. Li MMH, Lau Z, Cheung P, Aguilar EG, Schneider WM, Bozzacco L, et al. TRIM25 Enhances the Antiviral Action of Zinc-Finger Antiviral Protein (ZAP). Fernandez-Sesma A, editor. PLOS Pathogens. 2017; 13: e1006145. https://doi.org/10.1371/journal.ppat.1006145 PMID: 28060952

21. Zheng X, Wang X, Tu F, Wang Q, Fan Z, Gao G. TRIM25 Is Required for the Antiviral Activity of Zinc Finger Antiviral Protein. Diamond MS, editor. J Virol. 2017; 91: e00088–17, /jvi/91/9/e00088-17.atom. https://doi.org/10.1128/JVI.00088-17 PMID: 28202764

22. Yang E, Li MMH. All About the RNA: Interferon-Stimulated Genes That Interfere With Viral RNA Processes. Front Immunol. 2020;11. https://doi.org/10.3389/fimmu.2020.605024 PMID: 33362792

23. Garcia-Moreno M, Noerenberg M, Ni S, Järvelin AI, González-Almela E, Lenz CE, et al. System-wide Profiling of RNA-Binding Proteins Uncovers Key Regulators of Virus Infection. Molecular Cell. 2019; 74: 196–211.e11. https://doi.org/10.1016/j.molcel.2019.01.017 PMID: 30799147

24. Choudhury NR, Heikel G, Trubitsyna M, Kubik P, Nowak JS, Webb S, et al. RNA-binding activity of TRIM25 is mediated by its PRY/SPRY domain and is required for ubiquitination. BMC Biol. 2017; 15: 105. https://doi.org/10.1186/s12915-017-0444-9 PMID: 29117863

25. Ficarelli M, Neil SJD, Swanson CM. Targeted Restriction of Viral Gene Expression and Replication by the ZAP Antiviral System. Annu Rev Virol. 2021; 8: 265–283. https://doi.org/10.1146/annurev-virology-091919-104213 PMID: 34129371

26. Goodier JL, Pereira GC, Cheung LE, Rose RJ, Kazazian HH. The Broad-Spectrum Antiviral Protein ZAP Restricts Human Retrotransposition. Malik HS, editor. PLoS Genet. 2015; 11: e1005252. https://doi.org/10.1371/journal.pgen.1005252 PMID: 26001115

27. Decorsière A, Mueller H, van Breugel PC, Abdul F, Gerossier L, Beran RK, et al. Hepatitis B virus X protein identifies the Smc5/6 complex as a host restriction factor. Nature. 2016; 531: 386–380. https://doi.org/10.1038/nature17170 PMID: 26983541

28. Nomura K, Klejnot M, Kowalczyk D, Hock AK, Sibbet GJ, Vousden KH, et al. Structural analysis of MDM2 RING separates degradation from regulation of p53 transcription activity. Nature Structural & Molecular Biology. 2017; 24: 578–587. https://doi.org/10.1038/nsmb.3414 PMID: 28553961

29. Koliopoulos MG, Esposito D, Christodoulou E, Taylor IA, Rittinger K. Functional role of TRIM E3 ligase oligomerization and regulation of catalytic activity. EMBO J. 2016; 35: 1204–1218. https://doi.org/10.15252/embj.201593741 PMID: 27154206

30. Pettersen EF, Goddard TD, Huang CC, Couch GS, Greenblatt DM, Meng EC, et al. UCSF Chimera—A visualization system for exploratory research and analysis. Journal of Computational Chemistry. 2004; 25: 1605–1612. https://doi.org/10.1002/jcc.20084 PMID: 15264254

31. Woodard LE, Wilson MH. piggyBac-ing models and new therapeutic strategies. Trends in Biotechnology. 2015; 33: 525–533. https://doi.org/10.1016/j.tibtech.2015.06.009 PMID: 26211958

32. Blighe K, Rana S, Lewis M. EnhancedVolcano: Publication-ready volcano plots with enhanced colouring and labeling. 2021. Available: https://github.com/kevinblighe/EnhancedVolcano

33. Huang DW, Sherman BT, Lempicki RA. Systematic and integrative analysis of large gene lists using DAVID bioinformatics resources. Nature Protocols. 2009; 4: 44–57. https://doi.org/10.1038/nprot.2008.211 PMID: 19131956

34. Huang DW, Sherman BT, Lempicki RA. Bioinformatics enrichment tools: paths toward the comprehensive functional analysis of large gene lists. Nucleic Acids Research. 2009; 37: 1–13. https://doi.org/10.1093/nar/gkn923 PMID: 19033363

35. Luu AP, Yao Z, Ramachandran S, Azzopardi SA, Miles LA, Schneider WM, et al. A CRISPR Activation Screen Identifies an Atypical Rho GTPase That Enhances Zika Viral Entry. Viruses. 2021; 13: 2113. https://doi.org/10.3390/v13112113 PMID: 34834920

36. Tourrière H, Chebli K, Zekri L, Courselaud B, Blanchard JM, Bertrand E, et al. The RasGAP-associated endoribonuclease G3BP assembles stress granules. The Journal of Cell Biology. 2003; 160: 823–831. https://doi.org/10.1083/jcb.200212128 PMID: 12642610

37. Kang W, Wang Y, Yang W, Zhang J, Zheng H, Li D. Research Progress on the Structure and Function of G3BP. Frontiers in Immunology. 2021;12. Available: https://doi.org/10.3389/fimmu.2021.718548 PMID: 34526993

38. Cristea IM, Carroll J-WN, Rout MP, Rice CM, Chait BT, MacDonald MR. Tracking and Elucidating Alphavirus-Host Protein Interactions*. Journal of Biological Chemistry. 2006; 281: 30269–30278. https://doi.org/10.1074/jbc.M603980200 PMID: 16895903

39. Cristea IM, Rozjabek H, Molloy KR, Karki S, White LL, Rice CM, et al. Host Factors Associated with the Sindbis Virus RNA-Dependent RNA Polymerase: Role for G3BP1 and G3BP2 in Virus Replication. Journal of Virology. 2010; 84: 6720–6732. https://doi.org/10.1128/JVI.01983-09 PMID: 20392851

40. Scholte FEM, Tas A, Albulescu IC, Žusinaite E, Merits A, Snijder EJ, et al. Stress Granule Components G3BP1 and G3BP2 Play a Proviral Role Early in Chikungunya Virus Replication. Diamond MS, editor. Journal of Virology. 2015; 89: 4457–4469. https://doi.org/10.1128/JVI.03612-14 PMID: 25653451

41. Kim DY, Reynaud JM, Rasalouskaya A, Akhrymuk I, Mobley JA, Frolov I, et al. New World and Old World Alphaviruses Have Evolved to Exploit Different Components of Stress Granules, FXR and G3BP Proteins, for Assembly of Viral Replication Complexes. Heise MT, editor. PLoS Pathog. 2016; 12: e1005810. https://doi.org/10.1371/journal.ppat.1005810 PMID: 27509095

42. Panas MD, Schulte T, Thaa B, Sandalova T, Kedersha N, Achour A, et al. Viral and Cellular Proteins Containing FGDF Motifs Bind G3BP to Block Stress Granule Formation. PLOS Pathogens. 2015; 11: e1004659. https://doi.org/10.1371/journal.ppat.1004659 PMID: 25658430

43. Götte B, Panas MD, Hellström K, Liu L, Samreen B, Larsson O, et al. Separate domains of G3BP promote efficient clustering of alphavirus replication complexes and recruitment of the translation initiation machinery. PLoS Pathog. 2019; 15: e1007842. https://doi.org/10.1371/journal.ppat.1007842 PMID: 31199850

44. Schulte T, Liu L, Panas MD, Thaa B, Dickson N, Götte B, et al. Combined structural, biochemical and cellular evidence demonstrates that both FGDF motifs in alphavirus nsP3 are required for efficient replication. Open Biology. 2016; 6: 160078. https://doi.org/10.1098/rsob.160078 PMID: 27383630

45. Kruse T, Benz C, Garvanska DH, Lindqvist R, Mihalic F, Coscia F, et al. Large scale discovery of coronavirus-host factor protein interaction motifs reveals SARS-CoV-2 specific mechanisms and vulnerabilities. Nat Commun. 2021; 12: 6761. https://doi.org/10.1038/s41467-021-26498-z PMID: 34799561

46. Takayama K, Suzuki T, Tanaka T, Fujimura T, Takahashi S, Urano T, et al. TRIM25 enhances cell growth and cell survival by modulating p53 signals via interaction with G3BP2 in prostate cancer. Oncogene. 2018; 37: 2165–2180. https://doi.org/10.1038/s41388-017-0095-x PMID: 29379164

47. Lim KL, Chew KCM, Tan JMM, Wang C, Chung KKK, Zhang Y, et al. Parkin Mediates Nonclassical, Proteasomal-Independent Ubiquitination of Synphilin-1: Implications for Lewy Body Formation. J Neurosci. 2005; 25: 2002–2009. https://doi.org/10.1523/JNEUROSCI.4474-04.2005 PMID: 15728840

48. Götte B, Utt A, Fragkoudis R, Merits A, McInerney GM. Sensitivity of Alphaviruses to G3BP Deletion Correlates with Efficiency of Replicase Polyprotein Processing. J Virol. 2020; 94: e01681–19. https://doi.org/10.1128/JVI.01681-19 PMID: 31941782

49. Kim YK, Maquat LE. UPFront and center in RNA decay: UPF1 in nonsense-mediated mRNA decay and beyond. RNA. 2019; 25: 407–422. https://doi.org/10.1261/rna.070136.118 PMID: 30655309

50. Balistreri G, Horvath P, Schweingruber C, Zünd D, McInerney G, Merits A, et al. The Host Nonsense-Mediated mRNA Decay Pathway Restricts Mammalian RNA Virus Replication. Cell Host & Microbe. 2014; 16: 403–411. https://doi.org/10.1016/j.chom.2014.08.007 PMID: 25211080

51. Kim W, Bennett EJ, Huttlin EL, Guo A, Li J, Possemato A, et al. Systematic and Quantitative Assessment of the Ubiquitin-Modified Proteome. Molecular Cell. 2011; 44: 325–340. https://doi.org/10.1016/j.molcel.2011.08.025 PMID: 21906983

52. Radivojac P, Vacic V, Haynes C, Cocklin RR, Mohan A, Heyen JW, et al. Identification, analysis, and prediction of protein ubiquitination sites. Proteins: Structure, Function, and Bioinformatics. 2010; 78: 365–380. https://doi.org/10.1002/prot.22555 PMID: 19722269

53. Mátyási B, Farkas Z, Kopper L, Sebestyén A, Boissan M, Mehta A, et al. The Function of NM23-H1/NME1 and Its Homologs in Major Processes Linked to Metastasis. Pathol Oncol Res. 2020; 26: 49–61. https://doi.org/10.1007/s12253-020-00797-0 PMID: 31993913

54. Yan N, Cherepanov P, Daigle JE, Engelman A, Lieberman J. The SET Complex Acts as a Barrier to Autointegration of HIV-1. PLOS Pathogens. 2009; 5: e1000327. https://doi.org/10.1371/journal.ppat.1000327 PMID: 19266025

55. Wigington CP, Williams KR, Meers MP, Bassell GJ, Corbett AH. Poly(A) RNA-binding proteins and polyadenosine RNA: new members and novel functions. WIREs RNA. 2014; 5: 601–622. https://doi.org/10.1002/wrna.1233 PMID: 24789627

56. Burgess HM, Richardson WA, Anderson RC, Salaun C, Graham SV, Gray NK. Nuclear relocalisation of cytoplasmic poly(A)-binding proteins PABP1 and PABP4 in response to UV irradiation reveals mRNA-dependent export of metazoan PABPs. Journal of Cell Science. 2011; 124: 3344–3355. https://doi.org/10.1242/jcs.087692 PMID: 21940797

57. Gao J, Tang Y-D, Hu W, Zheng C. When Poly(A) Binding Proteins Meet Viral Infections, Including SARS-CoV-2. Journal of Virology. 2022; 96: e00136–22. https://doi.org/10.1128/jvi.00136-22 PMID: 35293770

58. Jiao Y, Kong N, Wang H, Sun D, Dong S, Chen X, et al. PABPC4 Broadly Inhibits Coronavirus Replication by Degrading Nucleocapsid Protein through Selective Autophagy. Microbiology Spectrum. 2021; 9: e00908–21. https://doi.org/10.1128/Spectrum.00908-21 PMID: 34612687

59. Götte B, Panas MD, Hellström K, Liu L, Samreen B, Larsson O, et al. Separate domains of G3BP promote efficient clustering of alphavirus replication complexes and recruitment of the translation initiation machinery. Heise MT, editor. PLoS Pathog. 2019; 15: e1007842. https://doi.org/10.1371/journal.ppat.1007842 PMID: 31199850

60. Mark KG, Loveless TB, Toczyski DP. Isolation of ubiquitinated substrates by tandem affinity purification of E3 ligase–polyubiquitin-binding domain fusions (ligase traps). Nat Protoc. 2016; 11: 291–301. https://doi.org/10.1038/nprot.2016.008 PMID: 26766115

61. Komander D, Rape M. The Ubiquitin Code. Annu Rev Biochem. 2012; 81: 203–229. https://doi.org/10.1146/annurev-biochem-060310-170328 PMID: 22524316

62. Hornbeck PV, Zhang B, Murray B, Kornhauser JM, Latham V, Skrzypek E. PhosphoSitePlus, 2014: mutations, PTMs and recalibrations. Nucleic Acids Research. 2015; 43: D512–D520. https://doi.org/10.1093/nar/gku1267 PMID: 25514926

63. Lee SR, Pratt GA, Martinez FJ, Yeo GW, Lykke-Andersen J. Target Discrimination in Nonsense-Mediated mRNA Decay Requires Upf1 ATPase Activity. Molecular Cell. 2015; 59: 413–425. https://doi.org/10.1016/j.molcel.2015.06.036 PMID: 26253027

64. Serdar LD, Whiteside DL, Baker KE. ATP hydrolysis by UPF1 is required for efficient translation termination at premature stop codons. Nat Commun. 2016; 7: 14021. https://doi.org/10.1038/ncomms14021 PMID: 28008922

65. Fischer JW, Busa VF, Shao Y, Leung AKL. Structure-Mediated RNA Decay by UPF1 and G3BP1. Molecular Cell. 2020; 78: 70–84.e6. https://doi.org/10.1016/j.molcel.2020.01.021 PMID: 32017897

66. Götte B, Liu L, McInerney G. The Enigmatic Alphavirus Non-Structural Protein 3 (nsP3) Revealing Its Secrets at Last. Viruses. 2018; 10: 105. https://doi.org/10.3390/v10030105 PMID: 29495654

67. Chen W, Xiong S, Li J, Li X, Liu Y, Zou C, et al. The Ubiquitin E3 Ligase SCF-FBXO24 Recognizes Deacetylated Nucleoside Diphosphate Kinase A To Enhance Its Degradation. Molecular and Cellular Biology. 2015 [cited 9 Jan 2022]. https://doi.org/10.1128/MCB.01185-14 PMID: 25582197

68. Li C, Han T, Li Q, Zhang M, Guo R, Yang Y, et al. MKRN3-mediated ubiquitination of Poly(A)-binding proteins modulates the stability and translation of GNRH1 mRNA in mammalian puberty. Nucleic Acids Research. 2021; 49: 3796–3813. https://doi.org/10.1093/nar/gkab155 PMID: 33744966

69. Koepke L, Gack MU, Sparrer KM. The antiviral activities of TRIM proteins. Current Opinion in Microbiology. 2021; 59: 50–57. https://doi.org/10.1016/j.mib.2020.07.005 PMID: 32829025

70. Pérez-González A, Pazo A, Navajas R, Ciordia S, Rodriguez-Frandsen A, Nieto A. hCLE/C14orf166 Associates with DDX1-HSPC117-FAM98B in a Novel Transcription-Dependent Shuttling RNA-Transporting Complex. PLOS ONE. 2014; 9: e90957. https://doi.org/10.1371/journal.pone.0090957 PMID: 24608264

71. Pazo A, Pérez-González A, Oliveros JC, Huarte M, Chavez JP, Nieto A. hCLE/RTRAF-HSPC117-DDX1-FAM98B: A New Cap-Binding Complex That Activates mRNA Translation. Frontiers in Physiology. 2019; 10: 92. https://doi.org/10.3389/fphys.2019.00092 PMID: 30833903

72. Rodriguez A, Pérez-González A, Nieto A. Cellular Human CLE/C14orf166 Protein Interacts with Influenza Virus Polymerase and Is Required for Viral Replication. Journal of Virology. 2011; 85: 12062. https://doi.org/10.1128/JVI.00684-11 PMID: 21900157

73. Deutschmann J, Gramberg T. SAMHD1 . . . and Viral Ways around It. Viruses. 2021; 13: 395. https://doi.org/10.3390/v13030395 PMID: 33801276

74. Liang Y, Nandakumar KS, Cheng K. Design and pharmaceutical applications of proteolysis-targeting chimeric molecules. Biochemical Pharmacology. 2020; 182: 114211. https://doi.org/10.1016/j.bcp.2020.114211 PMID: 32866456

75. Gorchakov R, Wang E, Leal G, Forrester NL, Plante K, Rossi SL, et al. Attenuation of Chikungunya Virus Vaccine Strain 181/Clone 25 Is Determined by Two Amino Acid Substitutions in the E2 Envelope Glycoprotein. Journal of Virology. 2012; 86: 6084–6096. https://doi.org/10.1128/JVI.06449-11 PMID: 22457519

76. Brault AC, Foy BD, Myles KM, Kelly CLH, Higgs S, Weaver SC, et al. Infection patterns of o'nyong nyong virus in the malaria-transmitting mosquito, Anopheles gambiae. Insect Molecular Biology. 2004; 13: 625–635. https://doi.org/10.1111/j.0962-1075.2004.00521.x PMID: 15606811

77. Morrison TE, Whitmore AC, Shabman RS, Lidbury BA, Mahalingam S, Heise MT. Characterization of Ross River Virus Tropism and Virus-Induced Inflammation in a Mouse Model of Viral Arthritis and Myositis. Journal of Virology. 2006; 80: 737–749. https://doi.org/10.1128/JVI.80.2.737-749.2006 PMID: 16378976

78. Rice CM, Levis R, Strauss JH, Huang HV. Production of infectious RNA transcripts from Sindbis virus cDNA clones: mapping of lethal mutations, rescue of a temperature-sensitive marker, and in vitro mutagenesis to generate defined mutants. Journal of Virology. 1987; 61: 3809–3819. https://doi.org/10.1128/JVI.61.12.3809-3819.1987 PMID: 3479621

79. Bick MJ, Carroll J-WN, Gao G, Goff SP, Rice CM, MacDonald MR. Expression of the Zinc-Finger Antiviral Protein Inhibits Alphavirus Replication. Journal of Virology. 2003; 77: 11555–11562. https://doi.org/10.1128/jvi.77.21.11555-11562.2003 PMID: 14557641

80. Frolova EI, Fayzulin RZ, Cook SH, Griffin DE, Rice CM, Frolov I. Roles of Nonstructural Protein nsP2 and Alpha/Beta Interferons in Determining the Outcome of Sindbis Virus Infection. Journal of Virology. 2002; 76: 11254–11264. https://doi.org/10.1128/jvi.76.22.11254-11264.2002 PMID: 12388685

81. Atasheva S, Krendelchtchikova V, Liopo A, Frolova E, Frolov I. Interplay of Acute and Persistent Infections Caused by Venezuelan Equine Encephalitis Virus Encoding Mutated Capsid Protein. Journal of Virology. 2010; 84: 10004–10015. https://doi.org/10.1128/JVI.01151-10 PMID: 20668087

82. Hayakawa S, Shiratori S, Yamato H, Kameyama T, Kitatsuji C, Kashigi F, et al. ZAPS is a potent stimulator of signaling mediated by the RNA helicase RIG-I during antiviral responses. Nat Immunol. 2011; 12: 37–44. https://doi.org/10.1038/ni.1963 PMID: 21102435

83. Feng Q, Jagannathan S, Bradley RK. The RNA Surveillance Factor UPF1 Represses Myogenesis via Its E3 Ubiquitin Ligase Activity. Molecular Cell. 2017; 67: 239–251.e6. https://doi.org/10.1016/j.molcel.2017.05.034 PMID: 28669802

84. Landthaler M, Gaidatzis D, Rothballer A, Chen PY, Soll SJ, Dinic L, et al. Molecular characterization of human Argonaute-containing ribonucleoprotein complexes and their bound target mRNAs. RNA. 2008; 14: 2580–2596. https://doi.org/10.1261/rna.1351608 PMID: 18978028

85. Labun K, Montague TG, Gagnon JA, Thyme SB, Valen E. CHOPCHOP v2: a web tool for the next generation of CRISPR genome engineering. Nucleic Acids Res. 2016; 44: W272–W276. https://doi.org/10.1093/nar/gkw398 PMID: 27185894

86. Ran FA, Hsu PD, Wright J, Agarwala V, Scott DA, Zhang F. Genome engineering using the CRISPR-Cas9 system. Nat Protoc. 2013; 8: 2281–2308. https://doi.org/10.1038/nprot.2013.143 PMID: 24157548

87. Lacoste A, Berenshteyn F, Brivanlou AH. An Efficient and Reversible Transposable System for Gene Delivery and Lineage-Specific Differentiation in Human Embryonic Stem Cells. Cell Stem Cell. 2009; 5: 332–342. https://doi.org/10.1016/j.stem.2009.07.011 PMID: 19733544

88. Li MMH, Aguilar EG, Michailidis E, Pabon J, Park P, Wu X, et al. Characterization of Novel Splice Variants of Zinc Finger Antiviral Protein (ZAP). Heise MT, editor. J Virol. 2019; 93: e00715–19, /jvi/93/18/JVI.00715-19.atom. https://doi.org/10.1128/JVI.00715-19 PMID: 31118263

89. Mayank AK, Pandey V, Vashisht AA, Barshop WD, Rayatpisheh S, Sharma T, et al. An Oxygen-Dependent Interaction between FBXL5 and the CIA-Targeting Complex Regulates Iron Homeostasis. Molecular Cell. 2019; 75: 382–393.e5. https://doi.org/10.1016/j.molcel.2019.05.020 PMID: 31229404

90. Jami-Alahmadi Y, Pandey V, Mayank AK, Wohlschlegel JA. A Robust Method for Packing High Resolution C18 RP-nano-HPLC Columns. JoVE (Journal of Visualized Experiments). 2021; e62380. https://doi.org/10.3791/62380 PMID: 34057454

91. Cox J, Mann M. MaxQuant enables high peptide identification rates, individualized p.p.b.-range mass accuracies and proteome-wide protein quantification. Nature Biotechnology. 2008; 26: 1367–1372. https://doi.org/10.1038/nbt.1511 PMID: 19029910

92. Perez-Riverol Y, Bai J, Bandla C, García-Seisdedos D, Hewapathirana S, Kamatchinathan S, et al. The PRIDE database resources in 2022: a hub for mass spectrometry-based proteomics evidences. Nucleic Acids Research. 2022; 50: D543–D552. https://doi.org/10.1093/nar/gkab1038 PMID: 34723319

93. Jimenez-Morales D, Rosa Campos A, Von Dollen J. artMS: Analytical R tools for Mass Spectrometry. R package version 1.4.2. 2019.

# Appendix 2: Interaction of chikungunya virus glycoproteins with macrophage factors controls virion production

Article

SOURCE DATA | TRANSPARENT PROCESS | OPEN ACCESS | CHECK FOR UPDATES

THE EMBO JOURNAL

# Interaction of chikungunya virus glycoproteins with macrophage factors controls virion production

Zhenlan Yao [1], Sangeetha Ramachandran[1], Serina Huang [2], Erin Kim[3], Yasaman Jami-Alahmadi [4], Prashant Kaushal [1,5,6], Mehdi Bouhaddou [1,5,6], James A Wohlschlegel[4] & Melody MH Li [1,6]✉

## Abstract

**Despite their role as innate sentinels, macrophages can serve as cellular reservoirs of chikungunya virus (CHIKV), a highly-pathogenic arthropod-borne alphavirus that has caused large outbreaks among human populations. Here, with the use of viral chimeras and evolutionary selection analysis, we define CHIKV glycoproteins E1 and E2 as critical for virion production in THP-1 derived human macrophages. Through proteomic analysis and functional validation, we further identify signal peptidase complex subunit 3 (SPCS3) and eukaryotic translation initiation factor 3 subunit K (eIF3k) as E1-binding host proteins with anti-CHIKV activities. We find that E1 residue V220, which has undergone positive selection, is indispensable for CHIKV production in macrophages, as its mutation attenuates E1 interaction with the host restriction factors SPCS3 and eIF3k. Finally, we show that the antiviral activity of eIF3k is translation-independent, and that CHIKV infection promotes eIF3k translocation from the nucleus to the cytoplasm, where it associates with SPCS3. These functions of CHIKV glycoproteins late in the viral life cycle provide a new example of an intracellular evolutionary arms race with host restriction factors, as well as potential targets for therapeutic intervention.**

**Keywords** Alphavirus E1 Glycoprotein; Chikungunya Virus; eIF3k; Evolutionary Selection; Macrophage
**Subject Categories** Evolution & Ecology; Microbiology, Virology & Host Pathogen Interaction
https://doi.org/10.1038/s44318-024-00193-3
Received 22 September 2023; Revised 16 July 2024; Accepted 17 July 2024
Published online: 11 September 2024

## Introduction

Macrophages are phagocytic innate immune cells with critical functions in first-line defense against virus infection, inflammation, and priming of the adaptive immune system (Murray and Wynn, 2011). The sensing of viral infection by pattern recognition receptors in macrophages rapidly establishes an antiviral state through activation of the interferon (IFN) response (McNab et al, 2015). However, some viruses, such as highly-pathogenic avian influenza H5N1 viruses can breach this antiviral immunity (Cline et al, 2017; Marvin et al, 2017; Short et al 2012), highlighting productive macrophage infection as an important determinant for viral virulence. Moreover, in individuals infected with human immunodeficiency virus (HIV)(Kruize and Kootstra, 2019; Brown and Mattapallil, 2014), macrophages are potential reservoirs for rebound viremia upon cessation of antiretroviral therapy (Kruize and Kootstra, 2019; Kumar et al, 2014). Therefore, targeting viral infection of macrophages is an attractive therapeutic strategy for virus eradication.

Chikungunya virus (CHIKV) is a highly-pathogenic arthropod-borne alphavirus that has expanded worldwide with emerging lineages in recent decades (Weaver et al, 2020; Gould and Higgs, 2009). The unprecedented outbreaks from the Indian Ocean islands to Southeast Asia were caused by the novel CHIKV Indian Ocean lineage (IOL), characterized primarily by the E1-A226V mutation that adapted the virus from its principal vector *Aedes aegypti* to *Aedes albopictus* (Tsetsarkin et al, 2007, 2014; Chen et al, 2021). Although CHIKV infection is typically cleared in a few days, a significant percentage of individuals develop incapacitating arthralgia for up to 20 months (Schwartz and Albert, 2010; Pialoux et al, 2007; Gunn et al, 2012). Interestingly, CHIKV RNA and proteins persist in monocyte-derived macrophages (MDMs) in the spleen or synovial tissue for months in macaques and humans suffering from chronic arthralgia (Dupuis-Maguiraga et al, 2012; Labadie et al, 2010; Hoarau et al, 2010). These studies propose a role for macrophages as a cellular reservoir for CHIKV persistence and a niche for inflammation that is recurrently activated by viral components (Dupuis-Maguiraga et al, 2012; Kril et al, 2021). However, it is not clear what mechanism drives CHIKV persistence and whether this pathogenic role of macrophages is found in all arthritogenic alphavirus infections.

In contrast, o'nyong'nyong virus (ONNV), an arthritogenic alphavirus that shares the most genetic identity with CHIKV, is confined to periodic outbreaks in Africa (Weaver et al, 2020; Cottis et al, 2023). ONNV causes similar symptoms in humans, but is less virulent in mouse models, requiring a higher dose than

[1]Department of Microbiology, Immunology and Molecular Genetics, University of California, Los Angeles, Los Angeles, CA, USA. [2]Department of Human Genetics, David Geffen School of Medicine, University of California, Los Angeles, Los Angeles, CA, USA. [3]Department of Chemistry and Biochemistry, University of California, Los Angeles, Los Angeles, CA, USA. [4]Department of Biological Chemistry, University of California, Los Angeles, Los Angeles, CA, USA. [5]Institute for Quantitative and Computational Biosciences, University of California, Los Angeles, Los Angeles, CA, USA. [6]Molecular Biology Institute, University of California Los Angeles, Los Angeles, CA, USA. ✉E-mail: Manhingli@mednet.ucla.edu

CHIKV to reach the same level of mortality (Seymour et al, 2013). The evolutionary similarities yet epidemiological differences make CHIKV-ONNV chimeras excellent molecular tools for probing viral determinants for host adaptation. However, these studies so far have mostly focused on their differential uses of mosquito vectors, such as transmission of ONNV by *Anopheles gambiae* (Saxton-Shaw et al, 2013; Vanlandingham et al, 2006), while little is known about the molecular mechanisms underlying infection of human cells relevant for viral dissemination, such as macrophages.

Viral infection is mostly abortive in macrophages as host restriction factors either basally expressed or amplified by the IFN response suppress specific viral life cycle stages (Tenthorey et al, 2022). Even though CHIKV replication is active in human MDMs, it is more restricted in MDMs than in epithelial cells and fibroblasts (Sourisseau et al, 2007), suggesting viral suppression by macrophage restriction factors. Host antiviral immunity can impose evolutionary selective pressures on viral proteins, propelling viruses to evade or antagonize these blockades, such as the arms race between myeloid-cell-specific SAMHD1 (SAM and HD domain containing deoxynucleoside triphosphate triphosphohydrolase 1) and HIV-2 Vpx (Hrecka et al, 2011; Laguette et al, 2012; Daugherty et al, 2014). This prompted us to question how and to what extent the evolutionary pressure brought on by the host-virus arms race has selected for increased CHIKV survival in human macrophages.

Here, we found that human primary monocyte and THP-1-derived macrophage infection with CHIKV (vaccine strain 181/clone 25) is much more efficient than that of ONNV at a step following genome replication. By utilizing a repertoire of CHIKV-ONNV chimeras, we mapped the viral determinant for efficient virion production in macrophages to the CHIKV E2 and E1 glycoproteins. Interestingly, evolutionary analysis of 397 CHIKV structural polyprotein sequences isolated from infected individuals uncovered signatures of positive selection mostly in E2 and E1 proteins. Mutating two of the positively selected residues in CHIKV to the homologous ones in ONNV (E2-V135L, E1-V220I) attenuates virion production in 293T and BHK-21 cells while the E1-V220I mutation completely abolishes virion production in macrophages. We further performed affinity purification-mass spectrometry (AP-MS) to identify macrophage interactors of CHIKV glycoproteins that are involved in CHIKV production. We discovered and validated that E1 interacts with signal peptidase complex subunit 3 (SPCS3) and eukaryotic translation initiation factor 3 subunit K (eIF3k), which block CHIKV production in macrophages. Importantly, the E1-V220I mutation significantly reduces E1 binding to both SPCS3 and eIF3k, suggesting that the positive selection signature is driven by these host restriction factors. Despite its role as a translation initiation factor, eIF3k exhibits both cytoplasmic and nuclear localization. Interestingly, we observed translocation of eIF3k from the nucleus to the cytoplasm and increased colocalization with SPCS3 upon CHIKV infection. Interrogation of eIF3k anti-CHIKV mechanism in CRISPR-Cas9 knockout (KO) cells showed that eIF3k specifically inhibits CHIKV production through its HAM protein domain in a translation-independent manner. Taken together, we found that, in addition to their critical function in viral entry and egress, CHIKV glycoproteins may interfere with cellular restrictions to facilitate virion production and spread in macrophages.

## Results

### CHIKV infects human macrophages more efficiently than other arthritogenic alphaviruses

To evaluate the susceptibility of macrophages to different arthritogenic alphaviruses, we infected human primary monocyte-derived macrophages with EGFP-expressing Sindbis virus (SINV), Ross river virus (RRV), ONNV, and CHIKV, and quantified infection levels at 24 h post infection (h.p.i.) by flow cytometry (Fig. 1A). Despite generally low infection rates with these alphaviruses (<1%), we observed a small percentage (0.76%) of macrophages highly infected with CHIKV, according to intracellular EGFP expression that spans 3 logs. We then compared the growth kinetics of CHIKV and its closest relative, ONNV, in infected human monocytic cell line THP-1-derived macrophages by quantifying virion production in the supernatant (Fig. 1B). We found that CHIKV produces two to three logs higher titers than ONNV throughout the infection time-course (up to $1.05 \times 10^7$ pfu/ml for CHIKV compared to $3.75 \times 10^4$ pfu/ml for ONNV), with the titers of both viruses peaking at 24 h.p.i. We also compared ONNV SG650 infection to infections with pathogenic CHIKV La Réunion (LR2006 OPY1) and Asian (AF15561) strains in THP-1 derived macrophages (Fig. EV1A). We demonstrated that pathogenic CHIKV infections result in higher levels of virion production in comparison to ONNV infection. These results suggest that a small number of CHIKV-infected macrophages are extremely efficient at producing viral progeny.

We asked whether the high level of CHIKV production is achieved by enhanced viral replication in macrophages. To bypass viral entry, we directly transfected in vitro transcribed genomic viral RNAs (vRNAs) of CHIKV and ONNV into THP-1-derived macrophages (Fig. 1C). We measured intracellular negative-sense viral RNA ((-) vRNA), the replicative intermediate, by TaqMan RT-qPCR assays. To our surprise, the (−) vRNA levels of ONNV are significantly higher than those of CHIKV following vRNA transfection, suggesting CHIKV infection is enhanced at a step after genome replication in macrophages. Nevertheless, virion production of CHIKV is dramatically more robust than that of ONNV and could be detected as early as 8 h post transfection (h.p.t.) (Fig. 1D). Taken together, human macrophage infection with CHIKV drives more superior virion production than that with ONNV.

### CHIKV E2 and E1 synergize to mediate efficient virion production in THP-1-derived human macrophages

To identify the viral determinants for CHIKV infection of human macrophages, we constructed several CHIKV-ONNV chimeras (Fig. 2A) and assessed their infection levels in THP-1 derived macrophages, compared to parental CHIKV and ONNV. Alphaviruses express four nonstructural proteins (nsP1-4) for viral replication, and five structural proteins from a subgenomic mRNA (capsid, E3, E2, 6K/TF, E1) for viral particle assembly and host cell entry (Kafai et al, 2022). These proteins are proteolytically processed from the nonstructural and structural polyproteins. Given the genome organization, we generated Chimera I that contains ONNV nsP1 to capsid in a CHIKV backbone, and Chimera III, that contains CHIKV nsP1 to capsid in an ONNV



 

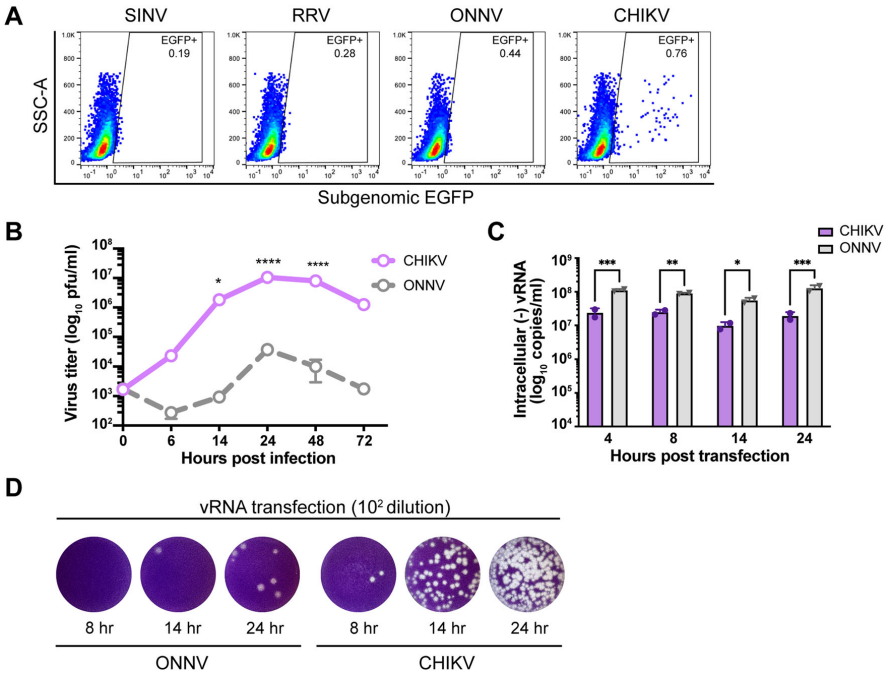


**Figure 1. Efficient CHIKV infection in human macrophages depends on a high level of virion production.**

(**A**) Human peripheral monocyte-derived macrophages were infected with EGFP-labeled alphaviruses (SINV TE/5′2 J, RRV strain T48, ONNV strain SG650, and CHIKV vaccine strain 181/clone 25) at MOI of 5 for 24 h. Levels of infection with different alphaviruses were determined by percent EGFP-positive cells evaluated by flow cytometry. Data are representative of 2 independent experiments performed in biological duplicates. (**B**) THP-1-derived macrophages were infected with CHIKV 181/clone 25 or ONNV SG650 at MOI 5. Titration of supernatant virus samples was performed at 0, 6, 14, 24, 48, and 72 h.p.i by plaque assay on BHK-21 cells. Data were representative of two independent experiments. Mean values of biological duplicates were plotted with SD. Asterisks indicate statistically significant differences as compared to ONNV (two-way ANOVA and Šidák's multiple comparisons test: 14 h $*p = 0.0128$; 24 h and 48 h $****p < 0.0001$). (**C**) Levels of intracellular (−) vRNAs, the viral replicative intermediate, at 4, 8, 14, and 24 h post transfection of THP-1 derived macrophages with CHIKV 181/clone 25 or ONNV SG650 viral RNAs (vRNAs) were quantified through RT-qPCR with specific TaqMan probes. Data were representative of two independent experiments. Mean values of biological duplicates measured in technical duplicates were plotted with SD (Two-way ANOVA and Šidák's multiple comparisons test: 4 h $***p = 0.0006$; 8 h $**p = 0.004$; 14 h $*p = 0.0299$; 24 h $***p = 0.0001$). (**D**) CHIKV and ONNV titers of supernatant samples collected from transfected THP-1 derived macrophages in (**C**) were determined by plaque assay. The incubation period for plaque assay took 40 h. Representative plaques of CHIKV and ONNV from two independent experiments (1:100 dilution) are shown. Source data are available online for this figure.

backbone. To account for potential discrepancies associated with mismatched subgenomic promoters located at the 3′ end of nsP4 and structural proteins, we also generated Chimeras II and IV, where the swapping of viral genes starts with the subgenomic promoters in CHIKV and ONNV nsP4. We found comparable levels of virion production of Chimeras I and II as CHIKV in the supernatant of infected macrophages, while Chimeras III and IV recapitulate ONNV production (Fig. 2B). These data demonstrate that the viral determinants for effective macrophage infection lie in the CHIKV E3-E2-6K-E1 structural polyprotein region.

To investigate the role of CHIKV structural proteins in virion production, we transfected vRNAs of CHIKV, ONNV, and Chimeras I-IV into THP-1-derived macrophages to bypass viral entry. We compared viral replication and production among the transfected cells at 24 h.p.t. based on intracellular positive-sense viral RNA ((+) vRNA) levels and supernatant titers (Fig. 2C). Consistent with Fig. 2B, transfection of viral genomes without CHIKV E3-E2-6K-E1 (ONNV, Chimera III, and Chimera IV) led to lower levels of virion production.

To further narrow down the viral determinants for CHIKV infection in macrophages, we constructed three additional chimeras in the context of Chimera III to include CHIKV E3 (Chimera III-I), E3-E2 (Chimera III-II), or E3-E2-6K (Chimera III-III) (Fig. 2D). Upon macrophage infection with CHIKV, ONNV, and the chimeras, we found that only Chimera III-II and Chimera III-III, both possessing CHIKV E2, partially enhance virion production at 24 and 48 h.p.i. although not significantly (Fig. 2E), suggesting that E2 alone is not sufficient. Chimera III-III with all the CHIKV structural proteins except E1 fails to fully rescue virion production in macrophages. Taken together, this supports the involvement of both CHIKV E2 and E1 in virion production.

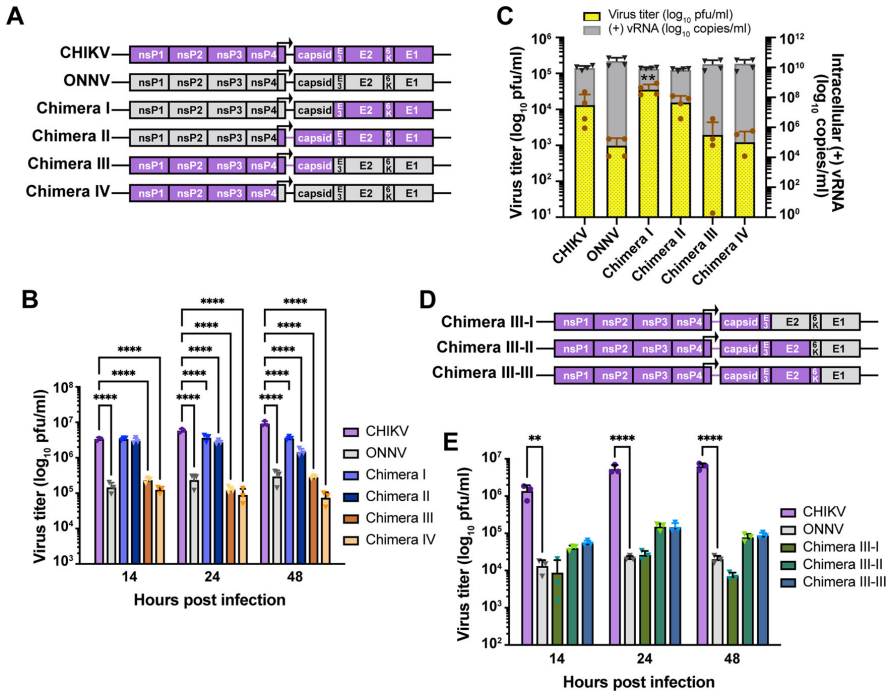


**Figure 2. Viral glycoproteins are critical determinants for macrophage tropism of CHIKV.**

(**A**) Schematic representation of CHIKV, ONNV, Chimera I, II, III, and IV. These chimeras consist of genomes from CHIKV vaccine strain 181/clone 25 and ONNV SG650 in different ratios: Chimera I contains the ONNV genome from nsP1 to capsid and the CHIKV genome from E3 to E1. Chimera II contains the ONNV genome from nsP1 to the region prior to the subgenomic promoter in nsP4 and the CHIKV genome from the subgenomic promoter to E1. Chimera III contains the CHIKV genome from nsP1 to capsid and the ONNV genome from E3 to E1. Chimera IV contains the CHIKV genome from nsP1 to the region prior to the subgenomic promoter in nsP4 and the ONNV genome from the subgenomic promoter to E1. (**B**) Titration of supernatant samples from THP-1 derived macrophages infected with CHIKV 181/clone 25, ONNV SG650, and 4 chimeras (I, II, III, IV). The macrophages were inoculated with the virus at MOI 5, and the supernatant samples were collected at 14, 24, and 48 h.p.i for plaque assay analysis. The incubation period for plaque assay took 28 h. Data were representative of three independent experiments. Mean values of biological triplicates were plotted with SD. Asterisks indicate statistically significant differences as compared to CHIKV (Two-way ANOVA and Dunnett's multiple comparisons test: 14, 24, and 48 h ****$p < 0.0001$). (**C**) THP-1-derived macrophages were transfected with 0.5 μg RNA of CHIKV 181/clone 25, ONNV SG650, or chimeras (I, II, III, IV). Virion productions were determined by intracellular (+) vRNA transcript levels and supernatant infectious particle titers through RT-qPCR and plaque assay, respectively. The incubation period for plaque assay took 40 h. Data were plotted with the mean value of four biological replicates from two independent experiments. The error bar represents SD. Asterisks indicate statistically significant differences as compared to CHIKV (two-way ANOVA and Dunnett's multiple comparisons test: viral titer of CHIKV vs Chimera I **$p = 0.0036$). (**D**) Schematic representation of Chimera III-I, III-II, and III-III. Chimera III-I contains the CHIKV genome from nsP1 to E3 and the ONNV genome from E2 to E1. Chimera III-II contains the CHIKV genome from nsP1 to E2 and the ONNV genome from 6K to E1. Chimera III-III contains the CHIKV genome from nsP1 to 6 K and ONNV E1. (**E**) Titration of supernatant samples from THP-1 derived macrophages infected with CHIKV 181/clone 25, ONNV SG650, or chimeras (III-I, III-II, III-III) for 14, 24, and 48 h. The infection conditions and virus titer assessments were performed as previously described in (**B**). Data were representative of two independent experiments. Mean values of biological triplicates measured were plotted with SD. Asterisks indicate statistically significant differences as compared to ONNV (two-way ANOVA and Dunnett's multiple comparisons test: 14 h CHIKV vs ONNV **$p = 0.0092$; 24 and 48 h CHIKV vs ONNV ****$p < 0.0001$). Source data are available online for this figure.

To pinpoint the impact of CHIKV E2 and E1 on virion production, we generated three chimeras in the ONNV backbone with CHIKV replacement of E2 (ONNV/CHIKV E2), E1 (ONNV/CHIKV E1), or both E2 and E1 (ONNV/CHIKV E2 + E1) (Fig. 3A). Neither single replacement of CHIKV E2 nor E1 rescues ONNV infection of macrophages to comparable levels as CHIKV (Fig. 3B). Surprisingly, macrophage infection with ONNV/CHIKV E1 is more attenuated than that with ONNV. In contrast, the simultaneous replacement of E2 and E1 with CHIKV homologs (ONNV/CHIKV E2 + E1) increased the supernatant titers to levels even higher than those of CHIKV. We then transfected vRNAs into macrophages to evaluate viral replication and production (Fig. 3C). All of the transfected vRNAs launched productive viral replication in macrophages; however, only the transfection of ONNV/CHIKV E2 + E1 RNA led to significantly enhanced virion production, albeit at levels lower than those for transfection of CHIKV RNA (Fig. 3C).

In order to further characterize the viral particles released by infected macrophages, we compared the particle-to-PFU ratios among ONNV, CHIKV, Chimera I (Fig. 2A), and ONNV/CHIKV E2 + E1 (Fig. 3A). Importantly, we found ONNV and CHIKV to

 

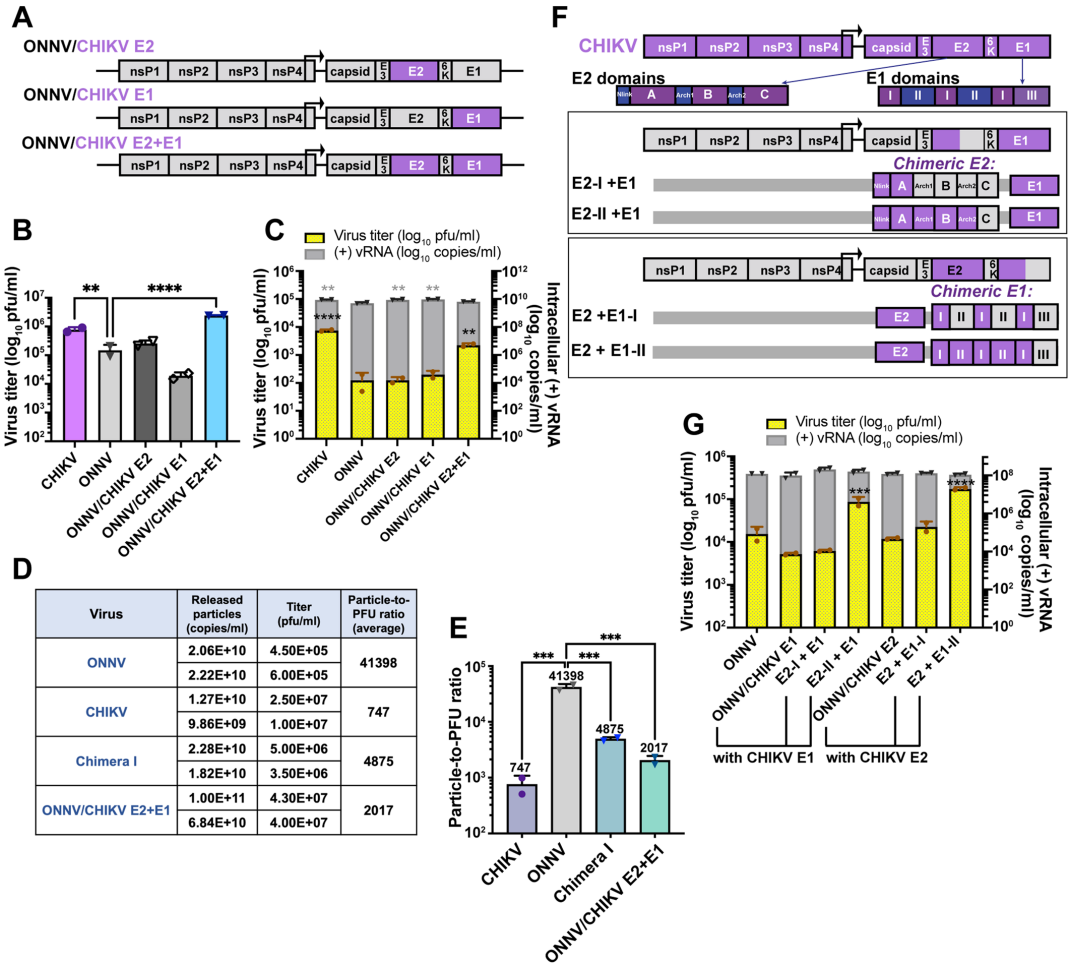


| Virus | Released particles (copies/ml) | Titer (pfu/ml) | Particle-to-PFU ratio (average) |
|---|---|---|---|
| ONNV | 2.06E+10 | 4.50E+05 | 41398 |
| | 2.22E+10 | 6.00E+05 | |
| CHIKV | 1.27E+10 | 2.50E+07 | 747 |
| | 9.86E+09 | 1.00E+07 | |
| Chimera I | 2.28E+10 | 5.00E+06 | 4875 |
| | 1.82E+10 | 3.50E+06 | |
| ONNV/CHIKV E2+E1 | 1.00E+11 | 4.30E+07 | 2017 |
| | 6.84E+10 | 4.00E+07 | |

have the highest (41398) and lowest (747) particle-to-PFU ratios, respectively (Fig. 3D,E). Consistent with that, either replacing the entire glyco-polyprotein or just E2 and E1 with the CHIKV homologs significantly decreased the particle-to-PFU ratios to 4875 and 2017, respectively, highlighting increased infectivity mediated by CHIKV glycoproteins. Since alphaviruses utilize the host secretory pathway for glycoprotein processing and maturation, we questioned whether the secretory pathway confers an advantage on CHIKV E2 and E1 proteins during the late stage of the viral life cycle in macrophages. We infected THP-1-derived macrophages, which had been treated with FLI-06 and Golgicide A (GCA), with ONNV, CHIKV, Chimera I, and ONNV/CHIKV E2 + E1 (Fig. EV1B). Golgicide A is a reversible inhibitor of Golgi-specific brefeldin A-resistance guanine-nucleotide exchange factor 1 (GBF1), an ARF-GEF (guanine-nucleotide exchange factors for ADP-ribosylation factor GTPases) in cis-Golgi, which leads to rapid disassembly of the Golgi and trans-Golgi network (TGN) (Saenz et al, 2009). FLI-06 interferes with cargo recruitment to ER-exit sites and disrupts Golgi without depolymerizing microtubules or interfering with GBF1 (Krämer et al, 2013). The plaque assay result shows that all the viruses are sensitive to secretory pathway disruption, however, the production of viruses containing CHIKV glycoproteins (CHIKV, Chimera I, and ONNV/CHIKV E2 + E1) is significantly more attenuated by FLI-06 and GCA. This demonstrates the greater dependence of CHIKV glycoproteins on the host secretory pathway for productive infection in macrophages.

In addition, we found that infections with ONNV, CHIKV, and chimeric viruses are less restricted in 293 T cells resulting in more robust virion production (over $10^8$ pfu/ml) (Fig. EV3A). There is no significant difference in virion production in 293T cells between CHIKV and ONNV, between CHIKV and Chimera I (Fig. 2A; ONNV with CHIKV poly-glycoproteins), between CHIKV and

**Figure 3. CHIKV E2 and E1 dramatically increase the specific infectivity of viral particles secreted from human macrophages without affecting viral RNA replication.**

(**A**) Schematic representation of chimera ONNV/CHIKV E2, ONNV/CHIKV E1 and ONNV/CHIKV E2 + E1. These three chimeric viruses were built on ONNV backbone with the replacement of CHIKV E2 (ONNV/CHIKV E2), E1 (ONNV/CHIKV E1), or both E2 and E1 (ONNV/CHIKV E2 + E1). (**B**) Titration of supernatant samples from THP-1 derived macrophages infected with CHIKV vaccine strain 181/clone 25, ONNV SG650, ONNV/CHIKV E2, ONNV/CHIKV E1, and ONNV/CHIKV E2 + E1. Macrophages were inoculated with the viruses at MOI 5, and the supernatant samples were collected at 24 h.p.i for plaque assay analysis. The incubation period for plaque assay took 28 h. Data were representative of two independent experiments. Mean values of biological duplicates were plotted with SD. Asterisks indicate statistically significant differences as compared to ONNV (two-way ANOVA and Dunnett's multiple comparisons test: ONNV vs CHIKV $^{**}p = 0.004$; ONNV vs ONNV/CHIKV E2 + E1$^{****}p < 0.0001$). (**C**) THP-1 derived macrophages were transfected with 0.5 μg RNA of CHIKV 181/clone 25, ONNV SG650, ONNV/CHIKV E2, ONNV/CHIKV E1, or ONNV/CHIKV E2 + E1. Virion production was determined by intracellular (+) vRNA transcript levels and supernatant infectious particle titers through RT-qPCR and plaque assay, respectively. The incubation period for plaque assay took 40 h. Data were representative of three independent experiments. Mean values of biological duplicates were plotted with SD. Asterisks indicate statistically significant differences as compared to ONNV (one-way ANOVA and Dunnett's multiple comparisons test: viral titer of ONNV vs CHIKV $^{****}p < 0.0001$; viral titer of ONNV vs ONNV/CHIKV E2 + E1$^{**}p = 0.0058$; viral copies of ONNV vs CHIKV $^{**}p = 0.0031$; viral copies of ONNV vs ONNV/CHIKV E2 $^{**}p = 0.0034$; viral copies of ONNV vs ONNV/CHIKV E1 $^{**}p = 0.0019$). (**D**, **E**) Particle-to-PFU ratios of ONNV, CHIKV, and chimeric viruses containing CHIKV glycoproteins. THP-1-derived macrophages were infected with ONNV SG650, CHIKV 181/clone 25, Chimera I (refer to Fig. 2A schematic), and ONNV/CHIKV E2 + E1 at MOI 5 for 24 h. The viral particle numbers in the supernatant were quantified by TaqMan qPCR assay with specific probes targeting nsP1 in (+) RNA. Virus titers were determined by plaque assay on BHK-21 cells. The incubation period for plaque assay took 28 h. Data were representative of two independent experiments, each of which has biological duplicate samples. The viral copy numbers and titers of each duplicate and their averaged values are shown in (**D**) and summarized as bar charts in (**E**). Asterisks indicate statistically significant differences as compared to ONNV (one-way ANOVA and Dunnett's multiple comparisons test: ONNV vs CHIKV$^{***}p = 0.0005$; ONNV vs Chimera I$^{***}p = 0.0008$; ONNV vs ONNV/CHIKV E2 + E1$^{***}p = 0.0006$). (**F**) Schematic representation of modified chimeras based on parental ONNV/CHIKV E1 + E2 that contain hybrid E2 or E1. E2 has three domains: A and B connected to A and C by two flanking β-ribbon arches, and C. E1 has three domains: I, II, and III, with a fusion loop in II. Chimera containing hybrid E2 that has arch-B-arch-C (E2-I + E1), or only domain C (E2-II + E1) from ONNV. Chimera containing hybrid E1 has domains II and III (E2 + E1-I), or only domain III (E2 + E1-II) from ONNV. (**G**) THP-1 derived macrophages were transfected with 0.5 μg RNA of ONNV SG650, ONNV/CHIKV E1 and chimeras (E2-I + E1, E2-II + E1), ONNV/CHIKV E2 and chimeras (E2 + E1-I, E2 + E1-II). Virion production was determined through RT-qPCR and plaque assays as described in (**C**). Data were representative of four independent experiments. Mean values of biological duplicates were plotted with SD. Asterisks indicate statistically significant differences as compared to ONNV (one-way ANOVA and Dunnett's multiple comparisons test: viral titer of ONNV vs E2-II + E1$^{***}p = 0.0008$; viral titer of ONNV vs E2 + E1-II$^{****}p < 0.0001$). Source data are available online for this figure.

Chimera III (Fig. 2A; CHIKV with ONNV poly-glycoproteins). Interestingly, infection of 293 T cells with ONNV/CHIKV E2 + E1 is significantly more productive than that with the parental CHIKV and ONNV viruses. These results clearly demonstrate that ONNV infection is not as attenuated in 293T cells as in macrophages, and hence the requirement for CHIKV structural proteins is highly specific to macrophage infection.

To map the viral determinants for virion production to specific domains, we strategically swapped in ONNV E2 or E1 domains in the context of ONNV/CHIKV E2 + E1. Alphavirus E2 comprises three domains (A, B, and C) connected by β-ribbon arches, with domains A and B functioning in receptor binding and cellular attachment (Li et al, 2010). Alphavirus E1 consists of three β-barrel domains: I, II, and III, with the fusion peptide embedded in domain II critical for viral fusion and uncoating. We generated two chimeras that contain total CHIKV E1 and partial domains of CHIKV E2 in the ONNV backbone (Fig. 3F, E2-I + E1 and E2-II + E1). We also constructed two chimeras that contain total CHIKV E2 and partial domains of CHIKV E1 in the ONNV backbone (Fig. 3F, E2 + E1-I and E2 + E1-II). We transfected macrophages with vRNAs of these chimeras in comparison with ONNV, ONNV/CHIKV E1, and ONNV/CHIKV E2 to measure virion production (Fig. 3G). We found that only the chimeras containing CHIKV E2 without domain C or E1 without domain III restore virion production to significantly high levels. These results suggest that glycoprotein determinants crucial for virion production in macrophages may lie in CHIKV E2 domain B and flanking β-ribbon arches, and E1 domain II.

## Positively selected residues in E2 and E1 are essential for CHIKV production in THP-1-derived human macrophages

Recent SARS-CoV-2 studies have harnessed the power of complementary selection analyses to reveal residues under positive selection that might promote virus adaptation and expansion in human hosts (MacLean et al, 2021; Maher et al, 2022; Kistler et al, 2022). CHIKV, like SARS-CoV-2, is a zoonotic virus well-adapted to humans. Therefore, we asked whether residues in the CHIKV glycoproteins have been under positive selection to overcome antiviral immunity and productively replicate in macrophages. We applied the same methodology from a highly cited SARS-CoV-2 study (MacLean et al, 2021) to analyze the evolutionary selection sites in the CHIKV structural proteins from patient isolates. The analysis pipeline is depicted in Fig. 4A: 397 CHIKV sequences isolated from infected individuals globally were obtained from the NCBI virus (Hatcher et al, 2017) database. The structural polyprotein sequences of these isolates were aligned through MUSCLE (Edgar, 2004) and built into a phylogenetic tree with IQ-TREE (Minh et al, 2020; Trifinopoulos et al, 2016) (Fig. EV2A) for positive selection site detection. The positively selected residues in CHIKV structural proteins were finally identified by the fixed effects likelihood (Kosakovsky Pond and Frost, 2005) (FEL, $p < 0.05$) and mixed effects model of evolution (Murrell et al, 2012) (MEME, $p < 0.05$). FEL identified four amino acid residues in E2, 6K, and E1 under pervasive positive selection; MEME identified 14 residues in the capsid, E2, 6K, and E1 under pervasive and episodic positive selection, including all four residues identified by FEL (Figs. 4B,C and EV2B).

Interestingly, the positively selected sites identified by MEME were concentrated in E2 and E1 (Fig. 4B). We found three residues in E2 (E2-V135, E2-A164, E2-A246) and three in E1 (E1-E211, E1-V220, E1-R366) to be different between our experimental strains, CHIKV vaccine strain 181/clone 25 and ONNV strain SG650 (Fig. EV2B). Next, we compared these six evolutionary sites in E2 and E1 of additional ONNV and CHIKV strains (Fig. EV2D,E). Four of these sites (E2-135, E2-246, E1-220, E1-366) are conserved among all ONNV strains (E2-135L, E2-246S, E1-220I, E1-366K) and all CHIKV strains (E2-135V, E2-246A, E1-220V, E1-366R). On



 

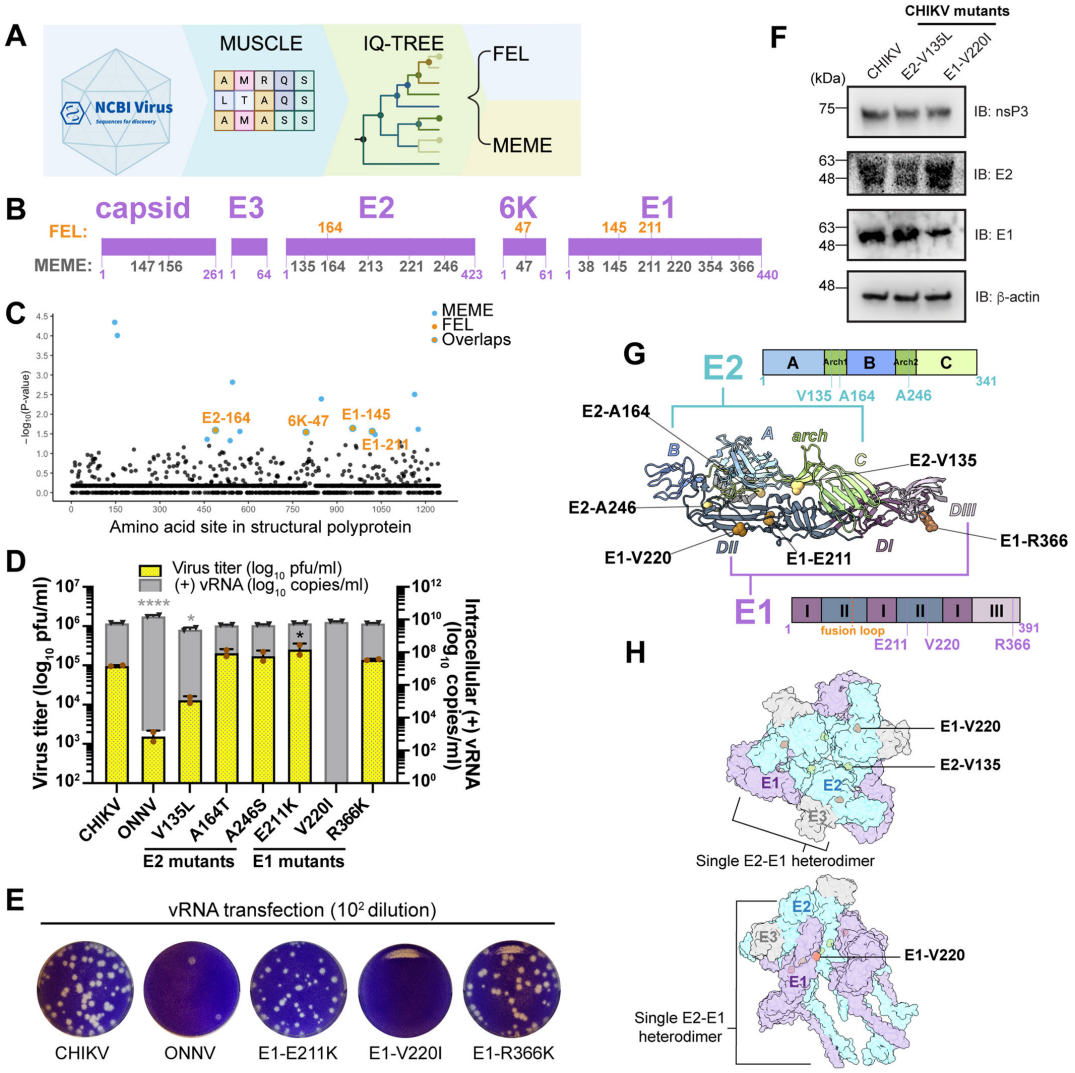


the other hand, the E2-164 and E1-211 sites encode for two different amino acids (E2-164T/A, E1-211K/E) that can be found in either one of the two viruses or both. These alignments suggest that most of the positively selected sites are conserved across different CHIKV strains.

To interrogate if these positively selected residues affect CHIKV production, we mutated them individually into the homologous residues in ONNV. We compared viral replication and production of these mutants (E2-V135L, E2-A164T, E2-A246S, E1-E211K, E1-V220I, and E1-R366K) with that of parental CHIKV in vRNA-transfected THP-1 derived macrophages (Fig. 4D). The E2-V135L mutation decreases virus titers by about 1 log and significantly reduces intracellular (+) vRNA levels. Strikingly, the E1-V220I mutation completely abrogates virion production in macrophages without affecting viral replication (Fig. 4D,E), suggesting a defect in the viral life cycle after genome replication. In contrast, both E2-V135L and E1-V220I mutations attenuate viral replication and production in 293T and BHK-21 cells (Fig. EV3B,C). In addition, the E2-V135L and E1-V220I mutations do not affect expression of the viral nonstructural protein nsP3 and only slightly reduce the expression of viral glycoproteins E2 and E1, respectively, further supporting a defect in virion assembly and/or exit after structural

**Figure 4. CHIKV E2 and E1 residues under positive selection are essential for virion production in human macrophages.**

(**A**) The pipeline for analyzing natural selection in the evolution of CHIKV structural proteins in human hosts. 397 CHIKV sequences isolated from infected individuals globally were downloaded from the NCBI virus database, and structural polyprotein sequence alignment was performed by MUSCLE(Edgar, 2004). The phylogenetic tree of CHIKV was constructed based on the maximum-likelihood (ML) optimality criterion with IQ-TREE (Minh et al, 2020; Trifinopoulos et al, 2016). The sites under positive selection were identified using mixed effects model of evolution (MEME) (Murrell et al, 2012) and fixed effects likelihood (FEL) (Kosakovsky Pond and Frost, 2005). (**B**) The positively selected sites identified by FEL or MEME are annotated in each CHIKV structural protein. The sites identified by MEME are colored in dark gray. Four of these sites (E2-164, 6K-47, E1-145, and E1-211) were identified with both methods and are colored in orange. (**C**) The positively selected sites in CHIKV structural proteins are plotted with the y-axis of $-\log_{10}$ *P* values (determined by MEME or FEL) and the x-axis of the amino acid locations in the full-length structural polyprotein (from the beginning of capsid to the end of E1). The *P* values are generated by the FEL or MEME algorithm and adjusted with Benjamini–Hochberg correction. The statistically significant sites identified by MEME ($p < 0.05$) are in blue, the ones identified by FEL (FEL $p < 0.05$) are in orange, and the ones identified by both methods (MEME $p < 0.05$ and FEL $p < 0.05$) are in orange with blue circles. (**D**) Comparison of virion production of CHIKV positive selection site mutants in THP-1 derived macrophages. The positive selection site in E2 or E1 of CHIKV 181/clone 25 was mutated to the homologous residue in ONNV, respectively, to generate six CHIKV mutants (E2-V135L, E2-A164T, E2-A246S, E1-E211K, E1-V220I, and E1-R366K). Macrophages were transfected with 0.5 μg RNA of CHIKV, ONNV, or CHIKV positive selection site mutants, and virion productions were determined by intracellular (+) vRNA transcript levels and supernatant infectious particle titers as previously described. Data were representative of three independent experiments. Mean values of biological duplicates were plotted with SD. Asterisks indicate statistically significant differences as compared to CHIKV (One-way ANOVA and Dunnett's multiple comparisons test: viral titer of CHIKV vs E211K $^{*}p = 0.0414$; viral copies of CHIKV vs ONNV $^{****}p < 0.0001$; viral copies of CHIKV vs V135L $^{*}p = 0.0228$). (**E**) Representative plaque images of CHIKV E1 positive selection site mutants (E1-E211K, E1-V220I, E1-R366K) in comparison with CHIKV and ONNV. Plaque assays were performed on supernatant samples from transfected THP-1-derived macrophages as mentioned in (**D**). The incubation period for plaque assay is 40 h. The representative plaques from the 1:100 dilution are shown here. (**F**) The expression levels of viral nonstructural and structural proteins of CHIKV wild-type, E2-V135L, and E1-V220I mutants in THP-1 derived macrophages. The THP-1-derived macrophages were transfected with viral RNAs of CHIKV, E2-V135L, or E1-V220I mutant for 48 h. The expression levels of viral nsP3, E2, and E1 proteins were evaluated through immunoblotting. (**G**) Visualization of positively selected sites in single E2/E1 heterodimer with the presence of E3 from infectious CHIKV 181/clone 25 virus particle. The heterodimer structure was downloaded from PDB (6NK7)(Basore et al, 2019) and visualized in Chimera X (Pettersen et al, 2021). The positively selected sites E2-V135, E2-A164, and E2-A246 are located in β-ribbon arches flanking domain B in E2. The positively selected sites E1-E211 and E1-V220 are located in domain II in E1. The positively selected site E1-R366 is in domain III in E1. (**H**) The locations of E2-V135 (yellow nodes) and E1-V220 (orange nodes) in trimerized E2/E1 heterodimers (PDB: 6NK7). The E2 (cyan), E1 (purple), and E3 (gray) were annotated to show a single heterodimer unit. Source data are available online for this figure.

protein translation (Fig. 4F). Given the importance of E2-V135 and E1-V220 in CHIKV production, we analyzed the amino acid heterogeneity at these two sites in the original 397 CHIKV primary isolates from NCBI Virus database (Fig. EV2C). Most of the amino acids at E2-135 and E1-220 are valine. This suggests that the valine residues at the positively selected sites E2-135 and E1-220 are crucial for CHIKV fitness and strongly selected during viral evolution.

While all six unique CHIKV residues are on the exterior of a single E2/E1 heterodimer (with E3) (Fig. 4G), E2-V135 and E1-V220 also interface with E2 from the neighboring heterodimer in trimerized E2/E1 heterodimer configuration (with E3) (Fig. 4H), according to the recently solved CHIKV vaccine strain 181/clone 25 structure (Basore et al, 2019). Meanwhile, E1-V220 is partially embedded in the groove formed by E1 and the neighboring E2, which may provide additional docking sites for host interactors (Fig. 4H). Interestingly, E2-V135 and E1-V220 are in the E2 β-ribbon arch and E1 domain II (Fig. 4G), respectively, that were identified to be critical for virion production in Fig. 3G. Taken together, the positively selected residue E1-V220 mediates efficient virion production likely by facilitating host factor binding in macrophages.

## Identification of cellular factors that interact with CHIKV glycoproteins in macrophages

Successful virion production requires the maturation of E2/E1 heterodimer for proper virion assembly which involves proteolytic processing of the precursor (E3-E2-6K-E1) to an intermediate form (p62/E1), and finally to the E2/E1 heterodimer in the secretory pathway (Brown et al, 2018; Helenius, 1995; Ren et al, 2022). To investigate intracellular macrophage factors that interact with the uncleaved precursors or mature glycoproteins to affect CHIKV production, we inserted a myc tag in the genome of CHIKV vaccine strain 181/clone 25 to label E2 N-terminally (CHIKV/myc-E2) that can also label the precursors in addition to E2/E1 heterodimers. We infected THP-1-derived macrophages in two independent experiments with either CHIKV/myc-E2 or untagged CHIKV vaccine strain 181/clone 25 (WT, negative control). We performed myc immunoprecipitation to enrich for uncleaved polyprotein E3-myc-E2-6K-E1, E3-myc-E2 in p62/E1 heterodimer and myc-E2 in mature E2/E1 heterodimer, followed by MS analysis of the resultant protein mixtures to identify interactors (Fig. 5A).

We identified 1157 proteins (Log2FC >0, $p < 0.05$) in the second experiment to be significantly enriched in CHIKV/myc-E2-infected cells compared to CHIKV WT infected cells (Fig. EV4A; Dataset EV1). Most of the candidate interactors showed more than twofold abundance, with the top enriched protein being S100 calcium-binding protein A9 (S100A9) (Log2FC = 7.89) (Fig. 5B). In addition to the bait protein E2 (Log2FC = 5.84, $p = 2.11E\text{-}5$) that was significantly pulled down in CHIKV/myc-E2-infected macrophages, we also detected E1 (Log2FC = 4.09, $p = 1.59E\text{-}3$) and E3 (Log2FC = 2.99, $p = 3.08E\text{-}2$) as expected. We then used CORUM, an experimentally confirmed, high-confidence protein–protein interaction database, to decipher multiprotein complexes among the host proteins co-immunoprecipitated in CHIKV/myc-E2-infected macrophages (Fig. 5C). The predominantly identified protein complexes that strongly interact with CHIKV glycoprotein precursors and E2/E1 heterodimers include the respiratory chain complex I, SNARE complex, spliceosome, mediator complex, signal peptidase complex, emerin complex I, oligosaccharyltransferase OSTC-III complex, and eIF3 complex. These results suggest that CHIKV glycoproteins may intersect with or co-opt different protein complexes involved in diverse biological processes. Interestingly, signal peptidases are hijacked for polyprotein maturations of several viruses, including alphavirus (Neufeldt et al, 2018; Zimmerman et al, 2023), however, the exact peptidases involved are still largely unknown.

 

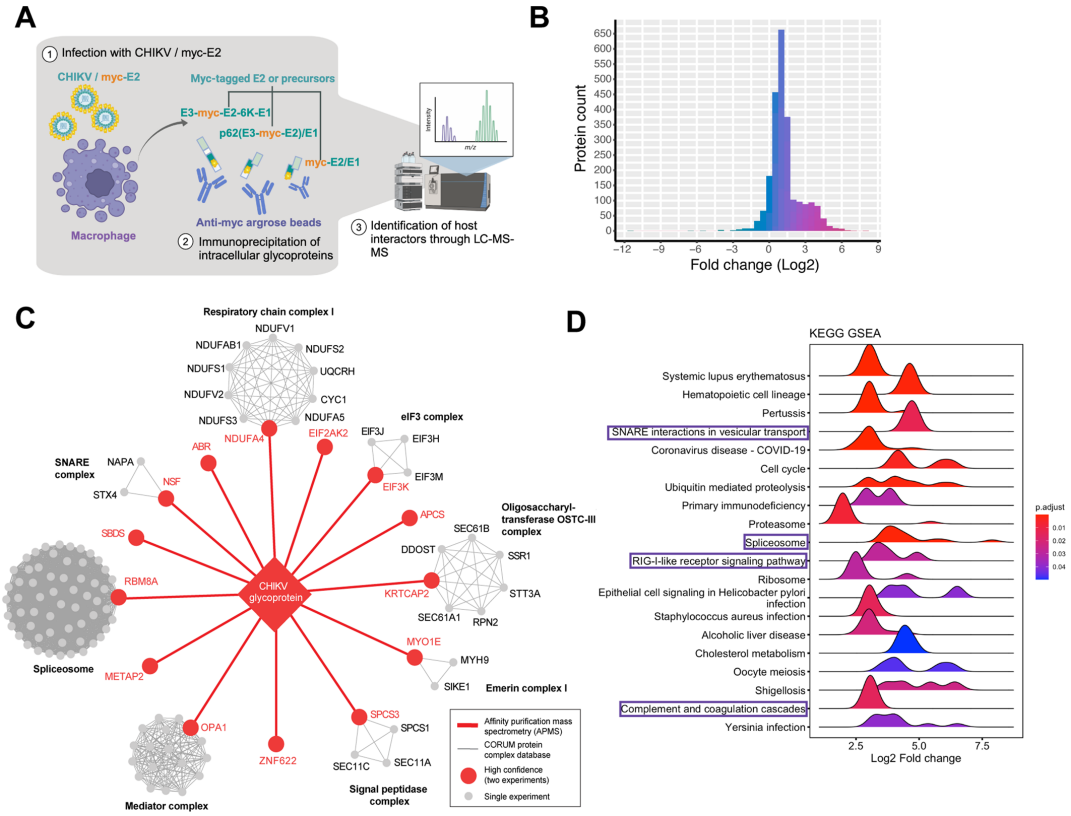


**Figure 5. Identifying host factors interacting with CHIKV glycoproteins in infected human macrophages by affinity purification-mass spectrometry (AP-MS).**

(**A**) The workflow of AP-MS analysis to identify host factors in THP-1 derived macrophages that interact with CHIKV glycoproteins. After 48 h infection with CHIKV/myc-E2, different forms of myc-tagged glycoproteins (polyprotein E3-myc-E2-6K-E1, E3-myc-E2/E1, myc-E2/E1) were pulled down by anti-myc agarose beads from the infected macrophage lysates and submitted to LC-MS/MS analysis to identify co-immunoprecipitated host factors. The co-immunoprecipitated proteins from untagged CHIKV vaccine strain 181/clone 25 (CHIKV WT)-infected macrophages serve as negative controls for proteomic analysis (not elaborated in this diagram). (**B**) The histogram of fold change distribution of all the identified macrophage proteins in the second independent AP-MS experiment that interact with myc-tagged glycoproteins (poly-glycoprotein E3-myc-E2-6K-E1, E3-myc-E2/E1, myc-E2/E1). (**C**) The interaction network between CHIKV glycoproteins and macrophage proteins. CHIKV glycoproteins interacting partners in THP-1 derived macrophages that were significantly enriched in both independent mass spectrometry experiments are depicted in red. Candidate interactors significantly enriched in at least one mass spectrometry experiment that belongs to existing red protein complexes are colored in gray. The protein complexes were identified through the CORUM database. (**D**) Gene set enrichment analysis (GSEA) of top 20 KEGG pathways in identified host factors summarized in ridgeplot. All the identified host factors are ranked according to the log2 expression fold change of proteins co-immunoprecipitated from CHIKV/myc-E2 infected macrophages with respect to proteins from CHIKV 181/clone 25 infected macrophages (x-axis). The significance of the KEGG enrichment is shown in a continuous color scale based on the adjusted *P* values, which are generated by Fisher's exact test and corrected by Benjamini–Hochberg. The histogram in each KEGG term is defined by the number of genes with a specific log2 fold change value. Created with BioRender.com.

Moreover, we visualized the overall biological processes of enriched host proteins through EnrichmentMap (Fig. EV4B). Consistent with the identified protein complexes, CHIKV glycoprotein interactors are mostly enriched in RNA processes (transcription regulation, pre-mRNA splicing), and secretory pathway (ER-Golgi transportation, intracellular vesicle transport, negative regulation of endopeptidase activity, signal peptide processing). Immune responses (type I IFN pathway/complement activation, antigen presentation) are also among the biological processes targeted by CHIKV glycoproteins. Consistent with the enriched protein complexes and biological processes, the KEGG analysis (Subramanian et al, 2005; Wu et al, 2021; Kanehisa et al, 2016) identified similar pathways (Fig. 5D, framed), suggesting that RNA processes, secretory pathway, and immune responses are critical for CHIKV glycoprotein interactions with macrophage factors.

## CHIKV E1 binding proteins exhibit potent anti-CHIKV activities

We next inquired whether the host factors interacting with the CHIKV glycoproteins are proviral or antiviral. We selected 13 host factors for further investigation, including ten hits identified in both AP-MS experiments, classical ISGs (APOBEC3F, OAS3), and a myeloid-specific gene (S100A9) which is an endogenous ligand for toll-like receptor 4 (TLR4) (Foell et al, 2007; Vogl et al, 2007) (Fig. 6A). We knocked down these genes with pooled siRNAs (Fig. EV5A) in THP-1 derived macrophages, followed by CHIKV infection (Fig. 6B). We included nontargeting (NT) siRNA as negative control and siRNAs targeting pro-CHIKV factors G3BP stress granule assembly factor 1 (G3BP1) and 2 (G3BP2) (Scholte et al, 2015; Kim et al, 2016) as a positive control. Knockdown of most of the host factors led to elevated CHIKV titers in macrophages compared to NT-transfected cells, except for G3BP1 + 2 knockdown, indicating that many of the candidate E2 interactors have antiviral activities. In addition to the previously reported anti-CHIKV restriction factors OAS3 and PKR (Bréhin et al, 2009; Gorchakov et al, 2004; Ryman et al, 2005), knockdown of the host genes SPCS3 and EIF3K significantly restores virion production by about fivefold. To confirm that the antiviral activities observed in Fig. 6B are specific to a step after viral entry, we knocked down the same host factors in THP-1-derived macrophages followed by transfection of CHIKV vRNA (Fig. 6C). We found that silencing of most of the genes enhances virion production in vRNA-transfected macrophages. CHIKV production in macrophages with OAS3, SPCS3, and EIF3K knockdown is significantly higher than that in NT-transfected cells, despite similar intracellular vRNA levels.

To confirm the interaction of CHIKV glycoproteins with host proteins demonstrating antiviral activities (OAS3, SPCS3, eIF3k, APOBEC3F, and PKR, Fig. 6B,C), we transfected 293T cells with plasmids expressing 3xflag-tagged host factors, followed by transfection with CHIKV vRNA (Fig. 6D) or CHIKV polyglycoprotein (E3-myc-E2-6K-E1) expressing plasmid (Fig. EV5B). The host factors were pulled down to probe for glycoproteins in precursor or mature forms. We consistently detected strong binding of E1 and moderate binding of E3-E2-6K-E1 to SPCS3 and eIF3k. However, it is surprising that neither SPCS3 nor eIF3k binds to E2 or p62, which is presumed to interact with E1 in heterodimer forms. To confirm the specific binding of SPCS3 and eIF3k to E1, we performed reciprocal immunoprecipitation. We transfected 293T cells with plasmids expressing the CHIKV polyglycoprotein and SPCS3/eIF3k followed by E1 or E2 pulldown (Fig. EV5C,D). The reciprocal immunoprecipitation validated the specific interaction of SPCS3 and eIF3k with E1, respectively, while we did not observe consistent pulldown of the host factors with E2.

Given the unexpected absence of E2 in both host factor and E1/E2 pulldown, it is possible that a group of free E1 proteins unassociated with E2 has distinct functions in interfering with cytoplasmic host factors for efficient virion production. It would be interesting to determine whether the E1 proteins that interact with SPCS3 and eIF3k localize to a different cellular compartment away from E2. To address this question, we applied confocal laser-scanning microscopy with an Airyscan detector to identify colocalization among E2, E1, and host factors (SPCS3 or eIF3k) (Fig. 7A,B). We found that the majority of E2 accumulates at the plasma membrane, while E1 mostly localizes to the region adjacent to the nucleus, potentially the endoplasmic reticulum (ER). According to the Pearson correlation coefficient analysis (Fig. 7A,B, violin plots), E1 colocalizes more with the host factors (SPCS3, eIF3k) than with E2. These results suggest that E2 and E1 may not always be together in heterodimer forms, and the cytoplasmic pool of E1 associates more with SPCS3 and eIF3k.

To further solidify the role of E1 interaction with macrophage restriction factors during viral evolution, we investigated the effects of replacement of the positively selected site E1-V220 in CHIKV with the isoleucine found in the homologous ONNV site. We previously showed that the E1-V220I mutation completely abrogates virion production in THP-1-derived macrophages (Fig. 4D). Consistent with that, E1-V220I dramatically reduces E1 binding to SPCS3 and to eIF3k (Fig. 7C). This implies that these host restriction factors may be involved in genetic conflict with CHIKV glycoproteins through the same E1 interface, which may engage with both SPCS3 and eIF3k in a complex.

To determine whether SPCS3 and eIF3k work together, we quantified their colocalization in CHIKV-infected 293T cells through Airyscan microscopy (Fig. 7D). SPCS3 is mostly localized to the cytoplasm while eIF3k is found in both the cytoplasm and nucleus, consistent with previous reports on the strong nuclear localization of eIF3k (Salsman et al, 2013). Some SPCS3 and eIF3k colocalize in mock-infected cells, and upon CHIKV infection their colocalization significantly increases (Pearson correlation coefficient increases from 0.4 to 0.6). This suggests that SPCS3 and eIF3k may work together to inhibit CHIKV upon infection. Interestingly, we observed eIF3k translocation from the nucleus to the cytoplasm in some CHIKV-infected cells (white arrows in Fig. 7D). This supports a novel cytoplasmic function of eIF3k upon CHIKV infection. Taken together, the viral E1 glycoprotein has been engaged in an evolutionary arms race with host restriction factors in human macrophages which is distinct from its conventional role in E2/E1 heterodimer formation.

## E1-binding protein eIF3k inhibits CHIKV production through its HAM domain in a translation-independent manner

Since neither SPCS3 nor eIF3k was previously reported as a restriction factor before, we further characterized their roles in CHIKV infection by validating their antiviral activities in CRISPR-Cas9 knockout (KO) 293T cells. Although we failed to generate a complete KO of SPCS3 consistent with a previous report (Zhang et al, 2016), we successfully obtained single-cell clones of eIF3k KO in 293T cells (Fig. 8A; Appendix Fig. S1B). We compared different arthritogenic alphavirus infections in eIF3k KO 293T cells (Fig. 8B), including SINV that shows similarly low infection levels in primary monocyte-derived macrophages as ONNV (Fig. 1A). We found that eIF3k KO leads to increased CHIKV titer by ~2.5-fold while having no effects on virion production of ONNV and SINV, confirming the specificity of CHIKV inhibition by eIF3k.

Next, we investigated how eIF3k antagonizes CHIKV production. Previously, we showed that eIF3k blocks virion production without affecting viral genome replication (Fig. 6C). Since viral structural polyprotein expression from the subgenomic mRNA precedes virion assembly, we asked whether eIF3k acts at the step of viral structural protein translation. We transfected a CHIKV



 

A

| Gene Symbol | Full Name | Log2FC | P value |
|---|---|---|---|
| S100A9 | S100 calcium binding protein A9 | 7.89124024 | 0.0364509 |
| RBM8A | RNA binding motif protein 8A | 6.32085395 | 0.0406373 |
| CHCHD2 | coiled-coil-helix-coiled-coil-helix domain containing 2 | 5.818015 | 0.0337427 |
| APOBEC3F | apolipoprotein B mRNA editing enzyme catalytic subunit 3F | 5.55268458 | 0.0466289 |
| KRTCAP2 | keratinocyte associated protein 2 | 4.77691911 | 0.0234857 |
| ZNF622 | zinc finger protein 622 | 3.6184588 | 0.0419445 |
| SBDS | SBDS ribosome maturation factor | 2.74946966 | 0.0132538 |
| EIF3K | eukaryotic translation initiation factor 3 subunit K | 1.87060632 | 0.00050938 |
| EIF2AK2 | eukaryotic translation initiation factor 2 alpha kinase 2 | 1.48996162 | 0.00307366 |
| SPCS3 | signal peptidase complex subunit 3 | 1.35257504 | 0.0040305 |
| OAS3 | 2′-5′-oligoadenylate synthetase 3 | 1.33637155 | 0.02704967 |
| METAP2 | methionyl aminopeptidase 2 | 0.9183056 | 0.0327671 |
| NSF | N-ethylmaleimide sensitive factor, vesicle fusing ATPase | 0.66010797 | 0.01576337 |

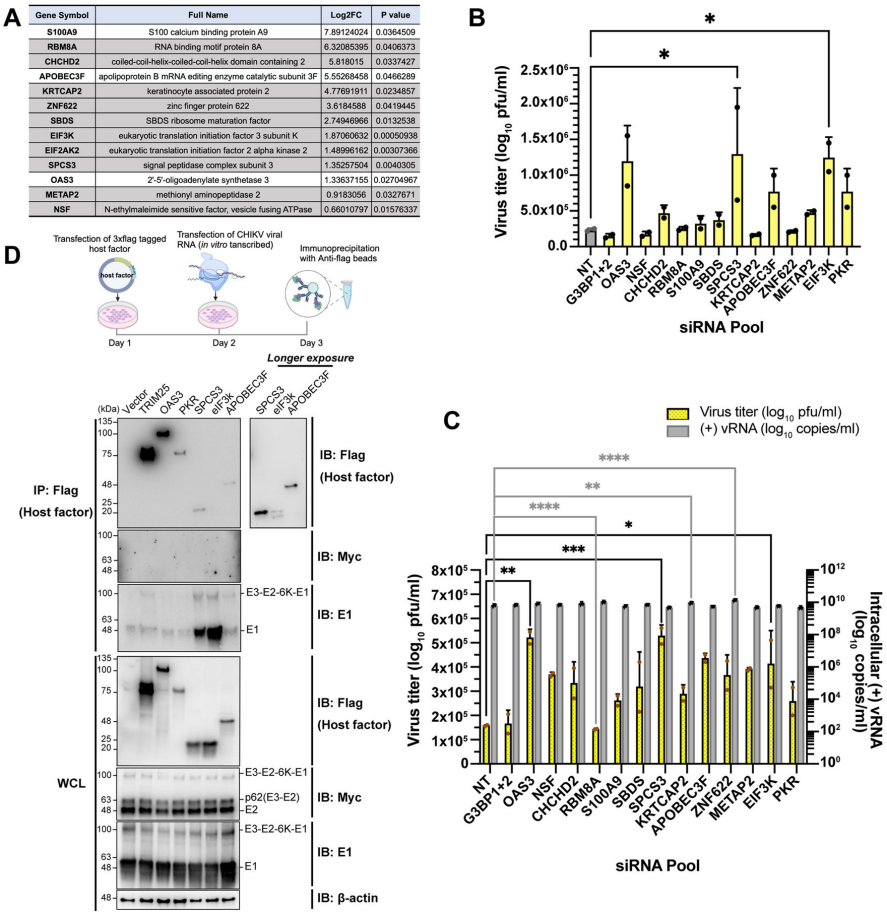


**Figure 6. CHIKV E1 interacts with macrophage host factors that block virion production.**

(**A**) Table of identified host factors that were chosen for siRNA knockdown assays in (**B**, **C**). Statistical analysis for protein differential expression is a moderated *t*-test from R package ArtMS3. The *P* values are adjusted with Benjamini–Hochberg for the multiple hypothesis correction. The gray-highlighted genes are significantly detected in 2 independent AP-MS experiments. (**B**, **C**) Evaluation of CHIKV infection (**B**) and production (**C**) in human macrophages with OAS3, NSF, CHCHD2, RBM8A, S100A9, SBDS, SPCS3, KRTCAP2, APOBEC3F, ZNF622, METAP2, EIF3K, or PKR knocked down. THP-1-derived macrophages were transfected with pooled siRNAs targeting specific host factors or nontargeting siRNAs (NT) for 48 h. The cells were then infected with CHIKV 181/clone 25 (MOI 5) (**B**) or transfected with CHIKV vRNA (**C**) for 24 h. The supernatant virus titers from cells treated with siRNAs targeting host factors were determined by plaque assay and compared to the titers from cells treated with NT siRNA to assess the anti- or proviral effects of specific host genes on CHIKV production. G3BP1 and G3BP2 (G3BP1 + 2) known to be proviral for CHIKV replication were knocked down together as control. For (**B**), data were representative of two independent experiments. The mean values of biological duplicates were plotted with SD (one-way ANOVA and Dunnett's multiple comparisons test: si-NT vs si-SPCS3 $*p = 0.031$; si-NT vs si-EIF3K $*p = 0.0421$.) For (**C**), data were representative of two independent experiments. The plaque assay results were plotted from biological duplicates with the mean values (one-way ANOVA and Dunnett's multiple comparisons test: viral titer of si-NT vs si-OAS3 $**p = 0.01$; viral titer of si-NT vs si-SPCS3 $***p = 0.0008$; viral titer of si-NT vs si-EIF3K $*p = 0.0194$). The qPCR results were plotted from biological triplicates with the mean values (one-way ANOVA and Brown-Forsythe test: viral copy of si-NT vs si-RBM8A $****p < 0.0001$; viral copy of si-NT vs si-KRTCAP2 $**p = 0.0054$; viral copy of si-NT vs si-ZNF622 $****p < 0.0001$). (**D**) 293T cells were transfected with plasmids expressing 3xflag-tagged host factors (TRIM25, OAS3, PKR, SPCS3, eIF3k, and APOBEC3F) or empty vector control for 24 h and later transfected with vRNA of CHIKV/myc-E2. The cells were lysed and immunoprecipitated by anti-flag agarose beads. Immunoblot was probed to check for E2/E1 binding to these host factors. 3xflag tagged TRIM25 (tripartite motif containing 25) was transfected into 293T cells for immunoprecipitation control. Data were representative of three independent experiments. Source data are available online for this figure.

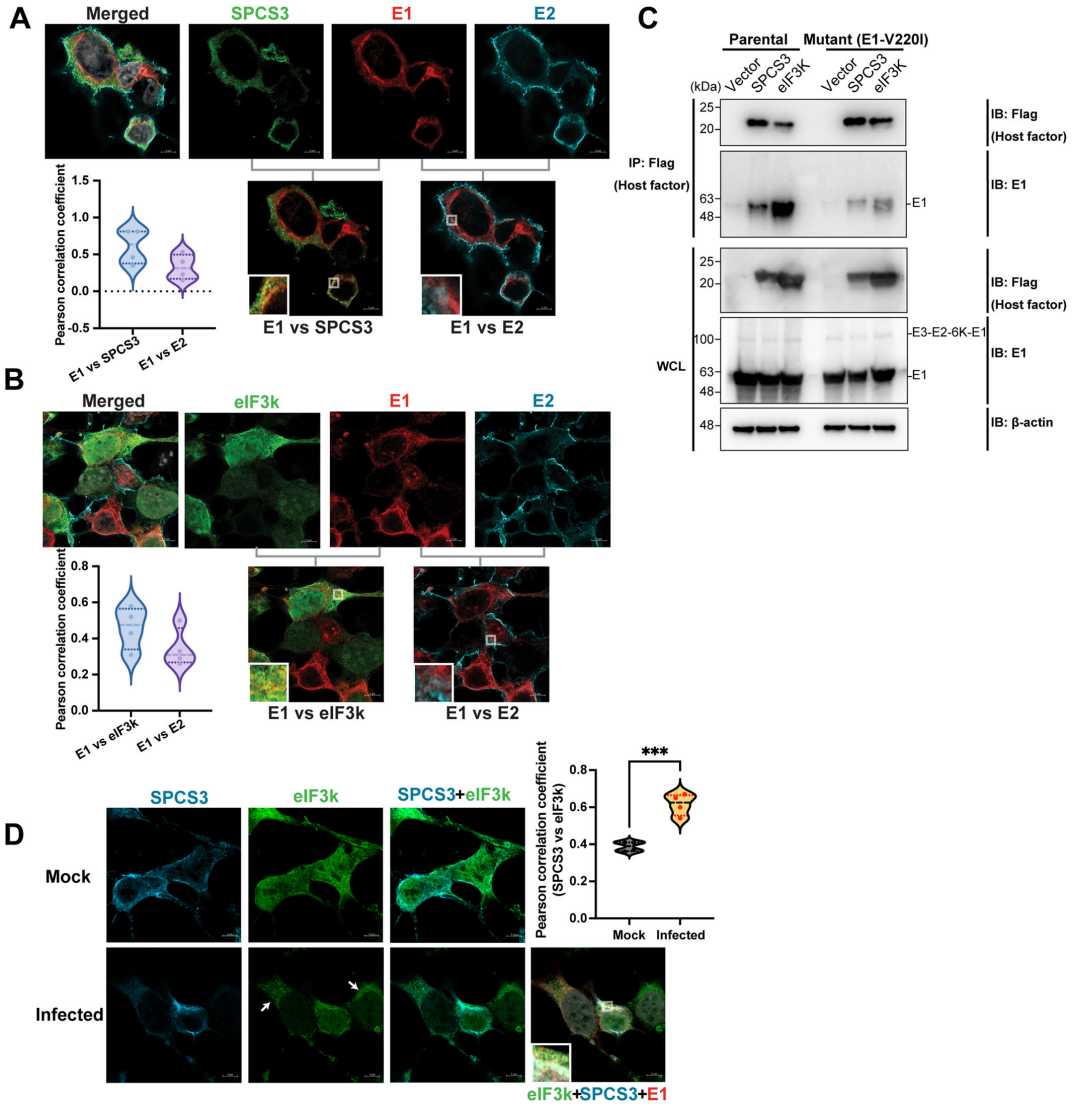


replicon where we replaced the viral structural polyprotein with EGFP into eIF3k KO 293T cells with or without overexpression of exogeneous 3xflag-tagged eIF3k (Fig. 8C). We found that restoration of eIF3k slightly reduces subgenomic promoter-driven EGFP expression while expression of the viral nonstructural protein (nsP3) is unaffected. We also transfected CHIKV vaccine strain 181/clone 25 into eIF3k KO 293T cells with or without 3xflag-tagged eIF3k expression (Fig. 8D). Again, eIF3k overexpression does not alter structural (E2 and E1) and nonstructural (nsP3) protein expression. These results suggest that eIF3k has no impact on CHIKV subgenomic or genomic RNA translation.

To further characterize the antiviral activity of eIF3k, we dissected the involvement of eIF3k protein domains. eIF3k contains two major domains: HEAT repeat-like HAM (HEAT analogous motif) domain, a winged-helix-like WH domain, and a C terminal long tail region (Wei et al, 2004; Chen et al, 2022) (Fig. 8E). Highly conserved hydrophobic residues from four of the helices in the HAM domain and the first helix from the WH domain form a hydrophobic core between the HAM and WH domains (Wei et al,

 

**Figure 7. A pool of free E1 separate from E2 associates with SPCS3 and eIF3k through the positively selected site E1-V220.**

**(A)** Colocalization analysis of CHIKV E1 with E2 or with SPCS3 through immunofluorescence. 293T cells were transfected with plasmids expressing 3xflag-SPCS3 and infected with CHIKV 181/clone 25 for 24 h 1 day later. flag-tagged SPCS3 (green), and CHIKV E1 (red) and E2 (cyan) were labeled through indirect staining with primary antibodies against flag, E1, and E2. The representative colocalization regions are enlarged on the bottom left of the overlaid images. Colocalization between CHIKV E1 and SPCS3 (E1 vs SPCS3) and between CHIKV E1 and E2 (E1 vs E2) are compared through Pearson correlation analysis and shown as violin plots. Pearson correlation coefficient values range from 1 to −1, where 1 is a total positive correlation, −1 is a total negative correlation, and 0 is no correlation. Scale bar: 5 μm. Representative results from two independent are shown here. Two field images were taken for each sample in each independent experiment, and four cells from one independent experiment were designated as region of interests (ROIs) for colocalization analysis. **(B)** Colocalization analysis of CHIKV E1 with E2 or with eIF3k through immunofluorescence. 293T cells were transfected with plasmids expressing 3xflag-eIF3k and infected with CHIKV 181/clone 25 for 24 h one day later. 3xflag-tagged eIF3k (green), and CHIKV E1 (red) and E2 (cyan) were labeled as previously described. The representative colocalization regions are shown in the bottom left of the overlaid images. Colocalization between CHIKV E1 and eIF3k (E1 vs eIF3k) and between CHIKV E1 and E2 (E1 vs E2) is compared through Pearson correlation analysis (refer to 7A) and shown as violin plots. Scale bar: 5 μm. Representative results from two independent are shown here. Two field images were taken for each sample in each independent experiment, and four cells from one independent experiment were designated as region of interests (ROIs) for colocalization analysis. **(C)** 293T cells were transfected with plasmids expressing 3xflag-tagged host factors (SPCS3, eIF3k) or empty vector control for 24 h followed by transfection with a plasmid expressing parental or E1-V220I-containing CHIKV polyglycoprotein (E3-myc-E2-6K-E1). The cells were lysed for immunoprecipitation with anti-flag agarose beads. Immunoblot was probed for parental or mutant E1 binding to host factors. Data are representative of 2 independent experiments. **(D)** Colocalization analysis of SPCS3 and eIF3k in uninfected and CHIKV-infected cells through immunofluorescence. 293T cells were co-transfected with plasmids expressing 3xflag-eIF3k and V5-SPCS3 followed by mock or CHIKV infection for 24 h 1 day later. V5-SPCS3 (cyan), 3xflag-eIF3k (green), and CHIKV E1 (red) were labeled through indirect staining with antibodies against V5, flag, and E1. The representative colocalization regions are shown on the bottom left of the overlaid images. Colocalization between SPCS3 and eIF3k (SPCS3 vs eIF3k) is compared in mock and CHIKV-infected 293T cells through Pearson correlation analysis (refer to 7A) and shown as violin plots (unpaired t-test: Mock vs Infected ***$p = 0.0004$). Scale bar: 5 μm. Representative results from two independent are shown here. Two field images were taken for each sample in each independent experiment, and four cells from one independent experiment were designated as region of interests (ROIs) for colocalization analysis. Source data are available online for this figure.

2004). To identify the domain(s) required for the antiviral activity of eIF3k, we constructed several 3xflag-tagged truncation mutants: HAM + WH mutant, Core mutant, and HAM mutant (Fig. 8F). The HAM + WH mutant contains the two eIF3k domains without the C terminal tail. The Core mutant contains HAM and the first helix from WH domain to include the hydrophobic core structure (Wei et al, 2004) (Fig. 8F). Except for the Core truncation, the HAM + WH and HAM truncations can be well expressed in eIF3k KO cells after transient transfection (Fig. 8G). To investigate the antiviral activities of HAM and WH domains, we transfected eIF3k KO 293T cells with HAM + WH and HAM truncation mutants and later infected the cells with CHIKV. The plaque assay results from all the independent experiments showed that the HAM alone is sufficient to inhibit CHIKV production though statistically insignificant (Fig. 8H).

Contrary to the dogma that viral glycoproteins only play essential roles in entry, assembly, and egress, our study provides one of the first comprehensive evidence that CHIKV glycoproteins actively interfere with intracellular blockades for efficient virion production and spread in human macrophages.

## Discussion

Macrophages are important cellular reservoirs for persistent CHIKV infection; however, the underlying mechanisms are largely unexplored. In this study, we interrogated the CHIKV proteins that hijack macrophages to produce and spread new infectious virus particles. We first demonstrated that both CHIKV glycoproteins E2 and E1 mediate efficient virion production from infected macrophages through comparative infection with CHIKV-ONNV chimeras. By performing evolutionary selection analysis on sequences of human CHIKV isolates from NCBI Virus (Hatcher et al, 2017), we identified E2-V135 and E1-V220 to be associated with elevated CHIKV production. We then uncovered two new host factors, SPCS3 and eIF3k, with inhibitory effects on CHIKV production that specifically interact with CHIKV E1. Unlike other translation initiation factors involved in virus infection, the anti-CHIKV activity of eIF3k is mediated by its HAM protein domain in a translation-independent manner. Mutating the positively selected site at CHIKV E1-V220 into the ONNV homologous residue attenuates its interaction with SPCS3 and eIF3k, respectively. Our results suggest that the evolutionary selection of CHIKV glycoproteins driven by intracellular antiviral host factors, including SPCS3 and eIF3k, contributes to efficient CHIKV production in macrophages.

According to previous studies (Brown et al, 2018; Voss et al, 2010), CHIKV E2 and E1 are always interacting with each other from single heterodimer formation in the ER to heterodimer trimerization before viral particle assembly. We found the CHIKV positively selected sites E2-V135 and E1-V220 on the exterior of a single E2-E1 heterodimer, suggesting that they may be involved in interactions with host factors, but they appear to not be engaged in the E2-E1 interaction in a single heterodimer (Fig. 4G). Interestingly, in trimerized spike structure, both of these residues are located at the interaction surface between two adjacent E2-E1 heterodimers (Fig. 4H) and may play a role in trimer formation. Unlike E2-V135, that is fully embedded in the center of the trimerized spike, E1-V220 is partially exposed and protruding into the groove formed by E1 and the E2 of the neighboring heterodimer, accessible to host factors. As such, mutating CHIKV E1-V220 to the ONNV residue (E1-V220I) may not only disrupt E2-E1 trimerization but also interfere with viral glycoprotein interaction with host factors. Similarly, swapping E2 or E1 with CHIKV glycoprotein in the ONNV backbone may also affect the interaction between neighboring E2 and E1 during trimerization, which may explain why neither ONNV/CHIKV E2 nor ONNV/CHIKV E1 rescues virion production in macrophages (Fig. 3B,C). Taken together, E2-V135 in a single heterodimer and E1-V220 in a single or trimerized heterodimer are all likely to interface with intracellular restriction factors in macrophages, driving positive selection at these sites to increase viral fitness and production.

While we found no impact of other positively selected sites on CHIKV production, it is possible that they are involved in adaptive

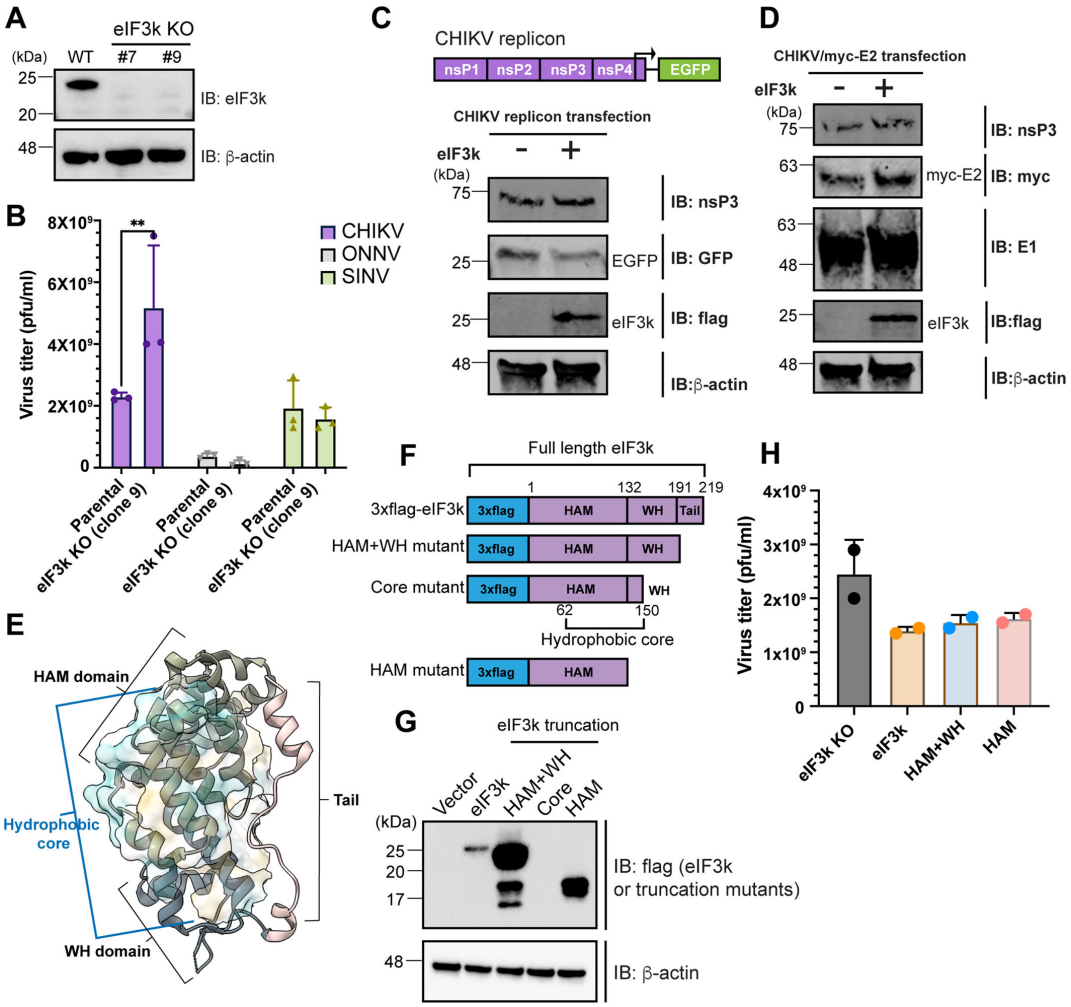


immune response, given that they are evolutionarily selected in the viral glycoproteins. Components of the adaptive immune response, such as virus-specific antibodies and T cells, can also select for escape mutations in viral glycoproteins (Tenthorey et al, 2022). We looked into the epitopes of currently characterized human CHIKV-neutralizing antibodies or broadly anti-alphavirus antibodies. They are mainly mapped to E2 domains A and B, responsible for receptor binding and cellular attachment, and E1 domain II, proximal to or within the fusion loop (Kim and Diamond, 2022; Kim et al, 2021; Pal et al, 2013). None of these reported antibodies target the six differential selection sites in CHIKV 181/clone 25 (Fig. EV2B, amino acids in red), suggesting that these residues are more likely selected by intracellular host restriction factors.

Among the candidate CHIKV glycoprotein interactors we identified, SPCS3 and eIF3k have inhibitory activities against CHIKV production in THP-1-derived macrophages (Fig. 6B,C). Surprisingly, the interaction with SPCS3 and eIF3k only engages CHIKV E1 but not E2. In infected cells, E1 is mostly localized to the cytoplasmic region adjacent to the nucleus, likely the ER, while E2 is predominantly found on the plasma membrane. The distinct localization patterns of E2 and E1 challenge previous knowledge that E2 and E1 always act together in heterodimer forms. Importantly, a previous study showed that alphavirus nsP3 (Götte et al, 2018), thought to always associate with membrane-bound viral replication complexes, can be freed to form large cytoplasmic aggregates. These findings support a model where a separate pool of

 

**Figure 8. The specific anti-CHIKV activity of eIF3k is translation-independent and mediated by its HAM domain.**

**(A)** Immunoblot validation of *EIF3K* CRISPR KO in 293T clones 7 and 9. **(B)** eIF3k KO 293T cells (clone 9) were infected with CHIKV 181/clone 25, ONNV SG650, or SINV Toto1101 at MOI 1 for 24 h. Virion production was evaluated by titering the supernatant infectious particles through plaque assay. Data were representative results of three independent experiments. The mean values of biological triplicates were plotted with SD (two-way ANOVA and Šidák's multiple comparisons test: Parental vs eIF3k KO for CHIKV infection $^{**}p = 0.0066$). **(C)** Translation of CHIKV replicon in eIF3k KO 293T cells (clone 7) with or without eIF3k reconstitution. The schematic for the CHIKV replicon is shown on top. Viral structural polyprotein downstream of the subgenomic promoter is replaced with the EGFP reporter. The eIF3k KO 293T cells were first transfected with an empty vector or plasmid expressing 3xflag-eIF3k followed by transfection with the CHIKV replicon RNA one day later. Twenty-four hours after the second transfection, protein expression of nsP3, EGFP, and 3xflag-eIF3k was detected by immunoblotting. As a GFP variant, EGFP was detected by a GFP antibody. Data were representative of three independent experiments. **(D)** The translation of CHIKV/myc-E2 in eIF3k KO 293T cells (clone 7) with or without eIF3k reconstitution. As mentioned in Fig. 5A, the myc tag is inserted at the N-terminal end of E2. The eIF3k KO 293T cells were first transfected with an empty vector or plasmid expressing 3xflag-eIF3k followed by transfection with CHIKV/myc-E2 RNA one day later. Protein expression of nsP3, myc (E2), E1, and (flag) eIF3k was detected by immunoblotting 24 h after the second transfection. Data were representative of three independent experiments. **(E)** The structure of human eIF3k with the protein domains labeled. The eIF3k crystal structure is downloaded from PDB (1RZ4)(Wei et al, 2004) and visualized in Chimera X. eIF3k consists of a HAM domain (khaki), WH domain (blue), and a long C-terminal tail region with α-helix at both ends (pink). The HAM domain contains a leading α-helix and 3 HEAT analogous repeats followed by a short helix. The WH domain contains three α-helices and three β-strands. **(F)** The diagram of eIF3k truncation mutants. The HAM + WH mutant that lacks the C-terminal tail terminates after residue S191 of full-length eIF3k. The Core mutant with a truncated WH domain terminates after residue Y150 of full-length eIF3k and includes the hydrophobic core formed by the highly conserved hydrophobic residues from HAM and the first helix of WH. The HAM-only mutant terminates after residue T132 of full-length eIF3k. All the eIF3k truncation mutants are tagged with an N-terminal 3xflag. **(G)** Validation of expression of eIF3k truncation mutants in eIF3k KO 293 T cells through immunoblotting. Since the Core mutant cannot be expressed, it is not followed up in (**8H**). **(H)** The anti-CHIKV activities of eIF3k truncation mutants. The eIF3k KO 293T cells (clone 7) were transfected with plasmids expressing full-length eIF3k or different truncation mutants. The cells were then infected with CHIKV at MOI 1 for 24 h 1 day following transfection. Levels of infectious particle production in supernatant samples were determined by plaque assay on BHK-21 cells. The incubation period for plaque assay is 28 h. Data were representative of five independent experiments. The mean values of biological duplicates were plotted with SD. Source data are available online for this figure.

free E1 interferes with cytoplasmic host restriction factors, further highlighting the enigmatic roles of alphavirus proteins in the viral life cycle.

To build on that model. we showed that mutation of the positively selected site in E1 (E1-V220) completely abrogates virion production in THP-1 derived macrophages and reduces E1 interaction with SPCS3 and eIF3k (Figs. 4D and 7C). These results clearly demonstrate that E1-V220 is a critical interaction site that has been evolutionarily selected by multiple restriction factors, including SPCS3 and eIF3k, to drive increased virion production in macrophages. To better elucidate the mechanism of these macrophage restriction factors, further studies need to be performed to determine the functional consequences of E1 binding to these anti-CHIKV factors, such as protein degradation or sequestration.

SPCS3 is one of the core components of the endoplasmic reticulum-associated signal peptidase complex (SPC) (Gemmer and Förster, 2020), which cleaves signal peptides during the translocation of protein precursors in the ER (Böhni et al, 1988, 11; Shelness et al, 1993). The signal peptidases are presumably usurped by flaviviruses, bunyaviruses, and alphaviruses for poly-glycoprotein cleavage (Zhang et al, 2016; Neufeldt et al, 2018; Zimmerman et al, 2023). However, it is unknown what exact peptidase releases p62, 6K, and E1 from the alphavirus poly-glycoprotein precursor (Frolov et al, 1996). A previous genome-wide CRISPR KO screen uncovered both SPCS1 and SPCS3 as proviral factors for flavivirus infection, and depletion of SPCS1 led to inefficient polyprotein cleavage disrupting flavivirus production (Zhang et al, 2016). Unexpectedly, we found that SPCS3 exhibits anti-CHIKV activity and strongly associates with CHIKV E1. SPCS3 overexpression does not affect CHIKV poly-glycoprotein cleavage (Fig. 6D), suggesting novel peptidase-independent antiviral activities. For the first time, we demonstrated the functional dualities of SPC proteins in different virus infection systems.

On the other hand, eIF3k is a subunit of the eukaryotic translation initiation factor 3 (eIF3) complex, which is the most complex and least characterized among the mammalian translation initiation factors containing at least 12 subunits (eIF3a-m)(Gomes-Duarte et al, 2017). eIF3 binds the small ribosomal subunit (40 S) and is involved in almost all steps of translation initiation (Wei et al, 2004; Aitken et al, 2016). Not as an essential component of the eIF3 complex, eIF3k is located on the outside of the eIF3 structure and can be easily dissociated from the complex (Gomes-Duarte et al, 2017).

The role of eIF3k in a viral context has not been explored previously. The most well-known example of translation shutoff as a general antiviral mechanism is mediated by protein kinase R (PKR). PKR, also known as eukaryotic translation initiation factor 2 alpha kinase 2 (EIF2AK2), senses double-stranded vRNAs in the cytoplasm leading to eIF2α phosphorylation and suppression of viral and host gene expression (Fros and Pijlman, 2016). Interestingly, PKR and other eIF3 subunits (eIF3h, eIF3j, eIF3m) were also identified in our AP-MS results (Figs. 5C, 6A). Therefore, it led us to hypothesize that the specific anti-CHIKV activity of eIF3k might involve viral translation inhibition. However, we showed that eIF3k neither inhibits CHIKV nonstructural nor structural protein translation, suggesting that eIF3k antiviral activity is not translation dependent (Fig. 8C,D). Although eIF3k is normally known for its role in translation initiation in the cytoplasm, it also interacts with promyelocytic leukemia protein (PML) and is associated with PML nuclear bodies in the nucleus (Salsman et al, 2013). Our results confirmed the strong nuclear localization of eIF3k (Fig. 7B,D mock infection) and revealed the translocation of eIF3k from nucleus to cytosol induced by CHIKV infection. Notably, eIF4E, which also has nuclear localization, was previously reported to mediate nuclear-cytoplasmic export of select transcripts (Osborne and Borden, 2015). It will be interesting to determine in future studies whether eIF3k also affects RNA export leading to modulation of the host antiviral response. Meanwhile, we also found that the anti-CHIKV activity of eIF3k potentially lie in the HAM domain (Fig. 8H). Previous structure analysis demonstrated that the eIF3k HAM domain consists of three HEAT analogous which can provide an interaction surface for protein–protein interaction (Wei et al, 2004). Further investigations are required to elucidate whether the eIF3k HAM domain recruits other antiviral host proteins to mediate anti-CHIKV activity.

Finally, although macrophages are widely recognized as persistent CHIKV reservoirs, most of the evidence came from the detection of viral components in nonhuman primates or patient samples. Here we used interdisciplinary approaches to uncover the advantage conferred by CHIKV glycoproteins in virion production in an in vitro macrophage model system. Future validations with ONNV-CHIKV chimeric virus infection in mammalian hosts will benefit the mechanistic understanding of how CHIKV glycoproteins facilitate virus dissemination through infected macrophages in a more physiologically relevant environment. Especially, while macrophages in vivo comprise heterogenous cell subsets, including both monocyte-derived macrophages and tissue-resident macrophages, the in vitro THP-1 derived macrophage model only represents monocyte-derived macrophages. Using in vivo models will address the question of whether resident macrophages, especially Langerhans cells from the skin and synovial macrophages from the joints, also exhibit greater susceptibility to CHIKV.

In summary, our study has unraveled a novel role of CHIKV glycoproteins in virion production in macrophages that is driven by an evolutionary arms race with intracellular antiviral factors, SPCS3 and eIF3k. Overall, this research not only challenges the prevailing paradigm that viral glycoproteins mainly play a role in entry, but also provides promising targets for therapeutic intervention to strengthen the antiviral status of macrophages in order to eliminate CHIKV reservoirs.

## Methods

**Reagents and tools table**

| Reagent/Resource | Reference or source | Identifier or catalog number |
|---|---|---|
| **Experimental Models** | | |
| THP-1 cells (*H. sapiens*) | ATCC | Cat#TIB-202 |
| Human primary PBMCs | UCLA/CFAR Virology Core Lab | N/A |
| HEK-293T cells (*H. sapiens*) | ATCC | Cat#CRL-3216 |
| BHK-21 cells (*Mesocricetus auratus*) | ATCC | Cat#CCL-10 |
| Lenti-X 293 T cells | Takara | Cat#631294 |
| **Recombinant DNA** | | |
| CHIKV 181/clone 25 | Scott Weaver, The University of Texas Medical Branch at Galveston (Gorchakov et al, 2012) | GenBank: AAA53256.3 |
| CHIKV 181/clone 25-EGFP | Nguyen et al, 2023 | N/A |
| pONN.AP3 | Stephen Higgs, Kansas State University (Brault et al, 2004) | GenBank: AF079456 |
| p5′dsONNic-foy | Stephen Higgs, Kansas State University (Brault et al, 2004) | N/A |
| SINV Toto1101 | Charles M. Rice, The Rockefeller University (Rice et al, 1987) | N/A |
| SINV TE/5′2 J/GFP | Charles M. Rice, The Rockefeller University (Pierro et al, 2003) | N/A |
| RRV T48-EGFP | Mark Heise, The University of North Carolina at Chapel Hill (Morrison et al, 2006) | N/A |
| CHIKV LR2006 OPY1 | Stephen Higgs, Kansas State University (Tsetsarkin et al, 2006) | GenBank: DQ443544 |
| CHIKV AF15561 | Scott Weaver, The University of Texas Medical Branch at Galveston (Gorchakov et al, 2012) | GenBank: EF452493 |
| Chimera I | This study | N/A |
| Chimera II | This study | N/A |
| Chimera III | This study | N/A |
| Chimera IV | This study | N/A |
| Chimera III-I | This study | N/A |
| Chimera III-II | This study | N/A |
| Chimera III-III | This study | N/A |
| ONNV/CHIKV E2 | This study | N/A |
| ONNV/CHIKV E1 | This study | N/A |
| ONNV/CHIKV E2 + E1 | This study | N/A |
| E2-I + E1 | This study | N/A |
| E2-II + E1 | This study | N/A |
| E2 + E1-I | This study | N/A |
| E2 + E1-II | This study | N/A |
| CHIKV/myc-E2 | This study | N/A |
| CHIKV-EGFP replicon | This study | N/A |
| pcDNA-3xflag-SPCS3 | This study | N/A |
| pcDNA-3xflag-EIF3K | This study | N/A |
| pcDNA-3xflag-APOBEC3F | This study | N/A |
| pcDNA-3xflag-PKR | This study | N/A |
| pcDNA-3xflag-OAS3 | This study | N/A |
| pcDNA-E3-myc-E2-6k-E1 | This study | N/A |
| pcDNA-3xflag-HAM | This study | N/A |
| pcDNA-3xflag-HAM + WH | This study | N/A |
| pcDNA-3xflag-Core | This study | N/A |
| CHIKV E2-V135L | This study | N/A |
| CHIKV E2-A164T | This study | N/A |
| CHIKV E2-A246S | This study | N/A |
| CHIKV E1-E211K | This study | N/A |
| CHIKV E1-V220I | This study | N/A |
| CHIKV E1-R366K | This study | N/A |
| lentiCRISPRv2 puro | Addgene | Cat#98290 |
| pMD2.G | Addgene | Cat#12259 |
| psPAX2 | Addgene | Cat#12260 |
| **Antibodies** | | |
| Anti-myc, mouse monoclonal | Cell Signaling Technology | Cat#2276 S |
| Anti-myc, rabbit monoclonal | Cell Signaling Technology | Cat#2272 S |
| Anti-flag, mouse monoclonal | Sigma-Aldrich | Cat#F1084 |
| Anti-flag, rabbit monoclonal | Cell Signaling Technology | Cat#14793 S |



 

| Reagent/Resource | Reference or source | Identifier or catalog number |
|---|---|---|
| Anti-CHIKV E1, rabbit polyclonal | GeneTex | Cat#GTX135187 |
| ChromoTek GFP antibody, rabbit polyclonal | Proteintech | Cat#pabg1 |
| Anti-β-actin-HRP, mouse monoclonal | Sigma-Aldrich | Cat#A3854 |
| Goat-anti-mouse HRP | Jackson ImmunoResearch | Cat#115-035-146 |
| Goat-anti-rabbit HRP | Thermo Fisher Scientific | Cat#31462 |
| Anti-V5, mouse monoclonal | Millipore Sigma | Cat#V8012 |
| Anti-CHIKV E2, mouse monoclonal | BEI Resources | Cat#NR-44002 |
| Anti-flag, Alexa Fluor 488, rat monoclonal | Invitrogen | Cat#MA1-142-A488 |
| Goat-anti-rabbit Alexa Flour 594 | Invitrogen | Cat#A-11012 |
| Goat-anti-mouse Cy5 | Invitrogen | Cat#A10524 |
| **Oligonucleotides and other sequence-based reagents** | | |
| Primers for overlap & normal PCR | This study | Dataset EV2A |
| Primers for NEBuilder HiFi assembly | This study | Dataset EV2B |
| Primers for CHIKV mutants | This study | Dataset EV2C |
| qPCR primers | This study | Dataset EV2D |
| siRNAs | Thermo Fisher Scientific | Ambion Silencer siRNA |
| **Chemicals, Enzymes and other reagents** | | |
| MEM | Gibco | Cat#11095098 |
| DMEM, high glucose | Gibco | Cat#11965092 |
| RPMI 1640 (ATCC modification) | Gibco | Cat#A1049101 |
| FBS | VWR | Cat#89510 |
| Penicillin/ streptomycin | Fisher Scientific | Cat#SV30010 |
| Non-essential amino acids | Gibco | Cat#11140050 |
| β-mercaptoethanol | Sigma-Aldrich | Cat#M3148 |
| DPBS | HyClone | Cat#SH30378 |
| Human AB serum | Omega Scientific | Cat#HS-20 |
| PMA | Sigma-Aldrich | Cat#P1585 |
| RosetteSep Human Monocyte Enrichment Cocktail | STEMCELL Technologies | Cat#15068 |
| Human recombinant M-CSF | STEMCELL Technologies | Cat#78057 |
| ImmunoCult-SF Macrophage Medium | STEMCELL Technologies | Cat#10961 |
| ACCUMAX | STEMCELL Technologies | Cat#07921 |
| TranIT-X2 transfection kit | Mirus Bio | Cat#MIR6004 |
| TransIT-mRNA transfection kit | Mirus Bio | Cat#MIR2225 |
| X-tremeGENE9 | Roche | Cat# 6365787001 |

| Reagent/Resource | Reference or source | Identifier or catalog number |
|---|---|---|
| Complete EDTA-free protease inhibitor mixture tablet | Roche | Cat# 11873580001 |
| FLI-06 | MCE | Cat# HY-15860 |
| Golgicide A | MCE | Cat# HY-100540 |
| NEBuilder HiFi DNA assembly kit | NEB | Cat#E5520 |
| Q5 site-directed Mutagenesis Kit | NEB | Cat# E0552S |
| Protoscript II First Strand cDNA Synthesis Kit | NEB | Cat# E6560L |
| TRIzol reagent | Thermo Fisher Scientific | Cat#E6560L |
| Direct-zol RNA Microprep Kit | Zymo Research | Cat#R2060 |
| MAXIscript SP6/T7 Transcription Kit | Thermo Fisher Scientific | Cat#AM1320 |
| Luna qPCR Dye | NEB | Cat#E6560 |
| Luna Universal Probe qPCR Master Mix | NEB | Cat#M3004 |
| PrimeTime One-Step RT-qPCR master mix | IDT | Cat# 10007065 |
| Nonidet P 40 Substitute (NP40) | VWR | Cat#M158 |
| EZview Red Anti-c-Myc Affinity Gel | Sigma-Aldrich | Cat#E6654 |
| EZview Red Anti-flag M2 Affinity Gel | Sigma-Aldrich | Cat#F2426 |
| Dynabeads Protein G | Invitrogen | Cat#10004D |
| 4–15% precast Mini-PROTEAN TGX Gel | Bio-Rad | Cat#4561086 |
| Laemmli Sample Buffer | Bio-Rad | Cat# 1610747 |
| Trans-Blot Turbo RTA Midi 0.2 µm PVDF Transfer Kit | Bio-Rad | Cat# 1704273 |
| ProSignal Pico ECL Reagents | Genesee Scientific | Cat#20-300B |
| Collagen-coated coverslips | Corning BioCoat | Cat#354089 |
| Formaldehyde (37% W/M) | Fisher Scientific | Cat# BP531-500 |
| Triton-X100 | Sigma-Aldrich | Cat# T8787 |
| Glycine | Sigma-Aldrich | Cat# 50046 |
| PpuMI | NEB | Cat#R0506 |
| NotI-HF | NEB | Cat#R3189 |
| ApaI | NEB | Cat#R0114 |
| PspXI | NEB | Cat#R0656 |
| BamHI-HF | NEB | Cat#R3136 |
| MfeI-HF | NEB | Cat#R3589 |
| EcoRI-HF | NEB | Cat#R3101 |
| NdeI | NEB | Cat#R0111 |
| SpeI-HF | NEB | R3133 |
| XbaI | NEB | R0145 |
| NheI-HF | NEB | R3131 |
| SacI-HF | NEB | R3156 |

| Reagent/Resource | Reference or source | Identifier or catalog number |
|---|---|---|
| BspEI | NEB | R0540 |
| EcoRV-HF | NEB | R3195 |
| **Software** | | |
| Graphpad Prism v9 | https://www.graphpad.com | N/A |
| FlowJo v10 | https://www.flowjo.com | N/A |
| ImageJ2 v2.14.0 | https://imagej.net | N/A |
| R Studio v2023.09 | https://posit.co/products/open-source/rstudio/ | N/A |
| Cytoscape v3.9 | https://cytoscape.org/ | N/A |
| **Other** | | |
| CFX96 OPUS | Bio-Rad | N/A |
| ChemiDoc | Bio-Rad | N/A |
| Dionex Ultimate 3000 UHPLC | Thermo Fisher Scientific | N/A |
| Nimbus electrospray ionization source | Phoenix S&T | N/A |
| Orbitrap Fusion Lumos Tribrid mass spectrometer | Thermo Fisher Scientific | N/A |
| ZEISS LSM 880 with (Airyscan) | ZEISS | N/A |
| MACSQuant Analyzer | Miltenyi Biotec | N/A |
| R package: ggplot2 | https://ggplot2.tidyverse.org/ | N/A |
| R package: ClusterProfile | Wu et al, 2021 | N/A |
| R package: ggmsa | Zhou et al, 2022 | N/A |
| R package: Biostring | https://rdrr.io/bioc/Biostrings/ | N/A |
| R package: ArtMS3 | https://bioconductor.org/packages/release/bioc/html/artMS.html | N/A |
| Cytoscape plugin: EnrichmentMap | Merico et al, 2010 | N/A |
| Image J plugin: Coloc 2 | https://imagej.net/plugins/coloc-2 | N/A |
| CRAPome database | crapome.org | N/A |
| CORUM database | Tsitsiridis et al, 2023 | N/A |
| DAVID database | david.ncifcrf.gov | N/A |
| KEGG database | kegg.jp | N/A |
| NCBI Virus database | https://www.ncbi.nlm.nih.gov/labs/virus/vssi/#/ (Hatcher et al, 2017) | N/A |
| MUSCLE v3.8.31 | https://drive5.com/muscle/ | N/A |
| HyPhy | https://hyphy.org/ | N/A |
| IQ-Tree v1.6.12 ModelFinder | http://iqtree.cibiv.univie.ac.at (Minh et al, 2020; Trifinopoulos et al, 2016) | N/A |

## Methods and Protocols

### *Cell culture, viruses, and infections*

BHK-21 cells (American Type Culture Collection (ATCC)) were maintained in Minimum Essential Media (MEM, Gibco) supplemented with 7.5% fetal bovine serum (FBS, VWR). HEK-293T cells (ATCC) were maintained in Dulbecco's Modified Eagle Medium (DMEM, VWR) supplemented with 10% FBS. THP-1 human monocytes (ATCC) were maintained in Roswell Park Memorial Institute 1640 Medium (RPMI 1640, Gibco) supplemented with 10% FBS, 1X penicillin/streptomycin (P/S, Fisher Scientific), 1X non-essential amino acids (NEAA, Gibco), and 0.05 mM β-mercaptoethanol (Sigma-Aldrich).

The infectious clone plasmids of enhanced GFP (EGFP)-expressing or unlabeled CHIKV vaccine strain 181/clone 25, EGFP-expressing (p5′dsONNic-foy) or unlabeled (pONN.AP3) ONNV strain SG650, EGFP-expressing SINV (TE/5′2 J/GFP) or unlabeled (pToto1101) SINV, and EGFP-expressing RRV (strain T48) have been previously reported(Pierro et al, 2003; Brault et al, 2004; Gorchakov et al, 2012; Morrison et al, 2006; Kuhn et al, 1991; Rice et al, 1987; Nguyen et al, 2023). The EGFP-expressing CHIKV, ONNV, and SINV have a 5′ duplicated subgenomic promoter that controls EGFP expression, while the EGFP-expressing RRV has a 3′ duplicated subgenomic promoter that controls EGFP expression. The infectious clone plasmids of pathogenic CHIKV La Réunion strain (LR2006 OPY1) (Tsetsarkin et al, 2006) and Asian strain (AF15561)(Gorchakov et al, 2012) are kind gifts from Stephen Higgs (Kansas State University) and Scott Weaver (The University of Texas Medical Branch at Galveston), respectively. Propagations and titrations of virus stocks were generated in BHK-21 cells as previously described (Yang et al, 2022; Luu et al, 2021). The pathogenic CHIKV stocks were prepared and titrated in a biosafety level 3 lab. To infect THP-1-derived macrophages or primary monocyte-derived macrophages, viruses were diluted in Dulbecco's phosphate buffered saline (DPBS) supplemented with 1% human AB serum (Omega Scientific) and 1% P/S, and added to cells at a multiplicity of infection (MOI) of 5 plaque-forming units (pfu)/cell. Typically, infection was carried out in a 12-well or 24-well plate with $5 \times 10^5$ or $2.5 \times 10^5$ macrophages seeded per well. Cells were incubated with the virus for 1 h and washed twice with PBS to remove the virus. Freshly made media was then added to cells, and supernatant samples were collected at the indicated timepoints for plaque assay as previously described.

### *Monocyte differentiation and transfection*

THP-1 human monocytes were differentiated into macrophages through a 24-h stimulation with 50 ng/ml phorbol 12-myristate 13-acetate (PMA, Sigma-Aldrich) in RPMI 1640 supplemented with 10% human AB serum, 1X NEAA, 1X P/S followed by a 24 h rest in human-serum containing RPMI 1640.

Human primary peripheral blood mononuclear cells (PBMCs) were obtained from donors through the UCLA/CFAR Virology Core Lab. The RosetteSep™ Human Monocyte Enrichment Cocktail (STEMCELL Technologies) was used to purify monocytes from the PBMCs. To differentiate the purified monocytes from macrophages, the monocytes were cultured in ImmunoCult™-SF Macrophage Medium (STEMCELL Technologies) supplemented with 50 ng/ml Human Recombinant M-CSF (STEMCELL Technologies) for 4 days. After differentiation, the macrophages were infected as described in the previous section.

### *Generation of EIF3K Cas9-CRISPR KO clones*

The designed guide RNAs (gRNAs) target exons 3 and 7 of *EIF3K* (Appendix Fig. S1A): sgRNA1: 5′-GTGCAAGTGCATGATC-GACC-3′; sgRNA2: 5′-GAAGATCTGCCCCGACTCGT-3′. The gRNAs were ligated into lentiCRISPRv2 puro vector (Addgene,

 

#98290). Lenti-X 293T cells (Takara) were transfected with lentiCRISPRv2, pMD2.G (Addgene, # 12259), and psPAX2 (Addgene, #12260) to generate CRISPR/Cas9 lentiviruses. 293T cells were transduced with lentiviruses and selected with 1 μg/ml puromycin for 5 days. The surviving cells were seeded at the density of 0.3 cell/well in a 96-well plate and expanded in DMEM supplemented with 10% FBS and 0.1 μg/ml puromycin. Clones 7 and 9 were verified by genomic DNA sequencing (Appendix Fig. S1B) and immunoblotting (Fig. 8A), and chosen for validation studies.

#### siRNA and viral RNA transfection

For gene silencing, three unique Ambion Silencer siRNAs (Thermo Fisher Scientific) targeting 13 host factors identified by AP-MS were pooled and transfected into THP-1 macrophages at a final concentration of 25 nM. To simultaneously knock down G3BP1 and G3BP2 as a positive control, two unique Ambion Silencer siRNAs, respectively, targeting G3BP1 and G3BP2 were pooled (25 nM) and transfected into THP-1 macrophage. The same amount of nontargeting siRNA (Thermo Fisher Scientific) was transfected into THP-1 macrophages as negative control. siRNA transfections were performed with TransIT-X2 Transfection Kit (Mirus Bio) following the manufacturer's instructions. Downstream assays were conducted 48 h after transfection.

To observe viral production in transfected macrophages, 500 ng of viral genomic RNA was transfected per well in 12-well plates through the TransIT®-mRNA Transfection Kit (Mirus Bio) following manufacturer's instructions.

#### Inhibition of secretory pathways

The secretory inhibitors FLI-06 and Golgicide A were purchased from MedChemExpress (MCE). The THP-1-derived macrophages were pretreated with 10 μM FLI-06 or 10 μM Golgicide A in RPMI 1640 containing 10% human serum for 30 min. The macrophages were then inoculated with ONNV, CHIKV, and ONNV/CHIKV E2 + E1 at MOI of 5 in DPBS containing 1% human AB serum for 1 h. After two washes with DPBS, the macrophages were again cultured in RPMI 1640 supplemented with 10% human AB serum and 10 mM secretory inhibitors. The macrophage supernatants were collected for plaque assay titration 24 h post infection.

#### Construction of CHIKV-ONNV chimeras, positively selected site mutants, myc-tagged CHIKV, and CHIKV-EGFP replicon

All the primers and restriction sites used in chimeras, mutants, reporter virus, and replicon constructions mentioned below are listed in Tables A, B, and C in Dataset EV2, respectively.

To construct Chimera I, gene regions amplified from the parental CHIKV vaccine strain 181/clone 25 and ONNV SG650 strains were fused into two chimeric fragments, Fragment 1 and Fragment 2, through PCR overlap extension (Appendix Fig. S2). Fragment 1 was inserted into the CHIKV 181/clone 25 backbone to generate an intermediate chimera with parts of nsP4 and capsid from ONNV. The fragment from the ONNV subgenomic promoter to the end of the CHIKV poly(A) tail was digested from the intermediate chimera and inserted into the ONNV backbone with Fragment 2 to obtain Chimera I.

To generate Chimera III, we first used overlapping PCR to generate Fragment 3 to replace the equivalent region in CHIKV 181/clone 25 to obtain the CHIKV/ONNV 5′UTR backbone. We then used the NEBuilder HiFi DNA Assembly Kit (New England Biolabs, NEB) to ligate the CHIKV/ONNV 5'UTR backbone with CHIKV subgenomic promoter and capsid (Fragment 4) and ONNV E3 to the end of the poly(A) tail (Fragment 5) (Appendix Fig. S2). Both Fragments 4 and 5 contained overlapping overhangs for HiFi ligation.

The cloning of Chimera II was based on Chimera I. We amplified the region from the CHIKV subgenomic promoter to the PspXI site in E2 with overlapping overhangs and used the NEBuilder HiFi DNA Assembly Kit to ligate the amplified product to the digested Chimera I backbone. To generate Chimera IV, we amplified the region from the ONNV subgenomic promoter to the intrinsic BamHI site in ONNV E2. We then used T4 ligase (NEB) to ligate the amplified fragment with a digested Chimera III backbone.

The other chimera clone plasmids (Chimera III-I, III-II, III-III, ONNV/CHIKV E1, ONNV/CHIKV E2, ONNV/CHIKV E2 + E1, E2-I + E1, E2-II + E1, E2 + E1-I, and E2 + E1-II) were generated in a similar fashion through multiple fragment ligations with the NEBuilder HiFi DNA Assembly Kit.

To construct the CHIKV positively selected site mutants (V135L, A164T, A246S, E211K, V220I, and R366 K), the region containing E2 or E1 was amplified from CHIKV 181/clone 25 and inserted into pCR-Blunt II-TOPO vector (Thermo Fisher Scientific) according to manufacturer's instructions. Corresponding site-directed mutagenesis was conducted on the intermediate TOPO constructs with specific mutation primers by using the Site-Directed Mutagenesis Kit (NEB). The mutated E2- or E1-containing fragments were digested from the TOPO constructs through intrinsic viral restriction sites and inserted back into CHIKV through T4 ligation.

To construct CHIKV with myc-tagged E2 (CHIKV/myc-E2), the myc tag was inserted between E3 and E2 through the NEBuilder HiFi DNA Assembly Kit. Fragment 6 was amplified from parental CHIKV 181/clone 25, containing the region from the subgenomic promoter in nsp4 to the end of E3. The segment of E2, from the start of E2 to the second NdeI site, was amplified from CHIKV 181/clone 25 as Fragment 7. The reverse primer of Fragment 6 and forward primer of Fragment 7 incorporates the myc tag into CHIKV 181/clone 25 through three-fragment assembly (Appendix Fig. S2).

To construct the CHIKV-EGFP replicon in which the structural genes in the genome of CHIKV vaccine strain 181/clone 25 were replaced with EGFP, the second subgenomic promoter, downstream structural genes, 3′UTR region, and polyA tail were removed from EGFP-CHIKV infectious clone plasmid through digestion at SpeI and NotI sites. The 3′UTR region and polyA tail were amplified from the CHIKV vaccine strain 181/clone 25 genome and reintroduced into the digested EGFP-CHIKV infectious clone plasmid through two-fragment assembly with NEBuilder HiFi DNA Assembly Kit.

#### Construction of host factor and CHIKV structural polyprotein plasmids

All the primers and restriction sites used in the construction of host factor and CHIKV structural polyprotein plasmids are listed in Table B in Dataset EV2, respectively.

The cellular mRNA from THP-1 cells was reverse transcribed with oligo-dT primer through the Protoscript II First Strand cDNA

Synthesis Kit (NEB) after TRIzol (Thermo Fisher Scientific) extraction. The host genes OAS3, PKR, SPCS3, EIF3K, and APOBEC3F were amplified with specific primers containing regions overlapping the pcDNA3.1-3xflag vector. The cDNAs of host factors were then incorporated into the NotI and XbaI sites of pcDNA3.1-3xflag vector through NEBuilder HiFi DNA Assembly Kit to transiently express N-terminally 3xflag-tagged host factors.

To construct the plasmid for CHIKV structural glycoprotein following capsid cleavage (pcDNA3.1-E3-myc-E2-6K-E1), the sequence spanning the beginning of E3 to the end of E1 was amplified from CHIKV/myc-E2 with primers containing overlapping regions with the pcDNA3.1 vector and incorporated into pcDNA3.1 through NEBuilder HiFi DNA Assembly Kit. To construct the plasmid expressing pcDNA3.1-E3-myc-E2-6K-E1-3xflag, the amplified E3-myc-E2-6K-E1 fragment was incorporated into the pcDNA3.1-3xflag vector, which transiently expresses the CHIKV poly-glycoprotein with a C-terminally 3xflag-tagged E1.

#### *Quantitative PCR*

For intracellular viral RNA detection, cells were lysed with TRIzol reagent (Thermo Fisher Scientific) followed by extraction of total RNAs through the Direct-zol RNA Microprep Kit (Zymo Research) according to the manufacturer's instructions. For quantifying viral copy number, viral RNAs from secreted particles in the cell culture supernatant samples were extracted through PureLink Viral RNA/DNA Kit (Invitrogen) according to the manufacturer's instructions. To enhance assay specificity, tagged reverse transcription primers targeting viral genes were used to synthesize viral cDNAs from total RNAs. The transcribed cDNAs were then quantified by SYBR Green or TaqMan qPCR.

The SYBR Green assay was used to evaluate the copy number of intracellular (+) vRNAs in the samples. To generate standard curve transcripts, full-length CHIKV E1 and partial ONNV E1 (SG650 bp 10092-11361) sequences were amplified with reverse primers containing the SP6 promoter and inserted into the pcDNA3.1 vector with an inherent T7 promoter at the 5′ terminal end. The (+) and (−) standard curve transcripts were synthesized with T7 polymerase using HindIII-linearized plasmid and Sp6 polymerase using NheI-linearized plasmid, respectively, through the MAXIscript™ SP6/T7 Transcription Kit (Thermo Fisher Scientific). The cDNAs of (+) standard curve transcripts and viral RNA in the samples were reverse transcribed with a reverse E1 primer containing a nongenomic tag sequence (Pinto et al, 2006) 5′-CAGACAGCACTCGTTCGTACAC-3′ through the Protoscript II First Strand cDNA Synthesis Kit (NEB). The (+) standard curve cDNAs were then serially diluted ten-fold from $10^{-1}$ to $10^{-8}$ and run through the SYBR Green assay (NEB) together with sample cDNAs. Specific forward primer targeting E1 and a reverse primer targeting the nongenomic tag were used in 20 ul SYBR Green reaction with 1x Luna qPCR Dye (NEB) according to the manufacturer's instructions. The reactions were run under the cycling conditions as previously reported (Luu et al, 2021).

The TaqMan assay was performed to determine the copy number of intracellular (−) vRNAs and supernatant (+) vRNAs from infected cells. The standard curve of (−)/(+) strand nsP1 from CHIKV or ONNV, tagged reverse transcription primers, qPCR primers, and TaqMan probes were designed and generated as previously described (Plaskon et al, 2009). Briefly, a portion of CHIKV or ONNV nsP1 was cloned into pcDNA3.1(+) with a T7 promoter at the 5′ terminus and an SP6 promoter at the 3′ terminus. The (−) and (+) transcripts of nsP1 were transcribed through SP6 and T7 promoters with MAXIscript SP6/T7 Transcription Kit (Invitrogen) respectively. For intracellular (−) viral RNA detection, the partial nsP1 cDNAs of (−) viral RNA in the samples were synthesized with a forward nsP1 primer containing a unique tag sequence 5′-GGCAGTATCGTGAATTC-GATGC-3′ by the Protoscript II First Strand cDNA Synthesis Kit. The appropriate reverse nsP1 primer, tag-specific forward primer, and FAM-labeled TaqMan probe (synthesized by Integrated DNA Technologies, IDT) were used in viral negative-strand quantification with Luna Universal Probe qPCR Master Mix (NEB). The reactions were run under the cycling conditions as follows: initial denaturation step at 95 °C for 1 min followed by 40 cycles of 95 °C for 15 s and 60 °C for 30 s. Data collection occurs during the 60 °C extension step. For supernatant (+) viral RNA detection, (+) nsP1 partial transcripts generated from standard curve plasmids were 10-fold serially diluted in water to create qPCR standard curves. The partial (+) nsP1 transcripts in the supernatant samples were amplified with specific primers but detected by the same FAM-labeled TaqMan probe that was used in (−) nsP1 qPCR with PrimeTime One-Step RT-qPCR Master Mix (IDT) according to the manufacturer's protocol.

Both SYBR Green and TaqMan reactions were performed in technical duplicates of cDNA/vRNA samples from biological replicates. All qPCR reactions were run on the CFX96 OPUS (Bio-Rad). The total copy number of viral RNA was determined by using the standard curve method. All the primers used in qPCR assays are listed in Table D in Dataset EV2.

#### *Positive selection analysis, E2 and E1 alignments*

Chikungunya virus (taxid: 37124) structural polyprotein sequences were downloaded from the NCBI Virus database. Sequences that were not isolated from a human host, less than 10,000 nucleotides in length, or had more than 0.5% of ambiguous characters were excluded; 556 sequences remained.

To guide the nucleotide alignment, the sequences were first translated to amino acids with HyPhy's Codon-aware MSA program (pre-msa). The amino acids were aligned with MUSCLE and used to align the nucleotide sequences with HyPhy's Codon-aware MSA program (post-msa). A maximum-likelihood phylogenetic tree was constructed by IQ-TREE (Minh et al, 2020). By using HyPhy's FEL (Kosakovsky Pond and Frost, 2005) and MEME (Murrell et al, 2012) methods, positive selection analyses were performed on 397 sequences after the exclusion of duplicates from the original 556 sequences.

To visualize the positively selected sites in E2 and E1 proteins of different CHIKV and ONNV strains. The structural polyprotein sequences of CHIKV 181/clone 25 (GenBank: AAA53256.3), CHIKV Asian strain (GenBank: ABO38821.1), CHIKV Caribbean strain (GenBank: AUS84054.1), CHIKV SL15649 strain (GenBank: ACZ72971.1), CHIKV LR2006 OPY1 strain (GenBank: ABD95938.1), CHIKV West African 37997 strain (GenBank: AAU43881.1), ONNV SG650 strain (GenBank: AAC97205.1), ONNV Gulu strain (GenBank: AAA46785.1), and ONNV Ahero strain (GenBank: AOS52786.1) were downloaded from NCBI database. The sequences were aligned with MUSLE, formatted with Biostrings and visualized with ggmsa (Zhou et al, 2022).

 

### Co-immunoprecipitation and immunoblot

To prepare samples for AP-MS, THP-1 monocytes were differentiated into macrophages in 36 15-cm dishes with $2 \times 10^7$ cells per dish. Half of the dishes were either infected with CHIKV vaccine strain 181/clone 25 or CHIKV/myc-E2 at an MOI of 5 pfu/cell. Forty-eight hours later, cells in each dish were lysed with 2 mL NP40 lysis buffer (100 mM Tris-HCl (pH 8.0), 5 mM EDTA, 150 mM NaCl, 0.1% NP40, 5% glycerol) supplemented with 1X PMSF, 2X PPI, 1 uM DTT, and Complete EDTA-free protease inhibitor mixture tablet (Roche). Cell lysates from every six dishes under the same treatment were combined and further centrifuged at 14000 × *g* for 15 min. The clarified supernatants were incubated with anti-myc agarose beads (EZview™ Red Anti-c-Myc Affinity Gel, Millipore) for 4 h at 4 °C. After washing with NP40 lysis buffer four times, proteins were eluted with urea buffer (8 M urea, 100 mM Tris-HCl (pH 8)) for mass spectrometry analysis.

To validate CHIKV glycoprotein interactions with host factors identified by AP-MS, 293T cells were seeded in six-well plates at a starting density of $1.5 \times 10^5$ cells/well, followed by transient transfection with plasmids expressing 3xflag-tagged host factors (OAS3, PKR, SPCS3, eIF3k, and APOBEC3F), empty vector, or control plasmid expressing 3xflag-tagged TRIM25 through X-tremeGENE9 (Roche). Immunoprecipitation of flag-tagged host factors in clarified supernatants with anti-flag agarose beads (EZview™ Red Anti-flag M2 Affinity Gel, Sigma-Aldrich) was performed at 4 °C for 45 min. After 4x washing, proteins were directly eluted with Laemmli Sample Buffer (Bio-Rad) containing 5% 2-mercaptoethanol and denatured by 99 °C 10-min incubation.

For E2 and E1 reciprocal immunoprecipitation (IP), CHIKV E2 antibody (CHK-48), or CHIKV E1 antibody (GeneTex) was conjugated to Dynabeads Protein G (Invitrogen) through 20 min room temperature incubation with rotation at the ratio of 2.2 µg antibodies per mg beads. The E2 antibody-conjugated Dynabeads were incubated with the lysates of 293T cells that were transfected with plasmids expressing 3xflag-SPCS3/eIF3k and CHIKV E3-myc-E2-6k-E1 for 20 min at room temperature to pull down E2. The pulldown efficiency of E2 was verified by myc antibody (Cell Signaling Technology) through immunoblot. For E1 immunoprecipitation, 293T cells were transfected with plasmids expressing 3xflag-SPCS3/eIF3k and E3-myc-E2-6k-E1-3xflag, followed by incubation of cell lysates with E1 antibody-conjugated beads. The pulldown of E1 was evaluated with flag antibody (Millipore Sigma) through immunoblot.

Proteins were resolved by SDS-PAGE in 4–15% precast Mini-PROTEAN TGX Gels (Bio-Rad) in conventional Tris/Glycine/SDS buffer. Proteins were blotted to the PVDF membrane (Bio-Rad) and detected with primary antibodies and HRP-conjugated secondary antibodies listed in the Reagent and tools table. Immunoblots were imaged by chemiluminescence with the ProSignal Pico ECL Reagents (Genesee Scientific) on a ChemiDoc (Bio-Rad).

### Mass spectrometry

Two independent AP-MS experiments were performed to identify macrophage proteins that interact with CHIKV glycoproteins. For mass spectrometry, protein disulfide bonds were subjected to reduction using 5 mM Tris (2-carboxyethyl) phosphine for 30 min, and free cysteine residues were alkylated by 10 mM iodoacetamide for another 30 min. Samples were diluted with 100 mM Tris-HCl at pH 8 to reach a urea concentration of less than 2 M, and then digested sequentially with Lys-C and trypsin at a 1:100 protease-to-peptide ratio for 4 and 12 h, respectively. The digestion reaction was terminated by the addition of formic acid to 5% (vol/vol) with centrifugation. Finally, samples were desalted using C18 tips (Thermo Scientific, 87784), dried in a SpeedVac vacuum concentrator, and reconstituted in 5% formic acid for LC-MS/MS processing.

Tryptic peptide mixtures were loaded onto a 25 cm long, 75-µm inner diameter fused-silica capillary, packed in-house with bulk 1.9 µM ReproSil-Pur beads with 120 Å pores as described previously (Jami-Alahmadi et al, 2021). Peptides were analyzed using a 140 min water-acetonitrile gradient delivered by a Dionex Ultimate 3000 UHPLC (Thermo Fisher Scientific) operated initially at 400 nL/min flow rate with 1% buffer B (acetonitrile solution with 3% DMSO and 0.1% formic acid) and 99% buffer A (water solution with 3% DMSO and 0.1% formic acid). Buffer B was increased to 6% over 5 min at which time the flow rate was reduced to 200 nl/min. A linear gradient from 6–28% B was applied to the column over the course of 123 min. The linear gradient of buffer B was then further increased to 28–35% for 8 min followed by a rapid ramp-up to 85% for column washing. Eluted peptides were ionized via a Nimbus electrospray ionization source (Phoenix S&T) by application of a distal voltage of 2.2 kV.

All label-free mass spectrometry data were collected using data-dependent acquisition on Orbitrap Fusion Lumos Tribrid mass spectrometer (Thermo Fisher Scientific) with an MS1 resolution of 120,000 followed by sequential MS2 scans at a resolution of 15,000. Data generated by LC-MS/MS were searched using the Andromeda search engine integrated into the MaxQuant 2 bioinformatic pipelines against the UniProt *Homo sapiens* reference proteome (UP000005640 9606) and then filtered using a "decoy" database-estimated false discovery rate (FDR) <1%. Label-free quantification (LFQ) was carried out by integrating the total extracted ion chromatogram (XIC) of peptide precursor ions from the MS1 scan. These LFQ intensity values were used for protein quantification across samples. Statistical analysis of differentially expressed proteins was done using the Bioconductor package ArtMS3. Samples were normalized by median intensity.

### Bioinformatic analysis of mass spectrometry data

Due to higher protein abundance, results from our second AP-MS experiment were visualized by histogram and volcano plot (ggplot2.tidyverse.org) to show the fold change distribution of host factors that were significantly enriched by myc pulldown in CHIKV/myc-E2 infected macrophages. To perform gene ontology analysis, candidate host interactors were first filtered by the cut-offs of $p$ value <0.05 and $\text{Log}_2$ fold change >0, based on the comparison of CHIKV/myc-E2 treatment group to CHIKV 181/clone 25 treatment group. We then used the CRAPome (contaminant repository for affinity purification) database (crapome.org) to remove potential contaminant proteins by a cutoff of $\geq$ 200 appearances in 716 recorded experiments. The filtered host factors were submitted to The Database for Annotation, Visualization and Integrated Discovery (DAVID: david.ncifcrf.gov) to analyze the enriched biological process (BP) categories. To have an intuitive view of all the BP categories, EnrichmentMap (Merico et al, 2010) in Cytoscape (Shannon et al, 2003) was used to generate the network of all the BP enrichment results. The KEGG pathway

analysis on host factors was performed by the latest online KEGG database (kegg.jp) downloaded in ClusterProfiler (Wu et al, 2021) in R, and the distribution of core enriched host factors for KEGG categories were visualized through ridgeplot in ClusterProfiler.

For the CORUM protein–protein interaction network, we recovered 37 hits from experiment 1 and 1157 hits from experiment 2 ($p$ value <0.05 and Log2 fold change >0). There were 14 hits overlapping between the two experiments. We first attempted to identify known host protein complexes among the overlapping hits using the CORUM database (Tsitsiridis et al, 2023), a manually curated database of high-confidence protein complexes, but found none. Next, we searched for protein complexes (again, using the CORUM database) in either experiment 1 or experiment 2, reasoning that although indirect protein–protein interactions may be lower abundance in the affinity purification they may be recovered in at least one of the experiments. Our final visualization (Fig. 5C) required that (1) protein complex members pass additional stringency criteria of $Log_2$ fold change >2 from either experiment 1 or 2 and (2) protein complexes possess at least one protein member that was an overlapping hit between experiments 1 and 2.

#### *Immunofluorescence staining and Airyscan microscopy*

To analyze the colocalization of CHIKV E1 with E2 or with host factors (SPCS3, eIF3k), 293T cells were grown on collagen-coated coverslips (Corning BioCoat) and transfected with plasmids expressing 3xflag-tagged SPCS3 or eIF3k followed by CHIKV infection one day later. Twenty-four-hours post infection, the 293T cells were fixed with 4% formaldehyde (Fisher Scientific) in PBS (v/v) for 15 min and sequentially washed with 300 mM glycine (Fisher Scientific) in PBS to quench unreacted formaldehyde residues. The cells were then permeabilized in 0.1% Triton-X100 (Sigma-Aldrich) in PBS (v/v) and blocked in 3% FBS/PBS at room temperature for 1 h. The cells were incubated with primary antibodies targeting CHIKV E1 (GeneTex) and E2 (CHK-48) (Fox et al, 2015) (BEI Resources) diluted in blocking buffer at 4 degrees overnight, followed by 2-h incubation with secondary antibodies and Alexa Fluor 488 conjugated flag antibody (Invitrogen). Coverslips were mounted on glass slides with Fluoromount-G (Invitrogen) and imaged by ZEISS LSM 880 with an Airyscan detector.

To evaluate the colocalization of SPCS3 and eIF3k, 293T cells were co-transfected with plasmids expressing 3xflag-tagged eIF3k and V5-tagged SPCS3 and infected with CHIKV 1 day after. Primary antibodies targeting CHIKV E1 (GeneTex) and V5 (Millipore Sigma) were diluted in the blocking buffer and incubated with the cells at 4 degrees overnight, followed by 2-hour incubation with secondary antibodies and Alexa Fluor 488 conjugated flag antibody. Mounting and imaging were performed as previously described. The antibodies used in the immunofluorescence staining are listed in the Reagent and tools table.

We used the Fiji Coloc2 plugin to analyze the colocalization of E1 and E2, E1 and host factors, and SPCS3 and eIF3k. For each analysis, we selected four cells that were identified to express all the relevant proteins as regions of interest (ROI) and calculated average Pearson correlation coefficient values.

#### *Flow cytometry*

After 24 h incubation with EGFP-labeled alphaviruses, primary human monocyte-derived macrophages were detached from 12-well plates by using ACCUMAX (Stemcell Technologies). Digested macrophages were washed with PBS two times in 96-well plates and fixed in fixation buffer (1% paraformaldehyde (PFA), 1% FBS in PBS). The intracellular EGFP expressions were detected by MACSQuant Analyzer (Miltenyi Biotec) with a minimum collection of 20,000 events per sample. The results were analyzed through FlowJo (Tree Star).

## Data availability

The datasets and computer code produced in this study are available in the following databases:

Protein interaction AP-MS data:
MassIVE repository
Accession number: MSV000094494
(https://massive.ucsd.edu/ProteoSAFe/dataset.jsp?task=db9adf314352491a8bbc20ca5291a838)

The source data of this paper are collected in the following database record: biostudies:S-SCDT-10_1038-S44318-024-00193-3.

Expanded view data, supplementary information, appendices are available for this paper at https://doi.org/10.1038/s44318-024-00193-3.

## Peer review information

A peer review file is available at https://doi.org/10.1038/s44318-024-00193-3

## References

Aitken CE, Beznosková P, Vlčkova V, Chiu W-L, Zhou F, Valášek LS, Hinnebusch AG, Lorsch JR (2016) Eukaryotic translation initiation factor 3 plays distinct roles at the mRNA entry and exit channels of the ribosomal preinitiation complex. eLife 5:e20934

Basore K, Kim AS, Nelson CA, Zhang R, Smith BK, Uranga C, Vang L, Cheng M, Gross ML, Smith J et al (2019) Cryo-EM structure of chikungunya virus in complex with the Mxra8 receptor. Cell 177:1725–1737.e16

Böhni PC, Deshaies RJ, Schekman RW (1988) SEC11 is required for signal peptide processing and yeast cell growth. J Cell Biol 106:1035–1042

Brault AC, Foy BD, Myles KM, Kelly CLH, Higgs S, Weaver SC, Olson KE, Miller BR, Powers AM (2004) Infection patterns of o'nyong nyong virus in the malaria-transmitting mosquito, *Anopheles gambiae*. Insect Mol Biol 13:625–635

Bréhin A-C, Casadémont I, Frenkiel M-P, Julier C, Sakuntabhai A, Desprès P (2009) The large form of human 2′,5′-oligoadenylate synthetase (OAS3) exerts antiviral effect against chikungunya virus. Virology 384:216–222

Brown D, Mattapallil JJ (2014) Gastrointestinal tract and the mucosal macrophage reservoir in HIV infection. Clin Vaccine Immunol 21:1469–1473

Brown RS, Wan JJ, Kielian M (2018) The alphavirus exit pathway: what we know and what we wish we knew. Viruses 10:89

Chen R, Plante JA, Plante KS, Yun R, Shinde D, Liu J, Haller S, Mukhopadhyay S, Weaver SC (2021) Lineage divergence and vector-specific adaptation have driven chikungunya virus onto multiple adaptive landscapes. mBio 12:e02738–21

Chen Y, Cao B, Zheng W, Sun Y, Xu T (2022) eIF3k inhibits NF-κB signaling by targeting MyD88 for ATG5-mediated autophagic degradation in teleost fish. J Biol Chem 298:101730

Cline TD, Beck D, Bianchini E (2017) Influenza virus replication in macrophages: balancing protection and pathogenesis. J Gen Virol 98:2401–2412

 

Cottis S, Blisnick AA, Failloux A-B, Vernick KD (2023) Determinants of chikungunya and O'nyong-Nyong virus specificity for infection of *Aedes* and *Anopheles* mosquito vectors. Viruses 15:589

Daugherty MD, Young JM, Kerns JA, Malik HS (2014) Rapid evolution of PARP genes suggests a broad role for ADP-ribosylation in host-virus conflicts. PLoS Genet 10:e1004403

de Bernardi Schneider A, Ochsenreiter R, Hostager R, Hofacker IL, Janies D, Wolfinger MT (2019) Updated phylogeny of chikungunya virus suggests lineage-specific RNA architecture. Viruses 11:798

Dupuis-Maguiraga L, Noret M, Brun S, Grand RL, Gras G, Roques P (2012) Chikungunya disease: infection-associated markers from the acute to the chronic phase of arbovirus-induced arthralgia. PLoS Negl Trop Dis 6:e1446

Edgar RC (2004) MUSCLE: a multiple sequence alignment method with reduced time and space complexity. BMC Bioinformatics 5:113

Foell D, Wittkowski H, Vogl T, Roth J (2007) S100 proteins expressed in phagocytes: a novel group of damage-associated molecular pattern molecules. J Leukoc Biol 81:28–37

Fox JM, Long F, Edeling MA, Lin H, van Duijl-Richter MKS, Fong RH, Kahle KM, Smit JM, Jin J, Simmons G et al (2015) Broadly neutralizing alphavirus antibodies bind an epitope on E2 and inhibit entry and egress. Cell 163:1095–1107

Frolov I, Hoffman TA, Prágai BM, Dryga SA, Huang HV, Schlesinger S, Rice CM (1996) Alphavirus-based expression vectors: strategies and applications. Proc Natl Acad Sci USA 93:11371–11377

Fros JJ, Pijlman GP (2016) Alphavirus infection: host cell shut-off and inhibition of antiviral responses. Viruses 8:166

Gemmer M, Förster F (2020) A clearer picture of the ER translocon complex. J Cell Sci 133:jcs231340

Gomes-Duarte A, Lacerda R, Menezes J, Romão L (2017) eIF3: a factor for human health and disease. RNA Biol 15:26–34

Gorchakov R, Frolova E, Williams BRG, Rice CM, Frolov I (2004) PKR-dependent and -independent mechanisms are involved in translational shutoff during Sindbis virus infection. J Virol 78(16):8455–8467

Gorchakov R, Wang E, Leal G, Forrester NL, Plante K, Rossi SL, Partidos CD, Adams AP, Seymour RL, Weger J et al (2012) Attenuation of chikungunya virus vaccine strain 181/clone 25 is determined by two amino acid substitutions in the E2 envelope glycoprotein. J Virol 86:6084–6096

Götte B, Liu L, McInerney GM (2018) The enigmatic alphavirus non-structural protein 3 (nsP3) revealing its secrets at last. Viruses 10:105

Gould EA, Higgs S (2009) Impact of climate change and other factors on emerging arbovirus diseases. Trans R Soc Trop Med Hyg 103:109–121

Gunn BM, Morrison TE, Whitmore AC, Blevins LK, Hueston L, Fraser RJ, Herrero LJ, Ramirez R, Smith PN, Mahalingam S et al (2012) Mannose binding lectin is required for alphavirus-induced arthritis/myositis. PLoS Pathog 8:e1002586

Hatcher EL, Zhdanov SA, Bao Y, Blinkova O, Nawrocki EP, Ostapchuck Y, Schäffer AA, Brister JR (2017) Virus variation resource – improved response to emergent viral outbreaks. Nucleic Acids Res 45:D482–D490

Helenius A (1995) Alphavirus and flavivirus glycoproteins: structures and functions. Cell 81:651–653

Hoarau J-J, Jaffar Bandjee M-C, Krejbich Trotot P, Das T, Li-Pat-Yuen G, Dassa B, Denizot M, Guichard E, Ribera A, Henni T et al (2010) Persistent chronic inflammation and infection by chikungunya arthritogenic alphavirus in spite of a robust host immune response. J Immunol 184:5914–5927

Hrecka K, Hao C, Gierszewska M, Swanson SK, Kesik-Brodacka M, Srivastava S, Florens L, Washburn MP, Skowronski J (2011) Vpx relieves inhibition of HIV-1 infection of macrophages mediated by the SAMHD1 protein. Nature 474:658–661

Jami-Alahmadi Y, Pandey V, Mayank AK, Wohlschlegel JA (2021) A robust method for packing high resolution C18 RP-nano-HPLC columns. J Vis Exp:e62380

Kafai NM, Diamond MS, Fox JM (2022) Distinct cellular tropism and immune responses to alphavirus infection. Ann Rev Immunol 40:615–649

Kanehisa M, Sato Y, Kawashima M, Furumichi M, Tanabe M (2016) KEGG as a reference resource for gene and protein annotation. Nucleic Acids Res 44:D457–D462

Kim AS, Diamond MS (2022) A molecular understanding of alphavirus entry and antibody protection. Nat Rev Microbiol 21:396–407

Kim AS, Kafai NM, Winkler ES, Gilliland TC, Cottle EL, Earnest JT, Jethva PN, Kaplonek P, Shah AP, Fong RH et al (2021) Pan-protective anti-alphavirus human antibodies target a conserved E1 protein epitope. Cell 184:4414–4429.e19

Kim DY, Reynaud JM, Rasalouskaya A, Akhrymuk I, Mobley JA, Frolov I, Frolova EI (2016) New world and old world alphaviruses have evolved to exploit different components of stress granules, FXR and G3BP proteins, for assembly of viral replication complexes. PLoS Pathog 12:e1005810

Kistler KE, Huddleston J, Bedford T (2022) Rapid and parallel adaptive mutations in spike S1 drive clade success in SARS-CoV-2. Cell Host Microbe 30:545–555.e4

Kosakovsky Pond SL, Frost SDW (2005) Not so different after all: a comparison of methods for detecting amino acid sites under selection. Mol Biol Evol 22:1208–1222

Krämer A, Mentrup T, Kleizen B, Rivera-Milla E, Reichenbach D, Enzensperger C, Nohl R, Täuscher E, Görls H, Ploubidou A et al (2013) Small molecules intercept Notch signaling and the early secretory pathway. Nat Chem Biol 9:731–738

Kril V, Aïqui-Reboul-Paviet O, Briant L, Amara A (2021) New insights into chikungunya virus infection and pathogenesis. Ann Rev Virol 8:327–347

Kruize Z, Kootstra NA (2019) The role of macrophages in HIV-1 persistence and pathogenesis. Front Microbiol 10:2828

Kuhn RJ, Niesters HGM, Hong Z, Strauss JH (1991) Infectious RNA transcripts from ross river virus cDNA clones and the construction and characterization of defined chimeras with sindbis virus. Virology 182:430–441

Kumar A, Abbas W, Herbein G (2014) HIV-1 latency in monocytes/macrophages. Viruses 6:1837–1860

Labadie K, Larcher T, Joubert C, Manniou A, Delache B, Brochard P, Guigand L, Dubreil L, Lebon P, Verrier B et al (2010) Chikungunya disease in nonhuman primates involves long-term viral persistence in macrophages. J Clin Invest 120:894–906

Laguette N, Rahm N, Sobhian B, Chable-Bessia C, Münch J, Snoeck J, Sauter D, Switzer WM, Heneine W, Kirchhoff F et al (2012) Evolutionary and functional analyses of the interaction between the myeloid restriction factor SAMHD1 and the lentiviral Vpx protein. Cell Host Microbe 11:205–217

Li L, Jose J, Xiang Y, Kuhn RJ, Rossmann MG (2010) Structural changes of envelope proteins during alphavirus fusion. Nature 468:705–708

Luu AP, Yao Z, Ramachandran S, Azzopardi SA, Miles LA, Schneider WM, Hoffmann H-H, Bozzacco L, Garcia G, Gong D et al (2021) A CRISPR activation screen identifies an atypical rho GTPase that enhances Zika viral entry. Viruses 13:2113

MacLean OA, Lytras S, Weaver S, Singer JB, Boni MF, Lemey P, Pond SLK, Robertson DL (2021) Natural selection in the evolution of SARS-CoV-2 in bats created a generalist virus and highly capable human pathogen. PLoS Biol 19:e3001115

Maher MC, Bartha I, Weaver S, di Iulio J, Ferri E, Soriaga L, Lempp FA, Hie BL, Bryson B, Berger B et al (2022) Predicting the mutational drivers of future SARS-CoV-2 variants of concern. Sci Transl Med 14:eabk3445

Marvin SA, Russier M, Huerta CT, Russell CJ, Schultz-Cherry S (2017) Influenza virus overcomes cellular blocks to productively replicate, impacting macrophage function. J Virol 91:e01417–16

McNab F, Mayer-Barber K, Sher A, Wack A, O'Garra A (2015) Type I interferons in infectious disease. Nat Rev Immunol 15:87–103

Merico D, Isserlin R, Stueker O, Emili A, Bader GD (2010) Enrichment map: a network-based method for gene-set enrichment visualization and interpretation. PLoS ONE 5:e13984

Minh BQ, Schmidt HA, Chernomor O, Schrempf D, Woodhams MD, von Haeseler A, Lanfear R (2020) IQ-TREE 2: new models and efficient methods for phylogenetic inference in the genomic era. Mol Biol Evol 37:1530–1534

Morrison TE, Whitmore AC, Shabman RS, Lidbury BA, Mahalingam S, Heise MT (2006) Characterization of Ross River virus tropism and virus-induced inflammation in a mouse model of viral arthritis and myositis. J Virol 80:737–749

Murray PJ, Wynn TA (2011) Protective and pathogenic functions of macrophage subsets. Nat Rev Immunol 11:723–737

Murrell B, Wertheim JO, Moola S, Weighill T, Scheffler K, Pond SLK (2012) Detecting individual sites subject to episodic diversifying selection. PLoS Genet 8:e1002764

Neufeldt CJ, Cortese M, Acosta EG, Bartenschlager R (2018) Rewiring cellular networks by members of the Flaviviridae family. Nat Rev Microbiol 16:125–142

Nguyen LP, Aldana KS, Yang E, Yao Z, Li MMH (2023) Alphavirus Evasion of Zinc Finger Antiviral Protein (ZAP) Correlates with CpG Suppression in a Specific Viral nsP2 Gene Sequence. Viruses 15:830

Osborne MJ, Borden KLB (2015) The eukaryotic translation initiation factor eIF4E in the nucleus: taking the road less traveled. Immunol Rev 263:210–223

Pal P, Dowd KA, Brien JD, Edeling MA, Gorlatov S, Johnson S, Lee I, Akahata W, Nabel GJ, Richter MKS et al (2013) Development of a highly protective combination monoclonal antibody therapy against chikungunya virus. PLoS Pathog 9:e1003312

Pettersen EF, Goddard TD, Huang CC, Meng EC, Couch GS, Croll TI, Morris JH, Ferrin TE (2021) UCSF ChimeraX: structure visualization for researchers, educators, and developers. Protein Sci 30:70–82

Pialoux G, Gaüzère B-A, Jauréguiberry S, Strobel M (2007) Chikungunya, an epidemic arbovirosis. Lancet Infect Dis 7:319–327

Pierro DJ, Myles KM, Foy BD, Beaty BJ, Olson KE (2003) Development of an orally infectious Sindbis virus transducing system that efficiently disseminates and expresses green fluorescent protein in *Aedes aegypti*. Insect Mol Biol 12:107–116

Pinto FL, Svensson H, Lindblad P (2006) Generation of non-genomic oligonucleotide tag sequences for RNA template-specific PCR. BMC Biotechnol 6:31

Plaskon NE, Adelman ZN, Myles KM (2009) Accurate strand-specific quantification of viral RNA. PLoS ONE 4:e7468

Ren SC, Qazi SA, Towell B, Wang JC-Y, Mukhopadhyay S (2022) Mutations at the alphavirus E1′-E2 interdimer interface have host-specific phenotypes. J Virol 96:e02149–21

Rice CM, Levis R, Strauss JH, Huang HV (1987) Production of infectious RNA transcripts from Sindbis virus cDNA clones: mapping of lethal mutations, rescue of a temperature-sensitive marker, and in vitro mutagenesis to generate defined mutants. J Virol 61:3809–3819

Ryman KD, Meier KC, Nangle EM, Ragsdale SL, Korneeva NL, Rhoads RE, MacDonald MR, Klimstra WB (2005) Sindbis virus translation is inhibited by a PKR/RNase L-independent effector induced by alpha/beta interferon priming of dendritic cells. J Virol 79:1487–1499

Saenz JB, Sun WJ, Chang JW, Li J, Bursulaya B, Gray NS, Haslam DB (2009) Golgicide A reveals essential roles for GBF1 in Golgi assembly and function. Nat Chem Biol 5:157–165

Salsman J, Pinder J, Tse B, Corkery D, Dellaire G (2013) The translation initiation factor 3 subunit eIF3K interacts with PML and associates with PML nuclear bodies. Exp Cell Res 319:2554–2565

Saxton-Shaw KD, Ledermann JP, Borland EM, Stovall JL, Mossel EC, Singh AJ, Wilusz J, Powers AM (2013) O'nyong nyong virus molecular determinants of unique vector specificity reside in non-structural protein 3. PLoS Negl Trop Dis 7:e1931

Scholte FEM, Tas A, Albulescu IC, Žusinaite E, Merits A, Snijder EJ, van Hemert MJ (2015) Stress granule components G3BP1 and G3BP2 play a proviral role early in chikungunya virus replication. J Virol 89:4457–4469

Schwartz O, Albert ML (2010) Biology and pathogenesis of chikungunya virus. Nat Rev Microbiol 8:491–500

Seymour RL, Rossi SL, Bergren NA, Plante KS, Weaver SC (2013) The role of innate versus adaptive immune responses in a mouse model of O'Nyong-Nyong virus infection. Am J Trop Med Hyg 88:1170–1179

Shannon P, Markiel A, Ozier O, Baliga NS, Wang JT, Ramage D, Amin N, Schwikowski B, Ideker T (2003) Cytoscape: a software environment for integrated models of biomolecular interaction networks. Genome Res 13:2498–2504

Shelness GS, Lin L, Nicchitta CV (1993) Membrane topology and biogenesis of eukaryotic signal peptidase. J Biol Chem 268:5201–5208

Short KR, Brooks AG, Reading PC, Londrigan SLY (2012) The fate of influenza A virus after infection of human macrophages and dendritic cells. J Gen Virol 93:2315–2325

Sourisseau M, Schilte C, Casartelli N, Trouillet C, Guivel-Benhassine F, Rudnicka D, Sol-Foulon N, Roux KL, Prevost M-C, Fsihi H et al (2007) Characterization of reemerging chikungunya virus. PLoS Pathog 3:e89

Subramanian A, Tamayo P, Mootha VK, Mukherjee S, Ebert BL, Gillette MA, Paulovich A, Pomeroy SL, Golub TR, Lander ES et al (2005) Gene set enrichment analysis: a knowledge-based approach for interpreting genome-wide expression profiles. Proc Natl Acad Sci USA 102:15545–15550

Tenthorey JL, Emerman M, Malik HS (2022) Evolutionary landscapes of host-virus arms races. Ann Rev Immunol 40:271–294

Trifinopoulos J, Nguyen L-T, von Haeseler A, Minh BQ (2016) W-IQ-TREE: a fast online phylogenetic tool for maximum likelihood analysis. Nucleic Acids Res 44:W232–W235

Tsetsarkin K, Higgs S, McGee CE, Lamballerie XD, Charrel RN, Vanlandingham DL (2006) Infectious clones of chikungunya virus (La Réunion Isolate) for vector competence studies. Vector Borne Zoonotic Dis 6:325–337

Tsetsarkin KA, Chen R, Yun R, Rossi SL, Plante KS, Guerbois M, Forrester N, Perng GC, Sreekumar E, Leal G et al (2014) Multi-peaked adaptive landscape for chikungunya virus evolution predicts continued fitness optimization in *Aedes albopictus* mosquitoes. Nat Commun 5:4084

Tsetsarkin KA, Vanlandingham DL, McGee CE, Higgs S (2007) A single mutation in chikungunya virus affects vector specificity and epidemic potential. PLoS Pathog 3:e201

Tsitsiridis G, Steinkamp R, Giurgiu M, Brauner B, Fobo G, Frishman G, Montrone C, Ruepp A (2023) CORUM: the comprehensive resource of mammalian protein complexes–2022. Nucleic Acids Res 51:D539–D545

Vanlandingham DL, Tsetsarkin K, Klingler KA, Hong C, Mcelroy KL, Lehane MJ, Higgs S (2006) Determinants of vector specificity of o'nyong nyong and chikungunya viruses in *Anopheles* and Aedes mosquitoes. Am J Trop Med Hyg 74:663–669

Vogl T, Tenbrock K, Ludwig S, Leukert N, Ehrhardt C, van Zoelen MAD, Nacken W, Foell D, van der Poll T, Sorg C et al (2007) Mrp8 and Mrp14 are endogenous activators of Toll-like receptor 4, promoting lethal, endotoxin-induced shock. Nat Med 13:1042–1049

Voss JE, Vaney M-C, Duquerroy S, Vonrhein C, Girard-Blanc C, Crublet E, Thompson A, Bricogne G, Rey FA (2010) Glycoprotein organization of Chikungunya virus particles revealed by X-ray crystallography. Nature 468:709–712

Weaver SC, Chen R, Diallo M (2020) Chikungunya virus: role of vectors in emergence from enzootic cycles. Ann Rev Entomol 65:313–332



 

Wei Z, Zhang P, Zhou Z, Cheng Z, Wan M, Gong W (2004) Crystal structure of human eIF3k, the first structure of eIF3 subunits. J Biol Chem 279:34983–34990

Wu T, Hu E, Xu S, Chen M, Guo P, Dai Z, Feng T, Zhou L, Tang W, Zhan L et al (2021) clusterProfiler 4.0: a universal enrichment tool for interpreting omics data. Innovation 2:100141

Yang E, Huang S, Jami-Alahmadi Y, McInerney GM, Wohlschlegel JA, Li MMH (2022) Elucidation of TRIM25 ubiquitination targets involved in diverse cellular and antiviral processes. PLoS Pathog 18:e1010743

Yu G, Smith DK, Zhu H, Guan Y, Lam TT-Y (2017) ggtree: an r package for visualization and annotation of phylogenetic trees with their covariates and other associated data. Methods Ecol Evol 8:28–36

Zhang R, Miner JJ, Gorman MJ, Rausch K, Ramage H, White JP, Zuiani A, Zhang P, Fernandez E, Zhang Q et al (2016) A CRISPR screen defines a signal peptide processing pathway required by flaviviruses. Nature 535:164–168

Zhou L, Feng T, Xu S, Gao F, Lam TT, Wang Q, Wu T, Huang H, Zhan L, Li L et al (2022) ggmsa: a visual exploration tool for multiple sequence alignment and associated data. Brief Bioinform 23:bbac222

Zimmerman O, Holmes AC, Kafai NM, Adams LJ, Diamond MS (2023) Entry receptors — the gateway to alphavirus infection. J Clin Invest 133:e165307

## Acknowledgements

We thank Dr. Stephen Higgs (Kansas State University) for providing the infectious clone constructs of CHIKV (La Réunion strain) and ONNV (SG650) and for his help with CHIKV-ONNV chimera constructions. We thank Dr. Scott Weaver (The University of Texas Medical Branch at Galveston) and Dr. Mark Heise (The University of North Carolina at Chapel Hill) for providing the infectious clone constructs of CHIKV (AF15561, 181/clone 25) and RRV (T48). We thank Dr. Charles M Rice for providing the infectious clone constructs of SINV (Toto1101, TE/5′2J/GFP). We thank Dr. Joyce Jose and her student Zeinab Elmasri (Pennsylvania State University), as well as Dr. Graham Simmons and Dr. Jing Jin (Vitalant Research Institute) for their help with the construction of the CHIKV E2 reporter virus. We express our gratitude to Dr. Sergei L Kosakovsky Pond (Temple University), and his students Jordan Zehr and Alexander Lucaci for their insights on positive selection analysis. We also thank Dr. Oliver Fregoso (UCLA) for his comments on this study. We thank the UCLA Proteome Research Center for their services. We thank the instructions and supports from Microscopy Core of UCLA Broad Stem Cell Reseaerch Center for setting up the Airyscanning. We thank the qPCR and flow cytometry platforms provided by UCLA AIDS Institute which is supported by the James B Pendleton Charitable Trust and the McCarthy Family Foundation. We also thank UCLA/CFAR Virology Core Lab (grant number 5P30 AI028697) for providing human primary monocytes. The following reagent was obtained through BEI Resources, NIAID, NIH: Monoclonal Anti-Chikungunya Virus E2 Envelope Glycoprotein, Clone CHK-48 (produced in vitro), NR-44002. This work was funded in part by NIH R01AI158704 (MMHL) and UC Cancer Research Coordinating Committee Faculty Seed Grant (CRN-20-637544; MMHL). JAW was supported by NIH GM089778 and R35GM153408. MB was supported by an HIV Accessory and Regulatory Complexes (HARC) Collaborative Development Award and a Center for AIDS Research Pilot Grant. ZY was supported by the Sydney Finegold Post-Doctoral Fellow Award. EK was supported by Ruth L. Kirschstein National Research Service Award AI007323.

## Author contributions

**Zhenlan Yao**: Conceptualization; Data curation; Software; Formal analysis; Validation; Investigation; Visualization; Methodology; Writing—original draft; Writing—review and editing. **Sangeetha Ramachandran**: Data curation; Formal analysis; Validation; Investigation; Visualization; Writing—original draft; Writing—review and editing. **Serina Huang**: Data curation; Software; Formal analysis; Visualization; Writing—original draft; Writing—review and editing. **Erin Kim**: Data curation; Investigation; Writing—review and editing. **Yasaman Jami-Alahmadi**: Data curation; Software; Formal analysis; Investigation; Writing—original draft. **Prashant Kaushal**: Data curation; Software; Formal analysis; Investigation. **Mehdi Bouhaddou**: Resources; Software; Formal analysis; Visualization; Writing—original draft. **James A Wohlschlegel**: Resources; Methodology; Writing—review and editing. **Melody MH Li**: Conceptualization; Resources; Data curation; Supervision; Funding acquisition; Methodology; Project administration; Writing—review and editing.

Source data underlying figure panels in this paper may have individual authorship assigned. Where available, figure panel/source data authorship is listed in the following database record: biostudies:S-SCDT-10_1038-S44318-024-00193-3.

## Disclosure and competing interests statement

The authors declare no competing interests.

# Expanded View Figures

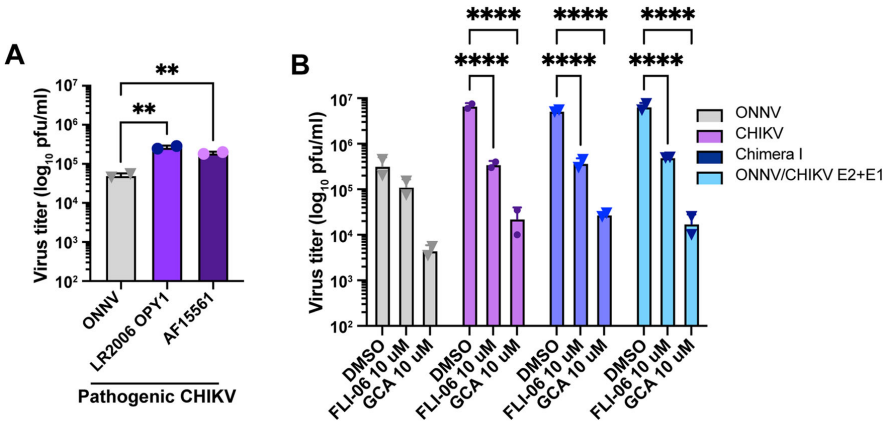


**Figure EV1. The advantage of virus production in macrophages is also recapitulated by pathogenic CHIKV and depends more on the host secretory pathway.**

(**A**) THP-1-derived macrophages were infected with ONNV SG650, CHIKV La Réunion strain (LR2006 OPY1), and CHIKV Asian strain (AF15561) at MOI 5. Titration of supernatant infectious particles was performed at 24 h.p.i by plaque assay on BHK-21 cells. The incubation period for plaque assay takes 28 h. Data were representative of three independent experiments. Mean values of biological duplicates were plotted with SD. Asterisks indicate statistically significant differences as compared to ONNV (One-way ANOVA and Dunnett's multiple comparisons test: ONNV vs LR2006 OPY1 $^{**}p = 0.0024$; ONNV vs AF15561 $^{**}p = 0.0082$). (**B**) The influence of secretary pathway inhibition on the infections of ONNV, CHIKV, Chimera I, and ONNV/CHIKV E2 + E1. The THP-1-derived macrophages were pretreated with 10 μM FLI-06 or GCA for 30 min prior to 1-h inoculation with ONNV, CHIKV, Chimera I, or ONNV/ CHIKV E2 + E1. The cells were then cultured with the inhibitors at the same concentration (10 μM) for 24 h. The virus titers from supernatants were analyzed by plaque assay as previously described. Data were representative of two independent experiments. Mean values of biological duplicates were plotted with SD. Asterisks indicate statistically significant differences as compared to ONNV (one-way ANOVA and Dunnett's multiple comparisons test: DMSO vs FLI-06/GCA with the infection of CHIKV, Chimera I, or ONNV/CHIKV E2 + E1 $^{****}p < 0.0001$).



 

A

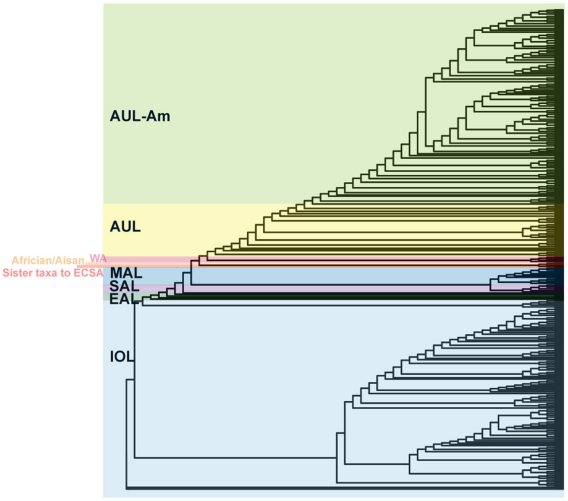


B

| AA location (structural polyprotein) | FEL (p<0.05) | MEME (p<0.05) | CHIKV 181/clone 25 | ONNV SG650 |
|---|---|---|---|---|
| 147 | | C-147 | Ala | Ala |
| 156 | | C-156 | Arg | Arg |
| 460 | | E2-135 | Val | Leu |
| 489 | E2-164 | E2-164 | Ala | Thr |
| 538 | | E2-213 | Thr | Thr |
| 546 | | E2-221 | Lys | Lys |
| 571 | | E2-246 | Ala | Ser |
| 795 | 6K-47 | 6K-47 | Thr | Thr |
| 847 | | E1-38 | Leu | Leu |
| 954 | E1-145 | E1-145 | Ser | Ser |
| 1020 | E1-211 | E1-211 | Glu | Lye |
| 1029 | | E1-220 | Val | Ile |
| 1163 | | E1-354 | Ile | Ile |
| 1175 | | E1-366 | Arg | Lys |

C

| | No. of sequences at E2-135 | No. of sequences at E1-220 |
|---|---|---|
| Valine (V) | 394 | 392 |
| Alanine (A) | 1 | 3 |
| Methionine (M) | 1 | 0 |
| Glutamic acid (E) | 0 | 1 |
| Glycine (G) | 1 | 0 |
| Isoleucine (I) | 0 | 1 |

D


E


**Figure EV2. Evolutionary selection analysis on CHIKV structural proteins.**

(**A**) Phylogenetic tree constructed by IQ-tree (Minh et al, 2020) using an alignment of the CHIKV structural polyprotein. The tree was visualized by ggtree (Yu et al, 2017). Tree branches were colored according to the latest CHIKV lineage classification (de Bernardi Schneider et al, 2019) used in CHIKVnext v3 (nextstrain.org/groups/ViennaRNA/CHIKVnext/v3.0). AUL-Am Asian urban + American lineage, AUL Asian urban lineage, EAL Eastern African lineage, IOL Indian Ocean lineage, MAL Middle African lineage, SAL South American lineage, WA Western African lineage. (**B**) Comparison of CHIKV positively selected sites with homologous sites in ONNV. MEME and FEL were used to analyze the positively selected sites in CHIKV structural proteins and generate *P* values. The *P* values are corrected with Benjamini–Hochberg. The positively selected CHIKV amino acids that are different from the homologous residues in ONNV were colored in red and highlighted in gray. (**C**) The heterogeneity of residues at E2-135 and E1-220 in 397 CHIKV patient isolates from NCBI Virus database. (**D**) The E2 alignment of different ONNV and CHIKV strains to compare the amino acid residues at E2-135, E2-164, and E2-246. CHIKV 37997 belongs to the West African lineage. CHIKV LR2006 OPY1 and CHIKV SL15649 belong to the East/Central/South African (ECSA) lineage. CHIKV Caribbean and CHIKV AF15561 belong to the Asian lineage. CHIKV AF15561 is the parental strain of CHIKV vaccine strain 181/clone 25. The alignment is visualized through ggmsa (Zhou et al, 2022). (**E**) The E1 alignment of different ONNV and CHIKV strains to compare the amino acid residues at E1-211, E1-220, and E1-366.

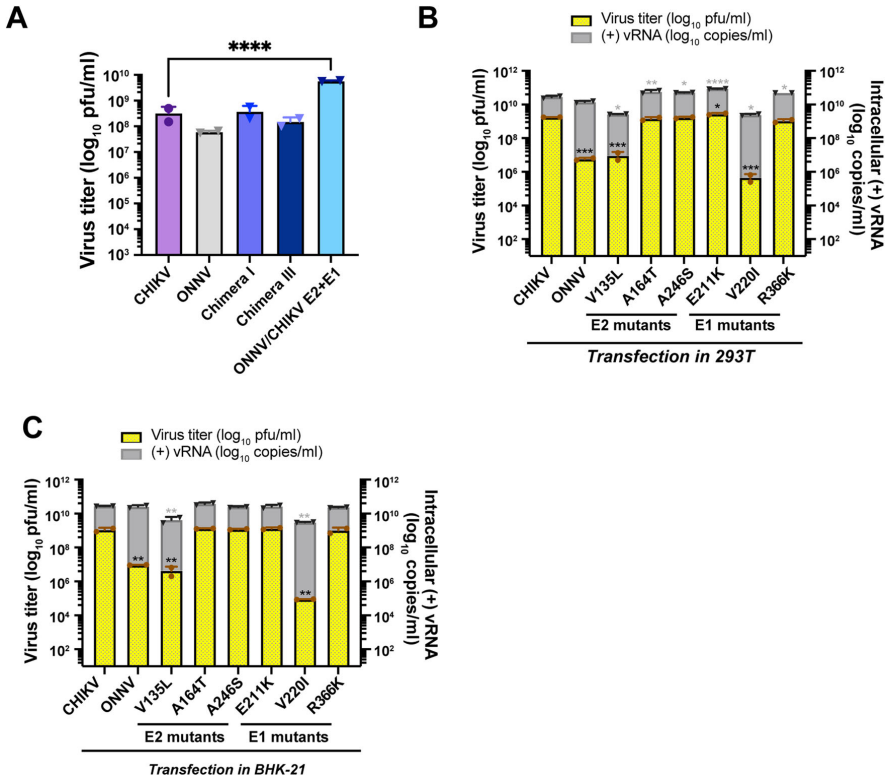


**Figure EV3. The superior virus production conferred by CHIKV structural proteins is macrophage-specific.**

(**A**) CHIKV, ONNV, Chimera I, Chimera III, and ONNV/CHIKV E2 + E1 infection in 293T cells. Virion production in the supernatant of infected 293T cells was titrated through plaque assay on BHK-21 cells as previously described. Mean values of biological duplicates were plotted with SD. Data were representative of two independent experiments. Asterisks indicate statistically significant differences as compared to CHIKV (one-way ANOVA and Dunnett's multiple comparisons test: CHIKV vs ONNV/CHIKV E2 + E1 ****$p < 0.0001$). (**B**, **C**) Infection of 293T (**B**) and BHK-21 (**C**) cells with CHIKV vaccine strain 181/clone 25 positive selection site mutants. Viral replication and production of positive selection site mutants (E2-V135L, E2-A164T, E2-A246S, E1-E211K, E1-V220I, and E1-R366K) were determined by levels of intracellular (+) vRNAs and secreted infectious particles as previously described. For EV3B, data were representative of two independent experiments. The plaque assay results were plotted from biological duplicates with the mean values. Error bars represent SD (one-way ANOVA and Dunnett's multiple comparisons test: viral titer of CHIKV vs ONNV ***$p = 0.0004$; viral titer of CHIKV vs E2-V135L ***$p = 0.0004$; viral titer of CHIKV vs E1-E211K *$p = 0.017$; viral titer of CHIKV vs E1-V220I ***$p = 0.0004$). The qPCR results were plotted from biological duplicates with the mean values. Error bars represent SD (one-way ANOVA and Brown-Forsythe test: viral copies of CHIKV vs E2-V135L *$p = 0.0116$; viral copies of CHIKV vs E2-A164T **$p = 0.0036$; viral copies of CHIKV vs E2-A246S *$p = 0.0156$; viral copies of CHIKV vs E1-E211K ****$p < 0.0001$; viral copies of CHIKV vs E1-V220I *$p = 0.011$; viral copies of CHIKV vs E1-R366K *$p = 0.0274$). For EV3C, data were representative of two independent experiments. The plaque assay results were plotted from biological duplicates with the mean values. Error bars represent SD (one-way ANOVA and Dunnett's multiple comparisons test: viral titer of CHIKV vs ONNV **$p = 0.006$; viral titer of CHIKV vs E2-V135L **$p = 0.0058$; viral titer of CHIKV vs E1-V220I **$p = 0.0057$). The qPCR results were plotted from biological duplicates with the mean values. Error bars represent SD (one-way ANOVA and Brown-Forsythe test: viral copies of CHIKV vs E2-V135L **$p = 0.0027$; viral copies of CHIKV vs E1-V220I **$p = 0.0019$).



 

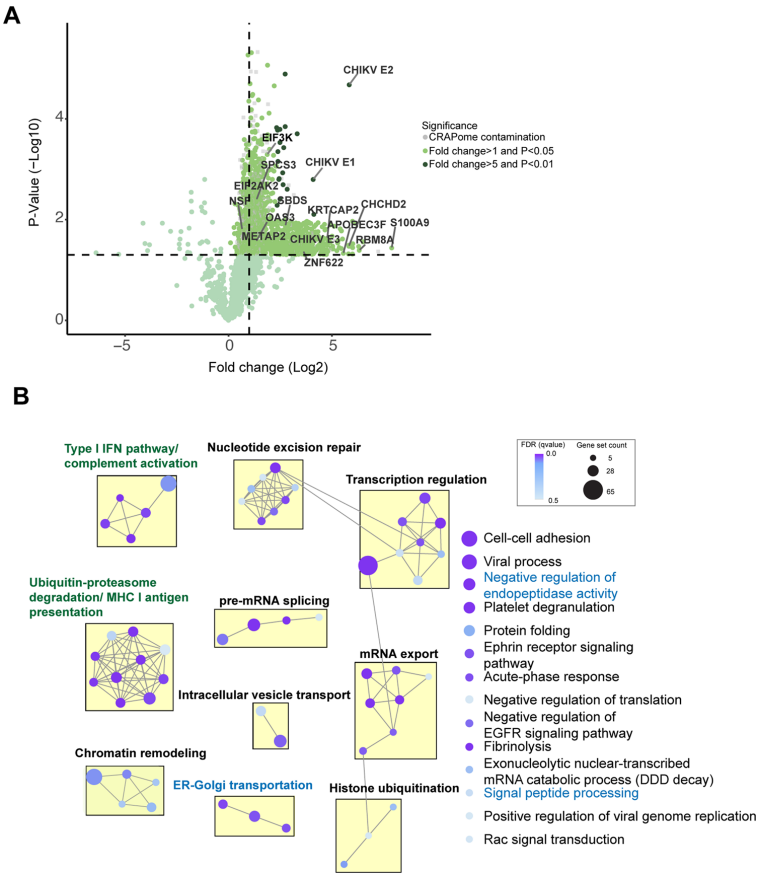


**Figure EV4. The macrophage host factors identified by AP-MS and representative biological processes of significantly enriched host factors.**

(**A**) Volcano plot depicting cellular interactors of CHIKV glycoproteins identified by mass spectrometry. A moderated *t*-test from R package ArtMS3 was used to generate the *P* values which were adjusted with Benjamini–Hochberg for the multiple hypothesis correction. The volcano plot is scattered by $-\log_{10}$ *P* value (y-axis) and $\log_2$ expression fold change (FC) of proteins co-immunoprecipitated from CHIKV/myc-E2 infected cells with respect to the proteins from CHIKV WT infected cells (x-axis). The dashed cut-offs of the adjusted *P* value and expression fold change are 0.05 ($-\log_{10}$ *P* value = 1.30103) and 2 ($\log_2$FC = 1), respectively. CHIKV glycoproteins (E3, E2, E1) and host factors for further investigation in Fig. 6A are annotated here. (**B**) Enrichment map that summarizes over-represented biological processes of identified host factors in groups. The enriched proteins identified by mass spectrometry were clustered by biological processes and organized into a network with edges connecting overlapping gene sets to reveal functional modules.

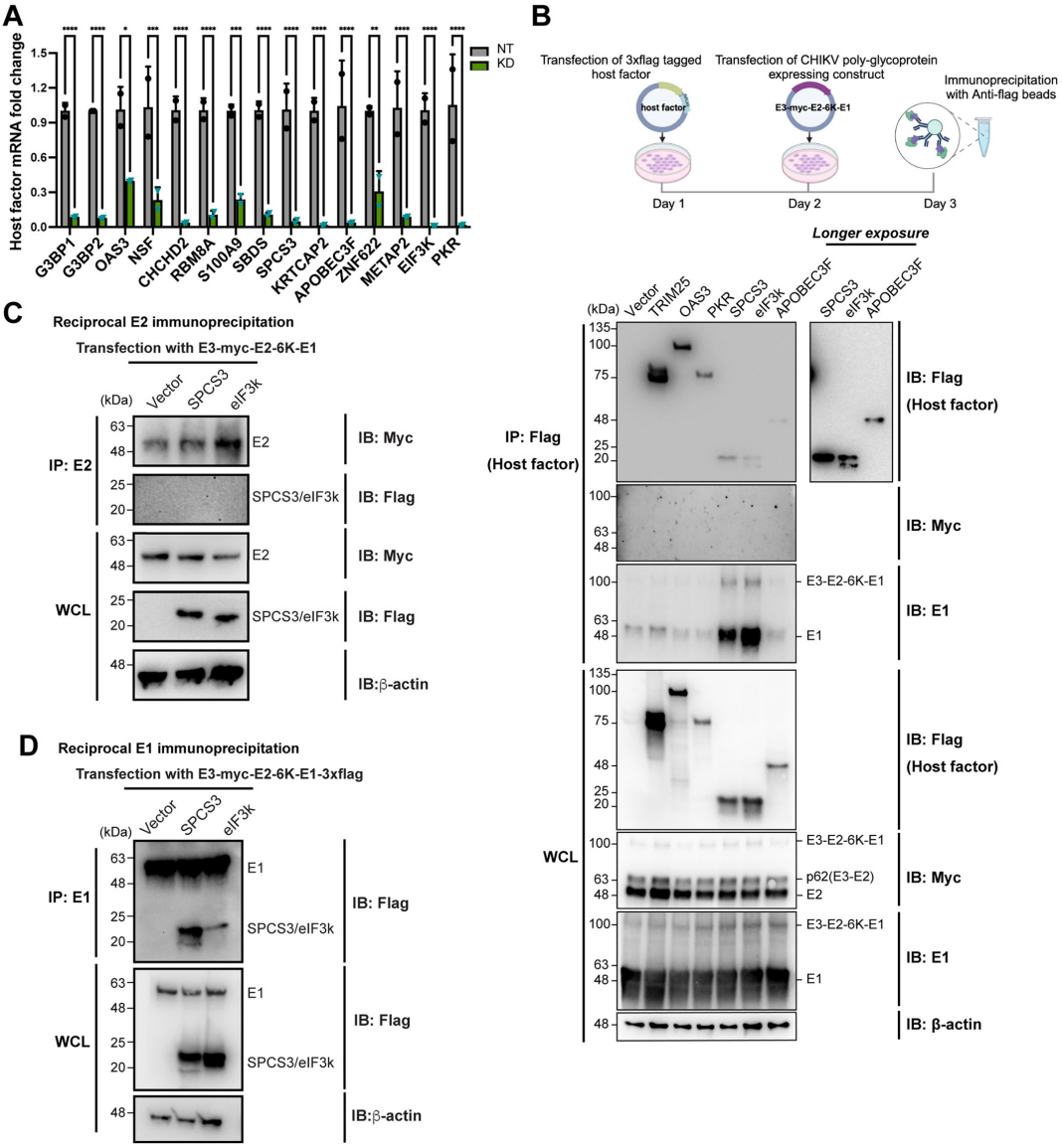




 

**Figure EV5. New antiviral host factors, SPCS3 and eIF3k, specifically interact with CHIKV E1.**

(**A**) The macrophages were transfected with 25 nM nontargeting siRNAs (NT) or pooled siRNAs targeting host factors (G3BP1, G3BP2, OAS3, NSF, CHCHD2, RBM8A, S100A9, SBDS, SPCS3, KRTCAP2, APOBEC3F, ZNF622, METAP2, EIF3K, and PKR). mRNAs of cells treated with siRNAs were extracted 48 h post transfection for RT-qPCR to evaluate the host factor knockdown efficiencies. Data were representative of two independent experiments. The mean values of biological duplicates were plotted with SD (two-way ANOVA and Šidák's multiple comparisons test: si-NT vs si-OAS3 $*p = 0.0118$; si-NT vs si-ZNF622 $**p = 0.0026$; si-NT vs si-NSF $***p = 0.0006$; si-NT vs si-S100A9 $***p = 0.0009$; si-NT vs si-G3BP1/G3BP2/CHCHD2/RBM8A/SBDS/SPCS3/KRTCAP2/APOBEC3F/METAP2/EIF3K/PKR $****p < 0.0001$). (**B**) 293T cells were transfected with plasmids expressing 3xflag-tagged host factors (TRIM25, OAS3, SPCS3, APOBEC3F, eIF3k, and PKR) or empty vector control for 24 h, and later transfected with plasmid expressing CHIKV glycoproteins (E3-myc-E2-6K-E1). The cells were lysed and immunoprecipitated by anti-flag agarose beads. Immunoblot was probed to check for E2/E1 binding to these host factors. TRIM25-3xflag was transfected into 293T cells for immunoprecipitation control. Data were representative of three independent experiments. (**C**) 293T cells were transfected with plasmids expressing 3xflag-tagged host factors (SPCS3, eIF3k) or empty vector control for 24 h, followed by transfection with the plasmid expressing CHIKV E3-myc-E2-6K-E1. The cells were lysed for immunoprecipitation with Dynabeads Protein G conjugated with E2 antibody (CHK-48) (Fox et al, 2015). Immunoblot was probed for host factor (SPCS3, eIF3k) binding to E2. Data were representative of two independent experiments. (**D**) 293T cells were transfected with plasmids expressing 3xflag-tagged host factors (SPCS3, eIF3k) or empty vector control for 24 h, followed by transfection with the plasmid expressing CHIKV E3-myc-E2-6K-E1-3xflag. The cells were lysed for immunoprecipitation with Dynabeads Protein G conjugated with E1 antibody. Immunoblot was probed for host factor (SPCS3, eIF3k) binding to E1. Data were representative of two independent experiments.

# BIBLIOGRAPHY

Abraham, R., Hauer, D., McPherson, R. L., Utt, A., Kirby, I. T., Cohen, M. S., Merits, A., Leung, A. K. L., & Griffin, D. E. (2018). ADP-ribosyl-binding and hydrolase activities of the alphavirus nsP3 macrodomain are critical for initiation of virus replication. *Proceedings of the National Academy of Sciences*, *115*(44), E10457–E10466. https://doi.org/10.1073/pnas.1812130115

Ahola, T., McInerney, G., & Merits, A. (2021). Chapter Four—Alphavirus RNA replication in vertebrate cells. In M. Kielian, T. C. Mettenleiter, & M. J. Roossinck (Eds.), *Adv Virus Res* (Vol. 111, pp. 111–156). Academic Press. https://doi.org/10.1016/bs.aivir.2021.07.003

Albert, J. M., Cao, C., Kim, K. W., Willey, C. D., Geng, L., Xiao, D., Wang, H., Sandler, A., Johnson, D. H., Colevas, A. D., Low, J., Rothenberg, M. L., & Lu, B. (2007). Inhibition of Poly(ADP-Ribose) Polymerase Enhances Cell Death and Improves Tumor Growth Delay in Irradiated Lung Cancer Models. *Clinical Cancer Research*, *13*(10), 3033–3042. https://doi.org/10.1158/1078-0432.CCR-06-2872

Alhammad, Y. M. O., & Fehr, A. R. (2020). The Viral Macrodomain Counters Host Antiviral ADP-Ribosylation. *Viruses*, *12*(4), Article 4. https://doi.org/10.3390/v12040384

Alhammad, Y. M. O., Kashipathy, M. M., Roy, A., Gagné, J.-P., McDonald, P., Gao, P., Nonfoux, L., Battaile, K. P., Johnson, D. K., Holmstrom, E. D., Poirier, G. G., Lovell, S., & Fehr, A. R. (2021). The SARS-CoV-2 Conserved Macrodomain Is a Mono-ADP-Ribosylhydrolase. *Journal of Virology*, *95*(3), 10.1128/jvi.01969-20. https://doi.org/10.1128/jvi.01969-20

Badiee, M., Kenet, A. L., Ganser, L. R., Paul, T., Myong, S., & Leung, A. K. L. (2023). Switch-like compaction of poly(ADP-ribose) upon cation binding. *Proceedings of the National Academy of Sciences*, *120*(19), e2215068120. https://doi.org/10.1073/pnas.2215068120

Bick, M. J., Carroll, J.-W. N., Gao, G., Goff, S. P., Rice, C. M., & MacDonald, M. R. (2003). Expression of the zinc-finger antiviral protein inhibits alphavirus replication. *Journal of Virology*, *77*(21), 11555–11562. https://doi.org/10.1128/jvi.77.21.11555-11562.2003

Bowman, J. D., Silva, N., Schüftan, E., Almeida, J. M., Brattig-Correia, R., Oliveira, R. A., Tüttelmann, F., Enard, D., Navarro-Costa, P., & Lynch, V. J. (2024). Pervasive relaxed selection on spermatogenesis genes coincident with the evolution of polygyny in gorillas. *eLife*, *13*. https://doi.org/10.7554/eLife.94563.1

Brault, A. C., Foy, B. D., Myles, K. M., Kelly, C. L. H., Higgs, S., Weaver, S. C., Olson, K. E., Miller, B. R., & Powers, A. M. (2004). Infection patterns of o'nyong nyong virus in the malaria-transmitting mosquito, Anopheles gambiae. *Insect Molecular Biology*, *13*(6), 625–635. https://doi.org/10.1111/j.0962-1075.2004.00521.x

Burgess, H. M., Richardson, W. A., Anderson, R. C., Salaun, C., Graham, S. V., & Gray, N. K. (2011). Nuclear relocalisation of cytoplasmic poly(A)-binding proteins PABP1 and PABP4 in response to UV irradiation reveals mRNA-dependent export of metazoan PABPs. *Journal of Cell Science*, *124*(19), 3344–3355. https://doi.org/10.1242/jcs.087692

Charron, G., Li, M. M. H., MacDonald, M. R., & Hang, H. C. (2013). Prenylome profiling reveals S-farnesylation is crucial for membrane targeting and antiviral activity of ZAP long-isoform. *Proceedings of the National Academy of Sciences*, *110*(27), 11085–11090.

Chen, S., Xu, Y., Zhang, K., Wang, X., Sun, J., Gao, G., & Liu, Y. (2012). Structure of N-terminal domain of ZAP indicates how a zinc-finger protein recognizes complex RNA. *Nature Structural & Molecular Biology*, *19*(4), 430–435. https://doi.org/10.1038/nsmb.2243

Chiu, H.-P., Chiu, H., Yang, C.-F., Lee, Y.-L., Chiu, F.-L., Kuo, H.-C., Lin, R.-J., & Lin, Y.-L. (2018). Inhibition of Japanese encephalitis virus infection by the host zinc-finger antiviral protein. *PLOS Pathogens*, *14*(7), e1007166. https://doi.org/10.1371/journal.ppat.1007166

Claflin, S. B., & Webb, C. E. (2015). Ross River Virus: Many Vectors and Unusual Hosts Make for an Unpredictable Pathogen. *PLOS Pathogens*, *11*(9), e1005070. https://doi.org/10.1371/journal.ppat.1005070

Cólon-Thillet, R., Hsieh, E., Graf, L., McLaughlin Jr., R. N., Young, J. M., Kochs, G., Emerman, M., & Malik, H. S. (2019). Combinatorial mutagenesis of rapidly evolving residues yields super-restrictor antiviral proteins. *PLOS Biology*, *17*(10), e3000181. https://doi.org/10.1371/journal.pbio.3000181

Cunningham, B. C., & Wells, J. A. (1989). High-Resolution Epitope Mapping of hGH-Receptor Interactions by Alanine-Scanning Mutagenesis. *Science*, *244*(4908), 1081–1085. https://doi.org/10.1126/science.2471267

Darwin, C., & Kebler, L. (1859). *On the origin of species by means of natural selection, or, The preservation of favoured races in the struggle for life*. London: J. Murray.

Daugherty, M. D., & Malik, H. S. (2012). Rules of engagement: Molecular insights from host-virus arms races. *Annual Review of Genetics*, *46*, 677–700. https://doi.org/10.1146/annurev-genet-110711-155522

Daugherty, M. D., Young, J. M., Kerns, J. A., & Malik, H. S. (2014). Rapid Evolution of PARP Genes Suggests a Broad Role for ADP-Ribosylation in Host-Virus Conflicts. *PLOS Genetics*, *10*(5), e1004403. https://doi.org/10.1371/journal.pgen.1004403

Delgado-Rodriguez, S. E., Ryan, A. P., & Daugherty, M. D. (2023). Recurrent Loss of Macrodomain Activity in Host Immunity and Viral Proteins. *Pathogens*, *12*(5), 674. https://doi.org/10.3390/pathogens12050674

Di Franco, A., Poujol, R., Baurain, D., & Philippe, H. (2019). Evaluating the usefulness of alignment filtering methods to reduce the impact of errors on evolutionary inferences. *BMC Evolutionary Biology*, *19*(1), 21. https://doi.org/10.1186/s12862-019-1350-2

Enard, D., Cai, L., Gwennap, C., & Petrov, D. A. (2016). Viruses are a dominant driver of protein adaptation in mammals. *eLife*, *2016*(5), e12469.

Fehr, A. R., Singh, S. A., Kerr, C. M., Mukai, S., Higashi, H., & Aikawa, M. (2020). The impact of PARPs and ADP-ribosylation on inflammation and host-pathogen interactions. *Genes & Development*, *34*(5–6), 341–359. https://doi.org/10.1101/gad.334425.119

Ficarelli, M., Antzin-Anduetza, I., Hugh-White, R., Firth, A. E., Sertkaya, H., Wilson, H., Neil, S. J. D., Schulz, R., & Swanson, C. M. (2020). CpG Dinucleotides Inhibit HIV-1 Replication through Zinc Finger Antiviral Protein (ZAP)-Dependent and -Independent Mechanisms. *Journal of Virology*, *94*(6), e01337-19. https://doi.org/10.1128/JVI.01337-19

Ficarelli, M., Neil, S. J. D., & Swanson, C. M. (2021). Targeted Restriction of Viral Gene Expression and Replication by the ZAP Antiviral System. *Annual Review of Virology*, *8*(1), 265–283. https://doi.org/10.1146/annurev-virology-091919-104213

Frolova, E. I., Fayzulin, R. Z., Cook, S. H., Griffin, D. E., Rice, C. M., & Frolov, I. (2002). Roles of Nonstructural Protein nsP2 and Alpha/Beta Interferons in Determining the Outcome of Sindbis Virus Infection. *Journal of Virology*, *76*(22), 11254–11264. https://doi.org/10.1128/jvi.76.22.11254-11264.2002

Gack, M. U., Shin, Y. C., Joo, C.-H., Urano, T., Liang, C., Sun, L., Takeuchi, O., Akira, S., Chen, Z., Inoue, S., & Jung, J. U. (2007). TRIM25 RING-finger E3 ubiquitin ligase is essential for RIG-I-mediated antiviral activity. *Nature*, *446*(7138), Article 7138. https://doi.org/10.1038/nature05732

Gao, F., Bailes, E., Robertson, D. L., Chen, Y., Rodenburg, C. M., Michael, S. F., Cummins, L. B., Arthur, L. O., Peeters, M., Shaw, G. M., Sharp, P. M., & Hahn, B. H. (1999). Origin of HIV-1 in the chimpanzee Pan troglodytes troglodytes. *Nature*, *397*(6718), 436–441. https://doi.org/10.1038/17130

Gao, G., Guo, X., & Goff, S. P. (2002). Inhibition of Retroviral RNA Production by ZAP, a CCCH-Type Zinc Finger Protein. *Science*, *297*(5587), 1703–1706.

Gao, J., Tang, Y.-D., Hu, W., & Zheng, C. (2022). When Poly(A) Binding Proteins Meet Viral Infections, Including SARS-CoV-2. *Journal of Virology*, *96*(7), e00136-22. https://doi.org/10.1128/jvi.00136-22

Gläsker, S., Töller, M., & Kümmerer, B. M. (2014). The alternate triad motif of the poly(ADP-ribose) polymerase-like domain of the human zinc finger antiviral protein is essential

for its antiviral activity. *The Journal of General Virology*, *95*(Pt 4), 816–822. https://doi.org/10.1099/vir.0.060988-0

Goldman, N., & Yang, Z. (1994). A codon-based model of nucleotide substitution for protein-coding DNA sequences. *Molecular Biology and Evolution*, *11*(5), 725–736.

Gonçalves-Carneiro, D., Takata, M. A., Ong, H., Shilton, A., & Bieniasz, P. D. (2021). Origin and evolution of the zinc finger antiviral protein. *PLOS Pathogens*, *17*(4), e1009545. https://doi.org/10.1371/journal.ppat.1009545

Gorchakov, R., Wang, E., Leal, G., Forrester, N. L., Plante, K., Rossi, S. L., Partidos, C. D., Adams, A. P., Seymour, R. L., Weger, J., Borland, E. M., Sherman, M. B., Powers, A. M., Osorio, J. E., & Weaver, S. C. (2012). Attenuation of Chikungunya Virus Vaccine Strain 181/Clone 25 Is Determined by Two Amino Acid Substitutions in the E2 Envelope Glycoprotein. *Journal of Virology*, *86*(11), 6084–6096. https://doi.org/10.1128/jvi.06449-11

Griffin, D. E., & Weaver, S. C. (2021). Alphaviruses. In P. M. Howley & D. M. Knipe (Eds.), *Fields Virology: Emerging Viruses—Volume 1* (7th Edition, pp. 194–245). Lippincott Williams & Wilkins.

Groslambert, J., Prokhorova, E., & Ahel, I. (2021). ADP-ribosylation of DNA and RNA. *DNA Repair*, *105*, 103144. https://doi.org/10.1016/j.dnarep.2021.103144

Guo, T., Zuo, Y., Qian, L., Liu, J., Yuan, Y., Xu, K., Miao, Y., Feng, Q., Chen, X., Jin, L., Zhang, L., Dong, C., Xiong, S., & Zheng, H. (2019). ADP-ribosyltransferase PARP11 modulates the interferon antiviral response by mono-ADP-ribosylating the ubiquitin

E3 ligase β-TrCP. *Nature Microbiology*, *4*(11), 1872–1884. https://doi.org/10.1038/s41564-019-0428-3

Guo, X., Carroll, J.-W. N., MacDonald, M. R., Goff, S. P., & Gao, G. (2004). The Zinc Finger Antiviral Protein Directly Binds to Specific Viral mRNAs through the CCCH Zinc Finger Motifs. *Journal of Virology*, *78*(23), 12781–12787. https://doi.org/10.1128/jvi.78.23.12781-12787.2004

Hahn, Y. S., Strauss, E. G., & Strauss, J. H. (1989). Mapping of RNA- temperature-sensitive mutants of Sindbis virus: Assignment of complementation groups A, B, and G to nonstructural proteins. *Journal of Virology*, *63*(7), 3142–3150. https://doi.org/10.1128/jvi.63.7.3142-3150.1989

Hayakawa, S., Shiratori, S., Yamato, H., Kameyama, T., Kitatsuji, C., Kashigi, F., Goto, S., Kameoka, S., Fujikura, D., Yamada, T., Mizutani, T., Kazumata, M., Sato, M., Tanaka, J., Asaka, M., Ohba, Y., Miyazaki, T., Imamura, M., & Takaoka, A. (2011). ZAPS is a potent stimulator of signaling mediated by the RNA helicase RIG-I during antiviral responses. *Nature Immunology*, *12*(1), Article 1. https://doi.org/10.1038/ni.1963

Hicke, L. (2001). Protein regulation by monoubiquitin. *Nature Reviews Molecular Cell Biology*, *2*(3), 195–201. https://doi.org/10.1038/35056583

Holmes, A. C., Basore, K., Fremont, D. H., & Diamond, M. S. (2020). A molecular understanding of alphavirus entry. *PLOS Pathogens*, *16*(10), e1008876. https://doi.org/10.1371/journal.ppat.1008876

Huang, S., Girdner, J., Nguyen, L. P., Sandoval, C., Fregoso, O. I., Enard, D., & Li, M. M. H. (2024). Positive selection analyses identify a single WWE domain residue that shapes

ZAP into a more potent restriction factor against alphaviruses. *PLOS Pathogens*, *20*(8), e1011836. https://doi.org/10.1371/journal.ppat.1011836

Iwasaki, A. (2012). A Virological View of Innate Immune Recognition. *Annual Review of Microbiology*, *66*, 177–196. https://doi.org/10.1146/annurev-micro-092611-150203

Kafai, N. M., Diamond, M. S., & Fox, J. M. (2022). Distinct Cellular Tropism and Immune Responses to Alphavirus Infection. *Annual Review of Immunology*, *40*(1), 615–649. https://doi.org/10.1146/annurev-immunol-101220-014952

Kajjo, S., Sharma, S., Chen, S., Brothers, W. R., Cott, M., Hasaj, B., Jovanovic, P., Larsson, O., & Fabian, M. R. (2022). PABP prevents the untimely decay of select mRNA populations in human cells. *The EMBO Journal*, *41*(6), e108650. https://doi.org/10.15252/embj.2021108650

Karlberg, T., Klepsch, M., Thorsell, A.-G., Andersson, C. D., Linusson, A., & Schüler, H. (2015). Structural basis for lack of ADP-ribosyltransferase activity in poly(ADP-ribose) polymerase-13/zinc finger antiviral protein. *The Journal of Biological Chemistry*, *290*(12), 7336–7344. https://doi.org/10.1074/jbc.M114.630160

Kerns, J. A., Emerman, M., & Malik, H. S. (2008). Positive selection and increased antiviral activity associated with the PARP-containing isoform of human zinc-finger antiviral protein. *PLOS Genetics*, *4*(1), e21. https://doi.org/10.1371/journal.pgen.0040021

Khaleghpour, K., Svitkin, Y. V., Craig, A. W., DeMaria, C. T., Deo, R. C., Burley, S. K., & Sonenberg, N. (2001). Translational Repression by a Novel Partner of Human Poly(A) Binding Protein, Paip2. *Molecular Cell*, *7*(1), 205–216. https://doi.org/10.1016/S1097-2765(01)00168-X

Kim, C., Wang, X.-D., & Yu, Y. (2020). PARP1 inhibitors trigger innate immunity via PARP1 trapping-induced DNA damage response. *eLife*, *9*, e60637. https://doi.org/10.7554/eLife.60637

Kimura, M. (1983). *The Neutral Theory of Molecular Evolution*. Cambridge University Press; Cambridge Core. https://doi.org/10.1017/CBO9780511623486

Kleine, H., Poreba, E., Lesniewicz, K., Hassa, P. O., Hottiger, M. O., Litchfield, D. W., Shilton, B. H., & Lüscher, B. (2008). Substrate-assisted catalysis by PARP10 limits its activity to mono-ADP-ribosylation. *Molecular Cell*, *32*(1), 57–69. https://doi.org/10.1016/j.molcel.2008.08.009

Kmiec, D., Lista, M. J., Ficarelli, M., Swanson, C. M., & Neil, S. J. D. (2021). S-farnesylation is essential for antiviral activity of the long ZAP isoform against RNA viruses with diverse replication strategies. *PLOS Pathogens*, *17*(10), e1009726. https://doi.org/10.1371/journal.ppat.1009726

Kosakovsky Pond, S. L., & Frost, S. D. W. (2005a). Datamonkey: Rapid detection of selective pressure on individual sites of codon alignments. *Bioinformatics*, *21*(10), 2531–2533. https://doi.org/10.1093/bioinformatics/bti320

Kosakovsky Pond, S. L., & Frost, S. D. W. (2005b). Not So Different After All: A Comparison of Methods for Detecting Amino Acid Sites Under Selection. *Molecular Biology and Evolution*, *22*(5), 1208–1222. https://doi.org/10.1093/molbev/msi105

Kosakovsky Pond, S. L., Murrell, B., Fourment, M., Frost, S. D. W., Delport, W., & Scheffler, K. (2011). A Random Effects Branch-Site Model for Detecting Episodic Diversifying

Selection. *Molecular Biology and Evolution*, *28*(11), 3033–3043. https://doi.org/10.1093/molbev/msr125

Kuttiyatveetil, J. R. A., Soufari, H., Dasovich, M., Uribe, I. R., Mirhasan, M., Cheng, S.-J., Leung, A. K. L., & Pascal, J. M. (2022). Crystal structures and functional analysis of the ZnF5-WWE1-WWE2 region of PARP13/ZAP define a distinctive mode of engaging poly(ADP-ribose). *Cell Reports*, *41*(4), 111529. https://doi.org/10.1016/j.celrep.2022.111529

Kwon, Y. T., & Ciechanover, A. (2017). The Ubiquitin Code in the Ubiquitin-Proteasome System and Autophagy. *Trends in Biochemical Sciences*, *42*(11), 873–886. https://doi.org/10.1016/j.tibs.2017.09.002

Lacoste, A., Berenshteyn, F., & Brivanlou, A. H. (2009). An efficient and reversible transposable system for gene delivery and lineage-specific differentiation in human embryonic stem cells. *Cell Stem Cell*, *5*(3), 332–342. https://doi.org/10.1016/j.stem.2009.07.011

Laguette, N., Rahm, N., Sobhian, B., Chable-Bessia, C., Münch, J., Snoeck, J., Sauter, D., Switzer, W. M., Heneine, W., Kirchhoff, F., Delsuc, F., Telenti, A., & Benkirane, M. (2012). Evolutionary and Functional Analyses of the Interaction between the Myeloid Restriction Factor SAMHD1 and the Lentiviral Vpx Protein. *Cell Host & Microbe*, *11*(2), 205–217. https://doi.org/10.1016/j.chom.2012.01.007

Lau, C., Aubry, M., Musso, D., Teissier, A., Paulous, S., Desprès, P., de-Lamballerie, X., Pastorino, B., Cao-Lormeau, V.-M., & Weinstein, P. (2017). New evidence for endemic circulation of Ross River virus in the Pacific Islands and the potential for emergence.

*International Journal of Infectious Diseases*, *57*, 73–76. https://doi.org/10.1016/j.ijid.2017.01.041

Law, L. M. J., Razooky, B. S., Li, M. M. H., You, S., Jurado, A., Rice, C. M., & MacDonald, M. R. (2019). ZAP's stress granule localization is correlated with its antiviral activity and induced by virus replication. *PLOS Pathogens*, *15*(5), e1007798. https://doi.org/10.1371/journal.ppat.1007798

Lee, J.-H., Ryu, S. W., Ender, N. A., & Paull, T. T. (2021). Poly-ADP-ribosylation drives loss of protein homeostasis in ATM and Mre11 deficiency. *Molecular Cell*, *81*(7), 1515-1533.e5. https://doi.org/10.1016/j.molcel.2021.01.019

Leung, A. K. L., Vyas, S., Rood, J. E., Bhutkar, A., Sharp, P. A., & Chang, P. (2011). Poly(ADP-Ribose) Regulates Stress Responses and MicroRNA Activity in the Cytoplasm. *Molecular Cell*, *42*(4), 489–499. https://doi.org/10.1016/j.molcel.2011.04.015

Li, M. M. H., Aguilar, E. G., Michailidis, E., Pabon, J., Park, P., Wu, X., Jong, Y. P. de, Schneider, W. M., Molina, H., Rice, C. M., & MacDonald, M. R. (2019). Characterization of Novel Splice Variants of Zinc Finger Antiviral Protein (ZAP). *Journal of Virology*, *93*(18), e00715-19.

Li, M. M. H., Lau, Z., Cheung, P., Aguilar, E. G., Schneider, W. M., Bozzacco, L., Molina, H., Buehler, E., Takaoka, A., Rice, C. M., Felsenfeld, D. P., & MacDonald, M. R. (2017). TRIM25 Enhances the Antiviral Action of Zinc-Finger Antiviral Protein (ZAP). *PLOS Pathogens*, *13*(1), e1006145. https://doi.org/10.1371/journal.ppat.1006145

Lim, E. S., Fregoso, O. I., McCoy, C. O., Matsen, F. A., Malik, H. S., & Emerman, M. (2012). The Ability of Primate Lentiviruses to Degrade the Monocyte Restriction Factor

SAMHD1 Preceded the Birth of the Viral Accessory Protein Vpx. *Cell Host & Microbe*, *11*(2), 194–204. https://doi.org/10.1016/j.chom.2012.01.004

Liu, C.-H., Zhou, L., Chen, G., & Krug, R. M. (2015). Battle between influenza A virus and a newly identified antiviral activity of the PARP-containing ZAPL protein. *Proceedings of the National Academy of Sciences*, *112*(45), 14048–14053.

Luo, X., Wang, X., Gao, Y., Zhu, J., Liu, S., Gao, G., & Gao, P. (2020). Molecular Mechanism of RNA Recognition by Zinc-Finger Antiviral Protein. *Cell Reports*, *30*(1), 46-52.e4. https://doi.org/10.1016/j.celrep.2019.11.116

Lüscher, B., Bütepage, M., Eckei, L., Krieg, S., Verheugd, P., & Shilton, B. H. (2018). ADP-Ribosylation, a Multifaceted Posttranslational Modification Involved in the Control of Cell Physiology in Health and Disease. *Chemical Reviews*, *118*(3), 1092–1136. https://doi.org/10.1021/acs.chemrev.7b00122

Ly, P. T., Xu, S., Wirawan, M., Luo, D., & Roca, X. (2022). ZAP isoforms regulate unfolded protein response and epithelial- mesenchymal transition. *Proceedings of the National Academy of Sciences*, *119*(31), e2121453119. https://doi.org/10.1073/pnas.2121453119

Malgras, M., Garcia, M., Jousselin, C., Bodet, C., & Lévêque, N. (2021). The Antiviral Activities of Poly-ADP-Ribose Polymerases. *Viruses*, *13*(4). https://doi.org/10.3390/v13040582

Maya-Mendoza, A., Moudry, P., Merchut-Maya, J. M., Lee, M., Strauss, R., & Bartek, J. (2018). High speed of fork progression induces DNA replication stress and genomic instability. *Nature*, *559*(7713), 279–284. https://doi.org/10.1038/s41586-018-0261-5

McDougal, M. B., Boys, I. N., De La Cruz-Rivera, P., & Schoggins, J. W. (2022). Evolution of the interferon response: Lessons from ISGs of diverse mammals. *Current Opinion in Virology*, *53*, 101202. https://doi.org/10.1016/j.coviro.2022.101202

McPherson, R. L., Abraham, R., Sreekumar, E., Ong, S.-E., Cheng, S.-J., Baxter, V. K., Kistemaker, H. A. V., Filippov, D. V., Griffin, D. E., & Leung, A. K. L. (2017). ADP-ribosylhydrolase activity of Chikungunya virus macrodomain is critical for virus replication and virulence. *Proceedings of the National Academy of Sciences*, *114*(7), 1666–1671. https://doi.org/10.1073/pnas.1621485114

Meagher, J. L., Takata, M., Gonçalves-Carneiro, D., Keane, S. C., Rebendenne, A., Ong, H., Orr, V. K., MacDonald, M. R., Stuckey, J. A., Bieniasz, P. D., & Smith, J. L. (2019). Structure of the zinc-finger antiviral protein in complex with RNA reveals a mechanism for selective targeting of CG-rich viral sequences. *Proceedings of the National Academy of Sciences*, *116*(48), 24303–24309. https://doi.org/10.1073/pnas.1913232116

Mitchell, P. S., Patzina, C., Emerman, M., Haller, O., Malik, H. S., & Kochs, G. (2012). Evolution-Guided Identification of Antiviral Specificity Determinants in the Broadly Acting Interferon-Induced Innate Immunity Factor MxA. *Cell Host & Microbe*, *12*(4), 598–604. https://doi.org/10.1016/j.chom.2012.09.005

Monit, C., Morris, E. R., Ruis, C., Szafran, B., Thiltgen, G., Tsai, M.-H. C., Mitchison, N. A., Bishop, K. N., Stoye, J. P., Taylor, I. A., Fassati, A., & Goldstein, R. A. (2019). Positive selection in dNTPase SAMHD1 throughout mammalian evolution. *Proceedings of the National Academy of Sciences*, *116*(37), 18647–18654. https://doi.org/10.1073/pnas.1908755116

Morrison, T. E., Whitmore, A. C., Shabman, R. S., Lidbury, B. A., Mahalingam, S., & Heise, M. T. (2006). Characterization of Ross River Virus Tropism and Virus-Induced Inflammation in a Mouse Model of Viral Arthritis and Myositis. *Journal of Virology*, *80*(2), 737–749. https://doi.org/10.1128/jvi.80.2.737-749.2006

Murrell, B., Moola, S., Mabona, A., Weighill, T., Sheward, D., Kosakovsky Pond, S. L., & Scheffler, K. (2013). FUBAR: A Fast, Unconstrained Bayesian AppRoximation for Inferring Selection. *Molecular Biology and Evolution*, *30*(5), 1196–1205.

Murrell, B., Wertheim, J. O., Moola, S., Weighill, T., Scheffler, K., & Kosakovsky Pond, S. L. (2012). Detecting Individual Sites Subject to Episodic Diversifying Selection. *PLOS Genetics*, *8*(7), e1002764.

Nguyen, L. P., Aldana, K. S., Yang, E., Yao, Z., & Li, M. M. H. (2023). Alphavirus Evasion of Zinc Finger Antiviral Protein (ZAP) Correlates with CpG Suppression in a Specific Viral nsP2 Gene Sequence. *Viruses*, *15*(4), Article 4. https://doi.org/10.3390/v15040830

Nguyen, L.-T., Schmidt, H. A., von Haeseler, A., & Minh, B. Q. (2015). IQ-TREE: A Fast and Effective Stochastic Algorithm for Estimating Maximum-Likelihood Phylogenies. *Molecular Biology and Evolution*, *32*(1), 268–274. https://doi.org/10.1093/molbev/msu300

Nielsen, R. (2005). Molecular Signatures of Natural Selection. *Annual Review of Genetics*, *39*(1), 197–218. https://doi.org/10.1146/annurev.genet.39.073003.112420

Odon, V., Fiddaman, S. R., Smith, A. L., & Simmonds, P. (2022). Comparison of CpG- and UpA-mediated restriction of RNA virus replication in mammalian and avian cells and

investigation of potential ZAP-mediated shaping of host transcriptome compositions. *RNA*, *28*(8), 1089–1109.

Park, E., & Griffin, D. E. (2009). The nsP3 macro domain is important for Sindbis virus replication in neurons and neurovirulence in mice. *Virology*, *388*(2), 305–314. https://doi.org/10.1016/j.virol.2009.03.031

Ranwez, V., Douzery, E. J. P., Cambon, C., Chantret, N., & Delsuc, F. (2018). MACSE v2: Toolkit for the Alignment of Coding Sequences Accounting for Frameshifts and Stop Codons. *Molecular Biology and Evolution*, *35*(10), 2582–2584. https://doi.org/10.1093/molbev/msy159

Rice, C. M., Levis, R., Strauss, J. H., & Huang, H. V. (1987). Production of infectious RNA transcripts from Sindbis virus cDNA clones: Mapping of lethal mutations, rescue of a temperature-sensitive marker, and in vitro mutagenesis to generate defined mutants. *Journal of Virology*, *61*(12), 3809–3819. https://doi.org/10.1128/jvi.61.12.3809-3819.1987

Rodrigue, N., Latrille, T., & Lartillot, N. (2021). A Bayesian Mutation-Selection Framework for Detecting Site-Specific Adaptive Evolution in Protein-Coding Genes. *Molecular Biology and Evolution*, *38*(3), 1199–1208. https://doi.org/10.1093/molbev/msaa265

Ryan, S. J., Carlson, C. J., Mordecai, E. A., & Johnson, L. R. (2019). Global expansion and redistribution of Aedes-borne virus transmission risk with climate change. *PLOS Neglected Tropical Diseases*, *13*(3), e0007213. https://doi.org/10.1371/journal.pntd.0007213

Sandoval, C., Nisson, K., & Fregoso, O. I. (2024). *HIV-1 Vpr-induced DNA damage activates NF-κB through ATM-NEMO independent of cell cycle arrest* (p. 2023.05.23.541990). bioRxiv. https://doi.org/10.1101/2023.05.23.541990

Sawyer, S. L., Emerman, M., & Malik, H. S. (2004). Ancient adaptive evolution of the primate antiviral DNA-editing enzyme APOBEC3G. *PLOS Biology*, *2*(9), E275.

Sawyer, S. L., Wu, L. I., Emerman, M., & Malik, H. S. (2005). Positive selection of primate TRIM5alpha identifies a critical species-specific retroviral restriction domain. *Proceedings of the National Academy of Sciences of the United States of America*, *102*(8), 2832–2837. https://doi.org/10.1073/pnas.0409853102

Schneider, W. M., Chevillotte, M. D., & Rice, C. M. (2014). Interferon-Stimulated Genes: A Complex Web of Host Defenses. *Annual Review of Immunology*, *32*, 513–545.

Schoggins, J. W. (2019). Interferon-Stimulated Genes: What Do They All Do? *Annual Review of Virology*, *6*(1), 567–584. https://doi.org/10.1146/annurev-virology-092818-015756

Schwerk, J., Soveg, F. W., Ryan, A. P., Thomas, K. R., Hatfield, L. D., Ozarkar, S., Forero, A., Kell, A. M., Roby, J. A., So, L., Hyde, J. L., Gale, M., Daugherty, M. D., & Savan, R. (2019). RNA-binding protein isoforms ZAP-S and ZAP-L have distinct antiviral and immune resolution functions. *Nature Immunology*, *20*(12), 1610–1620. https://doi.org/10.1038/s41590-019-0527-6

Shang, Z., Zhang, S., Wang, J., Zhou, L., Zhang, X., Billadeau, D. D., Yang, P., Zhang, L., Zhou, F., Bai, P., & Jia, D. (2024). TRIM25 predominately associates with anti-viral stress granules. *Nature Communications*, *15*(1), 4127. https://doi.org/10.1038/s41467-024-48596-4

Smith, D. W., Mackenzie, J. S., & Weaver, S. C. (2009). Alphaviruses. In *Clinical Virology* (pp. 1241–1274). https://doi.org/10.1128/9781555815981.ch54

Smith, M. D., Wertheim, J. O., Weaver, S., Murrell, B., Scheffler, K., & Kosakovsky Pond, S. L. (2015). Less Is More: An Adaptive Branch-Site Random Effects Model for Efficient Detection of Episodic Diversifying Selection. *Molecular Biology and Evolution*, *32*(5), 1342–1353. https://doi.org/10.1093/molbev/msv022

Stephenson, E. B., Peel, A. J., Reid, S. A., Jansen, C. C., & McCallum, H. (2018). The non-human reservoirs of Ross River virus: A systematic review of the evidence. *Parasites & Vectors*, *11*(1), 188. https://doi.org/10.1186/s13071-018-2733-8

Strauss, J. H., & Strauss, E. G. (1994). The alphaviruses: Gene expression, replication, and evolution. *Microbiological Reviews*, *58*(3), 491–562. https://doi.org/10.1128/mr.58.3.491-562.1994

Suskiewicz, M. J., Prokhorova, E., Rack, J. G. M., & Ahel, I. (2023). ADP-ribosylation from molecular mechanisms to therapeutic implications. *Cell*, *186*(21), 4475–4495. https://doi.org/10.1016/j.cell.2023.08.030

Takata, M. A., Gonçalves-Carneiro, D., Zang, T. M., Soll, S. J., York, A., Blanco-Melo, D., & Bieniasz, P. D. (2017). CG dinucleotide suppression enables antiviral defence targeting non-self RNA. *Nature*, *550*(7674), 124–127. https://doi.org/10.1038/nature24039

Tenthorey, J. L., Young, C., Sodeinde, A., Emerman, M., & Malik, H. S. (2020). Mutational resilience of antiviral restriction favors primate TRIM5α in host-virus evolutionary arms races. *eLife*, *9*, e59988. https://doi.org/10.7554/eLife.59988

Thorsell, A.-G., Ekblad, T., Karlberg, T., Löw, M., Pinto, A. F., Trésaugues, L., Moche, M., Cohen, M. S., & Schüler, H. (2017). Structural Basis for Potency and Promiscuity in Poly(ADP-ribose) Polymerase (PARP) and Tankyrase Inhibitors. *Journal of Medicinal Chemistry*, *60*(4), 1262–1271. https://doi.org/10.1021/acs.jmedchem.6b00990

Todorova, T., Bock, F. J., & Chang, P. (2014). PARP13 regulates cellular mRNA post-transcriptionally and functions as a pro-apoptotic factor by destabilizing TRAILR4 transcript. *Nature Communications*, *5*(1), Article 1. https://doi.org/10.1038/ncomms6362

Tritschler, F., Huntzinger, E., & Izaurralde, E. (2010). Role of GW182 proteins and PABPC1 in the miRNA pathway: A sense of déjà vu. *Nature Reviews Molecular Cell Biology*, *11*(5), 379–384. https://doi.org/10.1038/nrm2885

Ventoso, I., Berlanga, J. J., Toribio, R., & Díaz-López, I. (2024). Translational Control of Alphavirus–Host Interactions: Implications in Viral Evolution, Tropism and Antiviral Response. *Viruses*, *16*(2). https://doi.org/10.3390/v16020205

Vermeire, J., Naessens, E., Vanderstraeten, H., Landi, A., Iannucci, V., Van Nuffel, A., Taghon, T., Pizzato, M., & Verhasselt, B. (2012). Quantification of Reverse Transcriptase Activity by Real-Time PCR as a Fast and Accurate Method for Titration of HIV, Lenti- and Retroviral Vectors. *PLOS ONE*, *7*(12), e50859. https://doi.org/10.1371/journal.pone.0050859

Vivelo, C. A., Ayyappan, V., & Leung, A. K. L. (2019). Poly(ADP-ribose)-dependent ubiquitination and its clinical implications. *Biochemical Pharmacology*, *167*, 3–12. https://doi.org/10.1016/j.bcp.2019.05.006

Weaver, S. C., Winegar, R., Manger, I. D., & Forrester, N. L. (2012). Alphaviruses: Population genetics and determinants of emergence. *Antiviral Research*, *94*(3), 242–257. https://doi.org/10.1016/j.antiviral.2012.04.002

Wu, J., & Chen, Z. J. (2014). Innate Immune Sensing and Signaling of Cytosolic Nucleic Acids. *Annual Review of Immunology*, *32*, 461–488.

Xue, G., Braczyk, K., Gonçalves-Carneiro, D., Dawidziak, D. M., Sanchez, K., Ong, H., Wan, Y., Zadrozny, K. K., Ganser-Pornillos, B. K., Bieniasz, P. D., & Pornillos, O. (2022). Poly(ADP-ribose) potentiates ZAP antiviral activity. *PLOS Pathogens*, *18*(2), e1009202. https://doi.org/10.1371/journal.ppat.1009202

Yang, E., Huang, S., Jami-Alahmadi, Y., McInerney, G. M., Wohlschlegel, J. A., & Li, M. M. H. (2022). Elucidation of TRIM25 ubiquitination targets involved in diverse cellular and antiviral processes. *PLOS Pathogens*, *18*(9), e1010743. https://doi.org/10.1371/journal.ppat.1010743

Yang, E., & Li, M. M. H. (2020). All About the RNA: Interferon-Stimulated Genes That Interfere With Viral RNA Processes. *Frontiers in Immunology*, *11*, 3195.

Yang, E., Nguyen, L. P., Wisherop, C. A., Kan, R. L., & Li, M. M. H. (2022). The Role of ZAP and TRIM25 RNA Binding in Restricting Viral Translation. *Frontiers in Cellular and Infection Microbiology*, *12*. https://www.frontiersin.org/articles/10.3389/fcimb.2022.886929

Yang, Z. (2006). *Computational Molecular Evolution*. Oxford University Press.

Youn, J.-Y., Dunham, W. H., Hong, S. J., Knight, J. D. R., Bashkurov, M., Chen, G. I., Bagci, H., Rathod, B., MacLeod, G., Eng, S. W. M., Angers, S., Morris, Q., Fabian, M., Côté,

J.-F., & Gingras, A.-C. (2018). High-Density Proximity Mapping Reveals the Subcellular Organization of mRNA-Associated Granules and Bodies. *Molecular Cell*, *69*(3), 517-532.e11. https://doi.org/10.1016/j.molcel.2017.12.020

Yu, G., Smith, D. K., Zhu, H., Guan, Y., & Lam, T. T.-Y. (2017). ggtree: An r package for visualization and annotation of phylogenetic trees with their covariates and other associated data. *Methods in Ecology and Evolution*, *8*(1), 28–36. https://doi.org/10.1111/2041-210X.12628

Yuen, K. Y., & Bielefeldt-Ohmann, H. (2021). Ross River Virus Infection: A Cross-Disciplinary Review with a Veterinary Perspective. *Pathogens*, *10*(3). https://doi.org/10.3390/pathogens10030357

Zheng, X., Wang, X., Tu, F., Wang, Q., Fan, Z., & Gao, G. (2017). TRIM25 Is Required for the Antiviral Activity of Zinc Finger Antiviral Protein. *Journal of Virology*, *91*(9). https://doi.org/10.1128/JVI.00088-17

Zhou, Y., He, C., Wang, L., & Ge, B. (2017). Post-translational regulation of antiviral innate signaling. *European Journal of Immunology*, *47*, 1414–1426.

Zhou, Z., Qiu, Y., & Ge, X. (2021). The taxonomy, host range and pathogenicity of coronaviruses and other viruses in the Nidovirales order. *Animal Diseases*, *1*(1), 5.

Zhu, Y., Wang, X., Goff, S. P., & Gao, G. (2012). Translational repression precedes and is required for ZAP-mediated mRNA decay. *The EMBO Journal*, *31*(21), 4236–4246. https://doi.org/10.1038/emboj.2012.271

Zimmer, M. M., Kibe, A., Rand, U., Pekarek, L., Ye, L., Buck, S., Smyth, R. P., Cicin-Sain, L., & Caliskan, N. (2021). The short isoform of the host antiviral protein ZAP acts as an

inhibitor of SARS-CoV-2 programmed ribosomal frameshifting. *Nature Communications*, *12*(1), 7193. https://doi.org/10.1038/s41467-021-27431-0

Zimmerman, O., Holmes, A. C., Kafai, N. M., Adams, L. J., & Diamond, M. S. (2023). Entry receptors—The gateway to alphavirus infection. *The Journal of Clinical Investigation*, *133*(2). https://doi.org/10.1172/JCI165307